ROZPRAWA
DOKTORSKA

IChF
Institute of Physical Chemistry PAS

Krzysztof Niciński, MSc

Plasmonic nanostructures for bacteria and cancer cells analysis by Surface Enhanced Raman Spectroscopy

Institute of Physical Chemistry, Polish Academy of Sciences

Kasprzaka 44/52, 01-224 Warsaw

Supervisor:

Agnieszka Michota-Kamińska, PhD DSc

Assoc Prof. IPC PAS

This dissertation was prepared within the International PhD in Chemistry Studies at the Institute of Physical Chemistry of the Polish Academy of Sciences in Warsaw

Warsaw, December 2022

Table of contents

Acknowledgments

Abstract

The research presented in this dissertation concerns the practical application of surface-enhanced Raman spectroscopy (SERS). The newly developed techniques of SERS substrate production, accurate sample preparation and principal component analysis (PCA) allowed the collection and identification of spectra of a wide variety of bacteria, as well as different types of cancer cells and human body fluids.

The following work consists of a theoretical introduction (Chapters 1-5), aim of the thesis (Chapter 6), description of conducted experiments and their results (Chapter 7), as well as a summary and conclusions (Chapter 8). The theoretical part describes the basics of Raman techniques used in various analytical studies, current trends in the production of SERS substrates and their applications in research, involving biological materials, while the experimental section focuses on presentation of theses that guided the conducted research and results of, *inter alia*, spectroscopic measurements and chemometric analysis performed for different biological samples. The vast majority of the presented results have been published in the form of scientific publications and patent applications, the list of which may be found in Chapters 9 and 10. The list of tables, figures, equations, abbreviations, as well as appendix section are presented in Chapters 11-15, respectively.

The quoted information and presented data come from scientific articles, books and verified websites. These in turn may be found in the last, 16th Chapter of this thesis.

1. Introduction

The interaction of light with matter has always accompanied us in everyday life. The in-depth understanding of the nature of light, which in fact is electromagnetic wave, made it possible to determine the types of its interaction with matter and the manners to observe this phenomenon. It was demonstrated that different regions of the spectrum of electromagnetic radiation may provide different information about investigated compound / material, depending on the observed effect. The data that are most often recorded are presented in the form of a spectrum, i.e., the dependence of the intensity of the observed phenomenon as a function of its energy. The bands in the spectrum informs the observer whether the examined matter absorbed, let through or dispersed a certain amount of radiation with a given energy. Detailed analysis of this data allows to determine the energy state of a molecule, changes in its structure, e.g., the length and strength of bonds and angles between them, types of vibrations that occur in a given molecule, as well as their sizes, shapes or physical parameters, such as a dipole moment.

The phenomenon of light scattering both in elastic and inelastic manner, which is discussed in more detail in Chapter 2, allowed for discovery of an important branch of spectroscopy, known as Raman spectroscopy. Although the method enabled identification of different types of molecules, the observed effect was relatively week, as only one out of million photons is scattered in inelastic way. This, in turn, contributed to development of surface-enhanced Raman spectroscopy (SERS). The SERS technique which was discovered in 1974 and few years later explained on theoretical grounds, attracted researchers with new possibilities. The significantly increased sensitivity (by several orders of magnitude) allowed for measurements applying very low concentrations of analyte, down to single molecules. The data obtained in form of Raman spectra, and hence surface-enhanced Raman spectra, may be described as a set of unique bands characteristic for every compound from a exceedingly wide range of chemical or biochemical individuals. Therefore, it may be applied in research on the structure of organic and inorganic compounds, in experiments on reaction kinetics, as well as in measurements of biological materials such as eukaryotic and prokaryotic cells.

A cell is a basic unit of every organism constitute a collection of a large number of various chemical compounds. Their distribution, type, gene expression profile, and metabolism render a specific organism, tissue or body fluid unique. This feature translates into characteristic Raman / SERS spectrum. What is more, Raman-based spectroscopic

methods can be performed quickly and non-invasively on biological material and provide sufficiently characteristic data allowing its identification. The standard techniques used to identify material of biological origin are based on polymerase-chain reaction (PCR), biochemical tests, and / or immunochemical methods. Despite their high specificity and accuracy, they are usually time-consuming, invasive, and in many cases, relatively expensive.

The possibility of miniaturisation of spectrometers and omitting some sample preparation steps, e.g., cell culture, constitutes a great potential for the development of dispersive Raman techniques, which are nowadays widely applied in food and environmental studies, as well as clinical diagnostics. In addition, routine laboratory activities in quality control processes may also be accelerated and automated, as many samples subjected to the proposed spectroscopic analysis may not need pre-measurement preparation. In addition, the statistical analysis of the results may be performed by using customised computer software instead of empirical or manual analytical tools. All these features are crucial, as they may lead to information about the type of investigated sample in an extremely short time. Such time reduction of analysis enables quick response to detected food and water contamination or to start appropriate patient treatment due to rapid diagnosis of fatal diseases. This may become a fact by applying the SERS technique, but first it is required to perform a wide range of experiments related to production of the SERS substrates necessary to enhance Raman signal. Additionally, it is important to conduct basic research that allow to understand the variability and / or similarities in the spectra of analytes under study, as well the factors that have influence on the obtained result.

7

2.   Raman spectroscopy

2.1   Theoretical background

The scattered spectrum consists of photons of the same energy as incident ones (Rayleigh elastic scattering) and of photons of the changed, in relation to incident light, energy (inelastic scattering). Thus, Raman spectrum consists of the Rayleigh band which is placed in the centre, while the Stokes and anti-Stokes bands of correspondingly reduced and increased frequency are located on opposite sides of the Rayleigh band. Their intensity is generally about 1000 times weaker [1] than in the case of centrally located band, and their number and position depend on the structure of the scattering molecules. The possibility of observing the Stokes and anti-Stokes lines in a spectroscopic image means that the Raman spectroscopy is a technique that measures inelastic scattering of photons.

The described inelastic scattering is caused by rotational and vibration transitions in the molecules following their interaction with an electromagnetic wave. In the Raman spectroscopic techniques, a specific frequency of radiation from a monochromatic light source, most often a laser, is used to irradiate a sample. As a result, radiation scattered on the particle, differing from the energy of excitation radiation by one vibrational unit of energy, may be detected [2]. It should be noted that in the Raman techniques the energy of excitation radiation does not correspond to the electronic energy levels of a molecule and is not large enough to excite it from the ground state to the lowest electronic state. In this situation, the light beam interacts with the electron cloud around the nucleus and polarizes it. Consequently, the molecule is excited to the so-called virtual state between two energy states. The energy of virtual state depends on the frequency of applied electromagnetic radiation. A particle can remain in this state only for about 10^{-14} s, as it is formed only when a photon interacts with matter. For this reason, a molecule will return to its ground state when the light source is turned off.

The Rayleigh scattering can be described as the annihilation of a single photon under the influence of interaction with molecules, atoms, or crystals, and the immediate creation of a second photon with the same energy. As a result, the molecule neither loses nor gains energy. However, there is a probability that the created photon has less energy than the incident one. In this situation the energy difference is used to excite vibrations or rotations of the molecule. In consequence, the scattered light with a reduced frequency, registered in the form of the Stokes band is observed. The created photon may also have higher energy than the

8

incident one, which is related to the de-excitation of the molecule that transfers its excess of oscillatory or rotational energy to the created photon. In this case the anti-Stokes band is registered.

The intensity of the Stokes and anti-Stokes scattering depends on the population of different molecular states, which is represented by Boltzmann distribution:

$$\frac{n_h}{n_l} = \frac{g_h}{g_l} \times \exp(-\frac{\Delta E}{k_B T})$$

Equation 1

where $\frac{n_h}{n_l}$ is the ratio of energy levels, k_B is the Boltzmann constant, T is the temperature, and $\frac{g_h}{g_l}$ is the ratio of the degeneration of energy levels. The conclusion from this distribution is that at room temperature, at which experiments are usually performed, the number of particles in a higher, different than ground, energy state is exceedingly small. For this reason, the intensity of the spectral bands representing the anti-Stokes part of a spectrum will be much lower than for the ones from the Stokes part (*Figure 1*). This, in turn, is the reason why a typical Raman spectrum is usually limited to Stokes contribution.
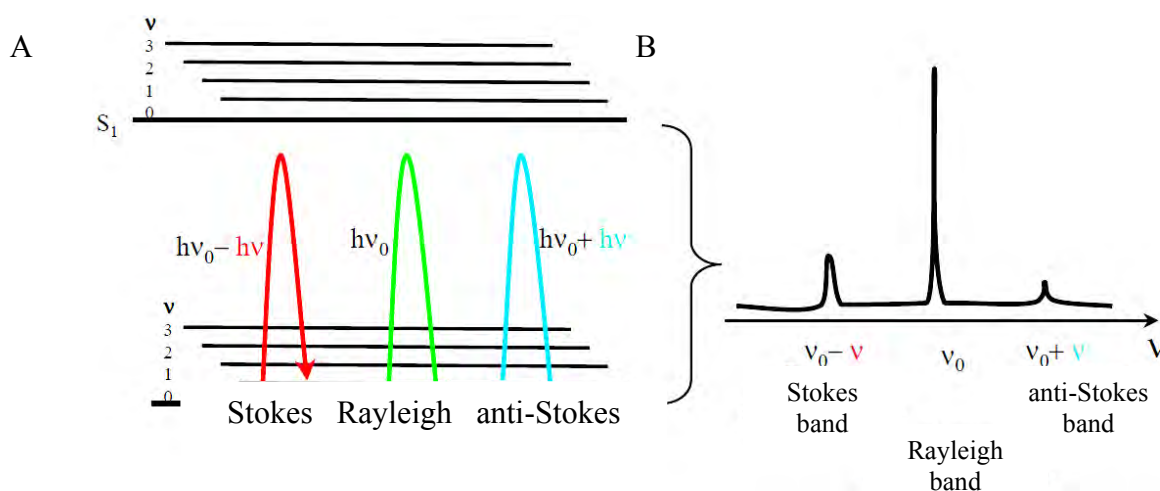
Figure 1. (A) The illustration of the Rayleigh and Raman scattering effect, (B) a schematic representation of the Stokes, Rayleigh and anti-Stokes bands in Raman spectrum [3].

The inelastic scattering effect was predicted theoretically by two independent scientists: Léon Brillouin in 1922 [4] and Adolf Smekal in 1923 [5]. Nonetheless, the Raman effect was named after Indian scientist, Chandrasekhara Venkata Raman, who proved its existence experimentally in 1928, with the assistance of his student, Kariamanikkam Srinivasa Krishnan [6]. For his discovery, Raman was awarded a Nobel Prize in Physics in 1930.

9

When particles are exposed to light, the electric component of electromagnetic wave interacts with the electron cloud, causing its shift. This causes the induction of a dipole moment which is proportional to the intensity of the electric component (E), of the incident electromagnetic wave:

$$\mu_{ind} = \alpha E.$$

Equation 2

Considering the time dependence of the induced electric dipole moment, the variation is described by the formula:

$$E = E_0 \cos 2\pi v_0 t$$

Equation 3,

where E_0 is the amplitude of intensity E and v_0 is the radiation frequency. Combining equations (2) and (3) together, we obtain:

$$\mu_{ind} = \alpha E_0 \cos 2\pi v_0 t$$

Equation 4

The generated dipole moment oscillates with the same frequency as the electric vector of the incident light beam and, at the same time, is a source of the electromagnetic wave. The described effect is observed as already mentioned Rayleigh scattering [7].

During vibration, the bonding force between electrons in the molecule fluctuates periodically, and therefore the polarizability can be expressed as a function of the normal coordinate of the vibration:

$$\alpha = f(q)$$

Equation 5

The dependence of molecular polarizability on normal coordinates can be expressed by using the Taylor series, which can be observed in equation (25). After adopting the harmonic oscillator approximation, we receive:

$$\alpha = \alpha_0 + q\left(\frac{\partial \alpha}{\partial q}\right)_0$$

Equation 6

During vibration the deflection is changing periodically:

$$q = q_0 \cos 2\pi v t$$

Equation 7

By combining equations (6) and (7) we obtain:

$$\alpha = \alpha_0 + q_0 cos2\pi vt\left(\frac{\partial \alpha}{\partial q}\right)_0$$

Equation 8

and by combining the equations (4) and (8) we receive:

$$\mu_{ind} = \alpha_0 E_0 cos2\pi v_0 t + \left(\frac{\partial \alpha}{\partial q}\right)_0 q_0 E_0 cos(2\pi v_0 t)cos(2\pi vt)$$

Equation 9

Having incorporated trigonometric formula for product of cosines:

$$cos\alpha cos\beta = \frac{1}{2}cos(\alpha - \beta) + \frac{1}{2}cos(\alpha + \beta)$$

Equation 10

we obtain:

$$\mu_{ind} = \alpha_0 E_0 cos2\pi v_0 t + \frac{1}{2}\left(\frac{\partial \alpha}{\partial q}\right)_0 q_0 E_0 cos2\pi(v_0 - v)t + \frac{1}{2}\left(\frac{\partial \alpha}{\partial q}\right)_0 q_0 E_0 cos2\pi(v_0 + v)t$$

Equation 11

As the above equation consists of three components, each characterised by different arguments, the following conclusion may be drawn: the induced dipole can oscillate with three different frequencies and generate an electromagnetic wave at v_0 , $v_0 - v$, and $v_0 + v$ wavenumbers [3].

2.2   Instrumentation for Raman spectroscopy

The Raman spectrometer is a device that allows for the observation of light scattering on the tested sample and filtration of the Rayleigh background radiation at the same time. It also enables registration and numerical representation of the collected data. The device consists of a light source, a scattered light collection zone, which usually has a form of a microscope, a spectrograph equipped with detector, filters, a diffraction hole or grating, and a computer control unit. Nowadays, there are handheld devices, table top devices and large spectrometers available on the market, which are equipped with many excitation lines, numerous detectors, and dedicated microscopes. The spectrometers, the design of which allows to use specific conditions of the experiment within the selected frameworks, are also widely popular. The most frequently used type of detector is a CCD (charge-coupled device) array - a system of many photosensitive elements, each registering an electrical signal proportional to the amount of light falling on it. It is commonly used in devices equipped with

11

a light source in the range from ultraviolet to near infrared. In the case of measurements in which the wavelength of the laser light is in the mid to far infrared range, the InGaAs detectors are used. Their name comes from the indium-gallium-arsenide alloy used in the photosensitive part of device and thus, are more resistant to the effects of high thermal energy associated with infrared radiation. On the other hand, the increase in temperature requires active cooling by using thermoelectric effect or liquid nitrogen. Another element, which is frequently observed in the case of spectrometers specialised in high optical resolution of signal acquisition, is a table moving in horizontal and vertical planes, the precise movements of which is possible due to piezoelectric actuators. Such a facility allows for mapping the studied area, i.e., collecting the spectra from equally distant areas with given geometric parameters. This type of signal collection allows obtaining information on the distribution of investigated compounds on a tested surface [8].

Importantly, especially for investigations requiring high resolution of a spectrum, the greater wavelength emitted by the exciting laser, the grater dispersion of light on the diffractive element is observed [9]:

$$I_{RS} \sim I_{laser}\, \bar{v}_{laser}^4\, |\, e_0^-\, \alpha e_s^-\, |^2 d\Omega$$

Equation 12

where e_0^- stands for the laser polarisation, e_s^- is the direction of observation, while and $d\Omega$ is the light-gathering solid angle. Unfortunately, based on the above proportionality, the high laser wavelength also lowers the signal intensity from the scattered light, sometimes making the experiment difficult to conduct.

The spectrum, i.e. the dependence of the intensity of registered phenomenon as a function of its energy, in the case of the Raman method is a plot showing the intensity of inelastically scattered light as a function of the Raman shift, defined as the energy difference between the scattered and the incident light. Therefore, the Rayleigh band in the Raman spectrum is represented by the wavenumber equal to 0 cm^{-1}, while the Stokes bands are usually observed for the range between 150 and 3200 cm^{-1}. The bands observed in the Raman spectrum typically come from molecular vibrations and thus constitute information about the sample.

2.3   Applications and properties of Raman spectroscopy

Almost every material / compound gives unique Raman signal, thus the Raman spectrum is so-called 'spectral fingerprint' of a tested substance. This technique is widely used in many types of laboratories and thus is considered as a standard analytical method. Considering reasonably applied light sources, the method allows for sample measurements in a non-destructive manner and for qualitative and quantitative analysis of solids, liquids or gases [10]. Due to digitisation of the Raman spectra libraries, the method is popular not only in academic community and specialized analytical laboratories, but also in archaeology, research related to art [11], pharmacy [12], studies of minerals and crystals [13], air research, or in forensics when examining secured organic and inorganic traces, e.g. gunpowder, explosives and drugs [14]. In scientific research, the most popular directions for the application of the Raman technique are related to nanomaterials, analysis of organic compounds, broadly understood analytical chemistry, and, for about three decades, biochemistry and medicine [15].

Another application of the Raman spectroscopy is connected with space missions, especially with unmanned missions on Mars. The Perseverance rover, currently present on the planet, is equipped with an arm-mounted device called SHERLOC (Scanning Habitable Environments with Raman & Luminescence for Organics & Chemicals) [16], which basically is a resonance Raman and fluorescence spectrometer utilising deep UV laser as a source of light. The spectrometer is used for studying the luminescence of martian minerals and organic molecules. Another device, also designed for Mars exploration, is the Raman Laser Spectrometer (RLS) [17], which is part of science payload of the European Space Agency's Rosalind Franklin rover. Its main task will be to find biosignatures and biomarkers on Mars.

Although the range of applications of the Raman spectroscopy is wide, the technique has also its drawbacks and limitations. The inelastic dispersion is an effect characterised by very low-intensity. Therefore, when considering weakly scattering material / surface / particle, or when the amount of the analysed material is insufficient, collecting a satisfactory Raman signal may not be feasible. What is more, most of the organic and biochemical compounds, characterized by high photoluminescence, may give a Raman spectrum dominated by intense photoluminescence signal. An additional signal loss is caused by the optics or components, e.g., monochromator, being a part of the used Raman device [18].

The mentioned limitations of the Raman spectroscopy make the technique difficult to apply in everyday practice. Thus, the performance reliable measurements often requires a lot

13

of experience from the operator as well as properly configured, for a given application, instrument. Nevertheless, in the mid-seventies of the last century, the so-called surface-enhanced Raman spectroscopy was discovered. In this technique the analytical signal is amplified multiple times. As a result, the obstacle in the form of low intensity of the Raman bands, hardware limitations, and reduced number of material molecules can be minimised.

3.   Surface-enhanced Raman spectroscopy (SERS)

3.1   Theoretical Background

Surface-enhanced Raman spectroscopy is a technique that allows to measure the inelastic scattering of molecules adsorbed to a metal surface or nanoparticles. To observe the SERS effect, the applied metal needs to be characterized by highly developed surface, that consist of sharp-edged structures. The presence of such structures results in a significant enhancement of the signal in relation to the classical Raman experiment.

The SERS effect was discovered accidentally in 1974, when Fleischmann and co-workers observed that the Raman spectrum of pyridine adsorbed to silver electrode was enhanced by several orders of magnitude in comparison to measurements in which the electrode was not applied. The researchers assumed that signal enhancement is related to a higher number of pyridine molecules in the measured spot, what in turn was connected with presence of crevices in metal structure in which molecules could be easily trapped. In 1977 two independent groups of researchers came to the conclusion that the observed by Fleischmann effect is generated due to a quantum processes [19]. The group of Jeanmaire and Duyne proposed the electromagnetic mechanism (EM) of the Raman signal enhancement [20], while Albrecht and Creighton - the charge transfer effect (CT), also known as chemical mechanism [21]. Nonetheless, until the present day, the real mechanism of the Raman signal amplification in SERS spectroscopy is a questionable topic.

Regardless of the theoretical attempts to describe the phenomenon, the most important condition to be met in every SERS experiment is the occurrence of adsorption process between the analyte and a rough metal surface. As commonly known, surface of a metal is covered with valence electrons of metallic bonds, which are not strictly connected with a specific atom and which are 'held' by the positive charge of the atomic nuclei. During the interaction of such electron gas with an electromagnetic wave, e.g., laser light, the electrons start to oscillate collectively. These types of oscillations are called surface plasmons [22]. The described phenomenon is illustrated in *Figure 2*.
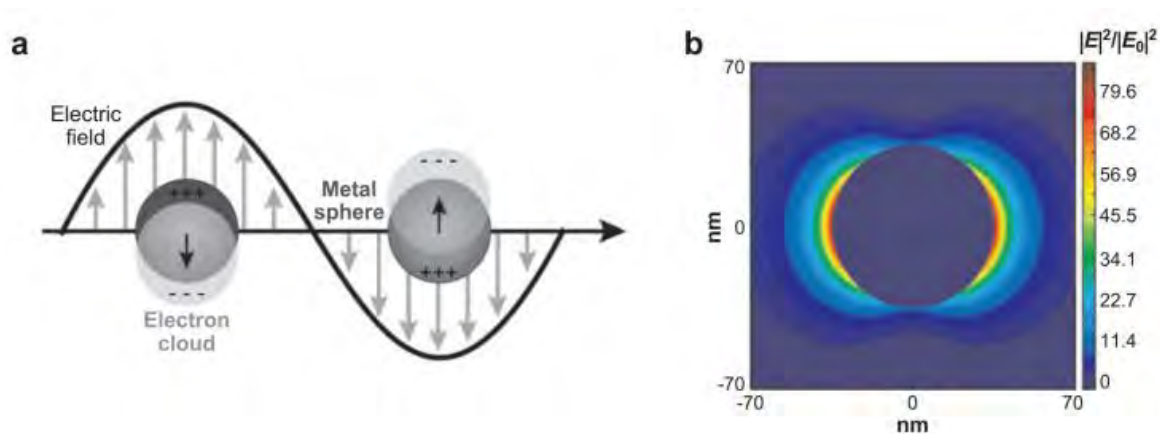
15

Figure 2. The diagrams of surface plasmons formed during the interaction of laser radiation with a metal nanoparticle; (a) the shift of electron cloud in relation to the charge of atomic nuclei under the influence of electric component of electromagnetic radiation, (b) the normalized electric field strength around the spherical silver nanoparticle placed under vacuum [23].

For surface plasmon excitation the light in the near ultraviolet (UV), visible or near infrared (NIR) range [24], as well as the metal structures of dimensions of several dozen nanometres are necessary. These structures may have different shapes, e.g., nanowires, nanorods or nanoparticles, and are usually made of silver, gold or copper. The mentioned metals are the most commonly used materials in the SERS substrate production due to their LSPR (Localized Surface Plasmon Resonance) that significantly covers visible and NIR infrared light ranges, resistance to solvents, and relatively low chemical reactivity. It should be emphasized that oscillations of electron gas also take place on smooth surfaces, but in such case the backscattered radiation, crucial in the vast majority of measurement systems, does not occur intensively enough to be recorded. This is why in the SERS technique the sharp edges, which enable the creation of LSPR and allow the intense dispersion of the incident light, are applied [2].

The EM mechanism is considered to give the main contribution to the signal enhancement in SERS. The particles adsorbed on the surface experience an extremely strong electromagnetic field. The observed effect of intensity increase of the bands is exceptionally strong because the amplification occurs twice: initially the field enhancement increases the intensity of the incident light and next, the Raman scattered signal is enhanced based on the same mechanism. At each stage the radiation is proportional to the square of the electric field gain and as a result the total signal gain is proportional to the fourth power of the field value.

The chemical mechanism, in turn, is a sum of three separate processes:

i. the non-resonant Raman enhancement connected with chemical interactions which take place at the basic level between the adsorbate and the metal surface; these interactions are not related to the excitation of the metal-adsorbate system;

ii. the resonant Raman enhancement where a resonance of the excitation wavelength and the molecular transition is present,

iii. the charge-transfer Raman enhancement where a resonance between the excitation wavelength and the transitions between the levels in the metal-adsorbate system is present.

It is estimated that the CT effect has the greatest influence on the chemical mechanism of the signal enhancement. During the formation of the metal-adsorbate system, there is a possibility of transferring the charge from the metal surface (a level close to the Fermi level) to the lowest vacant molecular orbital (LUMO) of the analyte. This process also occurs in the opposite direction. The transfer from highest occupied molecular orbital of the adsorbate to the Fermi level in the metal is also possible, however less likely to occur [25]. Due to the weak binding of electrons transferred between the levels, the electron density can be polarized more easily and, as a result, the Raman signal is enhanced [26, 27].

In order to compare materials that are active in the SERS technique, various parameters are used, for example: sensitivity, stability over time, repeatability, and enhancement factor. The Enhancement Factor (EF) tells us how many times the Raman signal is amplified for a given SERS-active material in comparison to the classical Raman experiment. The enhancement factor can reach very high values, potentially up to 10^{12}, for the objects such as nanoparticles. Informally these places (or actually the enhancements generated in these places) are called 'hot spots'. The strong amplification is an effect of dipolar coupled plasmon resonance and it depends on the location of a molecule within the gap formed between the nanoparticles. This relation is well presented in *Figure 3*.
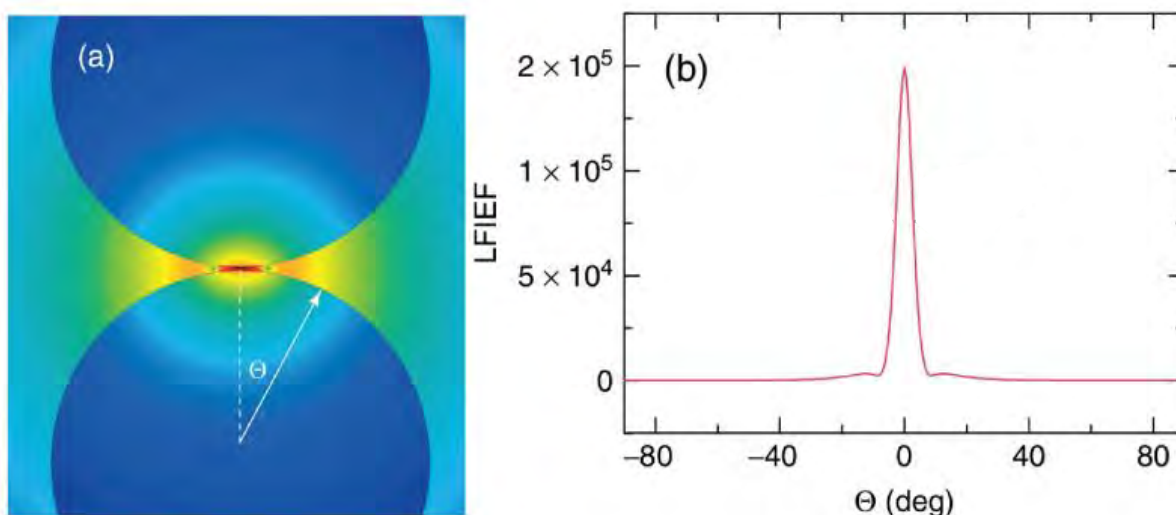
17

Figure 3.(a.) The spatial distribution of LFIEF (Local Field Intensity Enhancement Factor) in a 'hot spot' formed by two silver cylinders, each having 50 nm in diameter; red colour stands for the highest EF, while blue – for the lowest. The modelling was performed for a wavelength of 471 nm. (b); The enhancement factor on the surface of the lower cylinder is presented as a function of the angle (θ) [28].

As a rule of thumb, it may be assumed that, within a 'hot spot', a shift by ca. 5 nm changes the EF by one order of magnitude. In the case of anisotropic nanoparticles, the strongest electric field amplification is observed at the sharp tips and edges. Thus, a similar mechanism will occur for a highly rough gold or silver layers which are characterized by a high EF. The larger number of crevices in a metal structure or aggregates of metal atoms, the higher possibility to create a 'hot spot'. In addition, the value of the electric field intensity will greatly increase in the case of pointed structures such as needles or cones.

The EF is a relative quantity, i.e., we relate it to a certain base value. This value is calculated based on the signal intensity measured in standard Raman experiment and number of analysed molecules for which the signal was recorded. The obtained value allows to calculate EF, which is defined as the intensity ratio between the bands in the SERS (I_{SERS}) and Raman (I_{Raman}) spectra. During calculations it is necessary to consider as well the number of molecules (N_{SERS}, N_{Raman}) contributing to the intensity recorded in both types of measurements:

$$EF = \frac{I_{SERS}}{N_{SERS}} \cdot \frac{N_{Raman}}{I_{Raman}}$$

Equation 13

18

In order to receive reliable results, the measurements must be performed under the same experimental conditions. The maximum value of EF, ranging from 10^{10} to 10^{14}, according to scientific literature, is still a subject of dispute. The enhancement of the order of 10^{14}, obtained by Kneipp et.al. [29], is now considered as a mistake due to incorrect normalisation of the SERS signal to the Raman signal. Nowadays, the generally accepted, maximum EF value obtained in the laboratory, is about 10^9-10^{10}. This range of the Raman signal enhancement makes it possible to perform measurements even at level of single molecule [30].

3.2   SERS substrates

The SERS substrates, after adsorbing the analyte on their surface, enhance the analytical signal according to EM and CT mechanisms. The shape, size, repeatability, and arrangement of the sharp-edged nanostructures present on the SERS substrates affect the amplification of Raman signal. The materials from which they are made require the selection of measurement parameters and conditions in which it is performed. Therefore, the selection of an appropriate SERS substrate is a key to the success of the analysis.

As already mentioned, the most commonly used metals in the production of the SERS substrates are gold, silver and copper, but the signal amplification effect is also observed for other metals such as sodium, potassium and lithium [31]. However, due to the weak enhancement effect and high reactivity of these metals, they have no practical application in routine research. A large number of 'hot spots' on the metal surface is extremely desirable in the SERS technique, and thus over the last decades scientists developed multiple methods of SERS platforms production. These methods allow to obtain the nanostructures characterised by specific shapes, sizes, and chemical / mechanical properties. The technique which led to the enhancement of pyridine in Fleischmann's experiment and, as a result, discovery of the SERS effect, was based on the alternating oxidation-reduction electrochemical reactions of silver electrode in 0.1 M KCl solution [32]. With the development of nanotechnology, nanoparticles and their colloidal suspensions or solutions have become more popular, as their diameter, shape, concentration and dispersion in the solution could be controlled. Currently, nanoparticles with the shapes of ovals, cubes, wires, rods, flowers, columns, pyramids, etc., are synthesized [33]. Various types of commercially available substrates are presented on *Figure 4*.
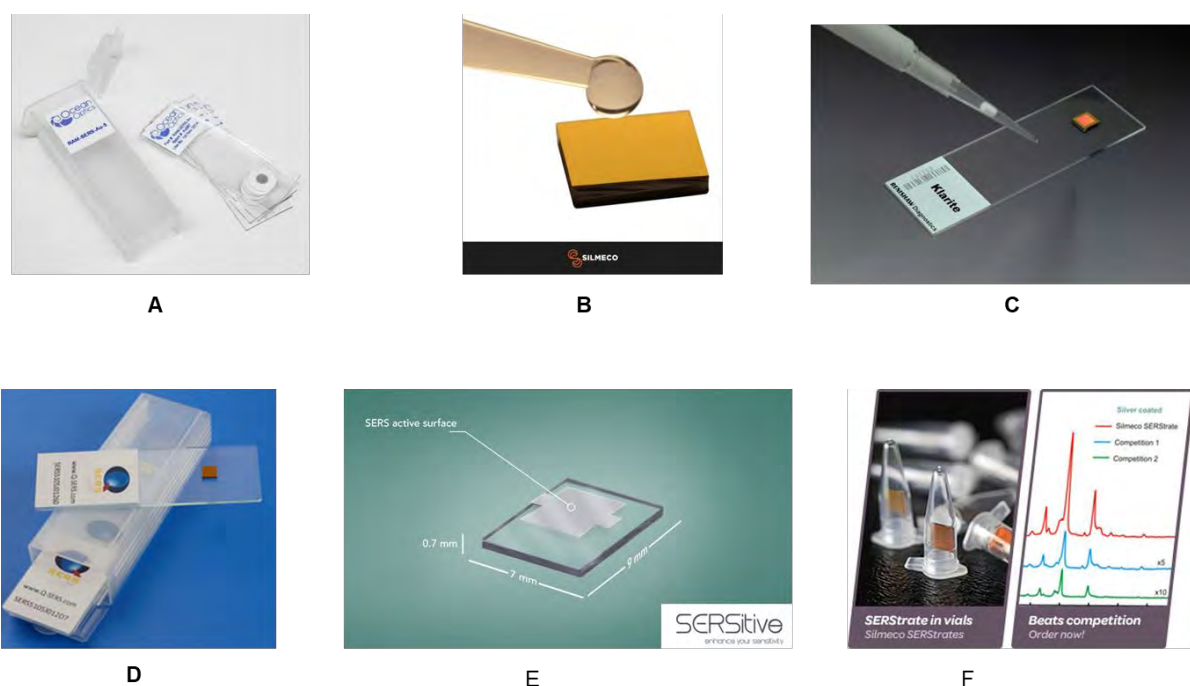
Figure 4. The commercially available SERS substrates (A) Oceaninsight [34](B) Silmeco [35](C) Renishaw (D) [36] Q-SERS [37] (E) Sersitive [38] (F) Serstrate [39].

In nanotechnology, there are generally two approaches for the fabrication of nanostructures: bottom up and top down [40]. In the top-down method the microscopic devices and nanofabrication techniques are used to produce and form the metal nanoobjects, while the bottom-up method uses self-assembled properties of molecules to obtain a desired structure. The bottom-up methods are most often based on chemical reactions initiated spontaneously around the grains suspended in a solution [41] or by other factors, e.g., specific light beam [42]. They may also apply oxidation-reduction reactions [43], photo-reduction [44], solvothermal synthesis [45] and sol-gel processes [46]. The top-down approach is mainly based on laser ablation, vapor deposition or chemical etching of the material with aggressive acids or bases.

Among numerous types of shapes of nanoparticles, we distinguish mainly nanospheres, nanorods and nanowires (*Figure 5*). The most common method for obtaining them is chemical reduction of silver nitrate (V) or chloroauric acid. In the first situation, the sodium citrate is usually used as a reducing agent, and, as a result, nanoparticles with diameter of about 60 nm are formed, while in the other case the reduction takes place with the use of $NaBH_4$. As a consequence, nanoparticles with an average size of about 20 nm are formed [32].

Another worth mentioning plasmonic nanostructures are core-shell nanoparticles, having interior and exterior usually made of different materials characterised by specific properties. The SERS-active metal can be either a shell or a core of a particle. When a noble metal acts as a core, it does not oxidise the analyte and, due to a properly functionalised shell, prevents nanoparticles from their quick aggregation and allows for longer measurement times. On the other hand, when a SERS-active metal acts as a shell, it is possible to introduce additional function to the core, e.g., by applying materials with magnetic properties. In such a situation the concentration of nanoparticles depends on the presence or absence of an external magnetic field. Their synthesis is possible due to reduction of $AgNO_3$ or by thermal decomposition of silver salts in the presence of a magnetic phase.

The plasmonic metal nanoparticles are often coated with silica (SiO_2) protective layer, which is usually formed due to decomposition of Na_2SiO_3, tetraethylorthosilicate (TEOS) or $(EtO)_4Si$ [47]. In the first case, the acidified Na_2SiO_3 solution is added to the sol of the previously prepared plasmonic nanoparticles, and next, the solution is left for about 6 days, being stirred. The second method, which is much faster, the silica layer is formed by ammonia catalysed decomposition of tetraethyl orthosilicate [48].

Another group of nanomaterials, namely nanorods, is characterised by high absorption in the near infrared and visible light range. This feature correlates with two types of electron plasmons, which are oscillating both along and perpendicular to the long axis of a nanomaterial. The superimposition of these two plasmonic vibrations is a source of strong electromagnetic enhancement at the ends of the rods [49]. In order to obtain silver nanorods, a solution containing pentagonal silver nanoseeds, sodium citrate, and silver nitrate is irradiated for 24 hours with light in the range of 600-750 nm. Depending on the light wavelength used to irradiate the solution, nanorods of different lengths and widths are obtained. In the case of light with a wavelength of 600 nm, nanorods with a length of 330 ± 85 nm and a width of 67 ±5 nm may be synthesised, while when applying the light of λ=700 nm, the average length and width of the obtained nanorods are 870 ±250 nm and 61 ±5 nm, respectively. These results demonstrate that the use of longer wavelength results in obtaining longer nanorods while maintaining similar width. When using shorter wavelength of light (500 nm), a mixture of nanorods, nanoprisms and bipyramid may be obtained [50].

The last group of plasmonic nanomaterials consists of nanowires (NW). They demonstrate the LSPR phenomenon for a wide range of excitation light - from ultraviolet, through visible, to near infrared [51]. In such case, the electromagnetic resonance is similar to the one observed for optical antennas. The resonance frequency can be adjusted during the

21

synthesis of nanowires, allowing to control their size, width, length [52], and thus – EF. The nanowires are synthesized using many techniques, such as polyol process [53], arc discharge or ultraviolet radiation photoreduction [54]. Hydrothermal growth is also popular technique, because of its simplicity – there is no need to use high temperature and pressure or add seeds to start the synthesis [55].
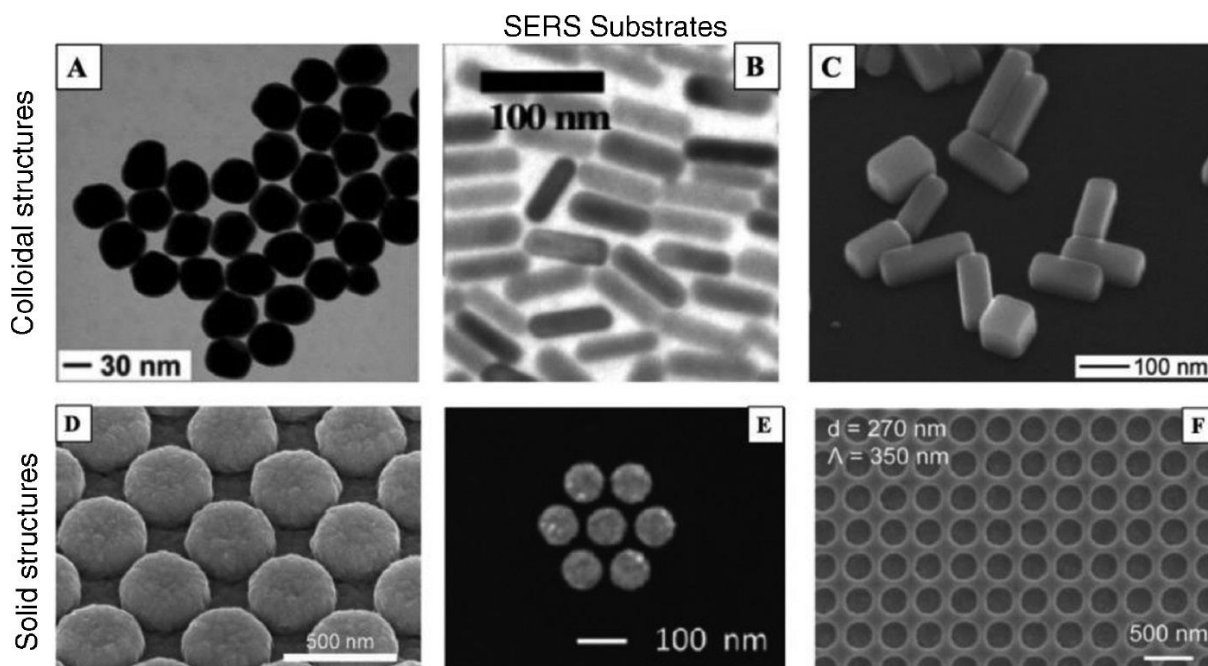

Figure 5. The SEM images of different types of the SERS substrates. (A) Spherical gold nanoparticles, (B) gold nanorods, (C) silver nanobars, (D) silver plasmonic nanodome array, (E) gold nanocluster, (F) gold nanoholes [56].

Despite numerous advantages mentioned above, the nanoparticles also possess drawbacks which make the SERS research difficult to conduct, e.g., low colloid stability over time or difficulties with obtaining particles of specific properties in different batches. Moreover, high sensitivity of the SERS technique makes it challenging to record a spectrum of pure investigated compound, as there is a high probability to detect impurities from reagents necessary in the production process of nanoparticles. As a result, the obtained spectrum is a 'mixture' of bands characteristic for analyte and reactants used in nanomaterial synthesis. Finally, it is practically impossible to map the liquid sample due to the solution dynamics [57].

In order to avoid the aforementioned difficulties, solid SERS platforms were designed as an alternative to nanoparticle suspensions. These substrates possess a well-defined structure and exhibit high stability and mechanical resistance over time. Additionally,

22

they can be characterised by two- or three-dimensional shape and tailored SPR mods for a stronger Raman signal enhancement. They are often build of solid inorganic template such as silicon [58], quartz [59] or silicon nitride [60], covered with SERS-active nanostructures what eliminates the problem of nanoparticle aggregation. In addition, a properly selected and controlled process of the production of plasmonic substrates allows to obtain desired distances between nanostructures. This, in turn, allows for the creation of 'hot-spots' of specific parameters.

Over the last decades, many methods of fabrication of the SERS platforms were invented. Based on the properties of the basic material they can be divided into conductors, semiconductors and insulators. The quite popular ones are carbon nanotubes immersed on a Si wafer [61] or functionalised carbon fibre cloth [62]. The methods used to modify their surface include lithography, dry reactive ion etching or metal vapor deposition and are often used to cover the solid substrates with SERS-active nanoparticles. It is also possible to obtain 'hot spots' directly on the surface of metals active in the SERS technique. In this case, electrochemical deposition in solutions characterised by an appropriately selected conductivity is most often used. This is usually obtained by applying highly soluble inorganic salts which are not spectrally active in the Raman scattering techniques [63]. The method can also be used for in-situ research in spectroelectrochemical techniques, where the analyte is deposited on the SERS substrate by applying voltage of an appropriate value [64].

3.3   SERS applications

As the SERS technique is an extension of the classical Raman spectroscopy, many practical applications for both methods are similar. Nevertheless, the increase in signal intensity by several orders of magnitude and the ability to detect single molecules opens enormous possibilities for the SERS technique. What is more, the main factor which is responsible for signal enhancement, i.e., a properly selected plasmonic substrate, as well as its parameters and production technique, broadens the range of the SERS applications.

Similarly, to the Raman technique, SERS is both qualitative and quantitative analytical method. In the case of quantitative measurements, the key factors are sensitivity and precision of the method, as they determine the reliability of obtained results. In addition, the use of chemometric and statistical analysis to draw calibration curves together with preparation of the analyte reference spectrum further improves the aforementioned parameters [65].

One of the crucial applications of the SERS-based quantitative analysis are immunoassays. It was observed that with the use of appropriate antibodies it is possible to determine concentration of the investigated molecules in a sample. Such experiments were conducted to detect tuberculosis marker (mannose-capped lipoarabinomannan) and pancreatic cancer markers in human blood serum [66]. For this type of research there is a need to select, optimise, and functionalize the SERS-active nanostructures and to perform measurements for different concentrations of the analyte. Usually, the higher enhancement factor, the greater signal to noise ratio. This allows to almost eliminate the background signals originating from the matrix solution and to obtain practically pure spectrum of the investigated analyte.

Another quantification method applied in SERS is 2D mapping. In this approach the spectra are recorded repeatedly for numerous 'hot spots' within selected area of the SERS substrate. Due to developed surface of the SERS substrate and thus increased adsorption area the accurate determination of the analyte concentration is possible. However, as the molecules of an analyte are randomly distributed on the SERS substance, it is necessary to perform time-consuming mapping of the surface, where the SERS signal is measured point by point. Thus, in some situations, the time of a single measurement needs to be extremely short and take, e.g., up to one second so that the entire procedure will not last long enough to face the issue of sample degradation. Importantly, the substrate must also dissipate the heat from the laser beam to omit local increase in temperature, which also leads to analyte degradation [67].

In the last century, the main problem of the Raman systems was connected with their low sensitivity influencing the limit of detection (LOD). Nowadays, the SERS technique, integrating substrates of different kinds and miniaturised, portable devices characterised by high spatial and spectral resolutions, meets the growing expectations raised by the scientific society. Additionally, due to development of microfluidic systems created by machining techniques [68], pouring moulds [69] or 3d printing [70], as well as optical fibres enabling light transmission, the method became even more popular. As microfluidics is a branch of science investigating the behaviour and parameters of fluids in channels from several to hundreds of micrometres in diameter, there is a possibility to apply it in SERS-based research. In such a scenario, both the nanoparticle suspension and the analyte can be introduced directly into the channels and mixed together. As a result, the SERS measurement can be performed in a small volume of liquid, improving the LOD. Such a form of experiment allowed to determine food contamination with melamine (LOD = 63 ppb) or thiram – commonly used fungicide (LOD = 50 ppt) [71]. Moreover, by applying electron beam lithography, it was also possible to fabricate gold-based SERS substrate directly in a microfluidic chip and next,

24

detect ochratoxin A – one of the most-abundant food-contaminating mycotoxins [72]. The authors of the publication demonstrated that the concentration of the analyte at the level of 2.5 μM could be easily detected. A similar technique was also used to determine the presence of levofloxacin – a drug which, as most antibiotics, is characterised by concentration dependent bacteria killing properties. In this case the LOD was at the level of 0.8 μM [73], proving once again, that the SERS technique can be successfully applied in clinical diagnostics.

As already mentioned, the SERS technique is suitable for identification and differentiation of various types of analytes, including biomolecules such as amino acids. The first attempts to detect DNA and RNA comprised the spectroscopic characterisation of thymine, guanine, cytosine, adenine and uracil. For this purpose the authors of the publication used electrochemically etched silver electrodes [74]. It was also demonstrated, that SERS allows to detect and identify proteins and peptides such as insulin [75] or β-amyloid [76]. These findings are crucial for development of clinical diagnostics, as determination of the level of insulin is essential for diabetics, while β-amyloid is most probably a causative agent of a neurodegenerative disorder, known as Alzheimer's disease.

Another application of the SERS technique is the possibility of detecting viruses both in a direct and indirect manner. In the first approach, due to capsid structure diversity, the spectra of viruses can be recorded directly on the SERS substrate [77]. It is also possible to identify their genetic material, however the method suffers from a lack of practical applications – viral DNA / RNA is quickly destroyed in extracellular matrix of infected organisms [78] and thus this direction of research is not popular. In the second approach the presence of viruses is determined based on the antibodies produced by immune system of many animals. Usually, in order to enhance the analytical signal of the described analytes they are additionally combined with a Raman reporter - a molecule characterised by a high cross-section for the Raman scattering and thus giving an intense SERS spectrum. Such a type of experiment was performed for human immunodeficiency virus (HIV) [79], rotaviruses [80], or respiratory syncytial virus (RSV) [81].

The SERS technique can be also applied in early detection of tumours. According to World Health Organization (WHO), cancer is the second most common cause of deaths among humans, responsible for ca. 9 million fatalities annually [82]. In was also observed that approximately one in six deaths is due to a multi-organ disease. Rapid diagnosis in the early stages of cancer is crucial in its prevention. It was proved multiple times that such possibility is offered by SERS. As the technique can be used directly in the analysis of body fluids it

25

http://rcin.org.pl

might be considered as alternative to currently used diagnostic methods. Koo et al. demonstrated that by means of SERS it is possible to predict risk of developing prostate cancer [83]. In this label-free approach the specific prostate cancer targets (T2: ERG, PCA3 and KLK2) in the form of microRNA (miRNA) were mixed with silver nanoparticles (Ø = 40 nm) and measured via SERS. Next, by applying principal component analysis (PCA), the results could be divided into three groups: (i) healthy individuals, (ii) patients with low risk of prostate cancer and (iii) patients with high risk of developing this disease. The entire analysis took ca. 1.5 h which should be considered a short time in comparison to standard clinical analysis which usually takes about 4 h.

Cancer cells may also be detected by functionalising the SERS substrate with the molecules that specifically interact with the selected marker and next with the Raman-reporter. This highly specialized strategy allows both the detection of small biomolecules such as tumour markers and the mapping of whole cancerous tissue. An example of such 'sandwich' structure was presented by Lee et al. [84]. The authors of the publication created a SERS platform based on gold nanopillars which were functionalised with an appropriate locked nucleic acid (LNA). Subsequently, the modified SERS substrates were incubated with three different types of miRNAs, which hybridised with the complementary LNA probes. Finally, the substrates were incubated with Cy3 Raman-reporter giving the characteristic SERS band at 1150 cm^{-1}. After preparing the calibration curve, the LOD reached the value of 1 attomole.

Due to miniaturisation of the Raman spectrometers, flexibility in selecting measurement parameters, many different types of the SERS substrates, short time of data collection, and the availability of statistical software, the SERS technique has become more popular. It was demonstrated that it can be also applied in biochemistry, immunology, microbiology, and medicine. In addition, SERS is commonly used at the airports as a detection method of drugs, explosives and flammable materials. It is also widely used in forensics when analysing the collected evidence material such as blood, gunpowder or trace amounts of specific substances [85]. The nanomaterials such as graphene, quantum dots or functionalized polymers, are also in the area of the SERS interest [86]. The identification of pharmaceuticals is a branch of science in which SERS can be also successfully 'employed' [87]. The same applies to analysis of materials surface in terms of their interaction with different compounds [88].

3.4 SERS in detection and identification of microorganisms and cancer cells

The diseases caused by pathogenic bacteria are still a serious problem nowadays. Thus, the new methods for rapid identification of infectious agents and time-effective diagnosis of bacterial diseases are needed. Currently, the most widely used methods of bacteria detection and identification are cultivation in specific culture media, flow cytometry, polymerase chain reaction, and enzyme-linked immunosorbent assay (ELISA) [89]. These methods are effective, well-developed, and standardly used in laboratories around the world. They are highly specific and selective, but also labour-intensive and time-consuming.

The procedure of detection of a specific pathogen may take up to several days, which makes immediate medical assistance highly difficult. The SERS technique, ensuring quick measurements, is a promising direction for development of clinical diagnostics. Nevertheless, in order to fully understand and implement this technique, there is a need to meet the challenge posed by microorganisms – bacterium as a viable cell may give distinct signals in different conditions. Thus, it is exceedingly important to ensure that all the parameters, both physical and chemical, are constant for all measurements and sample batches. As a result, one may obtain a pure and reliable SERS spectrum of bacteria.

In a label-free, direct detection of microorganism the signals observed in the SERS spectrum come directly from a cell membrane, a wall, and / or an envelope, as well as compounds adsorbed to these structures. The signals observed in the spectra of microorganisms come mainly from phenylalanine, bases that are part of DNA, RNA, FAD, NAD or ATP, bicarbonates and metabolites of purine degradation other than adenine and AMP, *e.g.*, guanine, xanthine, hypoxanthine, and uric acid (Premasiri, 2016, The biochemical origins of the surface-enhanced Raman spectra of bacteria: a metabolomics profiling by SERS), and other bacterial cell wall components, *e.g.,* phospholipids (Witkowska, 2018, Strain-level typing and identification of bacteria–a novel approach for SERS active plasmonic nanostructures) and proteins (Andrew, 2002, SERS of whole-cell bacteria and trace levels of biological molecules).Their presence and the intensity ratio depends on tested microorganisms. The typical assignments of bands present in bacterial spectra are given in *Table 1*.

27

Table 1. The assignment of the shifts observed in the SERS spectrum of microorganisms [90].

Raman shift (cm⁻¹)	Band assignment
550-575	C-O-C ring deformation
620-630	C-C twisting mode of phenylalanine (protein)
623	C–C twisting in protein
645-660	C-S stretching, C-C twisting vibration of proteins (tyrosine) COO⁻ deformation in amino acids. guanine and thymine (ring breathing modes)
655-665	C-S stretching., C-C twisting vibration of proteins (tyrosine)
656	C–S stretching, hypoxanthine, xanthine, guanine
720-735	Adenine (FAD, NAD, ATP, DNA)
735	Adenine (in-plane ring breathing mode of adenine)
735-750	C-S stretching
777-793	Ring breathing mode of cytosine, uracil, (O−P−O) symmetric stretching of nucleic acid
826	Stretching O-P-O
847-852	Thymine, ring breathing mode of tyrosine, C-C stretch of proline ring
850-860	Ring breathing mode of tyrosine & C-C stretch of proline ring
905	C-C skeletal stretching, tyrosine
954-965	C=C deformation, C-N stretching, C−O stretching, CH_3 symmetric stretching of proteins (α-helix)
960	C=C deformation, adenine, guanine, NAD+
1002	Phenylalanine, C-C aromatic ring stretching
1006	Phenylalanine, C-C aromatic ring stretching
1030	C-N stretching, C-C stretching (phospholipids, carbohydrates), C-H in-plane bending mode of phenylalanine,
1025-1035	C-N stretching, C-C stretching (phospholipids carbohydrates)
1025-1060	C–C stretching (phospholipids, carbohydrates), C–N stretching
1060-1070	C-C skeletal stretching (lipids)
1085-1095	PO_2^- symmetric stretching, C–O–C stretching modes in polysaccharides, adenine, polyadenine
1090-1110	O-P-O (DNA), C-C stretching, C-O-C stretching
1128	=C–O–C= in unsaturated fatty acids in lipids
1181	Tyrosine
1125-1130	=C-OC= (unsaturated fatty acids in lipids), C-O-C stretching modes in nucleic acids, PO_2– stretching in nucleic acid, C-O and C-C stretching in carbohydrates, C-N stretching in proteins
1125-1145	=C-OC= (unsaturated fatty acids in lipids)
1170-1195	C-O ring, aromatic aa (proteins)
1215	C–N stretching / Amide III / thymine
1230-1250	Amide III
1205-1230	Amide III (random), thymine
1240-1285	Amide III
1305-1320	Ring breathing mode of guanine, CH_3, CH_2tw.
1320-1335	CH_3CH_2 wagging in purine bases, NH_2 stretching in adenine and polyadenine
1330	CH_3 / CH_2 wagging in purine bases

1330-1345	Adenine, guanine, C–H deformation
1365-1380	Tryptophan, guanine
1370-1376	ring breathing modes of the DNA / RNA bases, COO$^-$ stretching, C-H bending (proteins)
1390-1415	COO– symmetric stretching
1395-1405	CH rocking, C=O symmetric stretching
1446-1465	CH$_2$ deformation
1450	CH$_3$ / CH$_2$ deformation
1570-1590	C=C bending mode (phenylalanine), guanine, adenine, tryptophan (protein)
1500-1530	Cytosine
1530-1565	Amide II, tryptophan
1570-1595	C=C bending mode (phenylalanine)
1581	the C=C bending mode of phenylalanine
1600-1630	Amide I of proteins, C=C bending mode (phenylalanine)
1665-1668	Amide I, C=C bending mode (phenylalanine)

The biggest challenge with this type of approach is the non-specific capture of bacteria suspended in the investigated liquid sample. This can be achieved simply by mechanical isolation on filters with holes smaller than the bacterial cells, by centrifugation, or by electrostatic interactions. The latter is possible due to the fact that bacterial cell membrane consists of, among others, lipopolysaccharides built of phosphates and carboxylates and as a result its net charge is negative. Such results were presented by Kalasin et al. who used positive charge of nanomaterials to easily isolate *Staphylococcus aureus* cells from a liquid suspension [91]. In other studies, a positively charged poly-L-lysine covered with gold nanopillars was used as a SERS platform [92]. The authors functionalised its surface with 4-mercaptophenylboronic acid (4-MPBA) which acted as a Raman reporter. Additionally, due to the fact that 4-MBA compound possess both thiol and boron groups, it binds to gold / silver surface and to peptidoglycans found in bacterial cell wall at the same time. This allowed the scientists to prove that it is possible to design a platform which captures *Salmonella* Typhimurium cells and provides a high sensitivity of the experiment due to strong Raman signal from the Raman reporter.

Another promising method of immobilising and concentrating bacteria on the SERS platform is dielectrophoretic effect. Electrophoresis is the force generated on a charged particle by an electric field. In the case of dielectrophoresis (DEP), the particle is neutral (globally uncharged or characterised by a low net charge) but polarisable - it possesses a dipole moment when exposed to an electric field. If the constant field does not create any resultant on a globally neutral but polarised particle, the gradient of a spatially alternating

field creates the resultant: the dielectrophoretic force. With the help of this force, depending on the variant of the experiment, the attraction (positive DEP) or repulsion (negative DEP) of the bacteria takes place. In this manner it is possible to direct the flow of the bacteria in microfluidic systems or to concentrate a small number of microorganisms on a defined area. Moreover, the DEP method allows to save time by focusing the measurement on a defined spot, without the need of mapping relatively large SERS platform area. It was already shown by Wang and Yu [93] that by applying DEP and suspension of nanoparticles, is was possible to separate bacterial cells from blood sample and next, concentrate them in a specific area. Additionally, the authors used mineral oil to control the flow of separated phases. Due to this procedure a SERS-based analysis could be narrowed down to several spots.

In the case of label-based approach it is necessary to modify the selected SERS-active nanostructures with appropriate antibodies, aptamers or small molecular ligands. It was demonstrated by Duan et al. that aptamers can be used as substitute for antibodies for the sensitive and quick detection of *S*. Typhimurium and *Vibrio parahaemolyticus* [94, 95]. The method for the detection of *Salmonella* at a single cell level was also developed. For this purpose Tay et al. used nanoprobes called nanoaggregate embedded beads (NAEBs) which were linked to a specific spike protein from the capsid of P22 bacteriophage [96]. There were also attempts to apply bacteriophages in order to capture specific bacterial cells, e.g., Srivastava et al. used T4 bacteriophages to capture *Escherichia coli* cells, and next – a chip utilising metallic nanosculptured thin films to record the SERS spectra [97].

As mentioned in the previous chapter, SERS may be also applied in cancer cells detection. Cancer is a group of diseases caused by mutations in certain genes, which lead to uncontrolled, pathological tissue growth - neoplasm. As a result, cancer cells which does not differentiate into any known type of healthy cells, create a tumour which may grow into key organs, nerves, or blood vessels, impairing their function and causing death. Thus, there is a great need to develop a rapid method of cancer identification. This, in turn, allows for an immediate start of an accurate therapy.

Cancer detection is performed by determining the presence of specific biomarkers in patients' blood, computed tomography, positron emission tomography, ultrasound and / or endoscopic examinations. After locating a tumour, a sample is taken for histopathological analysis to confirm the initial diagnosis. In order to reduce the costs of analysis, mainly related to an invasive biopsy, it is desirable to develop novel diagnostic methods, such as the SERS technique.

In a label-free, direct detection of circulating tumour cells (CTCs, cancer cells that shred from tumour tissue into bloodstream and invade other organs) the signals observed in the SERS spectrum come directly from a cell membrane as well as adsorbed to it compounds. The location of the main SERS bands in case of CTCs and microorganisms is similar as their global biochemical composition is alike. Nevertheless, one should focus on presence of additional bands and signal intensity. In the case of the SERS spectrum of eukaryotes, the part above 1000 cm^{-1} dominates in terms of bands intensity. For microorganisms such as bacteria, the signals from tyrosine and adenine vibrations at about 630 cm^{-1} and 730 cm^{-1}, respectively, are usually the strongest signals of the entire spectrum. In the case of tumour cells measurements, the presence of an intense band in the range of 1130-1150 cm^{-1}, derived from vibrations of the porphyrin ring in lipids, is considered as a cancer marker. The rest of the signals origins from lipids, bicarbonates, tryptophan, and nucleobases that are part of DNA, RNA, FAD, NAD or ATP. The typical assignments of bands present in the CTCs spectra are given in *Table 2*. The use of the SERS technique in cancer analysis may lead to detection and identification of various types of cancers.

The high application potential of SERS was proved by Zhang and co-workers [98] who managed to distinguish three subtypes of non-small-cell lung cancer (H1229, H460, and A549) and leukocytes on a single-cell level. Other studies have demonstrated that SERS allows to identify melanoma [99] or cervical [100] and prostate [101] cancer. In these cases, studies were conducted on isolated, homogenized human and animal tissues and cultured cell lines. The measurements were carried out in the direct detection regime described in this section. Breast cancer identification research carried out by Jaeboom Choo et al. proved that silver nanoparticles, functionalized with silica shell and Raman-reporters are suitable for non-direct identification of this disease In this experiment, the functionalised nanoparticles were divided into three groups, each combined with a specific type of antigens. Such an approach allowed to identify three different subtypes of breast cancer [102].

The CTCs in human peripheral blood are the main cause of death in most cancer patients, however their detection is possible in early stages of the disease. The detection, identification and monitoring of CTCs is of great scientific significance and clinical application value. The high sensitivity of the SERS technique may be extremely important here, as it allows to detect single CTCs in relatively large volume of human blood, e.g., research conducted by Y.T. Lon et al. indicated the possibility of detecting even single HeLa cells mixed with 1 mL of peripheral blood. To obtain such result, the researchers applied gold nanoparticles functionalised with a Raman reporter and appropriate antigens [103].

31

In the recent years, it was demonstrated multiple times that the identification both of bacteria and cancer cells, which is crucial in medical studies and clinical diagnosis, can be performed with the help of fast spectroscopic fingerprinting. Thus, the SERS method gained great popularity among scientists and doctors [104]. Nonetheless, the research methodology related to SERS substrates, as well as the Raman spectroscopes still require further development. Additionally, the costs of the Raman spectrometers and disposable SERS substrates available on the market are still relatively high. In addition, obtaining a reproducible signal for different sample batches, is still a challenge, as it requires a thorough understanding of the origins of the SERS spectra variability. Finally, the creation of uniform procedures of statistical analysis, spectra collection, and data interpretation are necessary for the implementation of the SERS-based technology in non-laboratory venues. The concept of unique, total, spectral 'fingerprints' of the studied cell lines, presented in the next chapters of the following thesis, significantly simplifies the process of analyte identification and lowers the costs of preparing a single analysis for both microorganisms and cancer cells.

Table 2. The assignment of shifts observed in the SERS spectrum of CTCs [90].

Raman shift (cm^{-1})	Band assignment
652-658	Tyr (C-C twist) (protein assignment)
725 - 730	Trp (protein assignment) C-N head group choline $(H_3C)_3N+$ (lipid assignment)
785	PO_2 symm (nucleic acid assignment)
827	RNA backbone (nucleic acid assignment)
850	Tyr, Pro (protein assignment)
890	Structural protein modes of tumours
939	C-C str alpha-helix, Pro, Val C-C str alpha-helix, Pro, Val (protein assignment)
956	CH_3 def (protein assignment)
1003	Phe (protein assignment)
1030 - 1032	CH_2CH_3 bending modes of lipids
1094	C-N stretch (protein assignment); CC str chain, C-O str (lipid assignment); PO_2 symm (nucleic acid assignment)
1128	C-N str bk (protein assignment); Porphyrin (lipid assignment)
1170 - 1172	Tyr C-H in plane (protein assignment); T (nucleic acid assignment)
1212	C-C_6H_5 str in phenylalanine tyrosine (protein assignment)
1245	Amide III (beta sheet), (protein assignment)
1267 - 1270	Amide III (random coil) (protein assignment); CH=CH def (lipid assignment)
1325	purine bases of DNA (nucleic acid assignment)
1345	A, G (nucleic acid assignment)

32

1373	Sphingoglycolipids (lipid assignment)
1452	structural protein modes of tumours (protein assignment)
1552	A, G (nucleic acid assignment)
1597 - 1600	Phe, Tyr (protein assignment)
1616 - 1618	C-C str of Tyr and Trp (protein assignment)
1657 - 1695	Amide I (protein assignment); C=C str (lipid assignment)

4. Methods and analytical techniques

4.1 Microscopy

4.1.1 Electron microscopy

In the research on the structure and properties of matter, many different techniques and methods of imaging are being used. Their goal, regardless of the technique and the device used, is to obtain an enlarged image of small objects. When observing various types of objects with a wide range of imaging devices, the key parameter is resolution, i.e. the shortest distance between two points that can be identified as separate in the obtained image. In the case of classical light microscopy, a large limitation of the resolution is the wavelength of light, which allows to observe the object. In the case of visible light, this key length is in the range of 500-550 nm. Therefore, using the Abbe dependence, it is possible to determine the theoretical resolving power ρ for this optical microscope:

$$\rho = \frac{0,61\lambda}{\eta sin\alpha}$$

Equation 14

where λ is the wavelength of the radiation, η is the refractive index in the given centre, and α is the half of the lens aperture angle. Using this formula, at the end of the 19th century, it was possible to achieve the maximum theoretical image resolution of 200 nm in a light microscope. The reason for a limited capacity of a light microscope is diffraction of light, which makes the images of adjacent details in the tested sample indistinguishable, when the distance between them becomes close to the light [105]. The only solution is to use radiation with a wavelength shorter than the wavelength of visible light. The development of technology and the discoveries made at the beginning of the 20th century enabled to use the electron beam for imaging. It is a technique developed on the basis of theoretical optical microscopy. Electron microscopes are used in crystallographic and biological research, solid state physics, medicine and in various industries. In electron microscopy, a light beam is replaced by an electron beam after interaction with the sample material that can generate various signals depending on the type of interaction - from electrons, infrared photons, through visible light, up to X-ray radiation. These signals, depending on the needs, can be used to visualize the morphology of a surface or to study the distribution of the defects in

34

a crystal lattice. Theoretically, the electron microscopy techniques allow obtaining images with a resolution of 0.1 – 0.05 nm. Regardless of the type of an electron microscope, each one consists of three main parts: (i) an electron source, called an electron gun or emitter, (ii) an array of electromagnetic lenses and apertures that control focus, shape and size of the electron beam, and (iii) an array of detectors for collecting signals from the sample, which are then used to visualise the data. The electrons emitted by their source are accelerated in the potential difference. The mono-energetic primary electron beam is shaped through the condenser lens and the objective lens. Their appropriate arrangement ensures a change in the current induced by the electron beam, which bombards the test sample. It also provides beam convergence control depending on the technique used - a wide and parallel beam is used in the transmission technique and the convergent and focused beam – in the scanning technique.

Scanning Electron Microscopy (SEM) is the method in which only the sample surface is imaged. The beam of electrons with an energy of approximately 1-30 kV, the shape of which is determined by the system of magnetic lenses, reaches the sample. As a result of the interaction of the electron beam with the sample surface, secondary, backscattered or Auger electrons are emitted. The characteristic X-rays are also emitted. The detector captures the quanta of this radiation and uses a photomultiplier and a scintillator or a semiconductor matrix to convert the signal into an image of the sample. The SEM images are characterised by deep contrast and the possibility of observing objects as large as several nanometres. The richness of electron interactions with the sample enables the analysis of the material composition. One of such techniques is Energy Dispersive Spectroscopy (EDS). The detectors present in the microscope, e.g., the detectors of backscattered electrons, due to which the image of the surface topography is obtained, are semiconductors. The characteristic X-ray intensity reading, on which this analysis is based, is possible due to the formation of the electron-hole pairs. The characteristic radiation of each element is collected in parallel thanks to multi-channel detectors. Therefore, EDS analysis is one of the fastest methods available. Silicon Drift Detectors (SDD), on the other hand, allow to detect lighter elements. Additionally, they can work using relatively low voltages accelerating electrons and are characterised by resolution performance at low energies. Last but not least, they are much smaller than their predecessors [106]. However, it is important that the sample is electrically conductive. In case it is not, it should be sputtered with a conductive material, e.g., gold, carbon (optimally, deposited layer should be 3 nm thick) to remove the charge from the sample surface and improve imaging.

Another popular microscopic technique, Transmission Electron Microscopy (TEM), enables to visualise the internal structures of the low thickness samples. For this purpose, an electron beam of 60-300 kV energy is used. The measurements in TEM technique are possible even at the very high voltage accelerating the electrons, equal to ~1000 kV. After passing through a sufficiently thin specimen, the electron beam can be shaped in a form of light rays, using the objective and eyepiece system. In this case, instead of typical glass optical elements, a magnetic field from the coils is used, which changes the path of the beam consisting of charged particles. When the microscope works in the image mode, the beam creates an image of the specimen on the detector. The image created as a consequence of the interaction of the electrons with the sample structures is a two-dimensional projection onto a plane, e.g., of a screen imaging device. The contrast of the obtained image comes from the differences in the density of the material and its thickness. The thicker or denser the medium, the darker the image on the screen [107].

4.1.2 Atomic force microscopy (AFM)

Atomic force microscopy is a type of Scanning Probe Microscopy (SPM). It is an imaging technique with a resolution reaching atomic scale, which is over 1000 times greater than that conditioned by the diffraction limit in optical techniques and electron microscopy. This method was developed in 1986, and since then it has found application in numerous fields, including physics, biology, chemistry and engineering. Its key element is a small cantilever that interacts with the sample. The measured value is the force or potential energy between the tip and the sample. For this purpose, a cantilever is equipped with a force actuator and a force gauge. The basis of the experiment is alternately approaching and moving away the cantilever in relation to the sample's surface. By approaching it, its topography can be determined, and by moving away from it, the force of interaction with the analyte is measured. At its end, the cantilever is equipped with a tip, which may have different shapes and is made of a material suitable for the experiment. Depending on the need for resolution and measured properties of the tested matter, we can distinguish: optical deflection technique, fibre interferometry, current measurement and piezoresistive methods. Nowadays, most of the levers are made of silicon, silicon (IV) oxide or silicon (IV) nitride. For this purpose, micro-machining techniques are often used. When an optical system is used to detect cantilever movements, its back is covered with a reflective layer, most often made of metal. As the tip is brought closer to the sample surface, an increasing force of attraction is observed. As soon as

36

a certain distance is exceeded, this force becomes repulsive and the tip comes into contact with the sample. Therefore, we can use this technique in two different modes - contact and non-contact. The force of interaction with the sample is measured while withdrawing the cantilever from the sample. Its deflection is then observed, which is proportional to the force of interaction with the analyte. The value of this force is estimated on the basis of the Hooke's law. In another mode, also known as dynamic mode, the cantilever can be vibrated at a selected resonant frequency and the force of the interaction is calculated from changes in the amplitude, phase and resonant frequency [108].

From the forces of attraction, one can distinguish the van der Waals interactions, electrostatic force and chemical interactions. There are numerous theoretical models describing the latter, but the ones worth mentioning are the Morse potential and Stillinger-Weber potential. In repulsive interactions, which are considered as interactions between the spheres of short range and exponential decay, the Coulomb interactions between electrons and the Pauli-exclusion interaction are included.

The van der Waals interactions are based on the Coulombic forces between electrically neutral but locally charged atoms due to thermal oscillations. For a tip with a spherical shape and a given radius R and assuming the shape of the sample as a flat surface, the van der Waals potential (V_{vdW}) and force (F_{vdW}) can be calculated using [109]:

$$V_{vdW} = -\frac{A_H R}{6z}$$

Equation 15

$$F_{vdW} = -\frac{A_H R}{6z^2}$$

Equation 16

where z is the closest distance to the sample and A_H is the Hamaker constant, which depends on such values as the polarizability of the atoms and the density of the tip and the analyte.

The electrostatic force is generated between the analyte and the tip made of conductive material or charged to a certain amount. In the case of conductive material, the voltage U is applied between the cantilever and the sample. For the distance z which is less than the radius of the R tip, the electrostatic force (F_{el}) can be calculated:

37

$$F_{el}(z) = -\frac{\pi\epsilon_0 R U^2}{z}$$

Equation 17

where ϵ_0 is the vacuum permittivity.

The chemical interactions occur when atoms come closer together in the process of creating a molecule and thus form bonds. When forming a covalent bond the covalent force is present, which depends on the relative position and accuracy. These are short-range forces, on the order of tenths of a nanometre, and are considered in the field of quantum mechanics. They are described by the Morse potential (V_{Morse}) [108]:

$$V_{Morse} = -E_{bond}\left(2e^{-\kappa(z-\sigma)} - e^{-2\kappa(z-\sigma)}\right)$$

Equation 18

where E_{bond} is the bond energy, σ is the equilibrium distance and κ is the decay length.

When testing a hydrophilic surface, which in ambient conditions adsorbs water, a meniscus forms between the tip and the sample. This meniscus is the source of an attractive force called capillary force. The theoretical basis of the capillary force is already described by the van der Waals interaction between the atoms which build the tip and the molecules on the sample surface.

Regarding the repulsive forces between the tip and the analyte, the theoretical basis is the Pauli exclusion principle or the ionic repulsion. These forces arise when the wave functions of the electrons overlap for the atoms approaching each other, which causes a strong short-range repulsion. This phenomenon is described by the Lennard-Jones potential (V_{LJ}) [110]:

$$V_{LJ} = -4\epsilon\left(\frac{\sigma^6}{z^6} - \frac{\sigma^{12}}{z^{12}}\right)$$

Equation 19

where ϵ is the depth of the potential well and σ is the distance for which the force is equal to zero.

As for the atomic resolution of this technique, it is the result of short-range interactions. As the van der Waals interactions are long-range in nature, and are the result of the forces of cantilever tip atoms and samples, the chemical interactions of covalent crystals or electrostatic forces in ionic crystals are the most important contributors to such an excellent

38

resolution. For the surface of materials made of semiconductors, the chemical interactions seem to be the source of atomic resolution [108].

4.2   Spectrophotometry (UV-VIS)

Spectrophotometric measurement methods in the ultraviolet range (UV) and Visible radiation (VIS) are one of the oldest methods used in chemical analysis. These methods focus on obtaining and analysing electronic spectra.
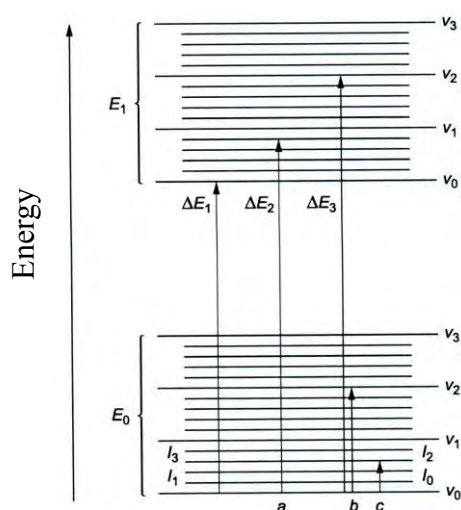
Figure 6. The diagram of electronic, oscillatory and rotational transitions in a diatomic molecule; E – electronic levels, v oscillatory levels, I – rotational levels, a - electronic transitions, b - oscillatory transitions, c - rotational transitions [3].

These spectra depict electronic transitions between the energy states of atoms and molecules governed by the selection rules which are described below (*Figure 6*).

The first states that in order for the radiation quantum to be absorbed, there must be two quantum states of the molecule, ψ_m and ψ_n, for which the energy difference corresponds to the energy value $h\nu$ of the incident radiation:

$$E_n - E_m = h\nu = \Delta E$$

Equation 20

Another rule specifies the situation in which absorption of a radiation quantum can take place. It must occur with the change of the dipole moment μ of the molecule. This condition quantitatively describes the moment of R_{nm} transition between electronic states. It determines the probability of absorption of a photon with an energy adjusted to the energy difference of the electron levels:

39

$$R_{nm} = \int \psi_n \mu \psi_m \, d\tau$$

Equation 21

where ψ_n *and* ψ_m are the wave functions of the two electronic states involved in the transition, μ is the transition moment operator, while $d\tau$ denotes the volume element

The above-described transition is allowed when $R_{nm} \neq 0$. The cases where the selection rules are not met are called forbidden passes.

When determining ion solutions, the so-called 'second law of absorption' is applied. According to it, when the solvent absorption coefficient is equal to zero, then monochromatic radiation after passing through a homogeneous solution of absorbent substance with a concentration of *C* is weakened:

$$I = I_0 \cdot e^{-kbC}$$

Equation 22

where:

I - the intensity of the radiation beam after it has passed through the absorbing medium

I_0 - the intensity of the monochromatic radiation beam incident on the absorbing medium

k - the absorption coefficient of the absorbing medium

b - the optical path length of the beam through the absorbing medium

According to this law, the dependence of absorbance A, i.e., the medium's ability to absorb radiation:

$$A = log\frac{I_0}{I} = abc$$

Equation 23

should be linear. In practice, its value is influenced, among others, by:

   i.   factors limiting the law,

  ii.   chemical factors,

 iii.   hardware factors.

They cause nonlinearity of absorbance and impose certain limitations on the measurement methods. It is highly important to develop a measurement procedure for the selected method, which includes, among others:

   i.   pH selection,

  ii.   choice of the solvent,

 iii.   selection of a complexing or binding agent,

 iv.   sample unification method,

40

v. selection of measuring cuvette sizes,

vi. determination of the degree of dilution,

vii. choice of the analytical light length.

For the method of comparing between an investigated and a known concentration, the dependence of the absorbance on the concentration of the analyte is plotted. This way a simple linear equation is obtained, which allows for an accurate and precise determination of the amount of the test substance.

4.3   X-ray Photoelectron Spectroscopy (XPS)

XPS was developed in the 1960s in Uppsala, Sweden, and in 1981 Siegbahn was awarded the Nobel Prize in Physics for his work applying this technique. It was developed to analyse the surface of various materials. A solid sample in a vacuum is irradiated with a monoenergetic X-ray beam and the scattered electrons are analysed in terms of their energy. The spectrum depicts the number of registered electrons of a certain energy as a function of their kinetic energy. Therefore, each element possesses its own characteristic spectrum. The spectrum obtained as a result of measuring a set of various elements is actually the sum of the signals from individual components of the surface of the tested material. Due to the fact that the average free path of electrons in solids is small, the detected electrons come from several outer atomic shells.

The physical basis of the XPS spectroscopy is the ability to emit an electron from the outer shell of an atom by light with the energy greater than that responsible for the binding of the electron in the atom. This discovery resulted in a Nobel Prize for Albert Einstein in 1921. These types of emitted electrons are called photoelectrons. During their emission, photons treated as energy carriers with zero rest mass and electrostatically non-charged are annihilated with complete energy transfer. If the energy carried by a photon is sufficient, an electron is emitted from an atom or ion and its kinetic energy is quantitatively measurable. This is a useful value as the electron binding energy is quantised and characteristic of the various elements [111].

MgK_α and AlK_α emission lines are often used to irradiate the surface of the analyte. The photon energy from these sources has a limited (at the level of 1-10 micrometres) penetration into the solids surface. The energy of the emitted electrons can be represented by the formula:

41

$$KE = hv - BE - \phi_s$$

Equation 24

where hv is the energy of the photon, BE is the binding energy of the atomic orbital from which the electron is emitted and ϕ_s is the work function of the spectrometer. It can be assumed that the binding energy is the difference between the initial and final state after photoelectron emission. Since there are many possibilities for the final ion states in any type of an atom building a surface, there is a wide variety of kinetic energies for photoelectrons that can be observed. Moreover, there is a different cross-section for the existence of a specific end state. As each element has its own unique electron binding energy distribution, XPS can be used in the identification and quantification of the content of a given element in the surface of the tested material. The differences in the bond energies, called chemical shifts, come from the differences in the chemical potential and the polarizability of the compounds, and can be used to identify the state of the material.

In addition to photoelectrons emitted during the photoelectric effect, the Auger electrons also may be emitted. These are the electrons whose emission results from the relaxation of the ions in the excited state after photoemission. The time that passes from the emission of the photoelectron to the emission of the Auger electron is about 10^{-14} seconds. In the process of emission of the Auger electron, the electron in the outer orbitals falls into the inner orbital. This transition is accompanied by a change in its energy, which is transferred by the simultaneous emission of a photon. Therefore, the Auger electron has a kinetic energy equal to the difference between the initial ion energy and the final double positive ion energy, and at the same time, depends on the initial ionisation mode [112].

Ultimately, photo-ionisation typically emits two electrons - a photoelectron and the Auger electron. The sum of their kinetic energies does not exceed the energy of the photons that caused the ionisation. The probability of an interaction of an electron with matter is many times higher for a photon penetrating deep into the surface of the material. Therefore, the depth at which photons penetrate the material is in the order of micrometres, while the path of electrons through the material is a tenth of the angstroms. Therefore, the ionisation can take place several millimetres deep into the surface, but only the electrons from the layers closest to the surface can leave it without losing energy, and their energy is also recorded as signals in the XPS spectrum. On the other hand, the energy of the electrons, which undergo the inelastic processes and the energy dissipation, is registered as a background. A potentially

42

competitive phenomenon in relation to the emission of the Auger electron is the fluorescence of the X-ray photon, but it is a minor process in this energy range [111].

The main elements of the XPS measurement system are the aforementioned X-ray source, ultra-high vacuum in the measurement chamber additionally shielded from external sources of the free electrons, an electromagnetic lens system, an energy analyser and a detector. In addition to the devices that are a common standard in laboratories, over the last decades, big centres have been developed where large synchrotrons are used to emit photons. They use the electrons with relativistic parameters, held on outer circles and accelerated by bent magnets or a set of wigglers and undulators in order to produce a beam of high-intensity and high-concentration photons. Synchrotron radiation can also be adjusted to a wide range of wavelengths and is additionally polarizable. In this way, by manipulating the parameters of the photon source, one can optimise the parameters to observe specific energy levels and low-density systems such as molecular or atomic adsorbates on the surface [113].

5. Principal component analysis (PCA)

Principal component analysis is a multivariate technique that belongs to statistical, chemometric methods for extracting information from specific data. Tabulated data is described by several inter-correlated quantitative dependent variables. The purpose of the method is to transform the relevant data from the table and represent it in a new coordinate system, described by new orthogonal variables called principal components. The quality of a PCA analysis can be verified by a cross-validation. The method has numerous applications, ranging from stock market analysis, through experimental data, to clinical trials [114].

In spectroscopic data analysis, for techniques such as the Raman and SERS, the method is used to interpret spectral data. It is based on the linear transformation of the spectra, treated as a set of N-dimensional vectors, where N is the number of measurement points in the spectrum into the new coordinate system. As a result, several principal components can be obtained from a large set of data forming a spectrum consisting of the intensity dependence of the Raman shift. The effect of this operation is that the first principal component is the representation with the greatest possible variance. Therefore, this component represents the largest part of the inertia of the analytical data. The second variant is computed in the orthogonality regime to the first component and in order to have the greatest possible inertia. If there is a need to calculate more, the rule for the second component is repeated in relation to the previous component. The values of the new variables for observations are called 'factor

43

scores' and can be represented geometrically as projections of the observations onto the principal components [115].

In PCA, components are obtained from singular value decomposition (SVD), which is the generalisation of the eigen-decomposition. The SVD decomposes a rectangular matrix into three simple matrices: two orthogonal matrices and one diagonal matrix [114]. In the case where the data table is X, where:

$$X = P\Delta Q^T$$

Equation 25

the $I \times L$ matrix of the factor scores, denoted as F, is obtained as:

$$F = P\Delta$$

Equation 26

The matrix Q gives the coefficients of the linear combinations used to compute the factors scores. This matrix may also be interpreted as a projection matrix because multiplying X by Q gives the values of the projections of the observations on the principal components. This can be demonstrated by combining *Equation 25* and *Equation 26* as:

$$F = P\Delta = P\Delta Q^T Q = XQ.$$

Equation 27

The components can also be geometrically represented by rotating the original axes (*Figure 7*). Abdi and Williams presented an example of PCA analysis for entries in a dictionary of meanings. For the selected words (X), two values have been assigned: the length of the word (Y) and the number of lines in the text (W) that constitute its definition. In this context, the matrix Q, also called a loading matrix, is interpreted as a matrix of direction cosines (because Q is orthonormal).. As such, the matrix X can be interpreted as the product of the factors score matrix by the loading matrix as [114]:

$$X = FQ^T \text{ with } F^Y F = \Delta^2 \text{ and } Q^T Q = I$$

Equation 28
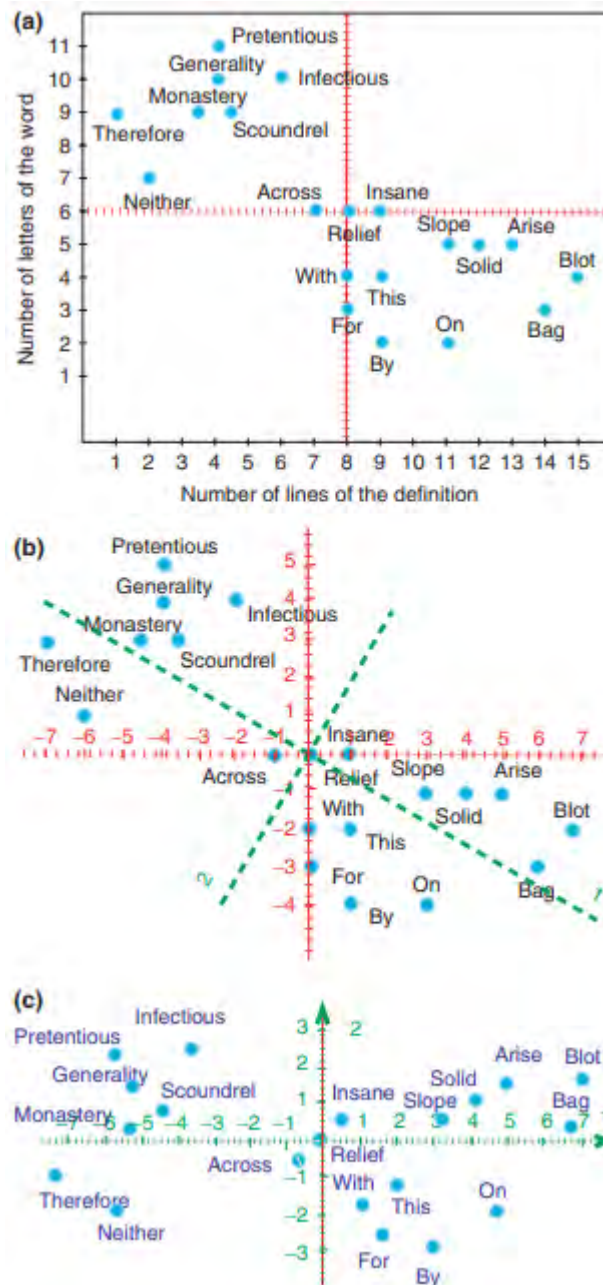
Figure 7. The geometric steps for finding the components of a principal component analysis. To find the components (1) centre the variables then plot them against each other. (2) Find the main direction, that is from now called the first component, of the group of points in such a manner that we have the minimum of the sum of the squared distances from the points to the component. Add a second component orthogonal to the first such that the sum of the squared distances is minimum. (3) When the components have been found, rotate the figure in order to position the first component horizontally and the second component - vertically. After that, original axes can be erased [114].

The similarities and differences between the samples represented by the different spectral data can be observed by plotting the principal component scores together. In the case of two principal components, we will be dealing with a two-dimensional plot, while in the

case of three principal components – with a three-dimensional representation. During the analysis, where a single spectrum is represented by a single point, it may be observed that similar spectra, located close to each other, will often overlap. Additionally, the spectral bands with the greatest influence on the spectral diversity can be represented by plotting loadings in the wavenumber or the Raman shift function [116]. The variables with high loading values have the greatest diagnostic value and thus are important in terms the uniqueness of the spectrum. In other words, the PCA method enhances futures which are difficult to observe with bare eye and thus allow to consider the SERS spectrum of a sample as its fingerprint.

In order to avoid human error in the comparison of the values obtained during the analytical tests of data and the unambiguous, mathematical representation of them, PCA is an extremely effective technique, which at the same time enables the parallel analysis of a large amount of data. In the context of data analysis in research on the identification of biological or clinical material, PCA is a not commonly used method and is applied, *inter alia*, to distinguish closely related analytes. These types of results, which allow to differentiate between biological samples, are presented in Chapter 6 and 7. Due to this method, SERS spectroscopy can be used to effectively and unambiguously discriminate between different species [117].

6.   The Aim of the thesis

Nowadays, the methods of identifying microorganisms or determining tumour markers are sensitive, accurate and enable the analysis of many types of samples. They are based on achievements in the field of biochemistry, biophysics, molecular biology and mass spectrometry [118]. Their main limitations are the time - consumption and sometimes high costs of the analysis. Additionally, the specificity of the method is sometimes very limited as in the case of enzyme-linked immunosorbent assays (ELISA). However, in the diagnosis of a patient, the most important period is from the moment the material is collected to the diagnosis and the treatment initiation. In the case of the analysis of the environmental samples, time also plays a significant role, as quick prevention effectively eliminates a potential source of infection.

Combining all the advantages of identification method in a single technique is extremely difficult and most probably – impossible. Nonetheless, it appears that spectroscopic techniques are a very promising area of research in this respect. Due to the spectral

46

representation of the sample composition, the SERS technique, along with the chemometric analysis, can be a serious alternative to the detection and the identification of microbiological hazards in clinical and environmental samples. Its significant limitations at this stage are the lack of repeatability and reproducibility, caused by a large variety of SERS substrates. Additionally, during SERS measurements, different laser lines, laser powers, measurement conditions and sample preparation methods may be applied. So far there have been no proposals to implement this technique to the existing guidelines on standard analytical procedures or food quality standards, which are regulated by the International Organization for Standardization (ISO) or European Union [119]. The research presented in Chapter 7 of current work is an attempt to solve the aforementioned problems and to bring the SERS method closer to real life analytical applications. Based on the achievements in this field, the SERS spectroscopy demonstrates a great potential for commercialisation. However, first and foremost, it has to be successfully implemented into the canon of certified analytical laboratories.

The main thesis for this dissertation can be formulated as follows: The efficient SERS-active structures along with the proposed SERS-measurement protocol, combined with the chemometric analysis of spectral data, may be an alternative analytical method for the detection and identification of selected bacteria and cancer cells in relation to the currently used techniques.

The individual goals of this thesis are:

1) Designing, testing and characterising properties of SERS substrates that will be suitable for the study of bacterial and cancer cells under label-free conditions. The fabrication process of the developed substrates ought to be controllable and scalable. The substrates should be stable over time and consist of uniformly distributed nanostructures on their surface, while their enhancement properties should allow for obtaining repeatable spectra of biological material.

2) Determining the optimal measurement parameters for selected species of bacteria.

3) Determining the optimal measurement conditions for bacteria and cancer cells obtained from cultures, as well as environmental and clinical samples.

4) The use of microfluidic systems along with dielectrophoresis for the separation of microbial material and cancer cells from liquid samples, including body fluids.

5) Assigning the bands present in the collected SERS spectra to the corresponding vibrations in the molecules.

6) Application of the PCA method for the analysis of bacteria and neoplastic cells spectra to identify the sample on the basis of the collected standard spectra.

7) Development of procedures for the sample preparation and their implementation in the experiments on numerous strains of bacteria and types of cancer cells.

7. Experimental Section

7.1 Experimental setup

All experiments performed with the use of the SERS effect, described in this section of the dissertation, were performed following the same procedure. A properly prepared sample, which is a suspension of the analyte in an aqueous buffer, was placed over the SERS substrate using a semi-automatic pipette. In order to prevent contact with the working surface, the substrate was previously attached to the microscopic slide (*Figure 8*).
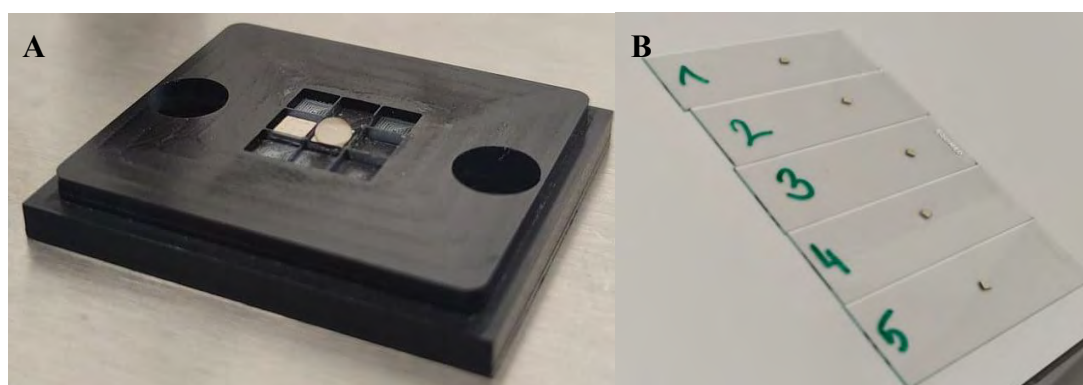
Figure 8. The comparison of the substrate with the freshly applied analyte (right) with the SERS substrate ready for deposition (left) on the microscope glass (A). The substrates were photographed against a black holder in which they were immobilized, while the sample was deposited. A series of five SERS media, mounted on basic microscope slides, ready for measurements (B).

After the water has evaporated, the slide with the fixed substrate was placed in the integration zone of the spectrometer selected for the experiment. In the experiments described below, two types of Raman spectrometers were used: (i) modular spectrometer, permanently mounted on a suitable optical table (Renishaw inVia Raman Spectrometer) and (ii) a portable handheld spectrometer (Bruker Barvo). Both measurement systems are presented in *Figure 9*

*Figure 9. The measurement station using the Bruker Bravo portable spectrometer (A). On the far-left side of the photo is located a tripod, which is used to hold the slide together with the SERS substrate, which is set in the centre of the hole in the cap, assembled in the device. Measurement station using the Renishaw inVia Raman spectrometer (B). *

The basic difference, which is immediately visible between the two devices, is their dimensions. However, in order to fully understand the measurement possibilities and to compare the similarities and the differences, it is necessary to compare the construction diagrams of both devices (*Figure 10*).
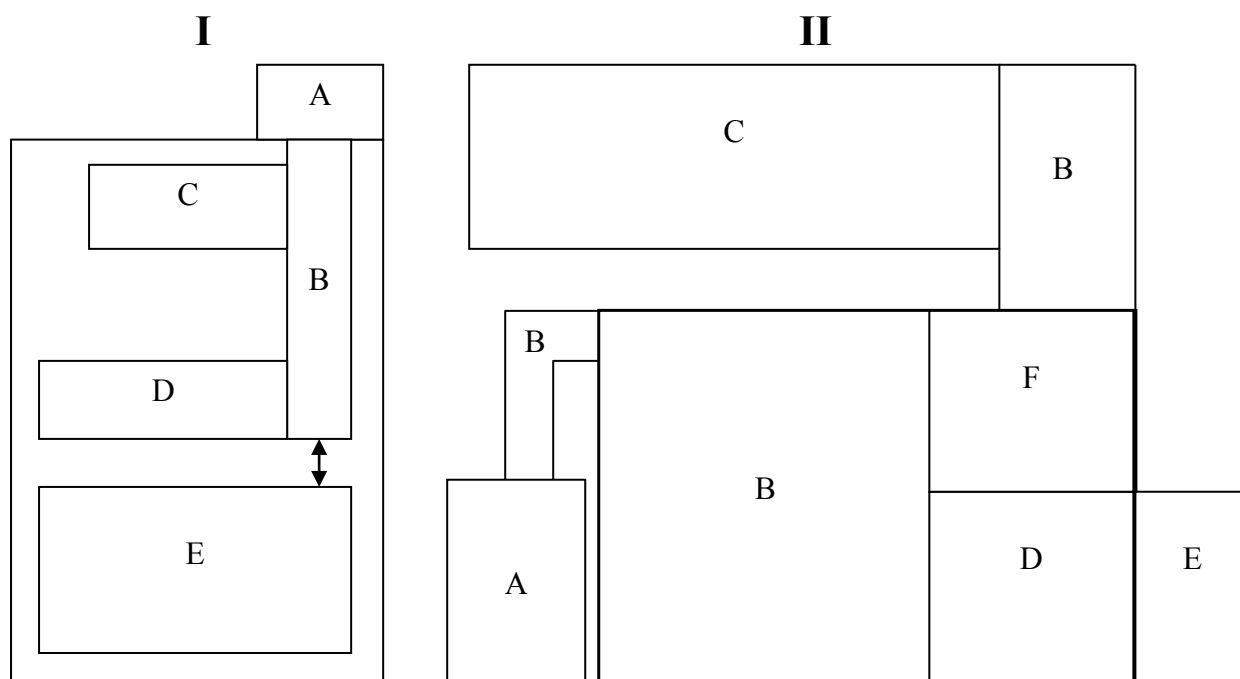
Figure 10. The comparison of the block diagrams of the Bruker Bravo (I) and the Renishaw inVia (II) spectrometer. The following letters denote the appropriate components: A - signal integration zone, B - line optics, C - laser line, D - spectrograph, E - control computer and screen, F - stepper motors for controlling line optics. In the block diagram II, the thicker line marks the elements of the device connected with each other in the central element of the spectrometer. The scale and the way of connecting individual elements or modules are not faithfully represented.

The modular design of the Renishaw inVia Raman spectrometer allows for using it in various types of experiments due to the possibility of applying many different laser lines and interchangeable and repositionable optics. In this way, for a selected laser line, a spectral resolution of 4 cm^{-1} can be obtained over the entire measuring range, i.e., from about 200 to 3200 cm^{-1}. In the case of the Bruker Bravo spectrometer, it is possible to obtain spectra in the range of 400-3200 cm^{-1}, while the range of 400-2000 cm^{-1} will be characterised by a spectral resolution of 4 cm^{-1} and the rest of the spectrum – at the level of 8 cm^{-1}. This is due to the lack of the optics of the device regulated by stepper motors.

What is more, the modular spectrometer is equipped with an optical microscope, which allows operator to preview the sample and its selected magnification. Consequently, it may be used to adjust the size of the laser spot on the sample. Due to the motorized table on which the sample is located, operator can precisely determine the area from which a single spectrum is collected or perform spectroscopic mapping for a selected surface area. The handheld spectrometer has fixed optics and thus it is not possible to change the size of the area from which the signal is collected. The mapping is also unavailable unless using

a custom-made sample alignment system. The optical table of the Renishaw inVia spectrometer suppresses mechanical vibrations, further improving the signal-to-noise ratio. A handheld Bruker Bravo spectrometer with a sample mounted in a suitable stand does not provide such high damping of vibrations.

The abovementioned features of both devices demonstrate the main strength of the modular structure of SERS spectrometers -it is crucial in determining the optimal conditions for measurements and the synthesis of signal-enhancing platforms. This topic was described precisely in Chapters 7.2.1, 7.2.2 and 7.2.3.

The spectrometer modularity is also a key factor in introducing a handheld device, such as Bruker Bravo, into regular SERS measurements of the biological material. It should be noted that a suitable and modern portable spectrometer, characterised by specified measurement criteria may nowadays preserve all the characteristics of his large counterpart. Its small size, relatively low mass, very high spectral resolution in the 'fingerprint' range of the spectra, together with the ability to work on batteries and in continuous mode with the use of a charging station make it a complete device. Thus, it was well suited for conducting research described in this paper.

7.2 Development of the SERS platforms for research on prokaryotic and eukaryotic cells.

7.2.1 Heat dispersive SERS substrate optimisation for microbiological sensing

A long-term exposure of the sample during the measurement of biological material may lead to its thermal degradation and thus - to the experiment failure. Thus there is a need for creation of a platform that would be able to dissipate the heat coming from laser light and at the same time would provide a large EF. It should also be characterised by a uniform signal enhancement.

The heat dissipation is crucial for few additional reasons. The molecules that are adsorbed to the SERS active metal surface can desorb at a temperature of 60-100 °C [120]. The decomposition of the analyte often leads to broadening of the observed spectral bands and to reduction of their intensity. This, in turn, may result in misinterpretation of analytical data [121, 122].

An additional advantage of the SERS platforms should be the low cost of production, synthesis process reproducibility and the possibility of using it in research on

various types of samples. One of the solutions is to use filters or filter-like materials with SERS-active nanostructures adsorbed to their surface. Stainless steel wire mesh (SSWM) was chosen as an alternative to the existing solutions based on polymer filters, fibres or meshes. There are four types of woven meshes: plain weave, twilled, plain Dutch, and twilled Dutch. All of these have a periodic structure which makes them an excellent base for SERS platforms. They are used as a filtration media in chemical industry due to high heat resistance, small aperture and reusability [123, 124]. For the purpose of creating a SERS substrate, Dutch SSWM has been chosen as the base and silver – as SERS-active metal, as it is characterised by good plasmonic performance in the near infrared excitation range. The metal was deposited on the base via the physical vapor deposition (PVD) technique and as a result the Ag/SSWM substrate was created. In order to find optimal conditions for SERS enhancement, six different thicknesses of silver layer on the SSWM substrates were tested: 5, 20, 35, 50, 70 and 100 nm. *P*-mercaptobenzoic acid was used as the Raman reporter, due to which the parameters of the platform enhancement were determined, while bacteria belonging to *Escherichia coli* and *Bacillus subtilis* species were selected as model microorganisms. **Details on the materials and devices used in the experiments may be found in Appendix 1.**

Preparation of the SERS Platform and Sample Measurement. The idea behind the preparation of those substrates, besides the context of plasmonic nanostructures, is to use the structural nanodefects existing on the surface of the grid and to cover them with a layer of plasmonically active silver of high purity (4N – 99.998% declared purity). In this way, the mesh was used as a template to create an analytical, signal enhancing, surface. Wire mesh sample (40×40 mm) was cut with scissors from big sheet (100×100 cm) and placed in beaker filled with acetone. In the first step the sample was sonicated for 10 min in an ultrasonic bath at a temperature of 50 °C. Then the acetone was exchanged with isopropyl alcohol and the step was repeated. Identical steps were taken with ethyl alcohol and water purified in Millipore system. The wire-mesh was next dried for 30 min at 50 °C and placed in a sterile Petri dish or immediately placed in PVD chamber. After the deposition process the samples were placed into a sterile Petri dish.

Characterisation of Wire Mesh and its Surface. Thermal conductivity of steel 316, from which the samples are made, is 16.3 $W \times m^{-1} \times K^{-1}$ [125]. In contrast to this value, the thermal conductivity of biodegradable polylactic acid (PLA), which is a fully biodegradable thermoplastic polyester and commonly used as a filament in 3D printing, is ca. 0.19 $Wm^{-1} \times K^{-1}$. This significant difference indicates the high thermal conductivity of

53

stainless steel. Thus, it can be a very good substrate material for the formation of a SERS platform. The numbers provided as the mesh type, e.g., 80×800 mesh, mean the numbers of warp (80) and weft (800) wires per inch. The mere choice of Twill Dutch weave enables the weft wires to be woven more densely and therefore it was possible to create holes with smaller diameters.
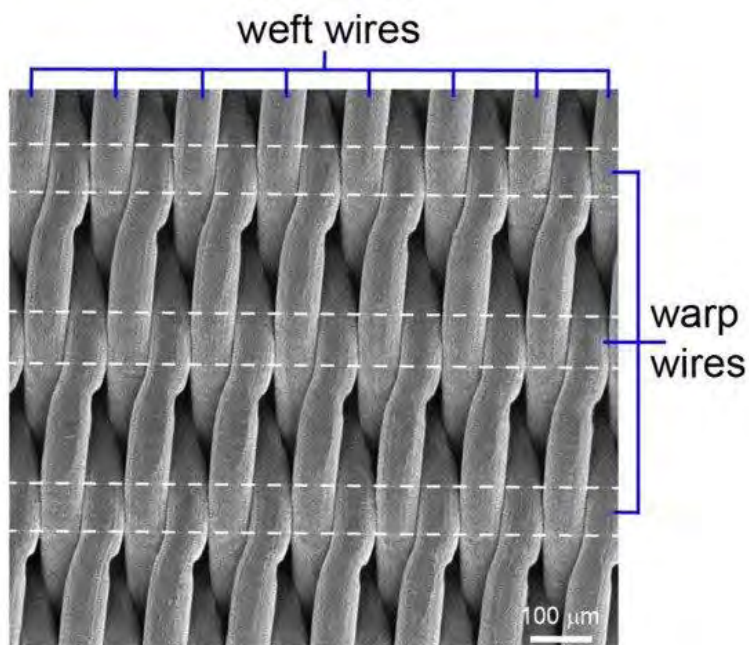
Figure 11. The twill consists of two types of wires: warp and weft. The SEM picture presents the 80×800 wire mesh [126].
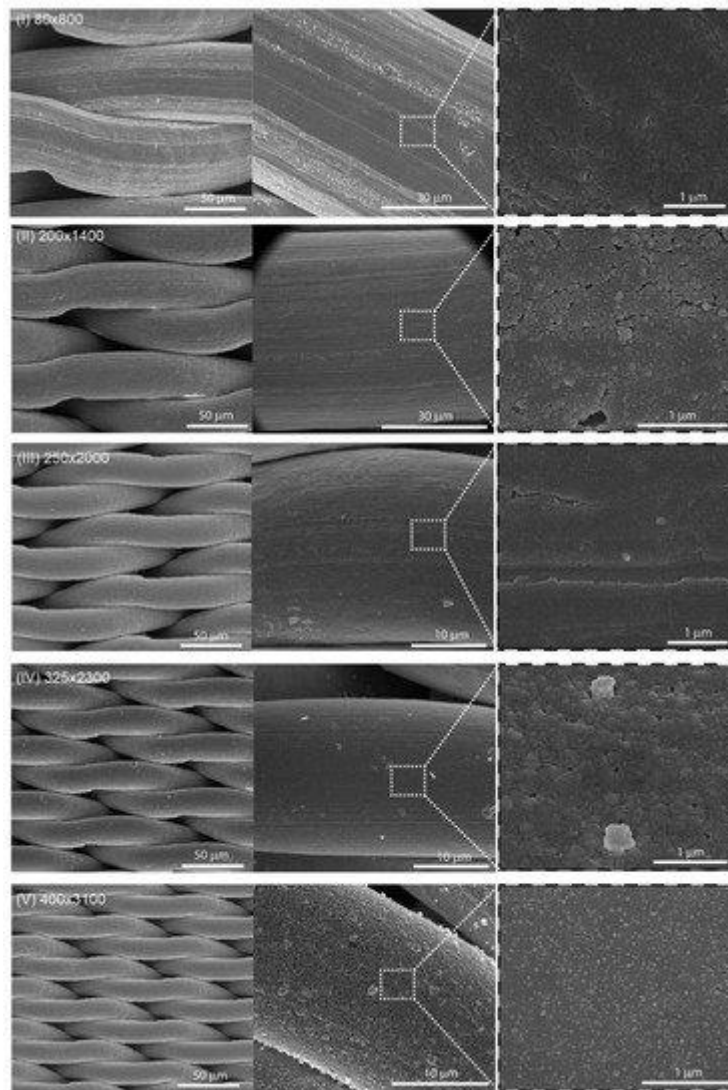
Figure 12. The SEM images of SERS-active platforms, sputtered with 50 nm layer of silver via PVD technique, at three different magnifications for comparison purposes [126].

The SEM images (*Figure 11, Figure 12*). demonstrate that silver nanostructures uniformly cover 80x800 steel-wool sample and were used to create a histogram of their size distribution. The mean size of the nanostructures on the substrate's surface for the tested sample was 33±14 nm and the median was 30 nm for the sample of 175 measurements of various structures. Each of them was measured three times and the result was averaged (*Figure 13*). The obtained values prove that the surface of the sample consist of the structures with optimal dimensions for the effective induction of LSPR.

55
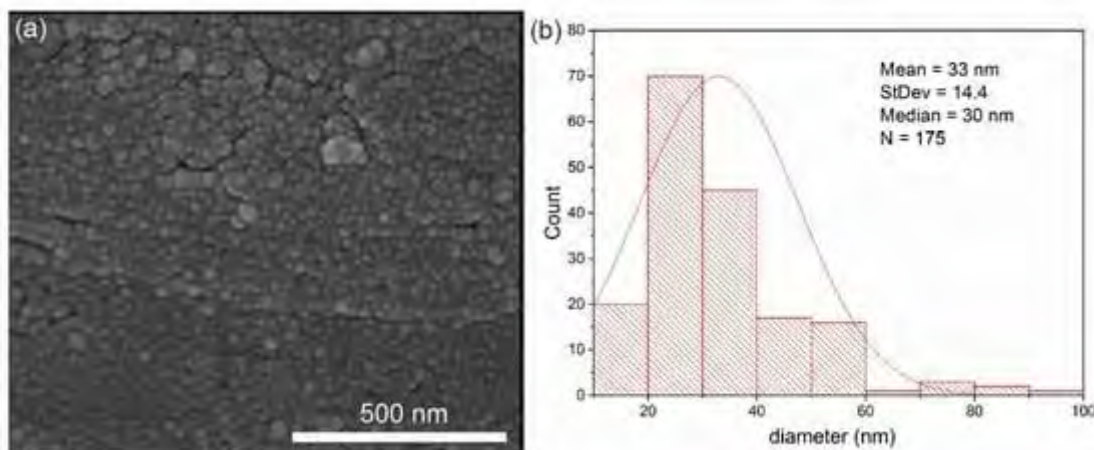
Figure 13. (a) The surface of 80x800 wire mesh sample covered with 50 nm layer of silver; (b) histogram of the size distribution of the Ag nanostructures on the surface [126].

SERS Properties of Ag/SSWM Substrate: In order to determine the sensitivity of the substrates, depending on the mesh used, their surface was functionalised with molecules of Raman reporters – *p*-MBA. As with SEM imaging, 5 different mesh weaves were tested: 80x800 (I), 200x1400 (II), 250x2000 (III), 325x2300 (IV), 400x3100 (V). Next, they were sputtered with 50 nm thick layer of silver. The *p*-MBA molecules bound to silver through thiol groups enabled the observation of the SERS effect. The *p*-MBA solution in ethanol with a concentration of 10^{-6} M was used to functionalize the Ag/SSWM samples. Each of the samples was immersed in 1 mL of such solution for 3 hours in order to completely cover their surface with a Raman reporter. The spectra I have obtained for the tested samples are presented in *Figure 14*.
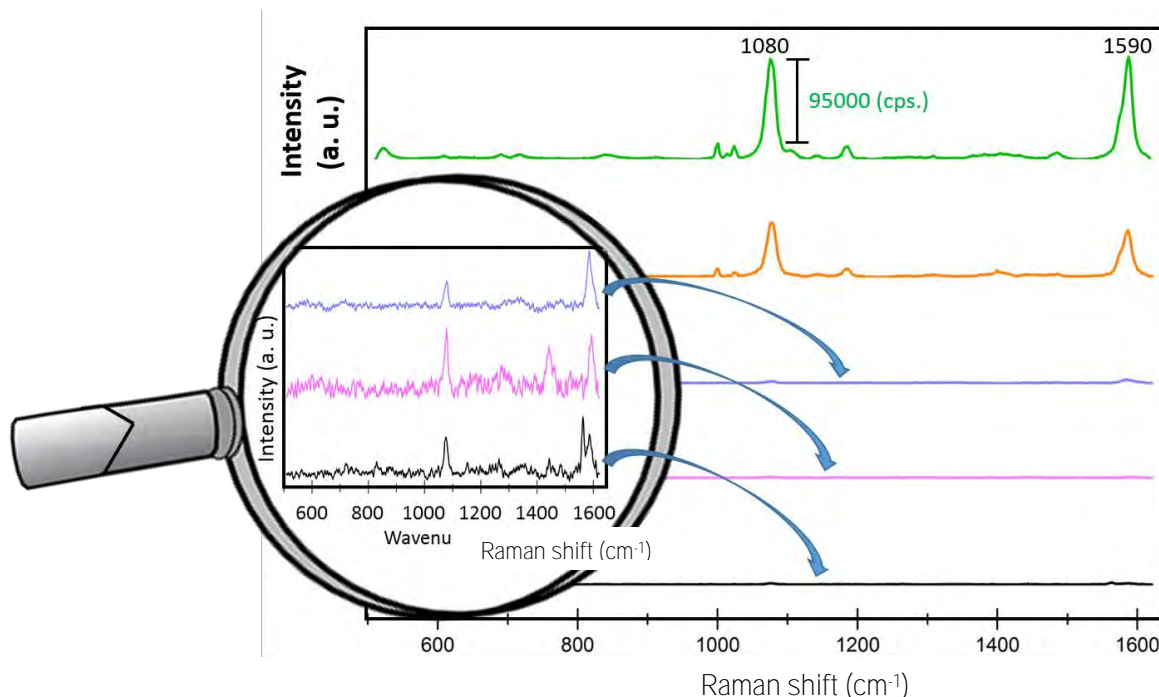
Figure 14. The SERS spectra of p-MBA recorded from five different SERS substrates (a-e) with varying morphology of a wire mesh. The experimental conditions: 5mW of 785 nm excitation, 2×5 seconds acquisition time. The image in magnifier presents the close view of the region with marker band at 1075 cm⁻¹ for SSWM surfaces demonstrating low EF. Every SERS spectrum is the result of averaging from twenty measurements in different places of SERS surface [126].

The Raman bands at around 690, 998, 1020, 1075 (Ag–S bonding), 1176 (in-plane vibrations of ring C–H), 1474 (non-bonded COO⁻ groups of the vertically oriented *p*-MBA molecules) and 1587 cm^{-1} (CC vibration with shoulder on the low-wavenumber side), that are present in the spectra, are characteristic for *p*-MBA. The bands at 689, 998, 1020 cm^{-1} and shoulder on 1587 cm^{-1} are characteristic for monosubstituted benzene derivatives [127]. Since the intensity of the obtained signals was the highest for the sample with 80×800 weave, it was chosen as the model sample in order to further optimize the platform preparation procedure. In the next stage, the thickness of the sputtering silver layer was optimised. For this purpose, the selected material was sputtered with 6 different thicknesses of silver: 5, 20, 35, 50, 70 and 100 nm. After sputtering the samples, they were functionalised again with *p*-MBA (in the same regime as before) and SERS measurements were conducted. The results are presented in *Figure 15*.
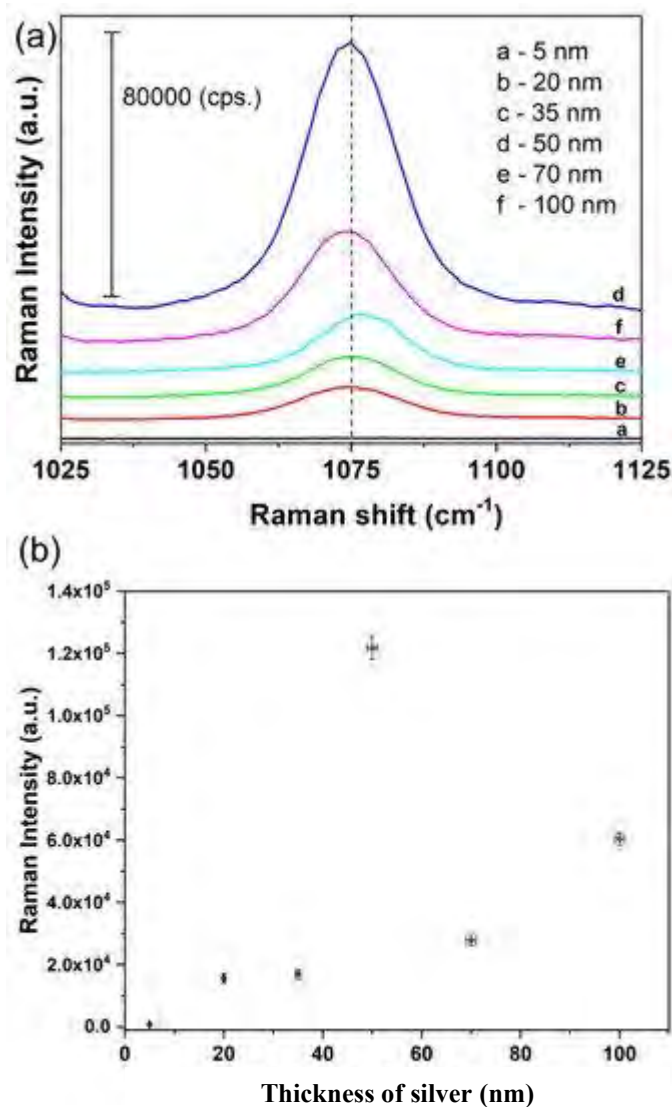
Figure 15. (a) The intensity of SERS band at 1075 cm^{-1} with varying Ag metal thickness for 80×800 mesh; (b) numerical values of Raman intensity. The error bars represent standard deviation of both thickness of the silver layer and Raman signal intensity [126].

The 1075 cm^{-1} band was selected to analyse the influence of the silver layer thickness on the substrate properties [128]. The highest intensity for this band was recorded for the sample covered with a 50 nm silver layer. Further increase in the thickness of the silver layer resulted in signal intensity decrease. Thus, a series of experiments, needed to calculate the EF for each of the wool samples, was performed using the optimal silver layer thickness of 50 nm. For this purpose, each of the Ag-covered samples was functionalized with *p*-MBA in the same regime as previously. In addition, the Raman spectrum of the solid *p*-MBA was measured under the same parameters as the SERS spectra were measured. The enhancement factor was calculated according to *Equation 13*. The effective illuminated volume *V* has been calculated using a formula recommended by Renishaw:

$$V = 3.21 \times \frac{\lambda^3 f}{D}$$

Equation 29

where f is the microscope objective focal length, D represents the effective laser beam diameter at the objective back aperture, and λ is the wavelength of the light used in the experiment. For the setup the calculated V was equal to 2012 µm³, so in rounded values it was equal to 2×10^3 µm³. The laser beam diameter, defined as twice the radius of the circle encompassing the area with 86% of the total power, was about 2.5 µm. Assuming the volume in a shape of a cylinder with the diameter of 5 µm, leads to the effective height of 100 µm. This value was confirmed by recording Raman spectra of Si, while varying the distance from the focal plane. Another important value is the number of molecules adsorbed on the surface of the substrate. The calculated number of molecules in the measured solution, according to the molecules concentration and the Avogadro constant, was 6.02×10^{14}. The surface area irradiated by the laser beam was 19.6 µm². The surface of the tested samples was 10 mm². Therefore, about 2.3×10^8 molecules were present in the laser beam spot. The normal Raman spectrum was observed for the cell filled with a pure *p*-MBA (molar mass of 154.19 g×mol⁻¹ and density of 1.06 g×cm⁻³). The effective illuminated volume for setup is 2×10^3 µm³. Under these conditions, number of molecules irradiated in normal Raman effect experiment was 8.1×10^{12}. From this data of the relative intensity and the number of molecules sampled from the regular Raman and SERS measurements, the enhancement factors for all studied SERS surfaces were calculated.

Table 3. The calculated EF factors for investigated Ag/SSWM substrates.

Mesh	Enhancement Factor (EF)
80×800	4.2×10^6
200×1400	1.3×10^5
250×2000	1.0×10^3
325×2300	1.2×10^3
400×3100	0.8×10^3

The above measurements indicate that the 50 nm thickness of the Ag metal film results in an optimal size and even distribution of silver nanostructures for a plasmon resonance effect in case of 785 nm laser line. The distribution of the nanostructures

determines the formation of 'hot spots' on the SERS substrate. In all experiments, the 785 nm excitation wavelength was used. The excitation wavelengths equal to 532 and 632.5 nm were also applied to compere the difference in intensity of the bands obtained after the measurements using all three laser lines. For this purpose, the band at 1075 cm^{-1}, defined as a marker band of *p*-MBA, was chose. The results are presented in *Table 4*.

Table 4. The intensities of the band at 1075 cm^{-1} of the representative SERS spectra of p-MBA adsorbed onto Ag/SSWM substrates.

Excitation wavelength (nm)	Intensity of 1075 cm^{-1} band of *p*-MBA (counts per second)
532	4500
632.5	98000
785	12000

Although the 1075 cm^{-1} band intensity for measurement performed with 632.5 nm line was ca. 8 times higher than in case of 785 nm line, the latter one was chosen as a compromise between the signal intensity and background fluorescence frequently observed for biological samples, which are the target analytes in described SERS experiments. The optimal size and distribution of silver nanostructures for a plasmon resonance effect for 785 nm laser line has been recently discussed in literature [129]. The reflectance spectra of SERS substrates are used for the detection of far-field electromagnetic enhancement mechanisms, whereas the near-field modes could be responsible of the strong long-wavelength resonances in the range of 700−850 nm [130]. The dark plasmons, called in such a way for non-radiating modes, detected in nanogaps and aggregated nanostructures, are indicated as potential origins of such huge Raman signal enhancements, despite expected weaker SERS effect [131].

Application of Ag/SSWM in differentiation between Gram-Positive and Gram-Negative bacteria species. In order to test the bioanalytical potential of the developed SERS surface, the SERS spectra I have recorded spectra of two different bacteria species: *E. coli* (Gram-negative) *B. subtilis* (Gram-positive). In the case of each species, bacteria were streaked on the Petri dishes with LB agar (Luria-Bertani broth agar) and incubated at 37 °C for 24 h. At first, three single bacterial colonies were suspended in 500 µL of saline solution (0.9% NaCl solution) and centrifuged for 5 min at 1070×g. Then, the supernatant was decanted and the pellet of bacterial cells was re-suspended in 500 µL of saline solution. The obtained concentration of the bacterial cells was $5×10^9$ mL^{-1}. This process was repeated three

times in order to acquire clean sample of microbial cells without any additional contamination form the cell culture medium. After discarding the supernatant in the last step of centrifugation, the bacteria cells were suspended in 20 μL of saline solution, transferred via pipette and placed onto SSWM substrate. The sample was left to dry for 5 min and then the SERS measurements were conducted. The growth of the bacteria was conducted at the Department of Molecular Microbiology, Faculty of Biology, University of Warsaw by Dr Dorota Korsak. **More details on the origin of the bacteria species may be found in Appendix 1.**
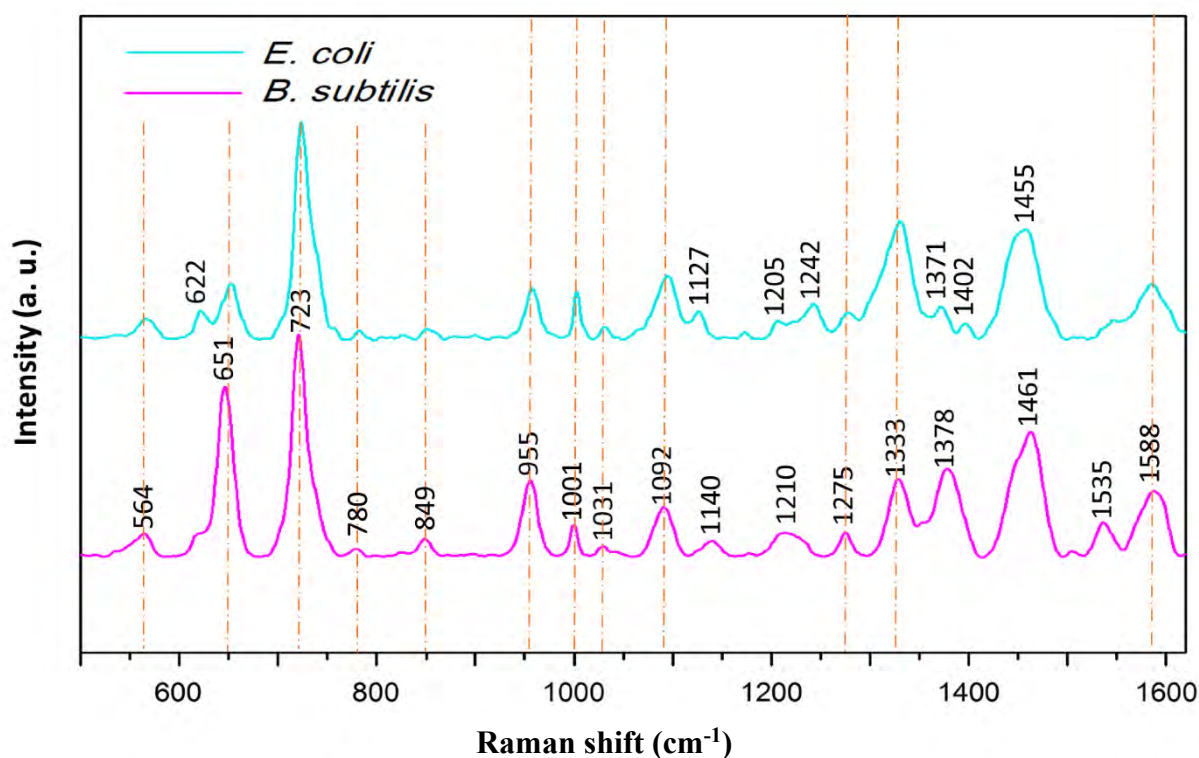
Figure 16. The SERS spectra of E. coli and B. subtilis recorded on Ag/SSWM (80×800 covered with 50 nm layer of Ag) SERS platforms. For all the collected spectra, excitation wavelength was at 785 nm, laser power was 5mW, and acquisition time was 30 seconds. Each of the presented spectra was averaged over 30 measurements in different places across the SERS surface using mapping mode [126].

As one may observe in the *Figure 16*, the obtained SERS spectra of both bacteria species exhibit major bands at around 650, 725, 960, 1000, 1100, 1330, 1375, 1460 and 1590 cm^{-1} and less intense bands at around 565, 780, 850, 1030, 1275 cm^{-1}. The band at 565 cm^{-1} originates from C–O–C ring deformation or C–C skeletal vibration, while the one at 650 cm^{-1} – from C–S stretching in methionine and / or C–C twisting mode of tyrosine [132-135]. The most intense band, located at 725 cm^{-1}, may be assigned to adenine derivatives. The band

at 780 cm^{-1} is a result of breathing modes in the DNA/RNA bases, the one at 850 cm^{-1} is derived from asymmetric O–P–O stretching and / or tyrosine [136, 137]. The bands at around 960 and 1000 cm^{-1} originate most likely from C–N stretching and from phenylalanine, respectively [138, 139]. The phospho-dioxy group (PO$_2$) from nucleic acids may be observed in the spectrum in a form of the band at 1092 cm^{-1}, while the Amide III and CH$_2$ wagging vibrations from glycine backbone and proline sidechains are detected as the band at 1275 cm^{-1} [140, 141]. Finally, the bands at around 1333, 1375, 1460 and 1590 cm^{-1} may be assigned to adenine, COO stretching, CH$_2$ bending and C=C olefinic stretching, respectively [142, 143].

Despite the similarities, the spectra can be distinguished and assigned to a specific species of bacteria. The bands at 620, 1127, 1205, 1242 and 1402 cm^{-1} may be observed only in the case of *E. coli* spectrum, while the bands located at 1140 and 1535 cm^{-1} are detected only in *B. subtilis* spectrum. Based on the above differences, Ag/SSWM SERS substrates can be applied for successful identification of bacteria.

To confirm the presence of bacteria in the measured area, SEM imaging of the examined platforms was performed *Figure 17*. The images depict the *E. coli* cells, approximately 2–2.5 μm in diameter, scattered uniformly over the steel wire *(Figure 17a)*. *Figure 17b* reveals that bacteria are arranged in lines. The reason for such an arrangement is connected with the structure of the stainless wire. The observed irregularities, which result from the process of stretching the steel fibre to the correct diameter and its subsequent spinning into a mesh, are in the scale of single micrometres and perfectly match the diameter of bacteria cells.
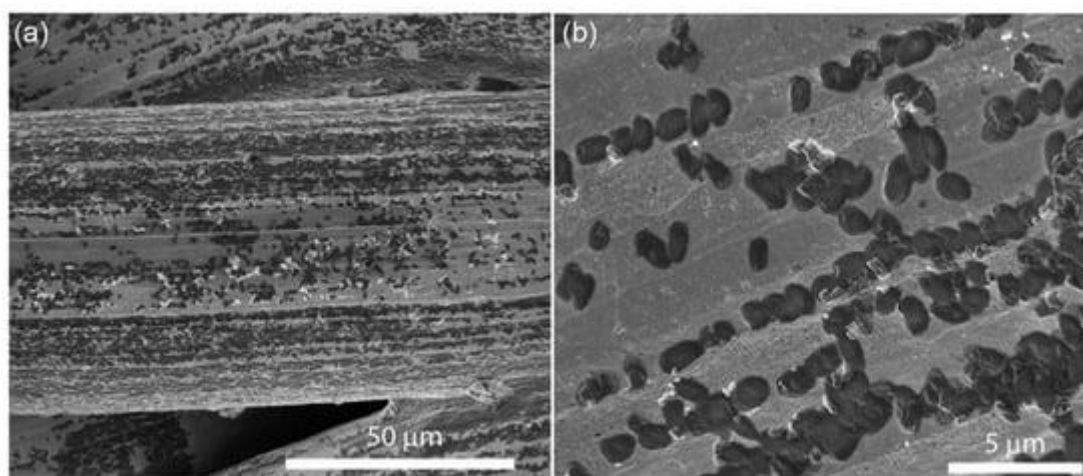
Figure 17. The SEM images of E. coli placed onto Ag/SSWM surface and collected at (a) lower and (b) higher magnification [126].

Reproducibility and thermal resistance of the SERS Substrate. To estimate the reproducibility of prepared Ag/SSWM substrates, I have calculated relative standard deviation (RSD) for SERS spectra of *p*-MBA, *B. subtilis*, and *E. coli* obtained in a mapping mode. *Figure 18* presents obtained results for optimised substrate. The calculated RSD values are equal to 6.4, 11.0, and 9.5%, respectively.
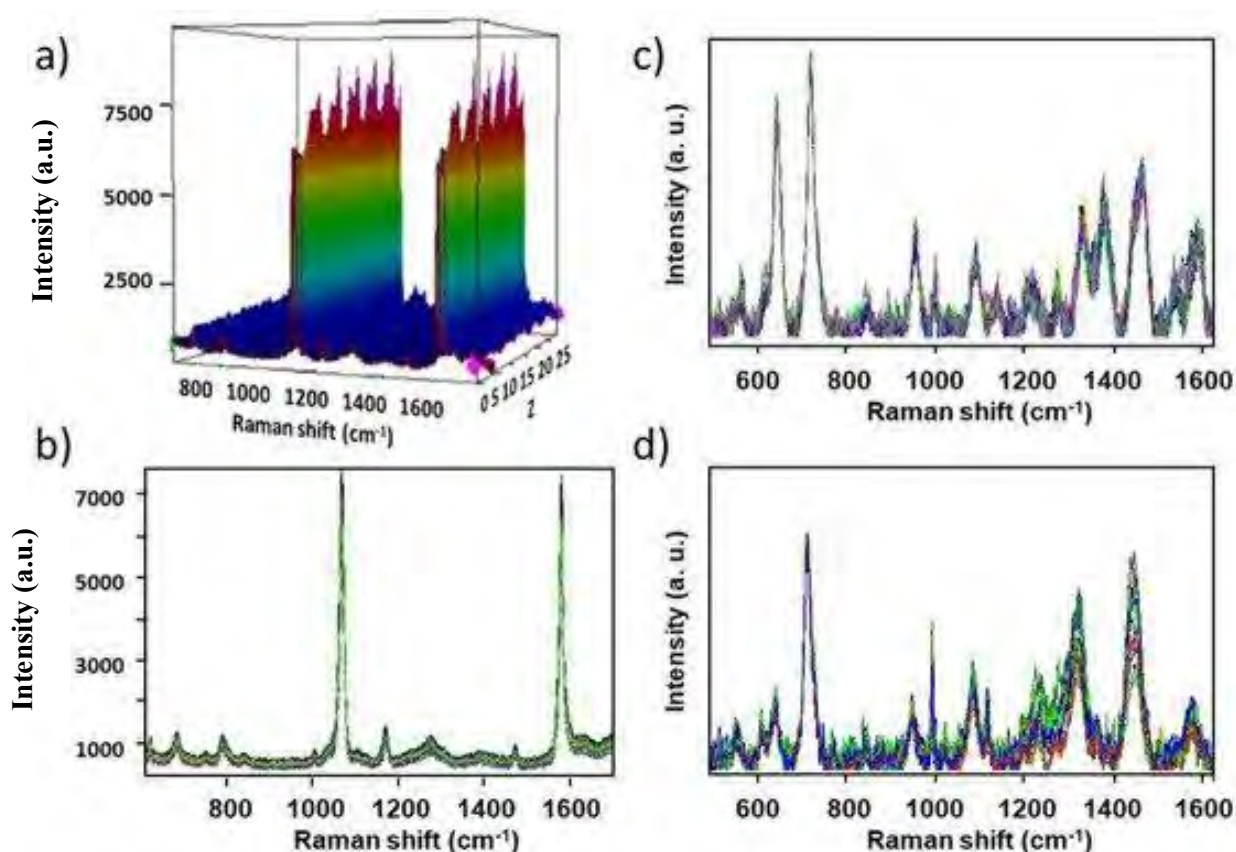
Figure 18. The SERS spectra of (a,b) p-MBA of concentration of 10^{-6}M, (c) B. subtilis, and (d) E. coli. The spectra were recorded from 30 different spots on the SERS surface using mapping mode. They were collected over a distance of 1mm with 10 μm steps. The power of 785 nm laser was 5mW [126].

The power of laser illuminating the sample strongly depends on the laser spot size and the magnification of the microscope that was used in the setup and results in the intensity of the scattered light. The biological samples are usually low-scattering analytes and thus – very sensitive to the radiation damage or local thermal decomposition.
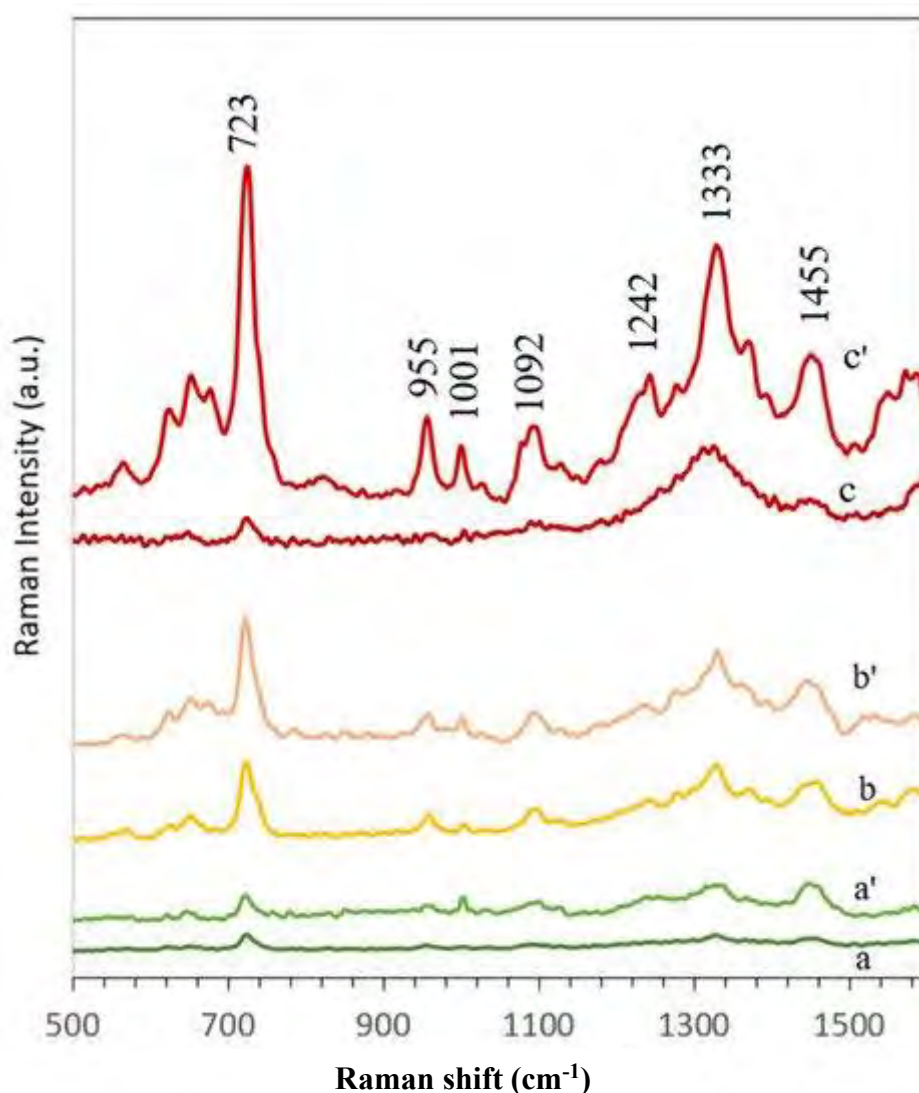
Figure 19. The SERS spectra of E. coli recorded on two different SERS substrates: modified with 50 nm of silver layer polymer mat — PLLA (a, b, c) and the stainless steel wire mesh – SSWM (a', b', c') recorded with different powers of 785 nm excitation wavelength: (a, a') 0.6 mW, (b, b') 1.3 mW, and (c, c') 14.5 mW.

To demonstrate the thermal capability of the developed SERS-active surfaces, the same volume of the same concentration of *E. coli* in saline solution was deposited onto two different types of the SERS substrates. First was based on poly-L-lactic acid (PLLA), while the second – on SSWM. The substrates based on PLLA were prepared similarly to Ag/SSWM platforms – by sputtering 50 nm silver layer on their surface via PVD technique. The SERS data that were recorder at various intensities of excited laser power are presented in *Figure 19*.

The burning or photo-degradation of biological samples, especially over prolonged period of excitation at too high laser power often results in appearance of the additional band in the recorded SERS spectrum at ca. 1500 cm^{-1} (*Figure 20*). The presence of the mentioned

band is usually associated with the formation of amorphous carbon originating from organic matter [144]. Additionally, because of sample decomposition, many chemical bounds simply break. This results in law spectra quality and invaluable information for the band analysis.
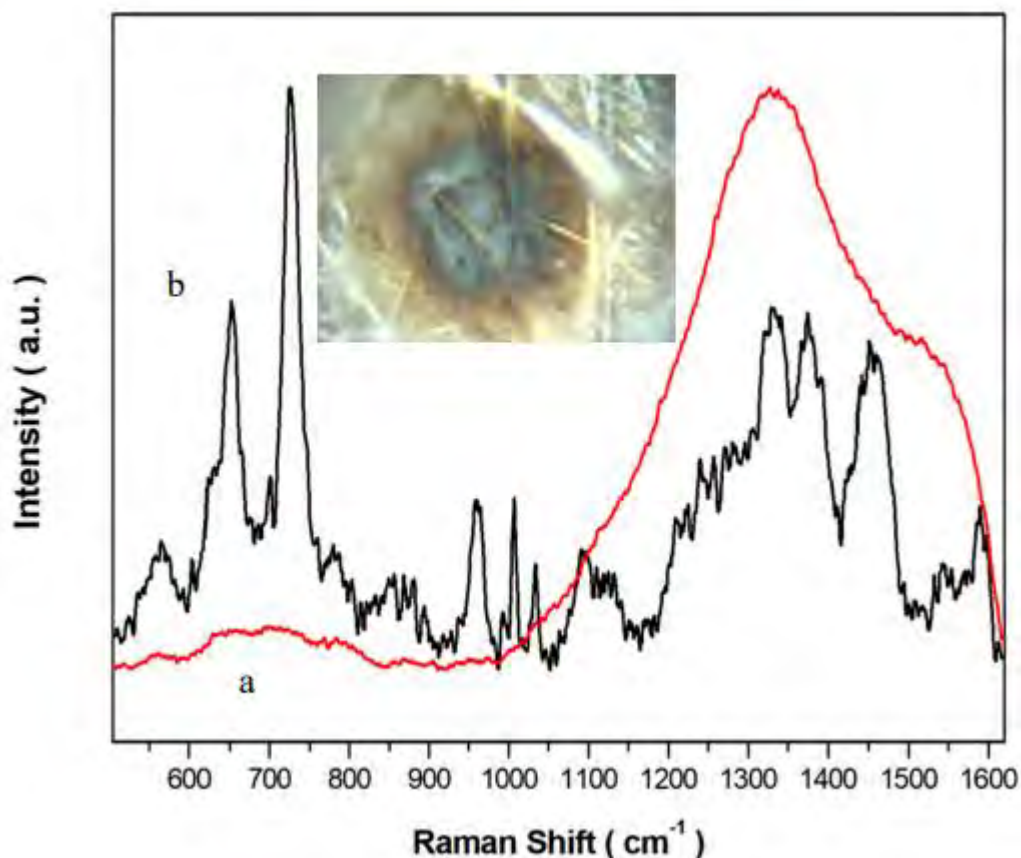
Figure 20. The SERS spectra of E. coli recorded onto polymer mat – PLLA modified with 50 nm of silver layer at different power of the 785 nm excitation wave length: (a) 1.3 mW, and (b) 14.5 mW. The additional insert presents the image of a destroyed sample observed via optical microscope.

Conclusions. The research described above presents a process of synthesis and optimisation of a new, low-cost, efficient and repeatable in terms of EF platforms, which are based on a mesh made of stainless steel. The influence of the fibres diameter, their morphology, and the thickness of the sputtered silver layer were investigated. The parameters guaranteeing high SERS signal enhancement were selected based on the Raman-reporter *p*-MBA measurements. Due to the high value of thermal conductivity, the SERS substrate exhibits excellent heat dissipation properties and prevents thermal decomposition of biological samples. Thanks to this, it is possible to extend the measurement time of the analyte or increase the laser power per unit area. This, in turn, allows to obtain spectra that, thanks to good parameters, allow to determine what type of research material is investigated.

65

This way, it was possible to differentiate Gram-positive from Gram-negative bacteria, identify them, and map the area of their occurrence with a maximum RSD of 11% along a 1 mm long section. The parameters of the obtained substrates were very satisfactory and these were used in subsequent experiments. The research conducted and described in this subsection led to the fulfilment of the first and fifth of the individual thesis goals.

7.2.2 Optimisation of bacterial culture conditions, measurement parameters for SERS-based microbiological material analysis.

The first experiments demonstrated that the developed Ag/SSWM platform has the potential to be used in the detection and identification of bacteria. The selection of both the metal covering the mesh surface, and laser line were based mainly on the achievements to date and / or literature data. The developed experiments conditions, presented in the further part of the present thesis, are considered as the basis for an effective work with the analysed material. The consistency of the measurement conditions would also guarantee the reproducibility of the experiments and the possibility of comparing the results obtained in them, despite the performance at different periods.

During the following SERS measurements four different laser lines: 325 nm, 514 nm, 633 nm, and 785 nm and six laser power levels of the selected laser line were tested. The impact of SERS-active metal / alloy and the duration of the experiment on the spectral image of bacteria was tested. Silver nanoparticles (NPs) and nanostructures are believed to be toxic to bacteria [145]. This toxic effect is connected with generation of reactive oxygen species when cells are exposed to silver nanoparticles. As the result of such interaction, nanoparticles may indirectly disrupt the function of cytoplasmic membrane, inactivate key enzymes, interact with nucleic acids, interfere with metabolic and respiratory processes, and cause death of the cell.

Additionally, the culture conditions effect on the structure and the chemical composition of bacteria and, thus, their SERS spectra, was investigated. The type of culture media and death of bacteria have been checked for impact on SERS spectrum band composition, as well their intensity and quality. Again, two model-bacterial species were investigated: Gram-negative *Escherichia coli* and Gram-positive *Bacillus subtilis*. **Details on the materials and devices used in the experiments may be found in Appendix 2.**

SERS substrates preparation and comparative analysis. In order to obtain a reliable comparative analysis of steel meshes with other substrates, I prepared additional substrates

based on silver discs, the nanoplasmonic surface of which is obtained by alternating electrochemical reduction and oxidation. The second type of comparative substrates used silicon as the base substrate, chemically etched with a 30% KOH base solution and then sputtered with metallic silver. Stainless steel mesh substrates were made according to the optimized procedure described in the previous section.

A smooth surface for further modification of the disc-based SERS substrates was obtained by mechanically polishing 4N-grade silver discs (Ø=10 mm, H=5 mm) with Al_2O_3 slurries in the SII OFL-12 Fibre Polisher (Seiko Instruments). First slurry contained particles with a size of 0.5 mm, whereas the second – particles with a size of 0.3 mm. The substrates were polished to a mirror-like surface. Then they were cleaned by sonication for 10 min in a 70% ethanol solution with distilled water and then again for 10 min in Millipore water. Subsequently, the discs were electrochemically roughened by oxidation / reduction cycles (ORCs) in the electrochemical cell filled with 0.1M KCl solution. The three ORCs were applied in total (0.5 V and − 0.5, both for 40 s; 0.5 V and − 0.5, both for 15 s; 0.5 V for 15 s and − 0.5 for 30 s). In the last step, the reduction potential of − 0.4 V was applied for 300 s. Finally, the silver discs were rinsed with Millipore water, dried, and used immediately in SERS experiments.

Another type of prepared substrates was based on silicon (100, n-doped) and covered with a layer of silver (Ag/Si). One-sidedly polished silicone plates (Ø = 25mm) were placed in a beaker filled with 30% KOH solution for 40 min at 50 °C. Next, having rinsed the plates in Millipore water, they were sonicated in an ultrasonic bath for 15 min at 50 °C in the following substances: acetone, isopropyl alcohol and Millipore water. Consequently, the platforms were dried for 30 min at 50 °C, placed in a PVD device and sputtered with a 10 nm layer of silver. After the deposition process the samples were placed into a sterile Petri dish. The substrates were used immediately after their preparation.

In this comparative experiment, *E. coli* and *B. subtilis* bacterial suspensions were prepared. For viable *E. coli* and *B. subtilis* cells, after 24 h of culture, three single colonies were placed via a sterile plastic inoculating loop into 200 μL of sterile 0.9% NaCl solution, mixed, and centrifuged for 3 min at 1070×g. The centrifugation process in the saline solution was repeated three times to obtain a solution of clean bacterial cells. Purified bacteria were finally suspended in 10 μL of sterile 0.9% NaCl solution. Then, bacteria samples were placed on a platform and immediately after drying, subjected to spectroscopic analysis. The SERS measurements were performed applying three accumulations of a single spectrum and were repeated three times for a single hot spot. The obtained results were next averaged. The time

67

needed to accomplish single accumulation was 4s. The spectra presented in the *Figure 21* were obtained in the mapping mode, and 30 measurements were averaged to obtain a single spectrum.
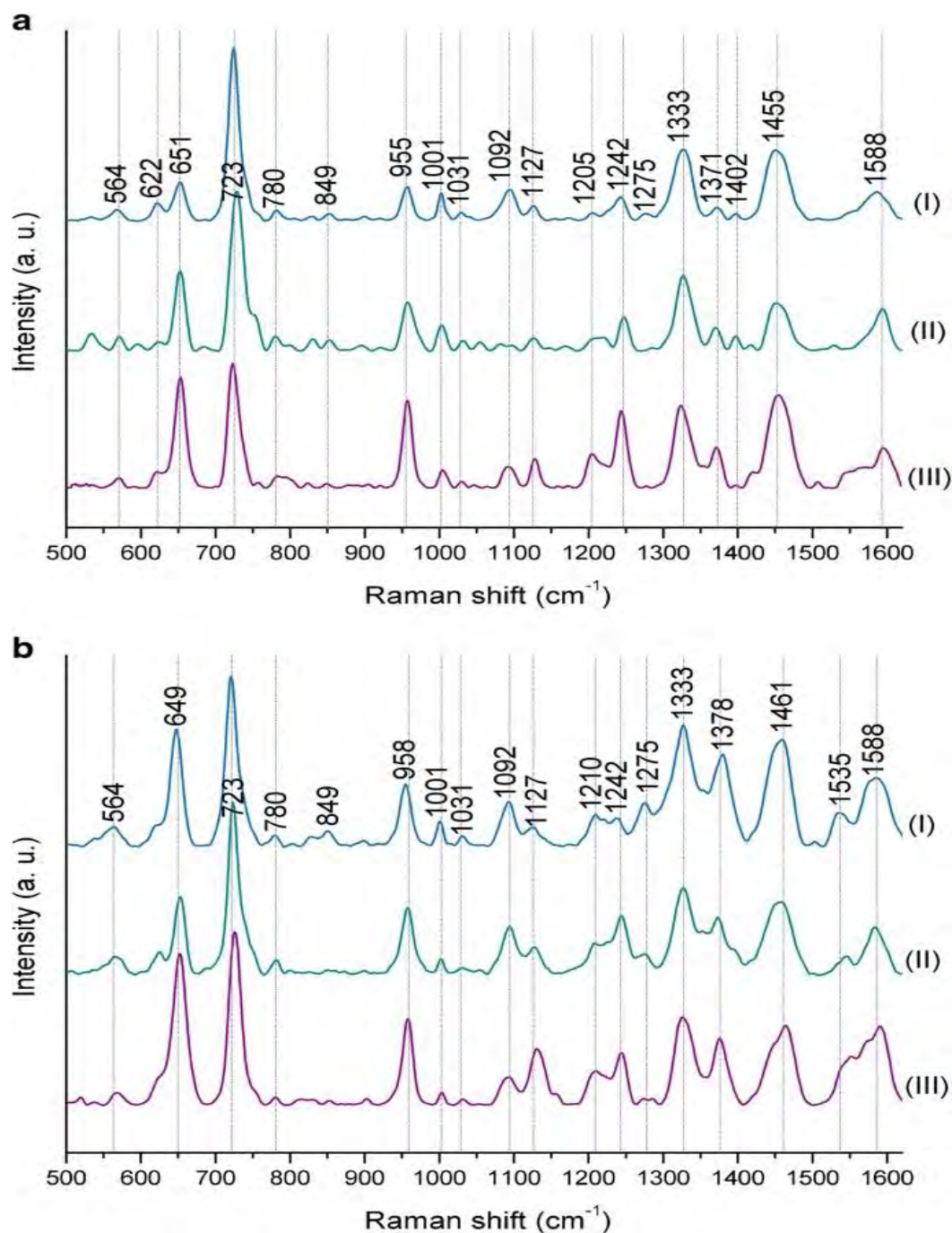
Figure 21. The SERS spectra of (a) E. coli and (b) B. subtilis measured on (I) Ag/SSWM, (II) Ag disc, and (III) Ag/Si SERS substrates. The bacteria were cultured on LB agar medium (24 h, 37 °C). All individually compiled spectra were averaged from 30 SERS measurements performed with the 785 nm laser line (1.5 mW), baseline corrected, smoothed, and normalized [146].

As in the previous section (7.2.1) the SERS spectra obtained with the use of the described SERS platforms were very similar within investigated bacterial species. In SERS spectra of both *E. coli* and *B. subtilis*, one may notice bands at around 565 cm^{-1} (C–S–S–C), 620 cm^{-1} (phenylalanine), 720 cm^{-1} (adenine in FAD and NAD), 955 cm^{-1} (C=C deformation), 1000 cm^{-1} (phenylalanine), 1090 cm^{-1} (C–C skeletal and C–O–C stretching from glycosidic link), 1240 cm^{-1} (Amide III), 1330 cm^{-1} (CH$_2$ / CH$_3$ wagging mode in purine bases of nucleic acids), 1450 cm^{-1} (CH$_2$ / CH$_3$ deformation of proteins and lipids), and 1590 cm^{-1} (phenylalanine, hydroxyproline, tyrosine) [137].
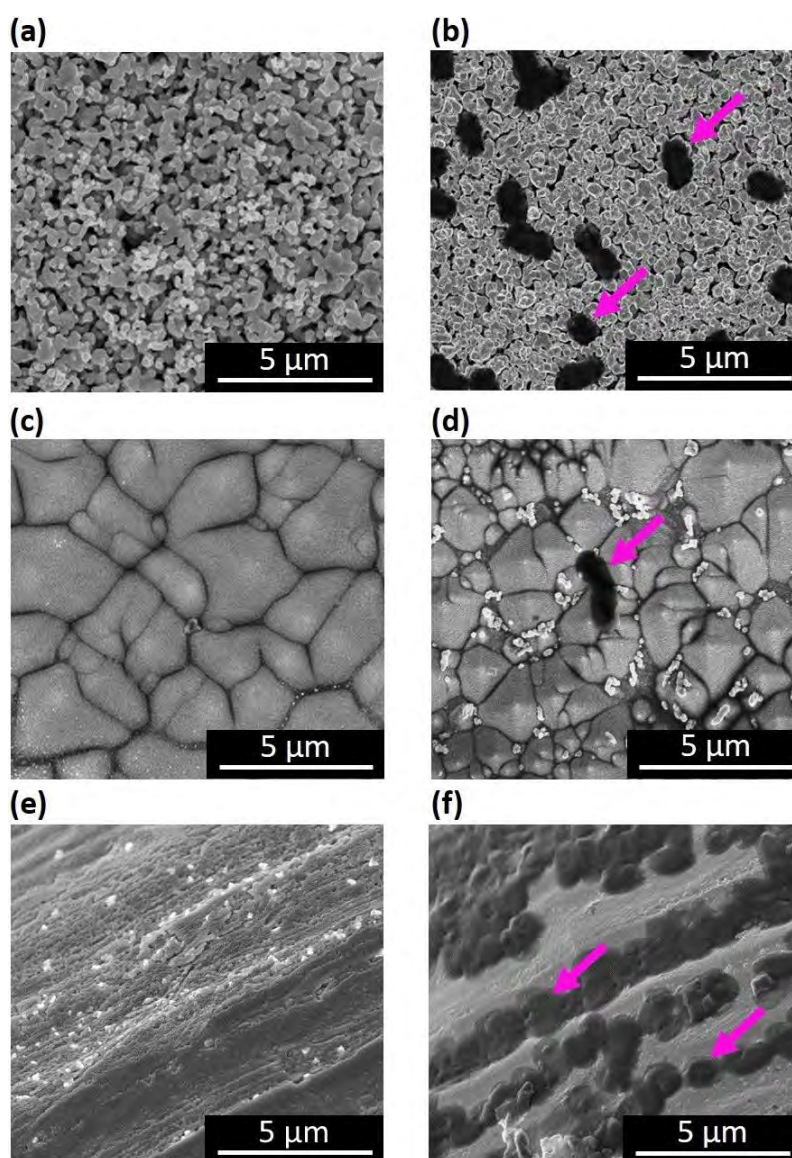
Figure 22. The SEM images of different SERS substrates and bacterial cells adsorbed on them: Ag disc (a) without and (b) with E. coli cells, chemically etched silicon covered with Ag layer (c) without and (d) with B. subtilis cell, and SSWM covered with Ag layer (e) without and (f) with E. coli cells. The bacterial cells are indicated with pink arrows [146].

69

Minor spectral dissimilarities may result from different properties of nanostructures present on SERS substrates (*Figure 22*). This includes their distinct sizes, shapes and characteristics of surface plasmon resonance. As one can see, the use of simple techniques for the production of SERS substrates, which do not require the use of organic, sparingly soluble reagents, positively affects the reproducibility of the spectra obtained on different substrates. Unfortunately, this in not always the case when comparing the results demonstrated in scientific publications. As a result, the same bacterial species may be represented by different SERS spectra [142, 147, 148]. Thus, it is crucial to avoid reagents which may interact with the analyte and / or contribute to overall spectroscopic image due to its characteristic SERS bands. Nevertheless, there are also other factors that may influence the SERS spectra of bacteria and their analysis is presented later in this work.

Comparison of the effects of various SERS-active metals in the production of SERS substrates. As silver, gold and copper are metals with the strongest observed signal enhancement in the SERS technique, they were selected for the experiment along with the gold and silver alloy with a mass ratio of 30/70. The parameters of the sputtering process of the metals on the surface of a steel mesh wire were the same, as in the case of silver in the previous experiment. The selected layer thickness was 50 nm, based on the optimisation experiments performed for Ag/SSWM substrates, demonstrated in section 7.2.1. The results of the experimental series for *E. coli and B. subtilis* are summarized below (*Figure 23)*.
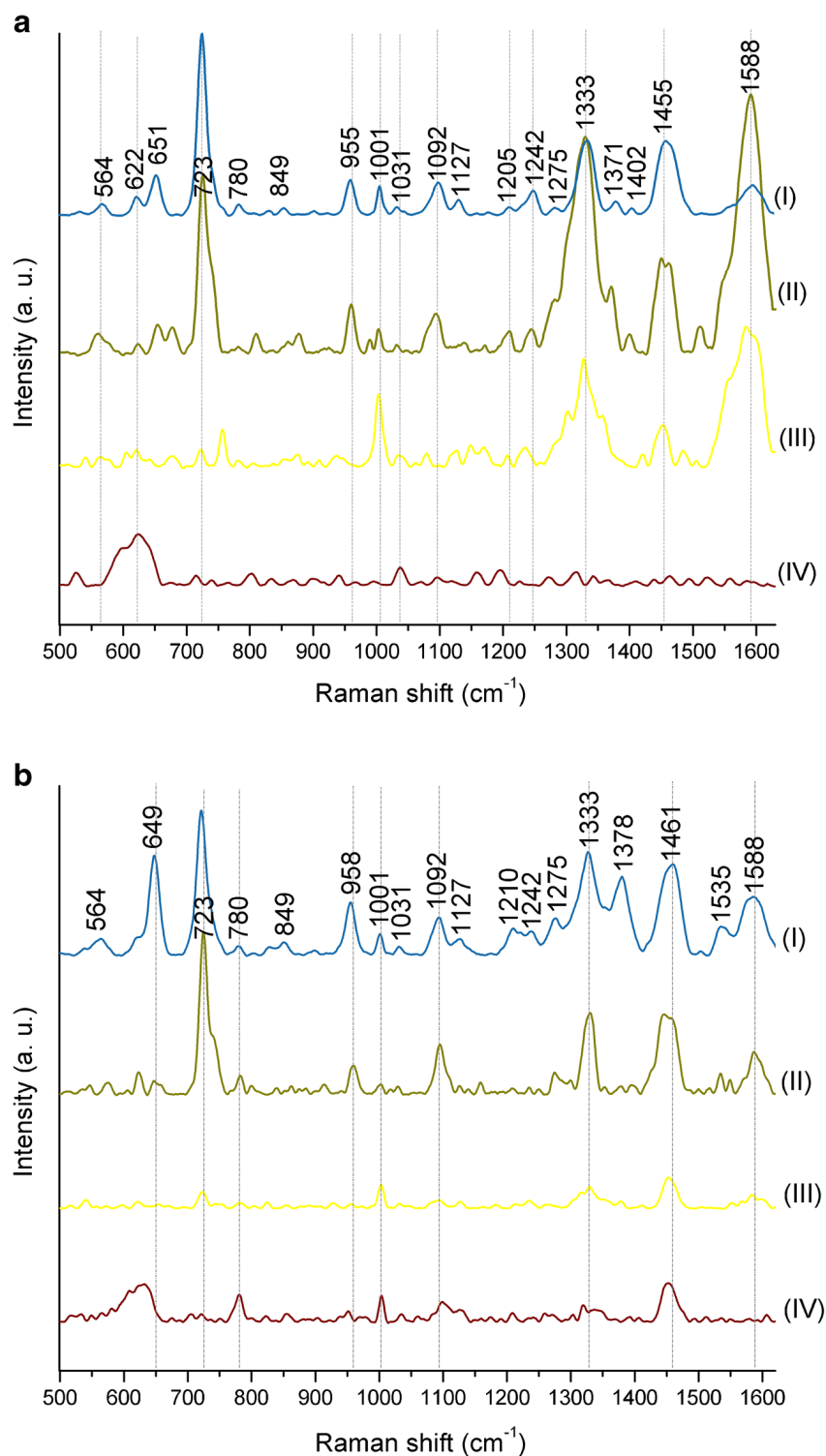
Figure 23. The SERS spectra of (a) E. coli and (b) B. subtilis measured on Ag/SSWM SERS substrates covered with 50 nm of (I) Ag, (II) Ag/Au alloy, (III) Au, and (IV) Cu. The bacteria were cultured on LB agar medium (24 h, 37 °C). All presented spectra were averaged from 30 SERS measurements performed with the 785 nm laser line (1.5 mW), baseline corrected, smoothed, and normalized [146].

The highest signal-to-noise ratio, the most intense SERS bands and the most representative SERS spectra were observed for Ag/SSWM and Au/Ag/SSWM platforms, for

71

both bacteria species. The Au/SSWM platform demonstrated some characteristic bands at around 1000 cm^{-1}, 1330 cm^{-1}, 1450, and 1590 cm^{-1}, but other bands typical for bacterial cells, e.g., at around 620, 650, 730, 960 and 1100 cm^{-1} were absent or hardly distinguishable from background noise. Moreover, the intensities of observed bands were very low in comparison to those obtained due to the presence of Ag and Ag/Au nanostructures. The copper substrate allowed for enhancing only one band, at around 620 cm^{-1}, originating from bacterial cell components of *E. coli* or exhibited only four bands at ca. 620, 780, 1000 and 1450 cm^{-1} in the case of *B. subtilis*. After the comparison of the SERS spectra obtained from all considered metals chosen for preparing the substrates, those consisting of silver allowed for the acquisition of the most characteristic and band-rich spectra for bacteria. The silver-coated SSWMs were selected for the next series of experiments, mainly due to the greatest diversity of spectra of both species of the tested bacteria, measured on these substrates. Additional advantage was a lower cost of their production compared to the application of a gold-silver alloy.

Investigation of the influence of the type of the laser lines and their power. I preformed SERS measurements of *E. coli* and *B. subtilis* with four different laser lines: 785 nm, 633 nm, 532 nm, and 325 nm on steel mesh substrate covered with Ag nanostructures. For all the bacterial samples, the same conditions of cell culture (37 °C, 24 h) and the sample preparation were maintained. The results are presented in *Figure 24*.

72
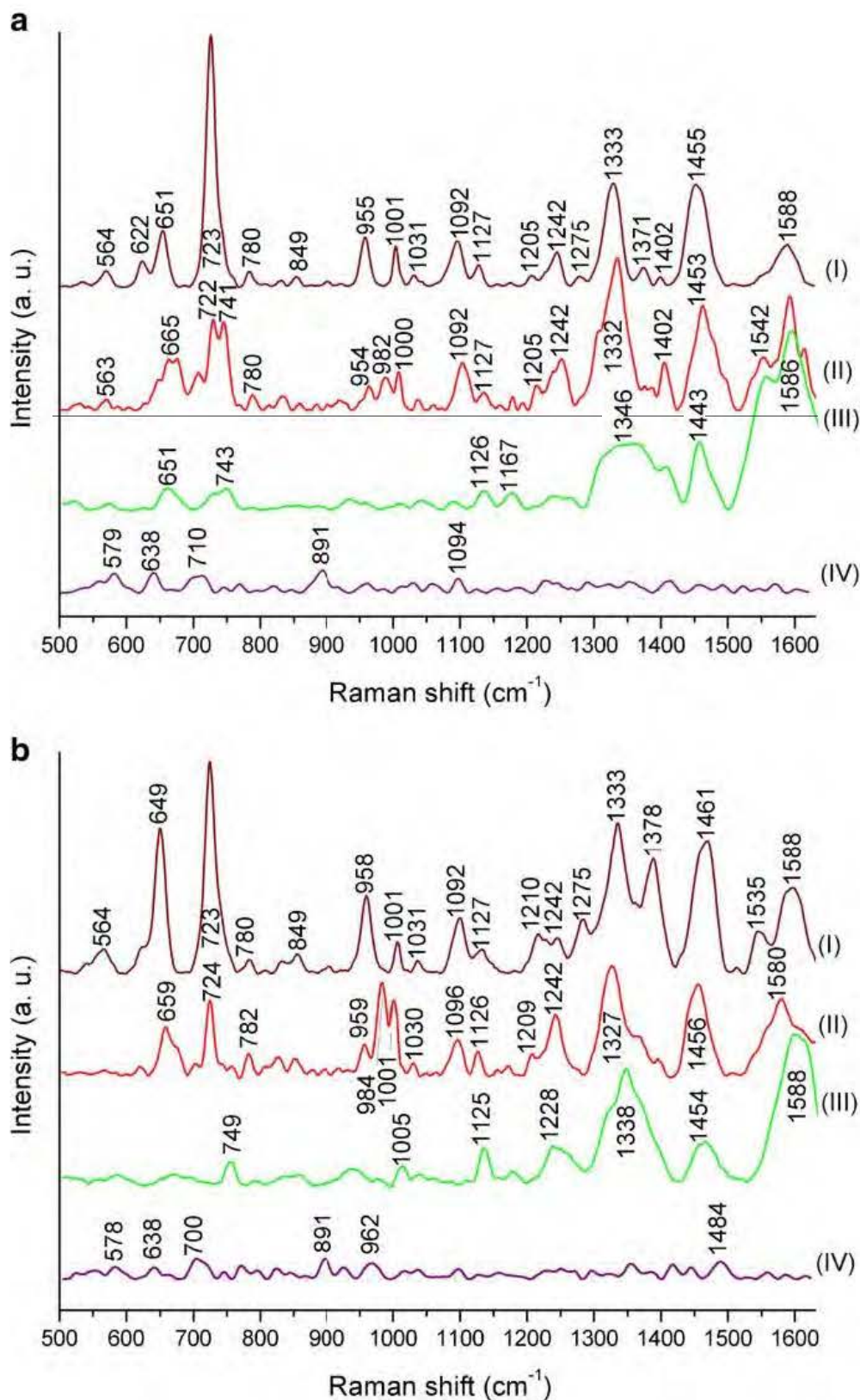
Figure 24. The SERS spectra of (a) E. coli and (b) B. subtilis measured with four different laser lines: (I) 785 nm, (II) 633 nm, (III) 532nm, and (IV) 325 nm. The bacteria were cultured on LB agar medium (24 h, 37 °C). All presented spectra were averaged from 30 SERS measurements performed on Ag/SSWM SERS substrates, baseline corrected, smoothed, and normalized [146].

73

The measurements performed with the use of 325 nm and 532 nm lines, resulted in almost-bandless spectra in the case of *E. coli* and few SERS signals for *B. subtilis*. In addition, the spectra obtained with the 532 nm line were characterized by a high fluorescence and in order to make them suitable for comparative analysis, background corrections had to be introduced. Both the 633 nm and 785 nm lines provided satisfactory results, however in the case of the experiment conducted with the use of 785 nm laser, a better signal-to-noise ratio and a higher intensity values were obtained.

It is worth mentioning again that the theory about the wavelength of maximum extinction for LSPR, located at around 400–500 nm, works well for silver nanoparticles, but is not entirely applicable to the tested substrates [149]. This phenomenon has been explained by the aforementioned plasmonic dark modes [130], which arise from the plasmon hybridisation in a set of interacting NPs. These dark modes tend to have a zero net dipole moment in contrast to dipole-active bright modes and usually do not appear in optical absorption experiments. Moreover, as all absorption measurements were conducted for metal nanoparticles, it was not likely that the extinction spectrum obtained from the colloidal suspension of metal nanoparticles would be the same as in the case of bulk SERS substrate. As the 785 nm line was confirmed as the best suitable for measuring a biological sample, it was used in subsequent experiments.

Selection of laser power. The thermal degradation of biological samples mentioned in the previous subsection is most often followed by the appearance of the 1500 cm^{-1} band in the spectrum, resulting from the formation of an amorphous carbon phase [144]. The selection of the optimal laser beam power was important as it affects the intensity of the spectrum and the signal-to-noise ratio, which are crucial for interpretation. I performed measurements of bacterial samples for different laser powers of 785 nm laser line. The results of these experiments are presented in *Figure 25*.

74
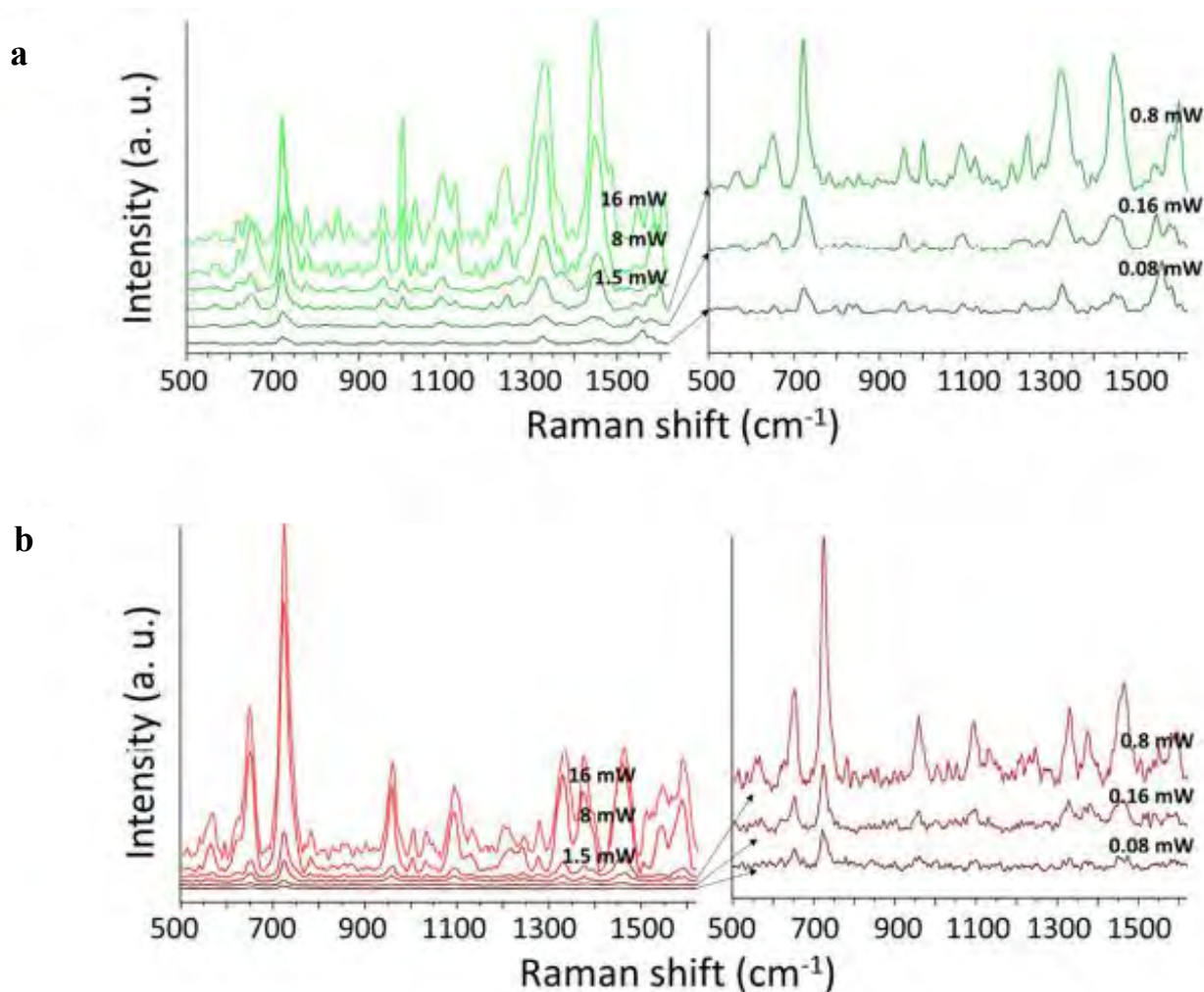
Figure 25. The SERS spectra of (a) E. coli and (b) B. subtilis measured with six different powers of 785 nm laser line: 0.08, 0.16, 0.8, 1.5, 8.0, 16.0 mW. The bacteria were cultured on LB medium (24h, 37°C). All presented spectra were averaged from 30 SERS measurements performed on Ag/steel mesh SERS substrates, baseline corrected, and smoothed.

In the case of power from 0.08 mW to 0.8 mW, the obtained intensity and signal-to-noise ratio were low. On the other hand, in the case of 8 mW and 16 mW power, when the measurements lasted over a minute, the bands related to the formation of amorphous carbon began to appear in the spectrum. Therefore, the power of 1.5 mW was selected for further applications of SERS spectroscopy in the study of bacteria.

Examination of the influence of the bacterial medium on the spectral image of the samples. Bacterial growth media contains substances necessary for the growth of microorganisms. Differences in their composition may cause significant changes in the growth characteristics of microorganisms and it has already been demonstrated that they

influence the SERS spectra of bacteria [150]. To study this dependency, few growth media available on the market were chosen: LB agar and BHI agar for cultivation of both *E. coli* and *B. subtilis*, MEYP agar for cultivation of *B. subtilis*, and TBX agar and CCA for cultivation of *E. coli*.
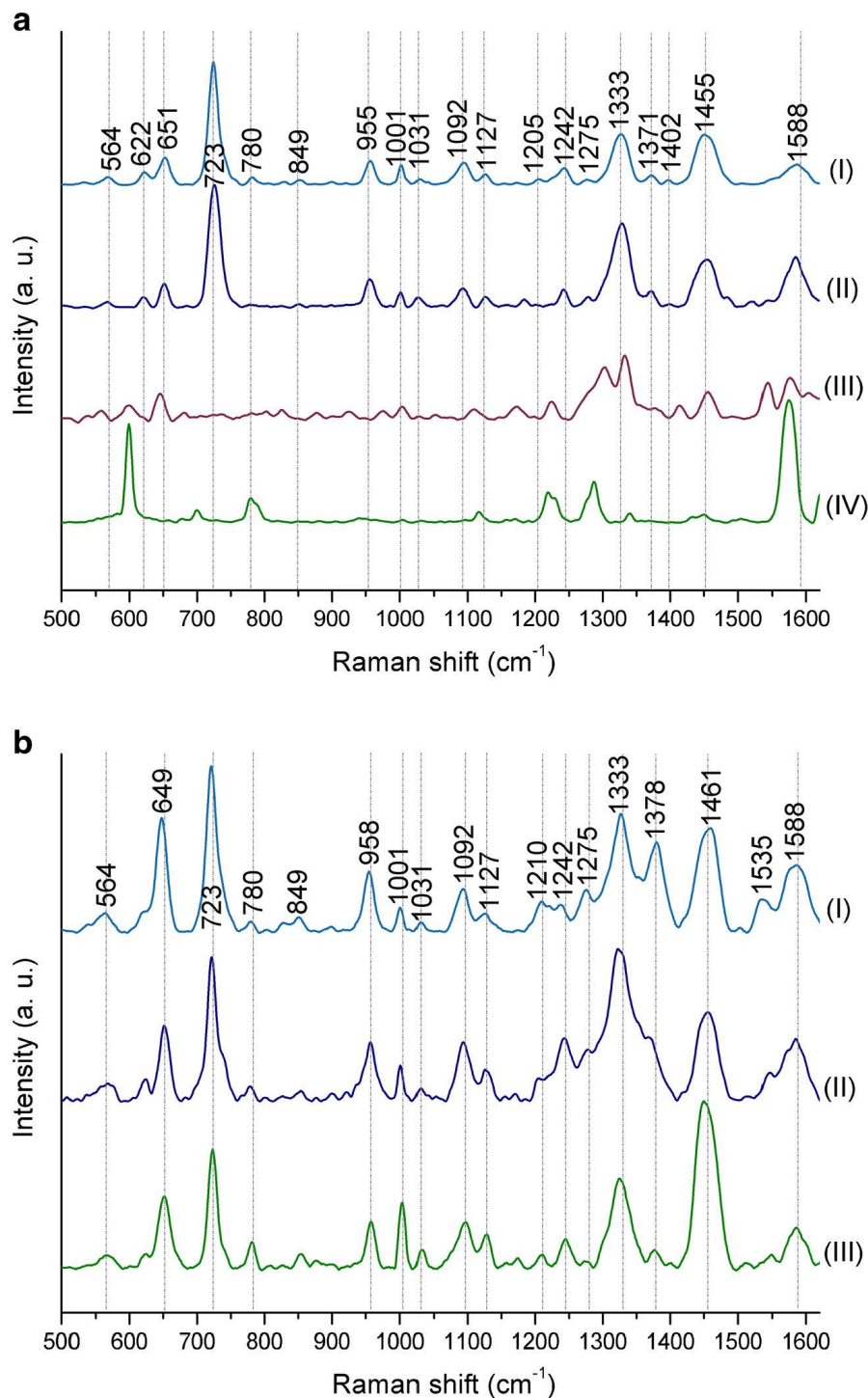
Figure 26. The SERS spectra of (a) E. coli cultured on (I) LB agar, (II) BHI agar, (III) TBX agar, and (IV) CCA media and (b) B. subtilis cultured on (I) LB agar, (II) BHI agar, and (III) MEYP agar media. The bacteria were cultured for 24 h in 37 °C. All presented spectra were averaged from 30 SERS measurements performed on Ag/SSWM SERS substrates with the 785 nm laser line (1.5 mW), baseline corrected, smoothed, and normalized [146].

76

The spectra of *E. coli* cultured on LB agar and BHI agar were very similar (*Figure 26*). The exceptions from those similarities may be observed at around 1330 cm^{-1} and 1590 cm^{-1} – intensities of these bands in the case of BHI agar are higher than for LB agar. In the case of measuring *E. coli* cultured on TBX agar and CCA media, the bands at around 620, 720, 955, 1092, and 1242 cm^{-1}, that were present for results obtained with LB and BHI agar, were absent. Moreover, the spectra of bacteria grown on TBX agar exhibited additional bands at 600, 1173, 1302, 1420, and 1546 cm^{-1}, while the spectra of bacteria from CCA medium demonstrated bands at around 600, 700, 1118, 1225 and 1290 cm^{-1}. Their presence is connected with the chromogenic compounds, which are released during bacterial growth and cover the SERS signal of bacterial cell. Characteristic bacterial bands that may still be observed on spectral image of the bacteria grow on TBX agar medium were 650, 1330, 1450 and 1590 cm^{-1}. In the case of CCA medium, the similarity to other spectra was due to presence of the band at around 1590 cm^{-1}. Its presence, however, is associated with the overlap of two bands: one assigned to bacterial cell and second to chromogenic substrate from CCA medium. That is because the band at around 1590 cm^{-1}, according to scientific sources, may be assigned to: phenylalanine, hydroxyproline, tyrosine, C–N stretching, NH$_2$ scissors, COOH antisymmetric stretching, or ring stretching of adenine / guanine.

Investigation of the influence of bacterial culture time on the spectral image. In order to determine the influence of bacterial growth time on their SERS spectrum, the tested bacteria were grown for 24, 48 and 72 h at 37 °C. For the experiment, the LB agar was selected, as it exhibited the smallest contribution to the spectral image of the bacteria. The composition, the structure, the amount along with the type of produced metabolites at different times of cultivation may influence the bands observed in the SERS spectrum. I have conducted measurements on optimized SERS platforms, after the indicated cultivation times has passed. For viable *E. coli* and *B. subtilis* cells, after 24 h, 48 h, or 72 h of cultivation, three single colonies were placed via a sterile plastic inoculating loop into 200 μL of sterile 0.9% NaCl solution, mixed, and centrifuged for 3 min at 1070×g. The centrifugation process in the saline solution was repeated three times to obtain a solution of clean bacterial cells. The purified bacteria were finally suspended in 10 μL of sterile 0.9% NaCl solution. Results are presented in *Figure 27*.

77
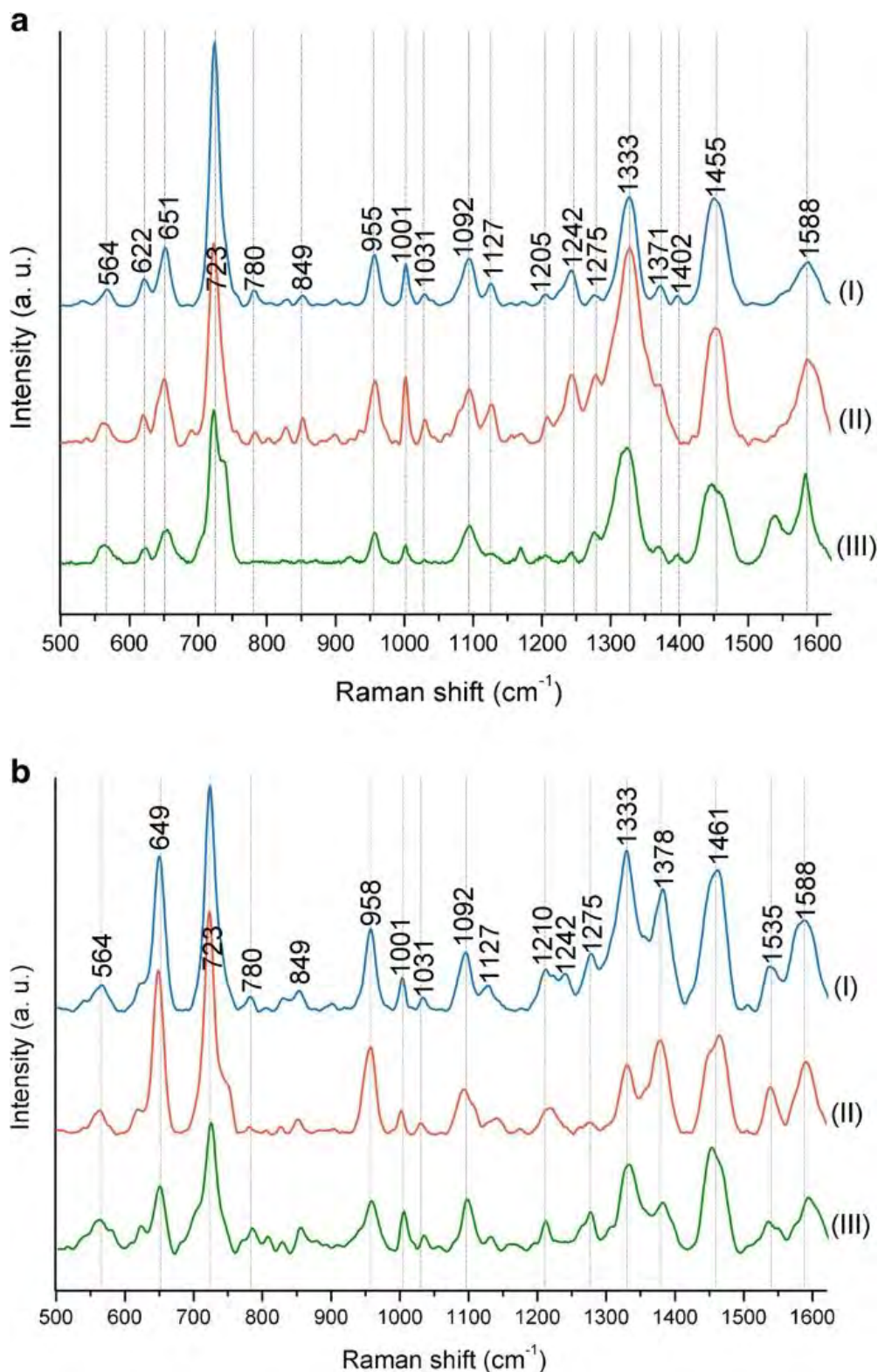
Figure 27. The SERS spectra of (a) E. coli and (b) B. subtilis after (I) 24h, (II) 48h, and (III) 72h of culture on LB agar medium (37 °C). All presented spectra were averaged from 30 SERS measurements performed on Ag/SSWM SERS substrates with the 785 nm laser line (1.5 mW), baseline corrected, and smoothed [146].

For both bacterial species, in the case of measurements performed after 24 and 48 hours of cultivation, most of the bands were well defined by a large signal-to-noise ratio, however in the case of *E. coli,* after 48 hours of cultivation, a slight decrease in the intensity of the band at 725 was observed. After 72 h, for the same bacteria, numerous bands displayed a lower intensity, that is: 780, 850, 1030 and 1130 cm^{-1}. It was similar in the case of *B. Subtilis* after 72 h – a significant decrease in the intensity of the bands at 650 cm^{-1} and 725 cm^{-1} was recorded. These regularities are most likely related to the number of bacterial cells which results in accumulation of metabolite compounds and consequently – death of the cells. As decrease in signal intensity is associated with a longer cultivation time, it is recommendable to apply 24h period of culture for the tested bacteria.

Investigation of the influence of various factors on the condition of bacteria, observable in the SERS spectrum. In order to cause death or structural changes of bacterial cells, previously purified cells of *E. coli* and *B. subtilis* were suspended in 70% ethanol, frozen in saline solution at $-80\ °C$ for 24 h, centrifuged (13.150×g) for 10 min, heated to 100 °C in saline solution for 1 h, and exposed to UV light for 1 h. The measurement conditions and the type of substrates were selected in accordance with the parameters developed in the above-described experiments.
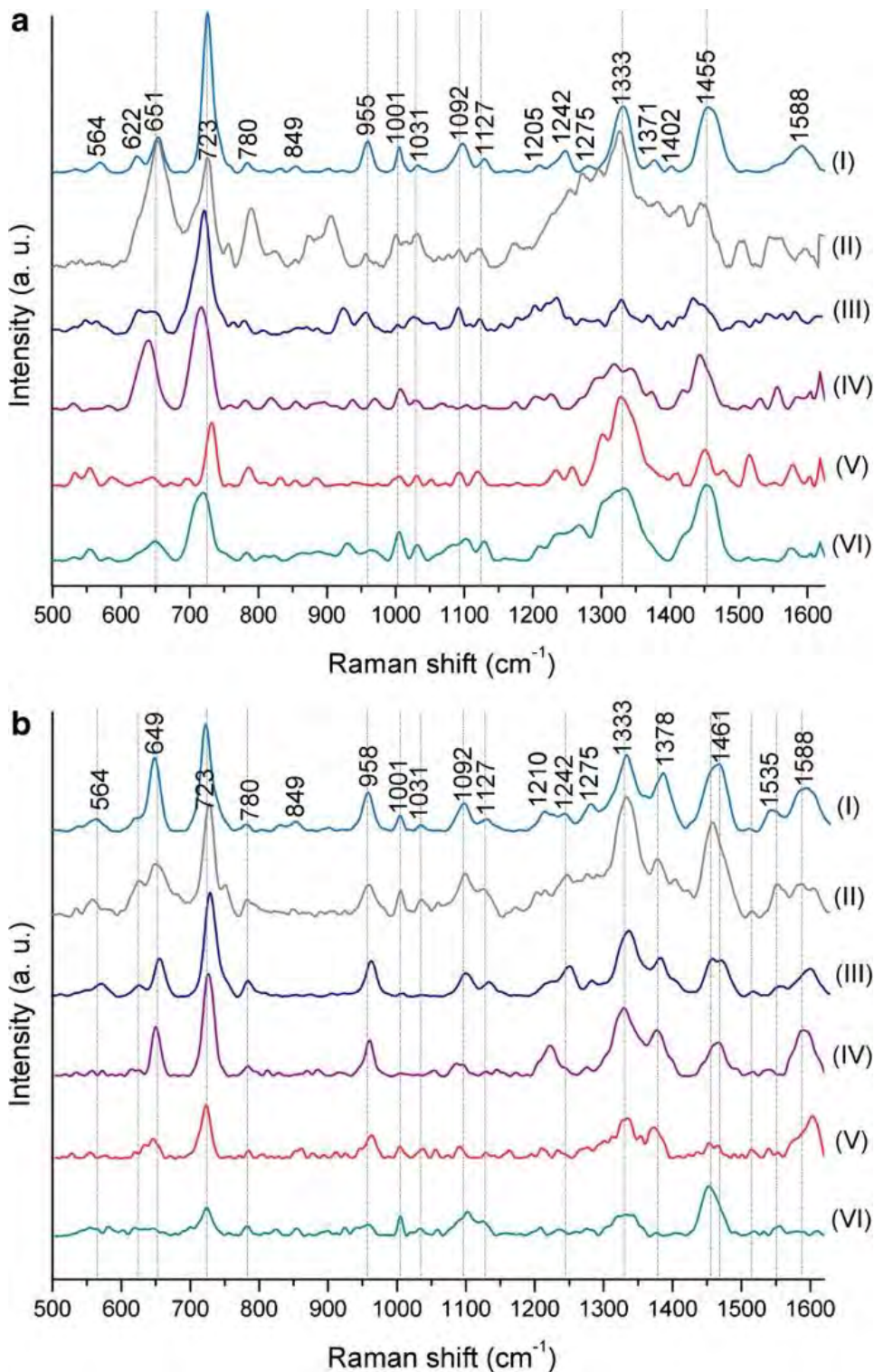
Figure 28. The SERS spectra of (a) E. coli and (b) B. subtilis after pre-treatment, by: (II) suspending in 70% ethanol, (III) freezing in − 80 °C, (IV) centrifugating (13.150×g), (V) heating up to 100 °C, and (VI) exposing to UV light. The averaged (blue) spectrum of the bacterial cells from 24 h culture in 37 °C (I) was given on top (a, b) for comparison. All presented spectra were averaged from 30 SERS measurements performed on Ag/SSWM SERS substrates with the 785 nm laser line (1.5mW), baseline corrected, smoothed, and normalized [146].

As can be noticed in the *Figure 28*, the spectra of both *E. coli* and *B. subtilis* changed drastically after their interaction with alcohol. In case of both species, the bands at around 650, 720, 1330 and 1450 cm^{-1} were unchanged. The same applies to the bands at around 960, 1000, and 1090 cm^{-1} in case of *B. subtilis.* However, the other spectral regions differed significantly. Additionally, in the case of *E. coli*, the increase of the band intensity at around 650 cm^{-1} was attained.

In another series of experiments, the bacteria were exposed to low temperatures. Freezing water, present in living cells, increases its volume and thus destroys the cellular structures. As in the case of ethanol treatment, the SERS spectrum of *E. coli* changed significantly. In comparison to viable bacterial cells, one may observe changes in the intensities and the shapes of various bands. Once again, the spectroscopic image of *B. subtilis* remains virtually the same, with only minor changes in several band intensities.

Similar conclusions might be drawn from the centrifugation experiment, performed at 15 000×g. This process caused significant reductions in *E. coli* vitality in comparison to the one conducted at 5000×g, as *E. coli* cells tend to be extremely sensitive to centrifugation in contrast to other bacterial species, what was demonstrated by Peterson et al [151]. The differences between spectra of 15 000×g and 5 000×g centrifuged *E. coli* were discernible with many bands simply disappearing after centrifugation. This was not the case for *B. subtilis*, as only minor differences may be observed in the region between 1040 and 1250 cm^{-1}.

After heating the bacteria to 100 °C, their proteins denature. Significant changes were visible in the spectra of both species of bacteria. Only the intensity of the 720 and 1330 cm^{-1} bands remained intense in relation to the background.

The SERS experiments were also performed in the case of bacteria exposed to radiation of UV light (more precisely, UVC range of 200-280 nm), as it possesses germicidal properties [152]. It was shown that it damages the DNA structure by dimerizing the thymine bases [153]. The spectra of both species exhibited bands with decreased intensities at around 720, 1000, 1090, 1330 and 1450 cm^{-1}. Other spectroscopic features, characteristic for bacteria, were difficult to observe at the same time.

In the next stage, the effect of the period spent by bacterial cells on the SERS substrate was tested. Having placed the bacteria on the platforms, I have carried out the measurements after 5, 15 and 45 minutes from the same place. The results without spectra normalisation are presented below (*Figure 29*).

81
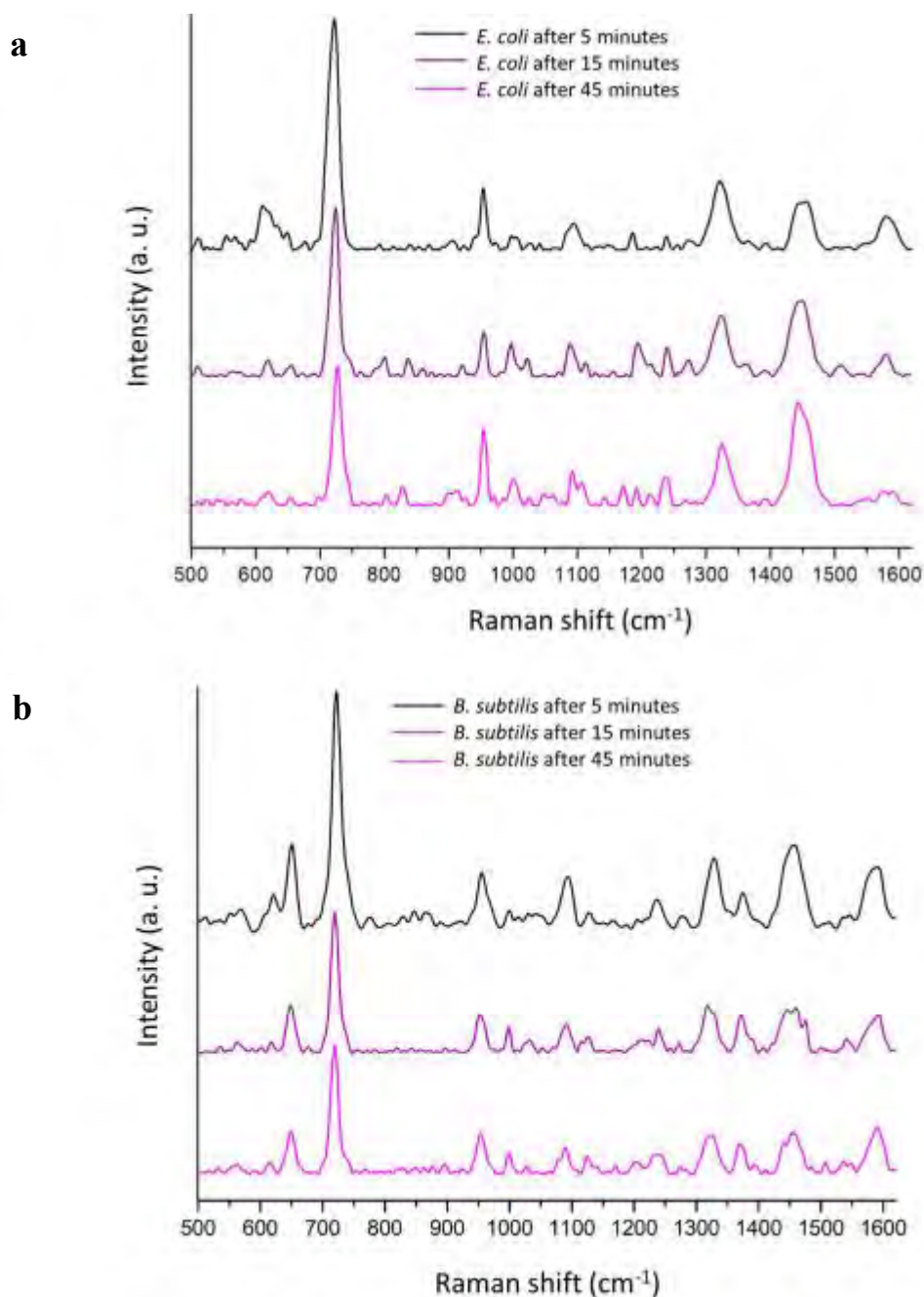
Figure 29. The SERS spectra of (a) E. coli and (b) B. subtilis after 5 (dark violet), 15 (violet) and 45 minutes (light violet) from the sample placement on the SERS substrate. the bacteria were cultured on LB medium (24 h, 37 °C). All measurements were performed on Ag/SSWM mesh SERS substrates with 785 nm laser line (1.5 mW), baseline corrected, and smoothed.

The analysis of the results depicts a decrease in the intensity of the 720 cm^{-1} band and 620 cm^{-1} in the case of both species and additionally the 650 cm^{-1} band in the case of *B. subtilis*. For *E. coli*, an increase in band intensity of around 1460 cm^{-1} was observed, while in the case of *B. subtilis* the intensity of this band decreased. The remaining parts of the spectra did not change significantly, apart from the general decrease in the intensity of the

82

entire spectrum. Due to observed intensity decrease of one of the most important diagnostic bands for bacteria, i.e., approximately 720-735 cm^{-1}, it is recommended that the experiment should begin as soon as possible after the samples have dried. Despite the expected bactericidal effect of silver nanostructures, the presence of bacteria on these structures for up to 45 minutes has minimal impact on the SERS spectrum, but the decrease in spectral intensity indicated a slow death of bacteria.

Conclusions. The results of all experiments indicated factors that influenced significantly the SERS spectra of bacterial cells from *E. coli* and *B. subtilis* species. From the point of view of qualitative analytics, they are of key importance in determining the measurement parameters and conditions for the cultivation and the experiment itself. The developed protocol demonstrates that the following conditions are optimal for conducting an effective SERS-based experiment:

i. Main substrate material ought to be characterized by high surface roughness and should not contribute to the measured SERS spectrum. If this condition is fulfilled, the type of base material used to produce the SERS substrate should not significantly affect the obtained SERS spectra.

ii. Experiments ought to be performed on SERS substrates covered with Ag or Ag/Au (70/30) nanostructures, for which the greatest signal enhancement is obtained.

iii. 633 nm and 785 nm laser lines provided the lowest background fluorescence and the most characteristic SERS spectra of the investigated bacterial cells. Nonetheless, the line 785 nm is recommended for bacteria measurements as it seems to be the best compromise between the signal intensity and background fluorescence. For the 785 nm line the best laser power, that did not cause damage to the sample, was 1.5 mW. Lower laser power, at around 0.80 mW, is also suitable, but to obtain similar intensity as in case of 1.5 mW, the duration of the experiment should be prolonged.

iv. The culture media of choice should not change the colour of the cells. This should only take place if special conditions need to be fulfilled. The example for such situation is the use of chromogenic agars during bacterial detection in food samples, when following ISO protocols. The best selected media, allowing further comparison of SERS spectra of different bacterial species or strains, are nonspecific ones, e.g., LB or BHI agar.

v. The cultivation of bacteria for investigation should not exceed 48 h. The minimum time of 24 h is often needed to obtain perceptible bacterial colonies, but exceeding 2 days results in relevant signal intensity decrease.

vi. Exposure of bacterial samples to conditions causing damage or their death should be avoided. In microbiological laboratories, particular attention must be paid to the optimal temperature window for bacterial cultivation and avoiding the UVC light, that is used to sterilize the laboratory surfaces. Additionally, during sample preparation and centrifugation, in order to separate potential contamination, the lowest possible revolutions per minute (RPM) values should be used.

vii. Duration of the conducted measurement should be as short as possible. Otherwise, the decrease of the band intensity at around 720-725 cm^{-1} may be observed. Additionally, thermal decomposition may take place, unless thermal dissipating SERS medium is used.

The research conducted and described in this subsection allowed for the fulfilment of the second, third and fifth individual thesis goals.

7.2.3 Photovoltaic (PV) cells in the detection of biomedical systems and spectroelectrochemistry using the SERS as a detection method

The developed substrates based on a stainless steel mesh presented in the previous Chapter showed a significant disadvantage. The fact that they are made of metals from the voltage series (on the negative side of the standard potentials in the case of iron and positive in the case of silver), remaining in constant contact with each other, may lead to electrochemical corrosion of the substrate in the perspective of their longer storage. Therefore, substrate preparation should preferably take place immediately before starting the experiment. Even storage in an atmosphere without access to oxygen and moisture does not provide sufficient protection. In addition, the growing cost of preparation, resulting from the need to prepare small batches, is not favourable in the long run. Moreover, studies performed on various types of SERS platforms did not indicate a significant effect on the spectral image of the analyte, irrelevant of the substrates used. Therefore, I developed, and characterized a completely novel type of the substrates based on the experience to date.

The most important factor in selecting a new material is potential to use structures already on its surface to create a plasmonically active material. Among the numerous candidates, fragments of photovoltaic cells that are not obvious in this application seem interesting. Their surface is well-developed for maximising the light scattering and its conversion into electric current using the semiconductor structure [154]. Additionally, they are equipped with electrical contacts, which enable an even voltage increase on the cell

84

surface, that can be used as an electrical contact in a system for spectroelectrochemical analyses. By using the well-known PVD technique to create a silver layer (Ag/PV) with plasmonic properties [155] on a matrix of nanostructures on the cell surface, an efficient platform for SERS measurements might be created. What is more, the platform may be low-cost due to the possibility of using waste from the production of photovoltaic panels in the production. Their usage is an additional advantage in the form of recycling of useless material.

In the following experiments, optimisation of the substrate preparation process, their physical characteristics was performed using SEM, and AFM, while XPS was used to determine the elemental composition of the panel. The enhancement factor was calculated from the intensities of the measured Raman and the SERS spectra for the *p*-MBA reporter Raman molecule. The SERS signal enhancement potential was then used to measure the bacterial signal and a selected tumour cell line. A series of spectroelectrochemical measurements were also performed to test the possibility of observing chemical reactions by means of a spectroscopic image with varying voltage between the electrode-SERS platform and the main solution [156, 157]. **Details on the materials and devices used in the experiments may be found in Appendix 3.**

Preparation and characterisation of Ag/PV SERS substrates. Photovoltaic sample at 40×40 mm was cut off with a glass cutter of a single PV-cell and placed in a beaker filled with an acetone. The first step was sonication for 10 minutes in an ultrasonic bath at 50 °C. Then the acetone was exchanged with isopropyl alcohol and the sample was sonicated again for 10 minutes at temperature of 50 °C. Then, the sample underwent the same procedure in distilled water (Millipore) at ambient temperature. The cleaned photovoltaic sample was subsequently dried for 30 minutes at 50 °C and placed in a sterile Petri dish or immediately placed in a Physical Vapor Deposition (PVD) device and sputtered with a layer of silver. Thus, the prepared SERS platform were ready to use.

In the experiments four different photovoltaic systems. They consisted of three main layers [154]: top layer consisting of blue silicon nitride anti-reflection coating deposited in plasma-enhanced chemical vapor deposition (PECVD) and silver busbars, which played the role of grid contacts (*Figure 31*). *Figure 30* presents the SEM images of the four types of analysed PV devices. Two polycrystalline silicon devices named 1m and 1-types, and two monocrystalline silicon systems named 2 and 3-types were tested. According to their description summarised in *Table* 5, the devices 1m and 1-types differ from each other in the method of preparing the silicon nitride layer (various chemical vapor deposition

processes), which was reflected in the visual properties of these panels, i.e., their colours and gloss.

Table 5. Types and parameters of PV devices used in experiments.

Name of the sample	Type of crystallite	Quantity of top silver busbars/single photo panel	Colour (visual observation)	Thickness of Si (µm)	Thickness range of antireflection layer (nm)
1-type	Poly	4	Different shades of blue from front and side	200 ± 20	88.5–98.8
1m-type	Poly	4	Blue or dark blue from front and dark blue from side	200 ± 20	88.5–98.8
3-type	Mono	34	Dark blue from front	210 ± 20	85.9–88.5
4-type	Mono	4	Black blue from front	210 ± 20	75.6–85.9
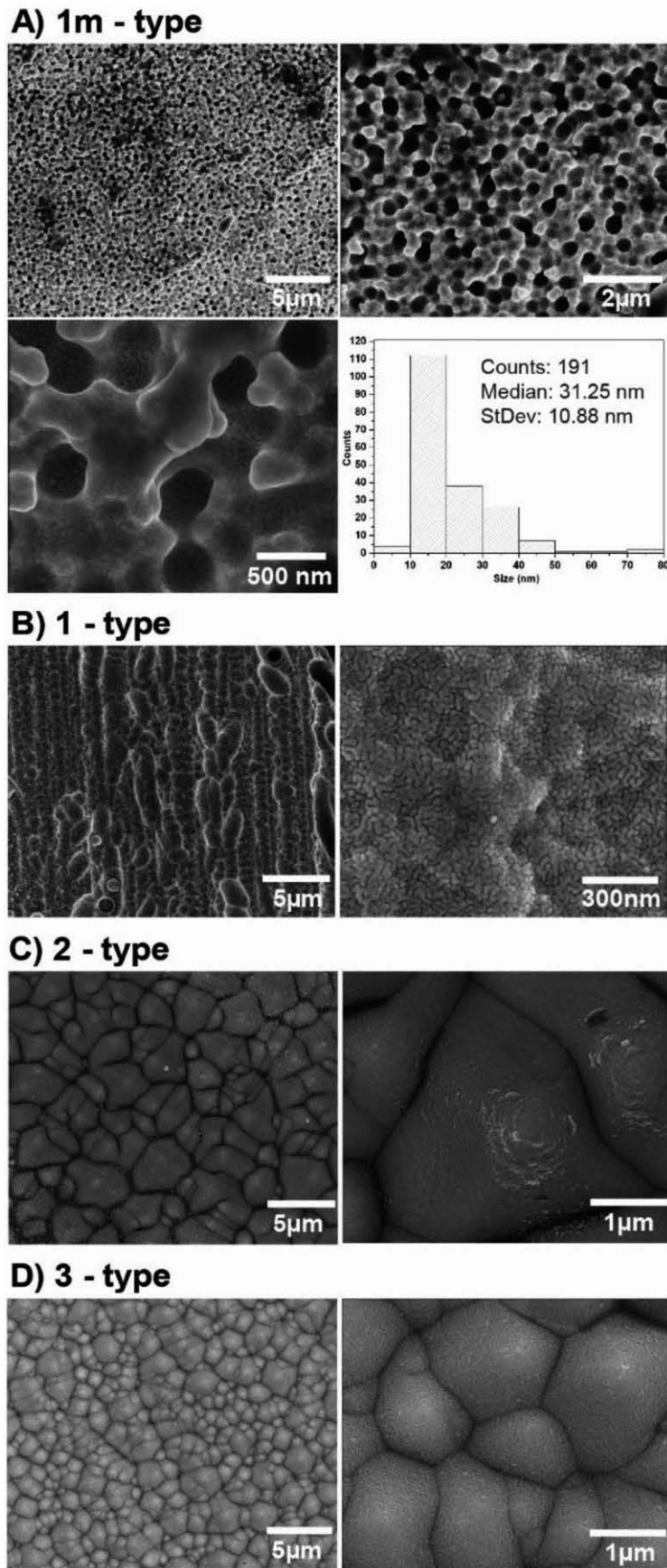
Figure 30. The comparison of SEM images at different magnifications of Ag/PV SERS-active substrates sputtered with 8 nm layer of silver via PVD technique [158].

87
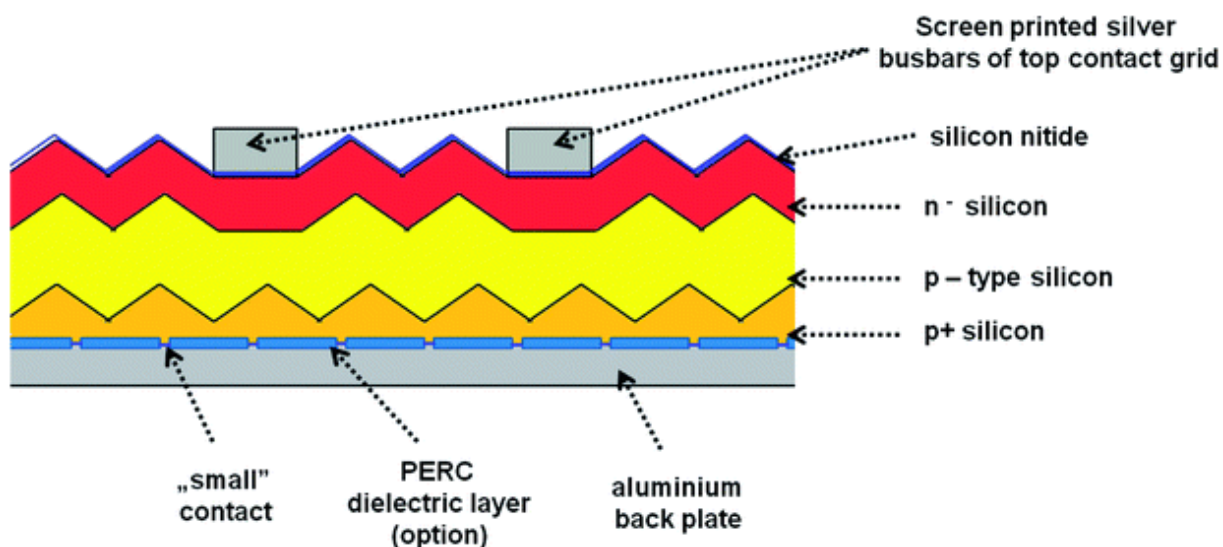
Figure 31. The diagram of the construction of photovoltaic cells [158].

Additionally, the SEM images presented in *Figure 30* of 1m and 1-types of devices, clearly revealed the difference in their morphology. The SEM image of 1m sample depicts that the porous silicon consisted of the network of apertures ranging from 200 to 400 nm. The sample named 1 revealed micrometre sized silicon barrels arranged into plait-like structures. The morphologies of samples named 2 and 3-types were completely different from morphologies of 1 and 1m-types of analysed samples but they were very similar to each other. Both, 2 and 3-types of PV devices exhibited the pyramid-like micrometre sized silicon structures.

The Figure 30 also depicts the results of the structure size analysis for the 1m-type substrate selected in the further part of the study. The calculations were conducted in Image J software by measuring and averaging the size of each of the structures selected in the SEM image three times. The results are presented in the form of a histogram. The size of the nanostructures on the surface was about 31 nm with a standard deviation of ±11 nm. In the case of the 1, 2 and 3-type samples, the sizes of the nanostructures were 42±19 nm, 43±18 nm and 35±18 nm, respectively. Subsequent SEM imaging did not demonstrate the effect of sputtering with the selected, optimal silver layer thickness on changes in the size of the structures that would exceed the value of the standard deviation.

A) Type - 1m

Height — 1.4 um — 2.0 um

Height — 3.5 um — 10.0 um

Roughness (R_a):120 ± 6 nm

B) Type - 1

Height — 2.0 um — 2.0 um

Height — 3.0 um — 10.0 um

Roughness (R_a): 239 ± 21 nm
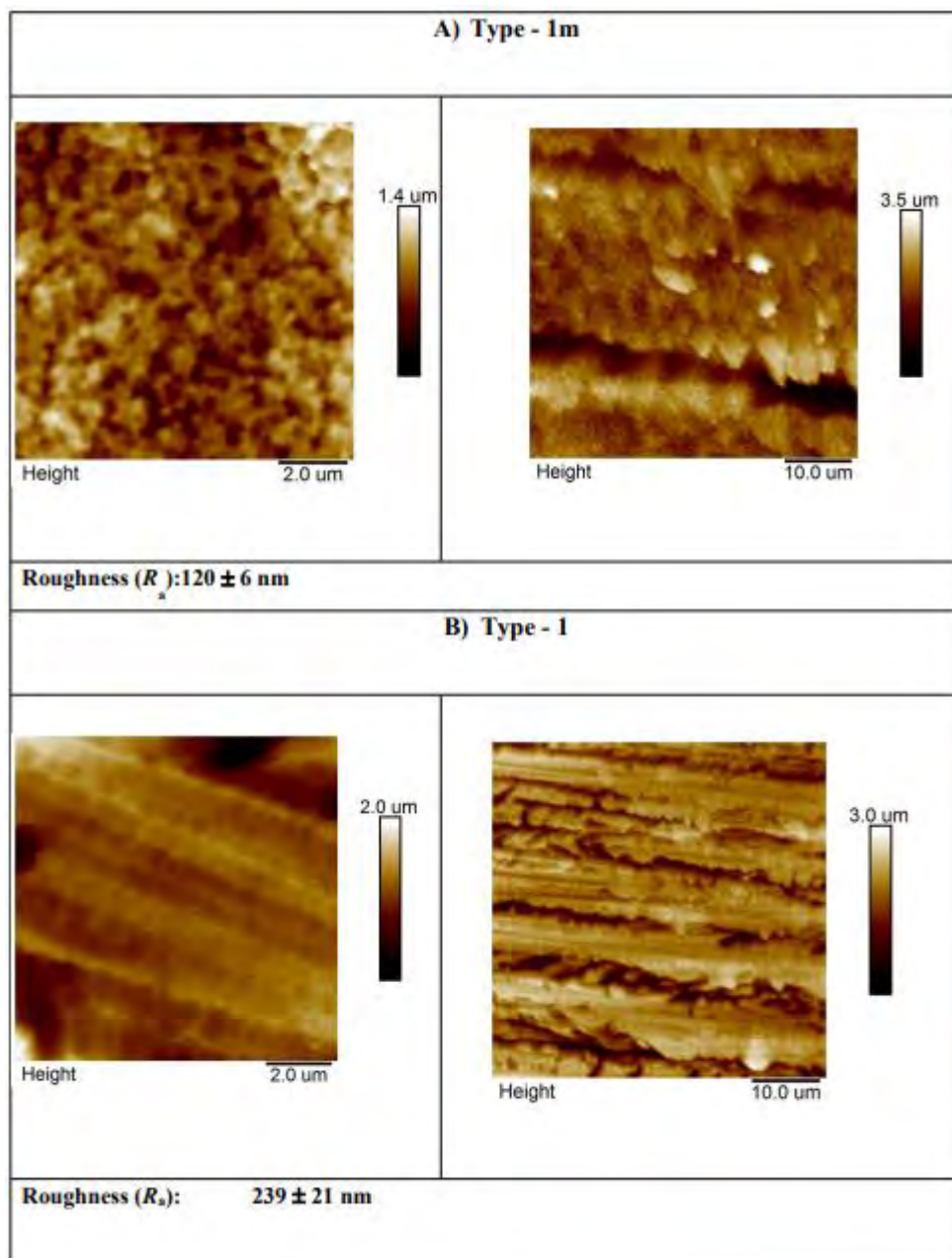
Figure 32. The AFM images at different magnifications of Ag/PV SERS-active platforms sputtered with 8 nm layer of silver via PVD technique.

89
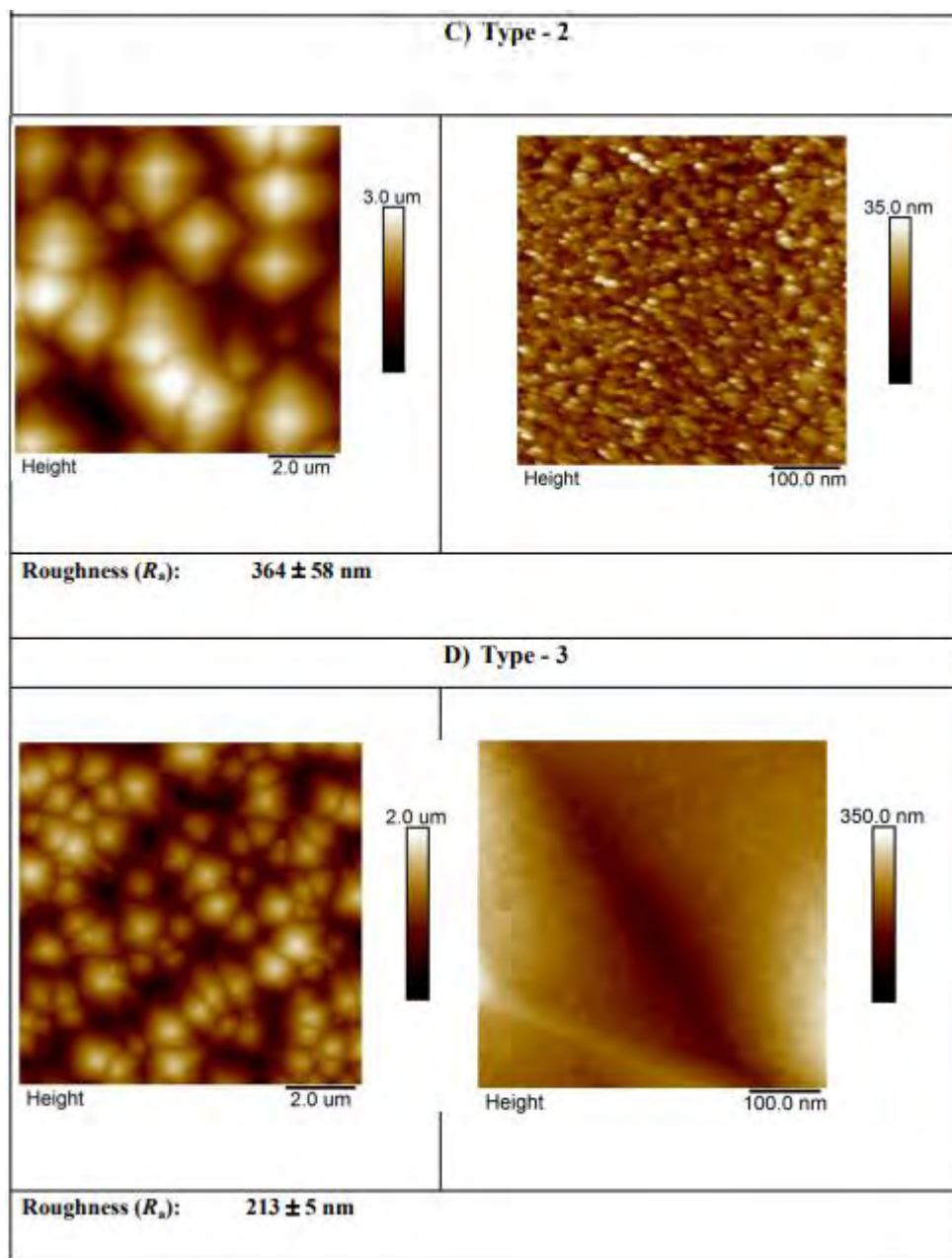
Figure 32. The continuation from page 89.

The above figure (*Figure 32*) presents the AFM images at two different magnifications of all tested Ag/PV SERS-active substrates sputtered with 8 nm layer of silver. These results confirm that sputtering method of fabrication of the SERS-active substrate offers homogeneous coverage of the PV surface with the layer of silver. The degree of the surface roughness RMS (root mean square) of all tested PV samples was determined and is summarised in *Table 6*.

Table 6. The calculated RMS and EF factors for four morphologically different surfaces.

Name of a sample	RMS (nm)	EF
1m-type	120 ± 6	2.1×10^6
1-type	239 ± 21	8.0×10^5
2-type	364 ± 58	1.5×10^4
3-type	213 ± 5	3.0×10^5

It should be highlighted, that all samples posses over 20 times higher value of RMS than the ion-etched silicon, that was tested simultaneously. For the PV based surfaces RMS varied from 120±6 nm to 364±58 nm, where etched silicon demonstrated roughness at a level of 6.6 ±0.6 nm. The effect of the surface roughness on plasmonic structures determinates the SERS efficiency [159]. The observed higher SERS activity for the rougher surfaces is related to the generation of a larger amount of 'hot-spots', which determine the localised plasmon effect and SERS intensity [160].

Table 7. The surface elements concentrations, obtained from XPS measurements.

Sample label	Atomic concentration (%)								
	O	Si	C	N	F	Sb	Pb	Na	Ag
1-type	29.0	25.6	23.5	21.0	0.5	0.2	0.1	<0.1	0.0
1m-type	29.6	34.8	12.8	22.2	<0.1	0.4	0.1	0.2	0.0
2-type	33.7	31.7	11.2	22.0	0.1	0.1	0.6	0.5	0.0
3-type	48.0	27.8	11.4	11.7	<0.1	0.6	0.3	0.3	0.0
1(Ag)	12.6	0.0	25.9	0.0	0.0	0.0	0.0	0.0	61.5
1m(Ag)	15.7	2.8	29.7	0.0	0.0	0.0	0.0	0.0	51.8
2(Ag)	15.2	2.8	22.6	0.0	0.0	0.0	0.1	2.0	57.4
3(Ag)	16.8	3.4	39.9	0.0	0.0	0.0	<0.1	0.0	39.8

The XPS results were summarised in *Table 7* and present the surface concentrations of the detected elements given in (%). As one may observe, for Ag coated PV substrates the major component detected through XPS corresponds to pure silver. The additional presence of oxygen and carbon-related XPS bands might be associated with certain sample contamination, which probably arose during the PVD procedure of applying the silver layer on top of the PV

91

surface [161]. In the case of samples 1m, 2 and 3 exceptionally weak bands at 155 eV appeared, that are attributed to Si (2s) crystalline Si bonding [162]. Crystalline silicon is the main compound of photovoltaic arrays. In the case of unsputtered photovoltaic samples the observed bands correspond to the surface composition of the PV samples.

__Raman-reporter SERS measurements and determination of the enhancement factor.__ I have used the *p*-MBA particle to optimize the thickness of the silver sputtering layer and to determine the value of the enhancement factor. The concentration of the solution from which the acid molecules were adsorbed on the surface of the SERS platforms was again 10^{-6} M, its volume was 2 mL and the adsorption time was 24 h. All four types of samples were sprayed with layers with thicknesses of 5, 8, 10, 15 and 20 nm. The intensity values of the 1078 cm^{-1} band are presented below (*Figure 33*).
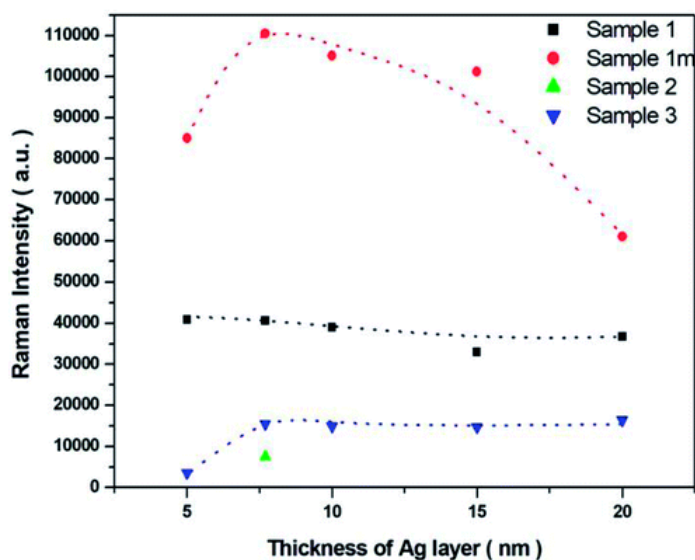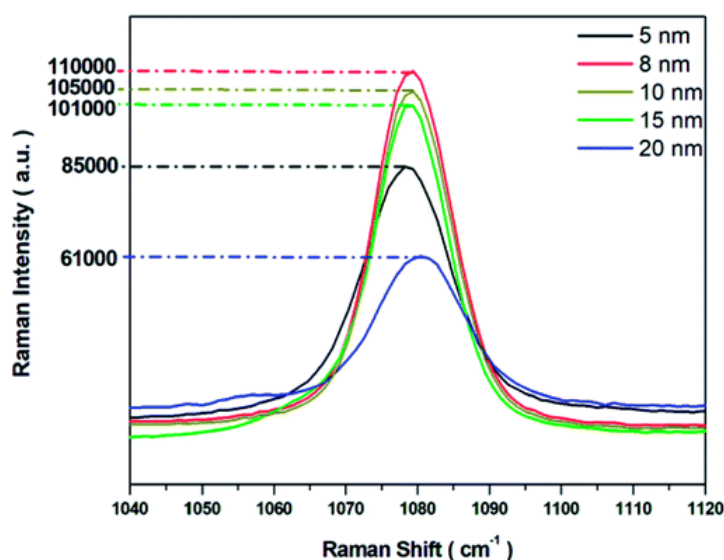
Figure 33. (A) The SERS intensity bands at 1078 cm^{-1} with different Ag metal thickness (5 nm, 8 nm, 10 nm, 15 nm and 20 nm) for the investigated PV surfaces. (B) The intensity of the band at 1078 cm^{-1} for the most SERS-sensitive 1m-type SERS substrate [158].

In case of a 1m-type sample increasing the thickness of the silver layer from 5 to 8 nm also increased the intensity of the band at 1078 cm^{-1}. Further increase in the thickness of the silver leads to a noticeable decrease in the intensity of this band. The 8 nm thick silver layer emerged as optimal to generate appropriate silver nanostructure shape, size and distribution for effective plasmon resonance effect. In the case of samples 1 and 3-type increasing the thickness of the silver layer from 5 to 20 nm led to a minor variety in the intensity of the 1078 cm^{-1} band. For sample 2-type, the SERS signal of the analysed band was only present for 8 nm of the deposited Ag. This sample exhibited exceedingly low SERS

activity due to its morphology: RMS value of 365 nm ± 58 nm was the highest for the all of the examined samples. Moreover, the SEM investigation indicated that the surface of this SERS platform-sample was non-uniform and was composed of different 'islands' of size ranging from hundreds of nm up to even five micrometres. Because of that, the number of possible 'hot-spots' was expected to be low, therefore for 8 nm thick silver layer the low enhancement was observed.
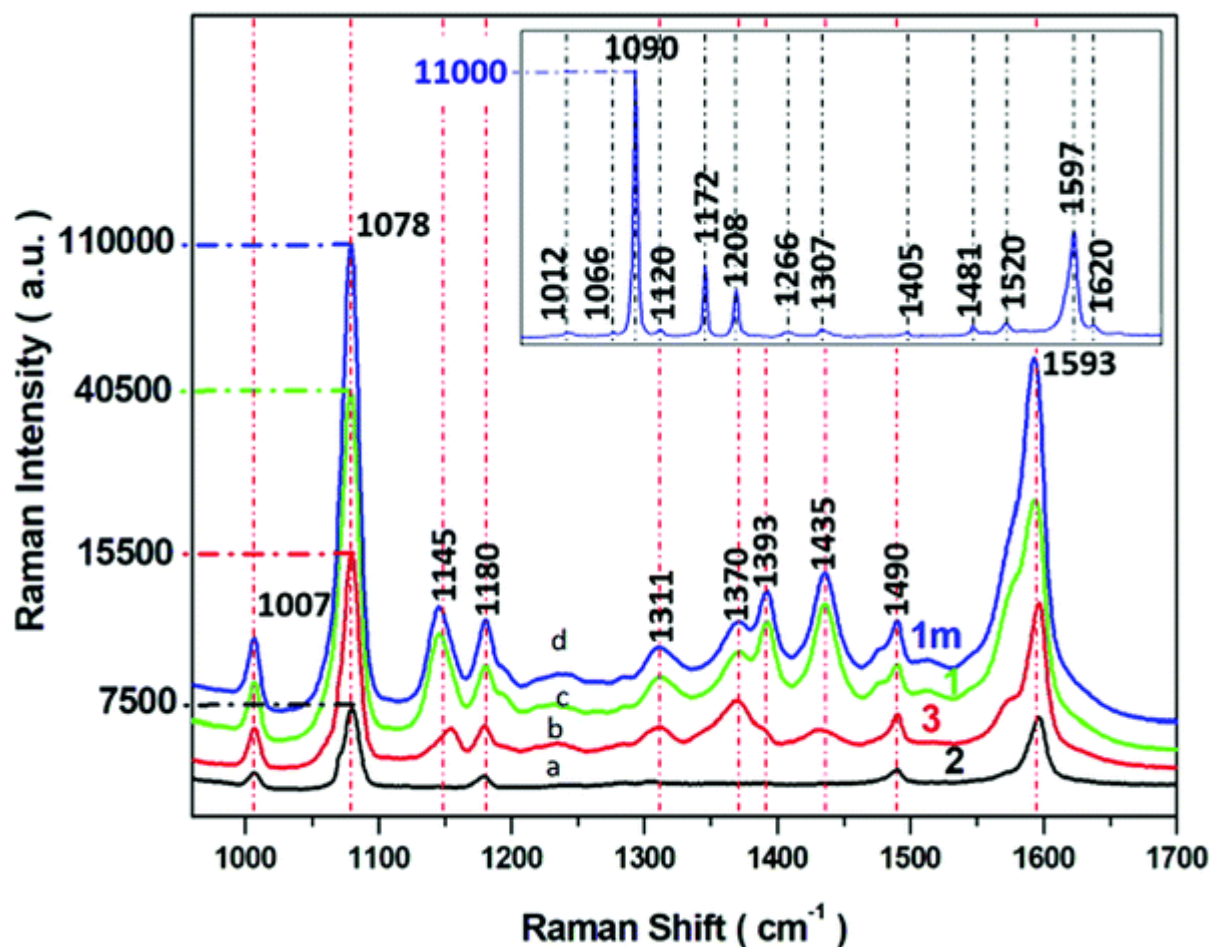
Figure 34. The SERS spectra of p-ATP recorded from four different SERS substrates (a–d) with varying morphology of the PV systems. The spectra acquisition took place under following parameters: 5 mW of 785 nm excitation, 2×2 seconds acquisition time. The insert presents the normal Raman spectrum of p-ATP in neat solid state. Each SERS spectrum was averaged from 40 measurements performed in different places on the SERS surface [158].

As in a previous tests the SERS efficiency of '1m-type' sample covered with a gold layer at different thicknesses was also tested (results are presented in *Figure 34*). The most intensive marker band at 1078 cm^{-1} appeared at 5 nm of Au thickness, but it was still 20 times lower that the intensity of this band recorded for the Ag layer.

The conclusion from the experiments, that included adsorbing and measuring the spectra of *p*-MBA on different silver-thicknesses, is that the 8 nm thickness of the Ag metal film led to the optimal morphology for the most efficient SERS response. This particular structure was applied to our further studies. In order to confirm the homogeneity of the substrate and the reproducibility of the SERS platform preparation process, compilation of non-averaged spectra collected in the mapping mode and a compilation of averaged spectra from several production series were made. The spectra from these analysis are presented in *Figure 35* and *Figure 36*.
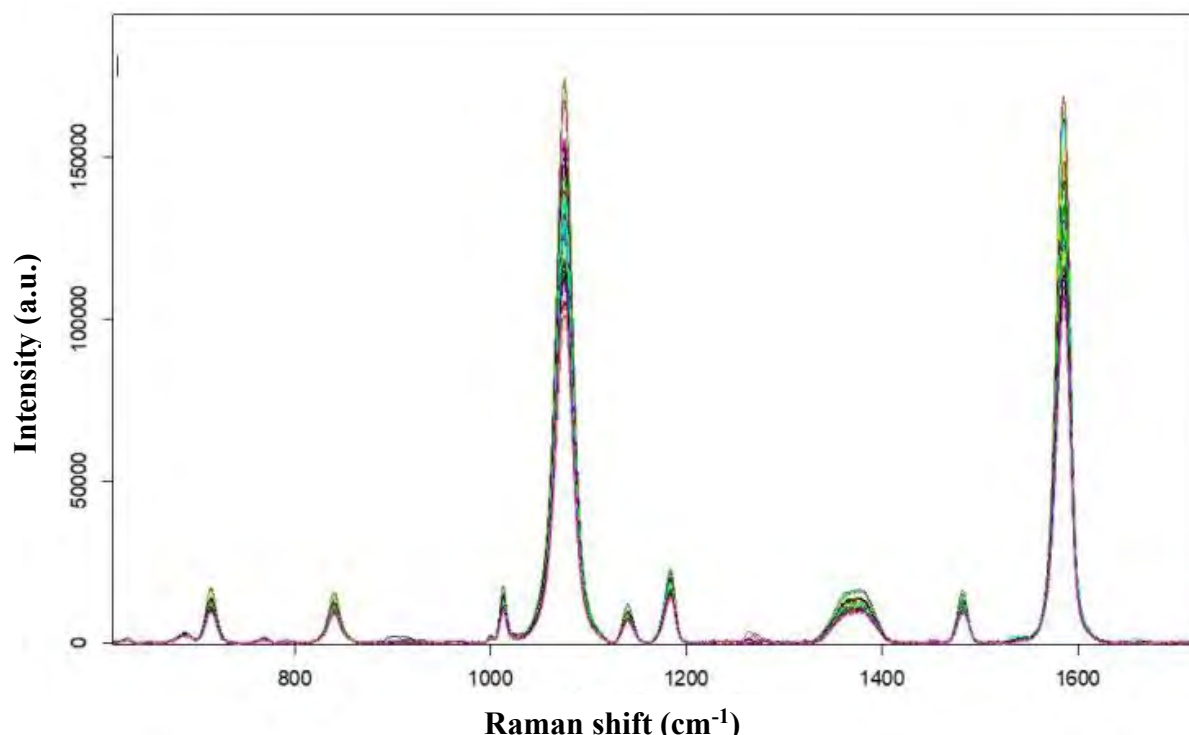
Figure 35. The SERS spectra of p-ATP solution in ethanol at 10^{-6} M concentration recorded from 40 different spots on the 1m-type SERS surface. The spectra were collected over an area 10x20 µm with 1.6 steps µm in mapping mode. The total of 40 spectra are presented. Each point in the map was recorded using 1.5 mW of 785 nm excitation with 18 seconds integration times [158].
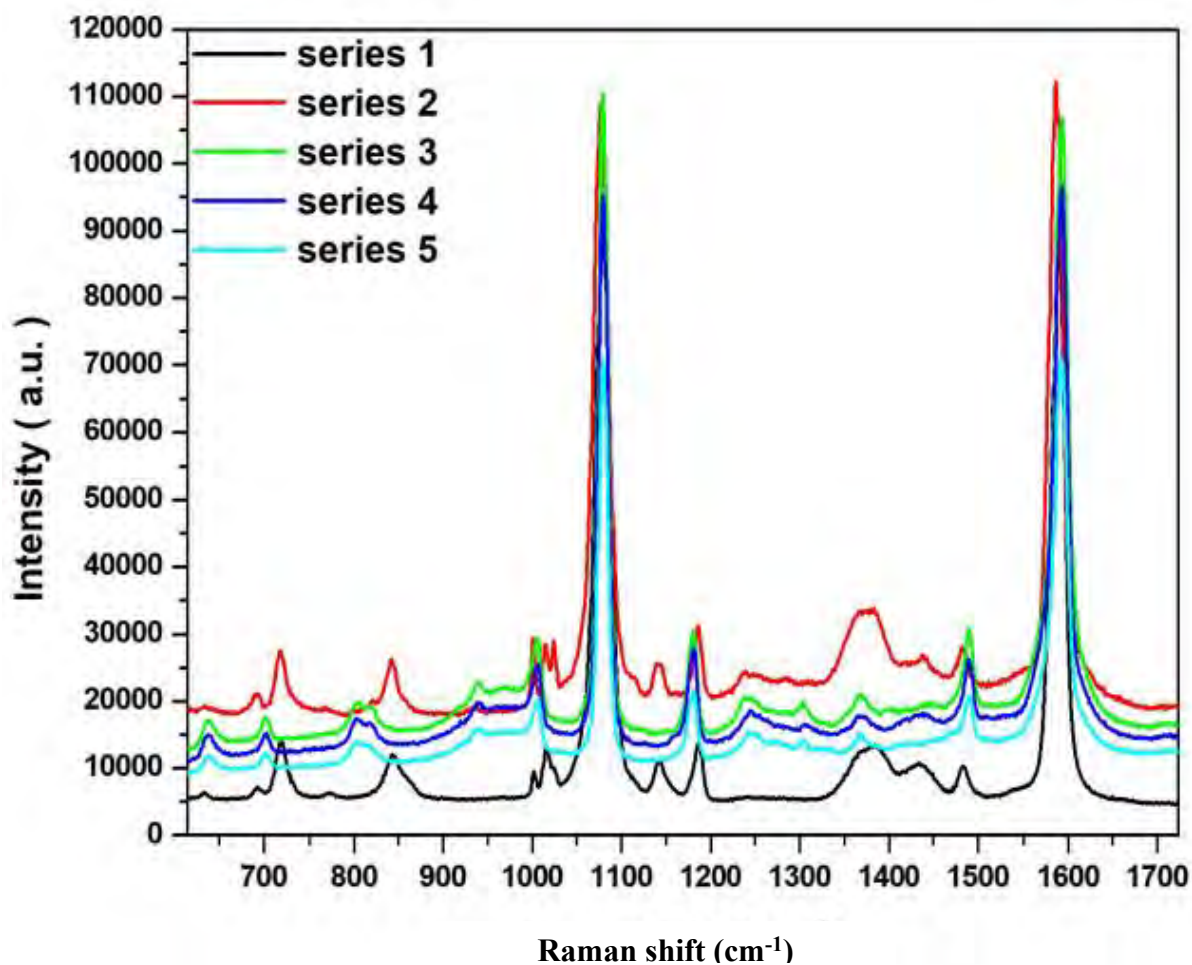
Figure 36. The SERS spectra of p-ATP solution in ethanol at 10^{-6} M concentration recorded from 40 different spots on the 5 different 1m-type SERS surfaces. The spectra were collected over an area 10x20 μm with 1.6 steps μm in mapping mode. The total of 40 spectra are presented. Each point in the map was recorded using 1.5 mW of 785 nm excitation with 18 seconds integration times [158].

The SERS efficiency of all obtained types of surfaces (1m, 1, 2, 3) was quantified by the calculated enhancement factor (EF) using *Equation 13*. The results are presented in the *Table 6*.

The obtained results clearly indicate that the optimal morphology corresponds to the roughness of the 1m-type sample. The calculated value of roughness (120±6 nm) corresponding to the most efficient SERS properties was the lowest among all the tested PV surfaces. Additionally, sample 1m-type exhibited completely different morphology than the rest of the studied samples. The remaining samples did not possess any porous structure and did not exhibited the pyramid / barrel-like structures with the dimensions in the micrometre range. The rough surface of 1m-type was responsible for the appropriate amount of 'hot-spots', which in consequence, most efficiently supported the localized plasmon resonance

response. These results demonstrates that, in addition to the thickness, also the roughness of the metallic layer was an important parameter in the SERS enhancement [163-165].

Spectral image of prokaryotic and eukaryotic cells obtained by the SERS effect on Ag/PV platforms. All of the experiments with eukaryotic material were performed on human cancer cell line Caki-1 that was commercially available. The cell line was purchased from the ATCC collection. The Caki-1 cells were cultured in RPMI-1640 medium, supplemented with 10% FBS, penicillin (100 $U \times mL^{-1}$), and streptomycin (100 $\mu g \times mL^{-1}$). The culture was maintained in a 95% humidified atmosphere of 5% CO_2 at 37 °C. For the experiments the cells were cultured in 25 cm^2 cell culture flasks. After reaching 80% of confluence, the cells were washed with PBS, trypsinised (0.05% trypsin, 0.02% EDTA solution), collected, and centrifuged at $250 \times g$ for 5 min at room temperature. Then, cells were washed with PBS and centrifuged again. After centrifugation, cells were re-suspended in 20 µl of PBS and stored on ice.

To multiply microbial organisms, they were cultivated in LB agar (Lysogeny broth agar) at 37 °C for 24 h. Consequently, 3-4 single bacterial colonies of ~2 µm in diameter were suspended in 500 µl of 0.9% NaCl solution (saline solution) and centrifuged for 5 min at 4000 rpm. Next, the supernatant was discarded and the bacterial cells were re-suspended in 500 µl of saline solution. The centrifugation process in the saline solution was repeated 4 times to obtain a solution of clean bacterial cells. In the final step, the supernatant was completely discarded and the bacteria cells were transferred via a pipette and placed onto a SERS substrate. The SERS measurements were taken after 10 minutes, to let the water evaporate. The SERS spectra of renal cell carcinoma (Caki-1), *Bacillus subtilis* and *Escherichia coli were recorded* as examples of a possibility of detection of cancer and bacterial species thanks to the novel, optimised platforms (*Figure 37*).

A) *B. subtilis*
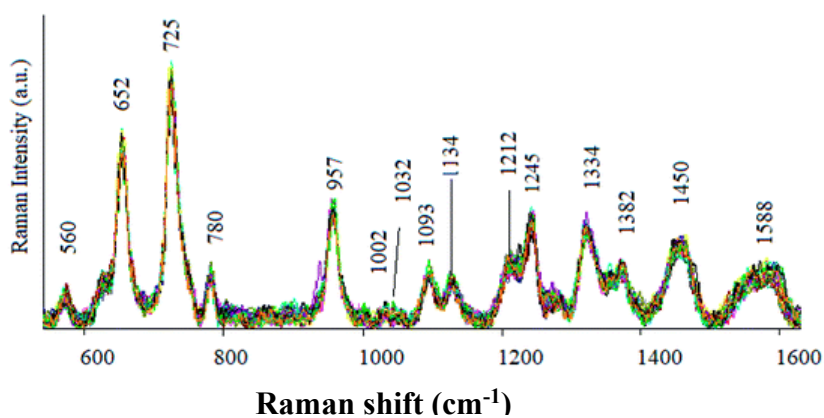
B) **Caki-1**
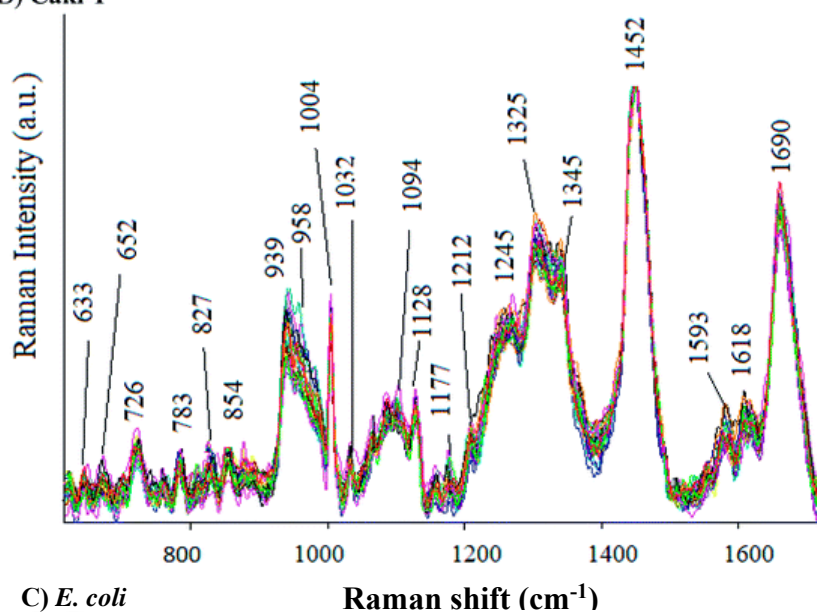
C) *E. coli*
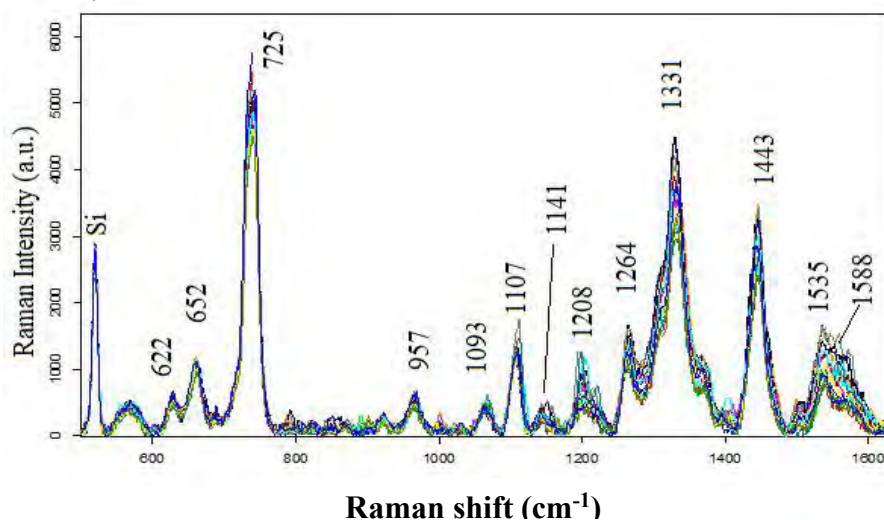
Figure 37. The SERS spectra of B. subtilis (A), Caki-1(B) and E. coli (C) recorded on Ag/PV substrate in mapping mode from 40 different points in mapping mode (10×20 μm). For all the spectra, excitation wave length was at 785 nm, laser power was 1.5 mW, and acquisition time was 3 seconds [158].

98

As in the previous experiments with *E. coli* and *B. subtilis*, strong bands may be observed at 652, 725, 957, 1093, 1275, 1334, 1382, 1450 and 1580 cm^{-1} and weaker bands at 560, 780, 850, 1002, 1030, 1212 cm^{-1}. As for the diagnostic bands that distinguish these two species are 622, 1265 and 1535 cm^{-1} and may be observed only in the spectrum of the *E. coli*, whereas the bands located at 1032, 1208 and 1245 cm^{-1} - only in the spectrum of *B. subtilis*. Also, the intensity differences of some bands should be taken into account while distinguishing them. It is noteworthy that in the case of the experiment with the bacterial detection, the spectra presented were collected from 70 measurement points in the mapping mode.

The SERS spectra of renal carcinoma cells (Caki-1) depict the spectroscopic features characteristic for the main component of eukaryotic cells [166], those are: lipids, nucleic acid, and proteins. The bands around 1245 and 1660 cm^{-1} may be assigned to Amide I and Amide III bands, respectively. Aromatic amino acid contributions appeared around 652 cm^{-1} (C–C twist of tyrosine); 726 cm^{-1} (C–S in protein, CH$_2$ rocking, adenine); 1004 cm^{-1} (C–C of phenylalanine); 1170 cm^{-1} (C–H in a plane of tyrosine or nucleic acid); 1618 cm^{-1} (vC[double bond, length as m-dash]C), tryptophan, tyrosine [167-171]. The vibrational modes of nucleic acid were revealed at 783 and 1094, 1325, and 1458 cm^{-1} [172]. The band at 1032 cm^{-1} (CH$_2$CH$_3$ bending modes of lipids) and 1452 cm^{-1} contributed to the structural protein modes of tumours [173, 174]. Phospholipids, elastin, and collagen were also recognized to exhibit a signal representation in this spectral region [175].

Additionally, the presence of bacteria and neoplastic cells on the surface of the media was confirmed by the SEM imaging (*Figure 38*). The dimensions of *E. coli* prokaryotic cells were in the range of 2.0-2.5 µm in length, while the much larger eukaryotic cells were approximately 23-27 µm in diameter.
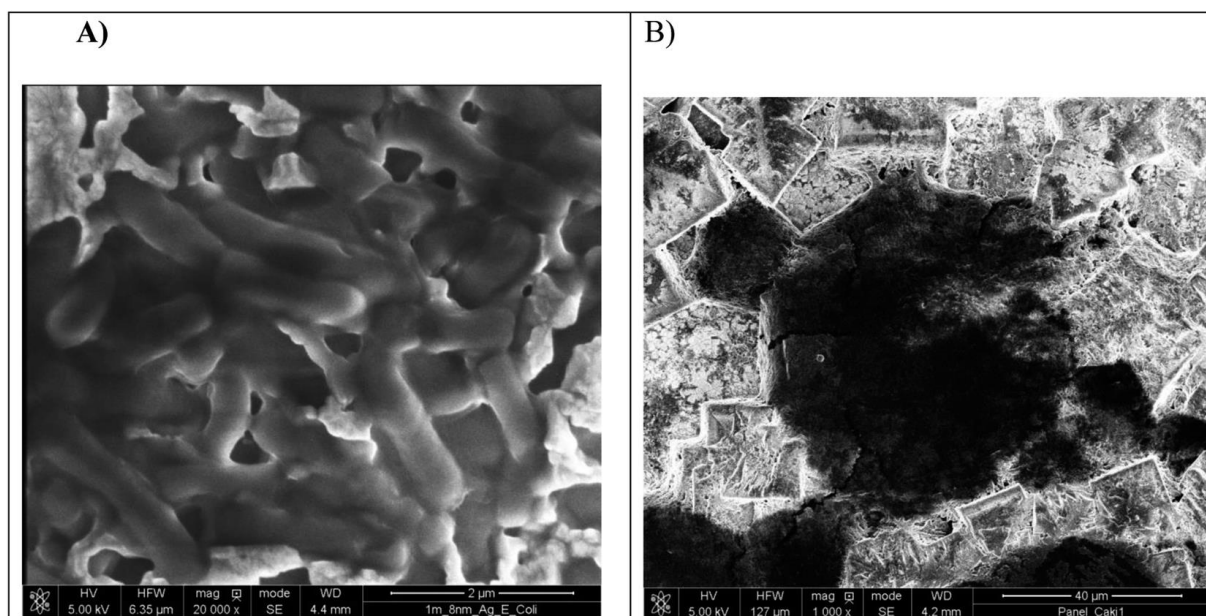
Figure 38. SEM images of E. coli(A) and Caki-1(B) placed onto 1m-type Ag/PV surfaces [158].

Spectroelectrochemical research. Due to the presence of a charge-transfer (chemical) SERS-enhancement mechanism in *p*-aminothiophenol (*p*-ATP) adsorbed onto Ag substrates, its molecule is to be studied in terms of the contribution of electromagnetic and CT to the total SERS enhancement [176-178]. It was demonstrated that spectral features of *p*-ATP originate from chemical (oxidative) transformation of p-ATP to 4.4′- dimercaptoazobenzene (DMAB, an azo compound) during the SERS measurements[179].
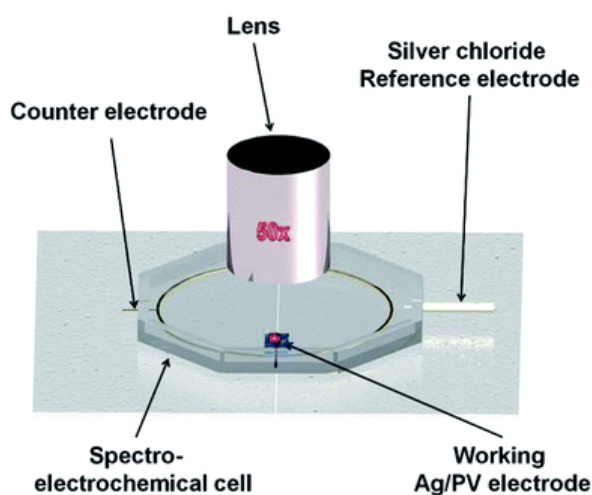
Figure 39. The schematic view of the spectroelectrochemical setup that was used for the analysis [158].

For the recording of *p*-ATP spectra, a 2 μl volume of the analyte solution was applied with a microlitre syringe onto the SERS substrate. The SERS spectra of cancer cells and pathogens were recorded immediately after placing the analysed sample onto the SERS substrate. All bacteria were at the same growth stage at the time of sample preparation. The recording of SERS spectra was completed after ∼10 minutes from placing the sample on the Ag/PV substrate.

The SERS spectra were recorded from 40 different points in mapping mode from a 20×40 μm area of the SERS substrate. The time required for completing a single SERS spectrum was 3 seconds for *p*-ATP and 6 seconds for bacterial and cancer cells, respectively. The electrochemical SERS measurements were performed in a self-designed spectro-electrochemical cell integrated with Renishaw inVia Raman system. The cell was fabricated from a polycarbonate with a window for the SERS measurements and three-electrode holders for the electrochemical control. The Ag/PV SERS-active surface was employed as a working electrode (WE). A platinum wire and Ag/AgCl electrode were used as the counter electrode (CE) and the reference electrode (RE), respectively. The electrode potential was given in reference to the Ag/AgCl electrode (+45 mV). The laser beam (spot size at 2.5 μm) was introduced via optical window and focused onto the three-phase boundary (gas–liquid–solid) formed on the immersed Ag/PV SERS substrate. The potential of a working electrode (Ag/PV) was swept at 2 mV×s^{-1} between −0.1 and −0.9 V in 0.1 M NaClO$_4$.
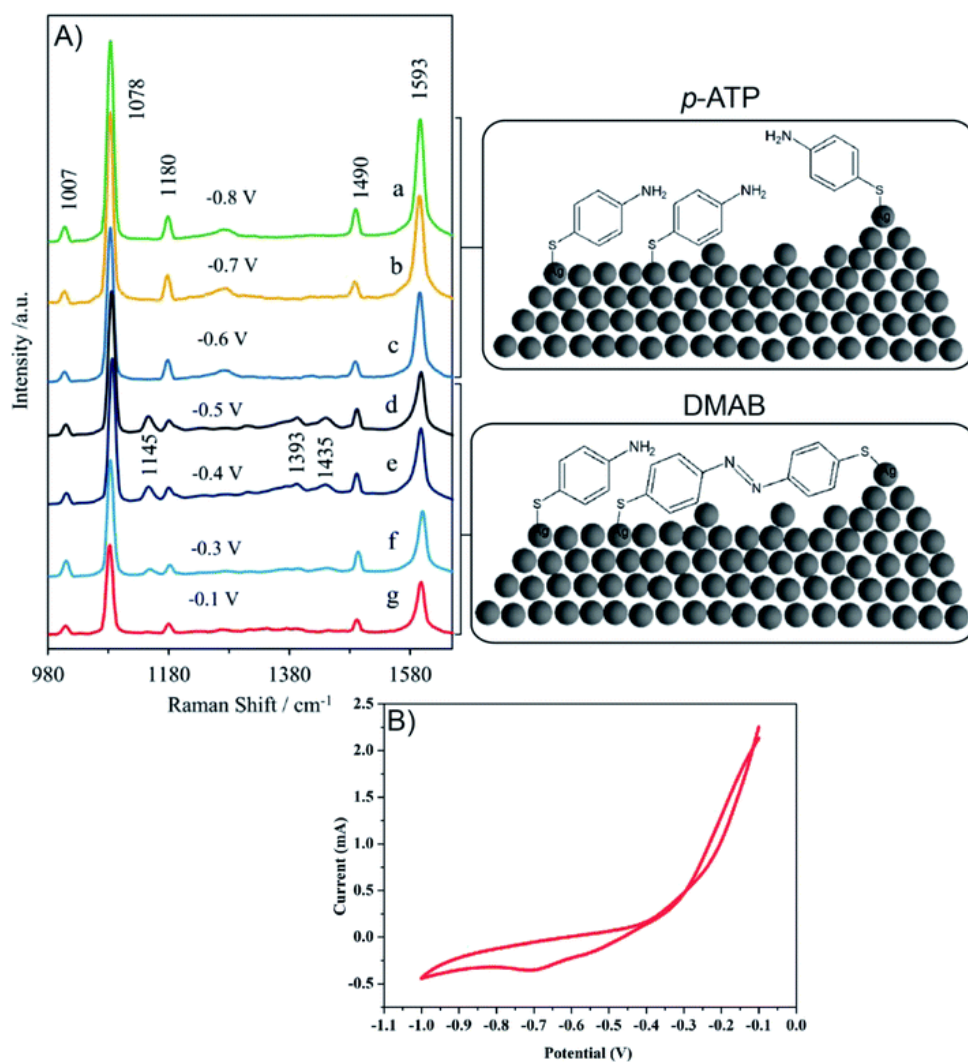
Figure 40. (A) The potential dependent SERS spectra of p-ATP adsorbed onto Ag/PV SERS surface from 10^{-6} M solution of p-ATP in 0.1 M NaClO₄, ('in situ' measurements). (B) The cyclic voltammogram recorded during spectro-electrochemical measurements [158].

The above figures present the spectro-electrochemical setup (*Figure 39*) used for analysis and *in situ* SERS spectra (*Figure 40*) of the SERS surface (working electrode) adsorbed onto Ag/PV in a 0.1 M NaClO₄ aqueous solution. The potential-depended SERS experiments were performed in the region from −0.1 to −1.0 V. According to the CT mechanism, by changing the potential of the SERS-active metal surface, the intensity of several modes may be significantly enhanced by generation of resonance-like Raman scattering [180]. At potential −0.5 V, the *p*-ATP started the transformation via oxidation of *p*-ATP to (DMAB), which was confirmed by the increasing of 'b2-type' modes intensity at 1145, 1393, and 1435 cm⁻¹ [179]. These bands achieved the maximum intensity at −0.4 V. When the potential was moved towards more negative values: ranging from −0.6 to −0.8 V, the recorded spectral features corresponded to presence of *p*-ATP molecule with the

102

characteristic bands at 1078, 1180, 1490 and 1593 cm^{-1}. These results agreed with the distinctive reduction band observed on the presented voltammogram at −0.7 V. The intensity of 'a1-type' modes was insensitive to the variation of electrode potential in comparison to the 'b2-type' modes, which is similar to data presented in literature [180].

Conclusions. I have developed and characterized the new type of SERS substrates. They have been optimised for the optimal LSPR with the selected thickness of the silver layer. In this way, a simple, low-cost procedure for the production of reproducible platforms has been achieved for the detection of bacterial, cancer cells, organic compounds and spectrochemical studies of the CT effect and obtaining a spectral image of the result of voltage-dependent oxidation-reduction cycles of the analyte. The mapping of the substrate has showed its high homogeneity in terms of the distribution of 'hot-spots'. The obtained results are promising for the application of this SERS platform - many types of analyses in the solid-liquid interface mode. The research conducted and described in this subsection led to the fulfilment of the first and fifth of the individual thesis goals.

7.2.4 Ag/PV-based SERS sensor for detection of spectroscopic signature of *Campylobacter*.

Diseases of the post-gastrointestinal tract caused by bacteria are a great threat and danger, especially to children, but also to adults. They are also responsible for economic damage [181]. For bacterial pathogens such as *Salmonella spp., Listeria monocytogenes, Cronobacter sakazakii,* their levels in foods used to be regulated by the Commission Regulation (EU) 2073/2005 [182], while the detection procedure, based mostly on conventional microbiology, is still standardised by International Organization for Standardisation (ISO) [183-185]. In 2017 new Commission Regulation [EU] 2017/1495 [186] has been enacted and indicates that food manufactures and business operators are henceforth responsible for the production and delivery of safe food. Unfortunately, it does not obligate distributors to check the food safety on poultry producers.

According to the European Union reports on zoonotic factors of food diseases among human in 2017 [187], *Campylobacter* was a major infectious agent. The standard methods of detecting thermotolerant bacteria of the genus *Campylobacter* in food are very time-consuming and labour-intensive. Moreover, the most popular methods, ELISA and PCR, permit multiplex detection of several bacterial cells, but require huge libraries of specific

103

antibodies and primers, respectively [188, 189]. Furthermore, in the PCR and ELISA techniques, the false-positive and false-negative results may appear. For this reason, it is desirable to develop modern, fast and cheap methods of detecting pathogens in food with the lowest possible probability of obtaining any false results. In the series of experiments described below, an attempt was made to combine the existing ISO procedure pathway and the detection and identification of *Campylobacter spp.* in food samples. The method involved the use of chemometric PCA for identification by analysing the similarities and differences in the spectra of the bacteria obtained from commercial collections (creating the first such spectral database for bacterial pathogens) and the spectra of bacteria from real food samples. **Details on the materials and devices used in the experiments may be found in Appendix 4.**

   Bacteria strains. Four different *Campylobacter* species, namely *C. jejuni* NCTC 11351, *C. coli* ATCC 33559, *C. upsaliensis* ATCC 43954, and *C. lari* ATCC BAA-1060, as well as *P. aeruginosa* ATCC 27853, were obtained from the Department of Applied Microbiology, Faculty of Biology, University of Warsaw (Poland). The cultures were maintained at −80 °C in Brucella Broth supplemented with 20% glycerol.

   The measurements of the SERS spectra and the PCA analysis of thermotolerant Campylobacter bacteria in order to create a spectral library for subsequent research on environmental material. In connection with the attempt to introduce the detection and identification of bacteria to the existing ISO standards using the SERS method, it is necessary to take a closer look at the chosen path, consistent with the content of the standard (ISO 10272-1: 2017). According to the standard, in order to detect *Campylobacter spp.*, the amount of bacteria in the tested products should be enriched, according to either of two scenarios:

   i.   low numbers of campylobacters and low level of background microflora and / or with stressed campylobacters (procedure A); for example, cooked and frozen products;

   ii. low numbers of campylobacters and high level of background microflora (procedure B); for example, raw milk and meats.

   Then, the food samples should be homogenized in an enriching medium - Bolton (procedure A) or Preston broth (procedure B), depending on the type of food sample. Next, the obtained mixtures ought to be incubated in a microaerobic atmosphere, at 37 °C for 5 hours and then at 41.5 °C for 44 hours (procedure A) or at 41.5 °C for 24 hours (procedure B). Consequently, the surfaces of mCCDA and a second medium, for example, Skirrow agar (procedure A) or only mCCDA agar (procedure B) should undergo an inoculation with

appropriate mixtures via 10 μL loop. Lastly, the samples ought to be incubated in a microaerobic atmosphere at 41.5 °C for 44 ± 4 hours.

At least one colony suspected of being a *Campylobacter* spp. among colonies that would grow is next selected and streaked onto non-selective blood agar plate, for example, Columbia blood agar. After cultivation in a microaerobic atmosphere (that is, with an oxygen level of 2-10%, much lower than that present in the Earth's atmosphere) at 41.5 °C for 24 to 48 hours, well-isolated colonies are used to identify bacteria.

At this point, or at an earlier stage - after growing on the selective mCCDA medium, their identification should take place using SERS spectroscopy combined with chemometric analysis of PCA. Before that, however, one need spectral data - references, i.e., a spectral library. To create it the spectra of *C. jejuni, C. coli, C. lari* and *C. upsaliensis were measured* on mCCDA, Columbia Blood Agar and a second selection medium as the standard does not indicate a specific type. Skirrow agar was selected for the second medium. As previous studies indicated that the type of medium influences the spectral image of bacteria, the database should take into account the type of medium in the PCA analysis process. In accordance with the above procedure, I conducted the measurements, the results of which are presented in *Figure 41*,

Figure 42 and *Figure 43*. All preprocessed data from the experiments, described in this section were subjected to the three-dimensional PCA and the cluster analysis.
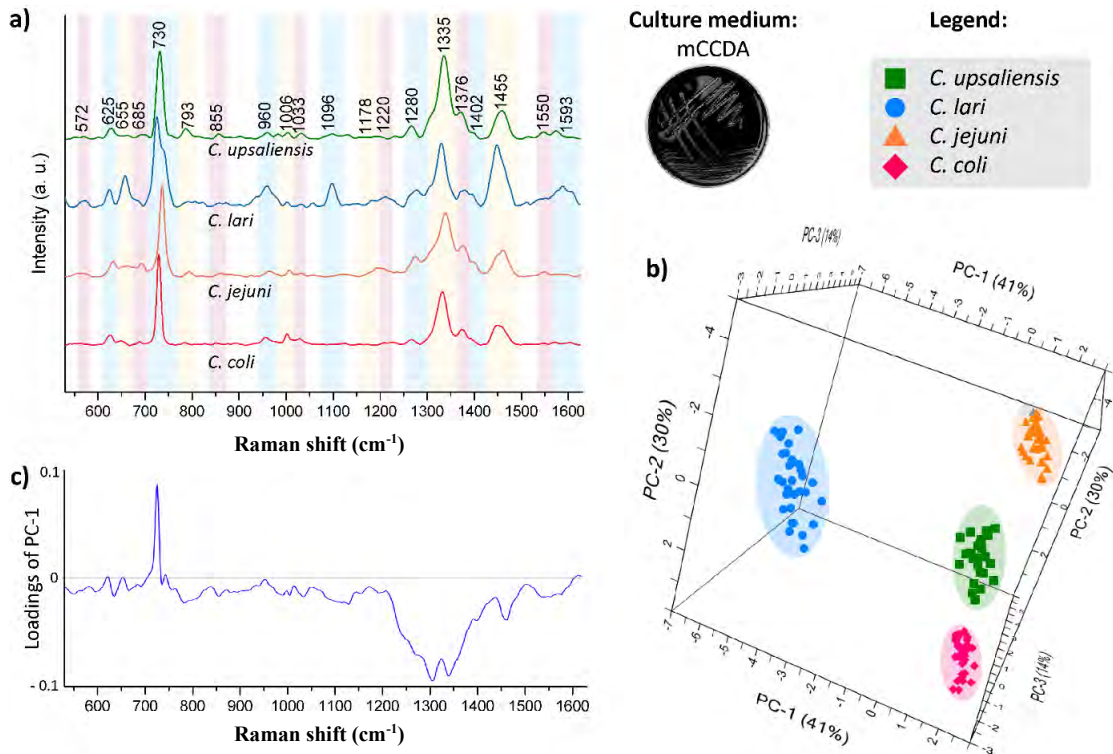
Figure 41. The SERS and PCA results obtained for Campylobacter spp. cultured on modified CCDA agar:(A) averaged SERS spectra, (B) 3D-PCA and (C) loadings plot of the first principal component (PC-1) [190].
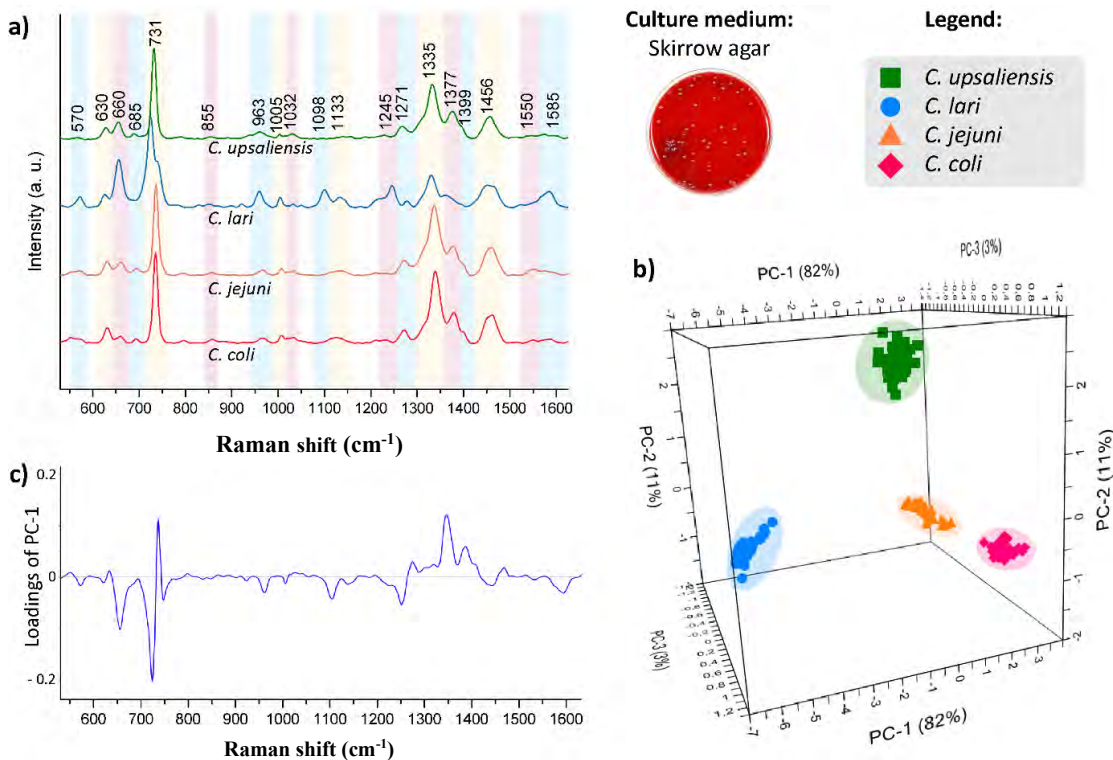
Figure 42. The SERS and PCA results obtained for Campylobacter spp. cultured on Skirrow agar:(A) averaged SERS spectra, (B) 3D-PCA and (C) loadings plot of the first principal component (PC-1) [190].
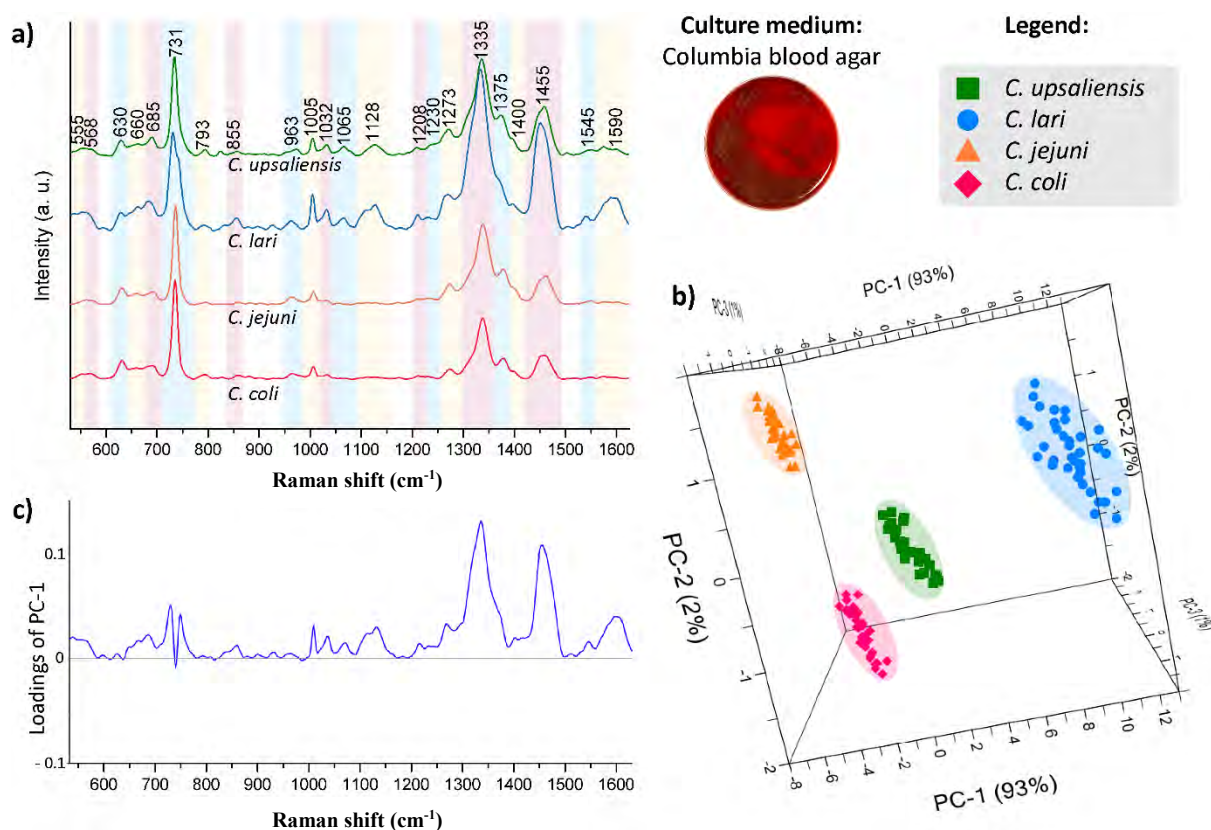
Figure 43. The SERS and PCA results obtained for Campylobacter spp. cultured on Columbia agar:(A) averaged SERS spectra, (B) 3D-PCA and (C) loadings plot of the first principal component (PC-1) [190].

In case of investigation based on mCCDA-medium the differences related primarily to the presence of additional bands and changes in their intensity and shape. In the case of the most prominent *C. lari*, intense bands at around 650, 960, 1100 and 1590 cm^{-1} may be observed. These bands were absent or weak in the case of the three other species. Additionally, in the case of this one, the band at 722 cm^{-1} has a 'shoulder' at about 732 cm^{-1}. It was also noticeable in the spectra of the bacterium cultured on the other two media. The band at 730 cm^{-1} corresponded to in-plane ring breathing mode of adenine or from other adenine-bearing molecules, for example, flavin adenine dinucleotide (FAD) or nicotinamide adenine dinucleotide (NAD) [191]. Additionally, intensity change of this band may appear due to the purine degradation [192]. As for the differentiation of the remaining three species of bacteria, they mainly resulted from the changes in the intensity of the bands at around 793, 1335, 1400, 1455 and 1550 cm^{-1}. Additionally, in the case of *C. upsaliensis*, faint bands around 975 and 1580 cm^{-1} may be observed, absent in the spectra of *C. coli* and *C. jejuni*. Their presence was, as described in previous experiments, related to the components of the bacterial cell wall and membrane. Despite the noticeable spectral

similarities between the bacteria after growing on the selective mCCDA medium, according to the PCA analysis and the combination of PC-1 Loadings in the wavenumber function, it was possible to distinguish them due to the characteristics of the band at around 730 cm^{-1} and the region between 1300 and 1350 cm^{-1}. PC-1, PC-2 and PC-3 summed up together accounted for 85% of the variance in the data.

The results of SERS measurements obtained for bacteria grown on Skirrow agar, that was chosen as a second selective medium to grow the bacteria in ISO procedure, were comparable to those attained from mCCDA. Again, the spectra indicate *C. lari* as the most prominent species and characterised by bands of around 570, 650, 960, 1100, 1130, 1245 and 1585 cm^{-1}, and a shoulder present at around 735 cm^{-1}. In the case of the three remaining species, the changes in the ratio of the intensity at around 630 and around 655 cm^{-1} , and the fluctuations in the intensity of the band around 1550 cm^{-1} were visible. As before, the PC-1 loading table in the wavenumber function showed the most important diagnostic variables in the analysed data set at around 655, 730 and 1330 cm^{-1}. PC-1 together with PC-2 and PC-3 were together accounted for 96% of variability.

In order to confirm the results obtained in the procedures A and B, the standard requires at least one *Campylobacter* suspect colony grown on one of the two selective media to be streaked on a non-selective medium, in our case the Columbia blood agar, for the development of well-isolated colonies. It was then tested to confirm *Campylobacter* identification. Analysing the spectral data again, *C. lari* proved to be the most prominent of the species. The arm at about 735 cm^{-1} was present again. The new details in the *C. lari* and *C. upsaliensis* spectra were visible as bands at approximately 1065 and 1208 cm^{-1}. Differences between *C. coli* and *C. jejuni* were virtually invisible. In the case of the *C. coli* spectrum, there was no band at 1550 cm^{-1}, which in turn was present in *the C. jejuni* spectrum. The analysis indicated the most important contribution to the differentiation of the bacteria studied, the bands at around 1335 and 1455 cm^{-1}, that corresponded to protein vibrational modes. This, in turn, suggested significant differences in the distribution of proteins in the bacterial cell walls. The calculated PC-1, PC-2 and PC-3 reached together the value of 96% of total variance.

In order to make it easier to compare the presence, assignment and intensity of the bands appearing in the spectra of Campylobacter bacteria (grown on different media), the following table was created:

Table 8. The main bands in the SERS spectra of thermotolerant Campylobacter spp.;(-) - absent, (vw) - very weak; (w) - weak, (m) - medium; (s) - strong, (vs) - very strong,(sh) - shoulder, def. - deformation, str. - stretching, tw. – twisting [193-198].

Band assignment	Range in which the band is observed (cm^{-1})	mCCDA				Skirrow agar				Columbia agar			
		Cc	Cj	Cl	Cu	Cc	Cj	Cl	Cu	Cc	Cj	Cl	Cu
C-O-C ring def.	550-575	-	w	w	vw	w	w	m	vw	w	w	m	w
C-C tw. (protein)	620-630	m	m	m	m	m	m	m	m	s	m	m	m
C-S str., C-C tw. of proteins tyrosine	655-665	vw	w	s	vw	w	m	s	m	m	m	m	m
Ring breathing mode of guanine	675-690	vw	m	w	w	w	w	-	vw	m	m	s	m
Adenine (FAD, NAD)	720-735	vs	vs	vs	vs	vs	vs	vs	vs	vs	vs	vs	vs
C-S stretch	735-750	-	-	sh	-	-	-	sh	-	-	-	sh	-
Ring breathing mode of cytosine, uracil	780-790	vw	w	vw	m	vw	vw	vw	vw	w	vw	vw	w
Ring breathing mode of tyrosine & C-C stretch	850-860	vw	vw	vw	w	vw	vw	vw	vw	w	vw	w	vw
C=C def., C-N str.	950-965	w	w	s	w	w	w	m	w	w	w	w	w
Phenylalanine, C-C aromatic ring str.	1000-1010	m	w	vw	w	w	w	w	vw	m	m	s	m
C-N str., C-C str. (phospholipids carbohydrates),	1025-1035	w	vw	vw	w	w	w	vw	vw	vw	vw	m	w
C-C skeletal str. (lipids)	1060-1070	-	-	vw	-	-	-	-	vw	-	-	w	w
O-P-O (DNA), C-C or C-O-C str.	1090-1110	-	-	s	w	-	-	m	-	-	-	m	-
=C-OC= (unsaturated fatty acids in lipids)	1125-1145	-	vw	-	w	w	w	w	-	-	-	s	m
C-O ring, aromatic aa (proteins)	1170-1195	-	w	vw	vw	-	-	-	-	vw	vw	-	-
Amide III (random), thymine	1205-1230	-	w	w	-	vw	-	m	vw	vw	w	m	w
Amide III	1240-1260	-	-	sh	-	-	-	m	-	-	-	-	-
Amide III	1270-1285	w	s	m	m	m	m	w	m	m	m	s	s
Ring breathing mode of guanine, CH$_3$, CH$_2$ tw.	1305-1320	-	-	sh	sh	sh	sh	sh	sh	-	-	-	sh
CH$_3$, CH$_2$ wagging	1325-1335	vs	vs	vs	vs	vs	vs	s	ws	vs	vs	vs	vs
Tryptophan, guanine	1365-1380	m	s	m	s	s	s	m	s	s	s	sh	s
CH rocking, C=O symmetric str.	1395-1405	sh	sh	sh	sh	sh	sh	sh	sh	sh	sh	m	sh
CH$_3$, CH$_2$ def.	1450-1465	s	s	vs	s	s	s	s	s	s	s	vs	s
Cytosine	1500-1530	-	-	vw	vw	-	-	vw	-	-	-	vw	vw
Amide II, tryptophan	1530-1565	-	w	w	w	vw	w	-	-	vw	vw	w	w
C=C bending mode (phenylalanine)	1570-1595	vw	-	s	w	vw	-	s	vw	vw	-	s	w
Amide I, C=C bending mode (phenylalanine)	1600-1630	vw	-	m	-	-	-	-	-	-	-	s	-

In order to verify the presence of bacteria on the surface of the SERS platforms, they were imagined by the SEM immediately after the experiment. The sample images for platform surfaces and *C. jejuni* NCTC 11351 are presented below (*Figure 44*).

109
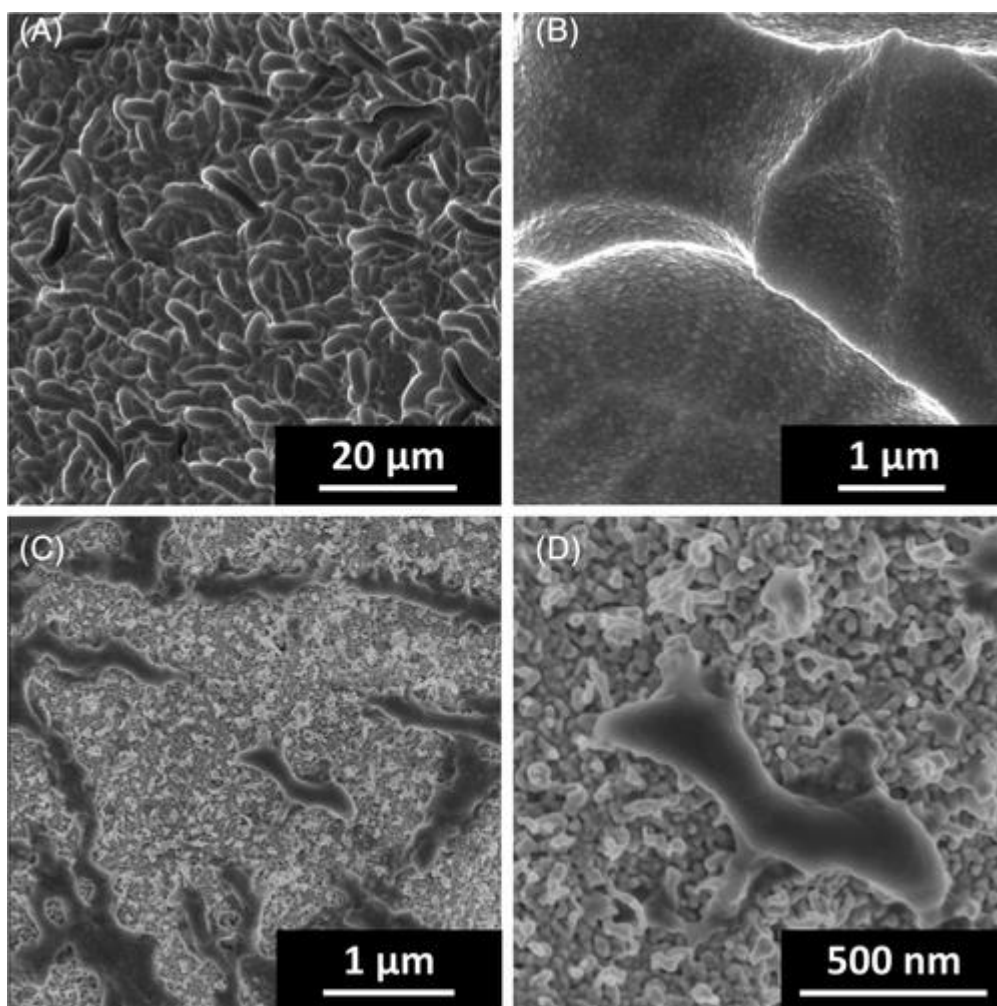
Figure 44. The SEM images, at different magnifications, of (A) and (B), bare surface of SERS substrate and (C), (D) - C. jejuni NCTC 11351 cells on SERS substrate [190].

The application of the ISO-SERS method in the detection of Campylobacter spp. bacteria in food samples. In order to test the proposed combination of the ISO methods with SERS detection, 10 samples of poultry were tested. The samples came from various stores and were packaged and shipped in sterile conditions at low temperature provided by ice and insulating packaging. For the sample preparation, 10×g of each batch of poultry were extracted in an aseptic manner and homogenized in enrichment broth (90 mL). Thus, homogenized meat samples were cultivated in microaerobic conditions at 41.5 °C. After 24 hours of incubation, the mCCDA plates were inoculated with ~10 μm of obtained mixture and cultured for 48 hours.

An important consideration in the examination process of food products is that not only campylobacters might be present on this type of growth medium. For this reason, all colonies differing in morphology were selected and collected with a disposable loop and

separately suspended in a sterile saline buffer. They were then genetically identified using 16S rRNA gene sequencing in the Department of Applied Microbiology, Faculty of Biology, University of Warsaw (Poland). As a result, *Proteus mirabilis*, *Escherichia coli*, and *Campylobacter jejuni* were identified. The last two species occurred only in one of the tested samples. To further enrich the species accompanying our main analyte, a *P. aeruginosa* ATCC 27 853 strain was added to the group of bacteria that were later subjected to the additional SERS identification. It was grown under the same conditions as the other bacteria tested in this part of the study. It is a representative of the cefoperazone-resistant *Pseudomonas* spp. The measurements and results for this experiment are presented in *Figure 45 and Figure 46*.
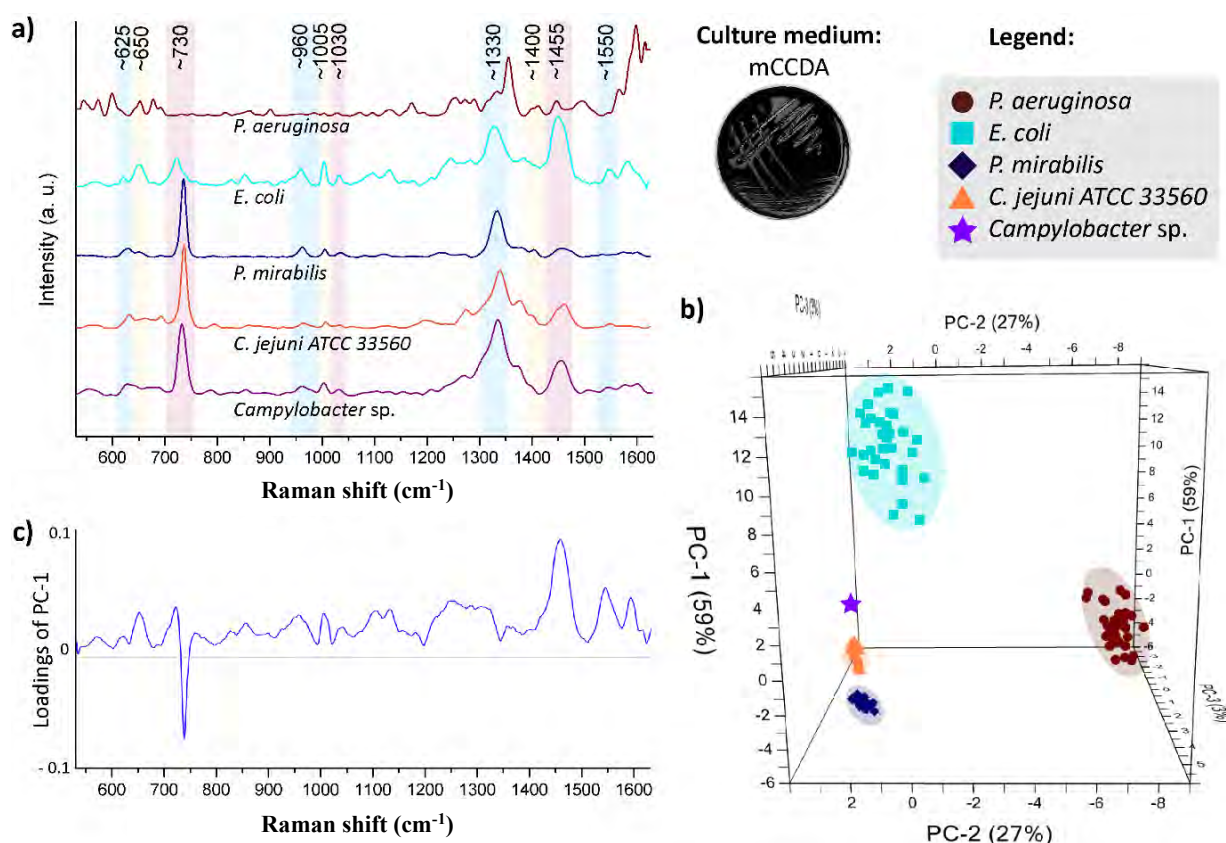
Figure 45. The SERS and PCA results obtained for different bacterial species present in poultry samples and detected on mCCDA; (A) averaged SERS spectra (the SERS spectrum of C. jejuni National Collection of Type Cultures (NCTC) 11351 was added as a control and was given for comparison), (B) 3D-PCA (the points described as C. jejuni NCTC 11351 were added to PCA as a control), and (C) loadings plot of the first principal component (PC-1). The Campylobacter sp. spectrum from image A and violet star from image B represent the averaged SERS spectrum of Campylobacter strain isolated from poultry sample [190].
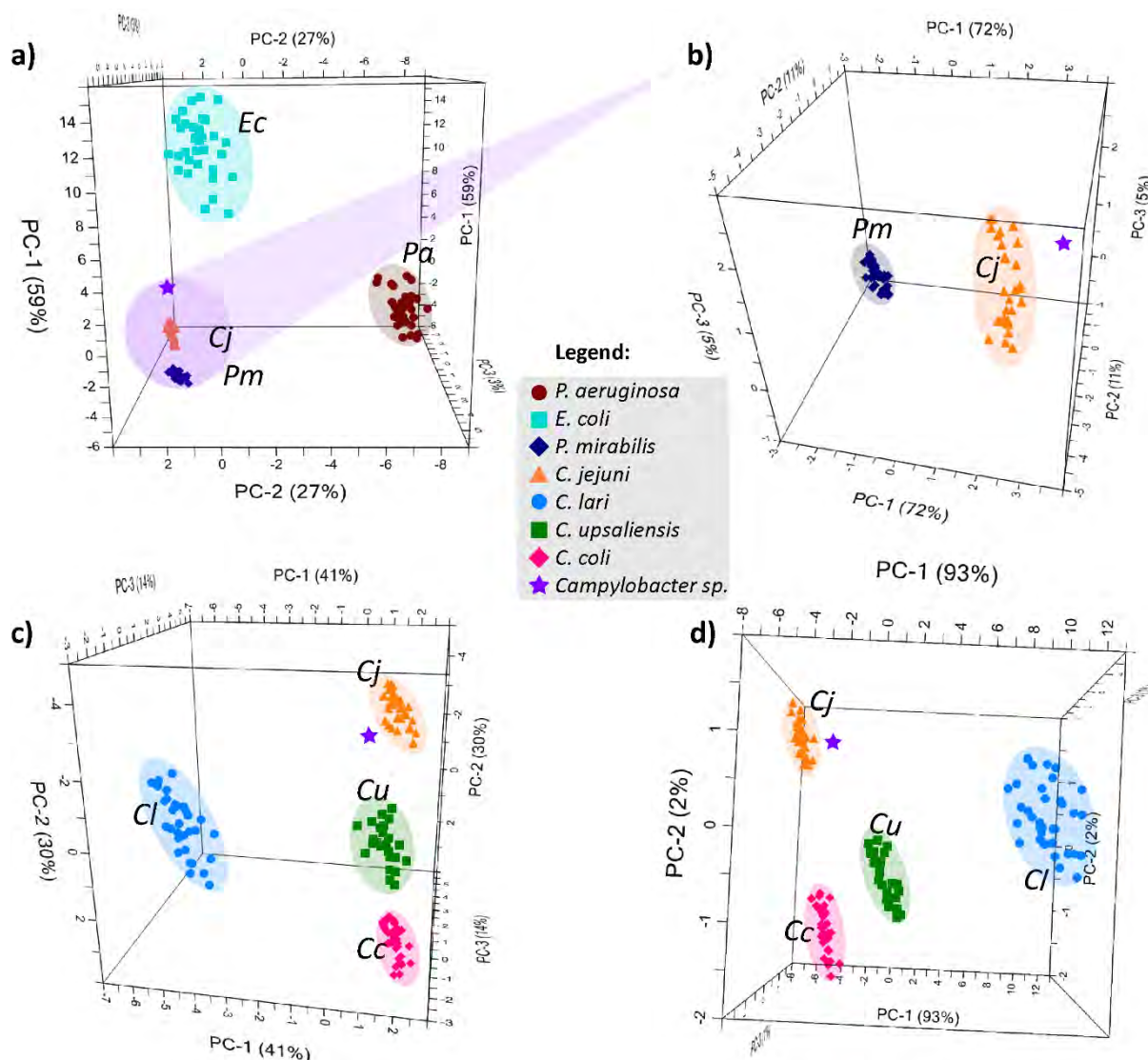
Figure 46. The three-dimensional principal component analysis results obtained for (A) all strains from the poultry samples growing on mCCDA, (B) additional PCA of violet region grouping together C. jejuni NCTC 11351, Campylobacter isolate, and P. mirabilis, all thermotolerant Campylobacter control strains and Campylobacter isolate cultured on (C), mCCDA, and (D), Columbia blood agar. The violet star represents the averaged SERS spectrum of Campylobacter sp. strain, which was detected in poultry sample [190].

The campylobacter strain isolated from a poultry sample, represented by a single averaged spectrum, in PCA analysis demonstrated the greatest similarity to the reference strain *C. jejuni* NCTC 11351 (database strain). The spectrum of *P. mirabilis* was also very similar. In contrast, the spectra of *E. coli* and *P. aeruginosa* presented many unique features, such as strong bands at around 650 and 1455 cm^{-1} and a weak band in the range of 720-730 cm^{-1}. The spectrum of *P. aeruginosa* displayed few bands characteristic of bacteria. The PCA analysis confirmed the close relationship of the *C. jejuni* NCTC 11351 and *P. mirabilis* strains in poultry and greater proximity to *E. coli* and *P. aeruginosa*. Calculated

89% of total variance in the case of the mentioned strains. The loading of PC-1 analysis exhibited the greatest effect on the separation of the results thanks to the bands at around 730 and 1455 cm^{-1}.

Due to the similarites between the bacteria, suspected of belonging to two campylobacterial strains, another PCA analysis was performed, this time for only 3 species. As one may notice, the violet star point is on the same side of the three-dimensional chemometric analysis representation as *C. jejuni* NCTC 11351. This indicates that this strain belongs to *C. jejuni* with a 72% separation of PC-1. This is sufficient to identify an unknown strain from a poultry sample. The lack of grouping of this point with the data for the strain from the database may be due to the fact that both tested samples may belong to two different strains of the same species. The strain differences may lead to sufficient spectral dissimilarities between the two analytes, and there are studies of SERS research indicating such cases [199, 200].

In the original trial to identify the closest similarity among *Campylobacter spp.* to the suspect strain, it may be noticed that the star representing it was found in the immediate vicinity of *C. jejuni* NCTC 11351. This sample was performed on both mCCDA and Columbia blood agar cultured bacteria and the obtained results were similar.

The conclusions. The above results indicate that SERS may be a powerful tool for the detection and identification of pathogenic bacteria in food samples. The elaborated method can be implemented in the chain of existing ISO procedures as an alternative to the costly and time-consuming classical identification methods. According to the diagram of the proposed procedure presented in *Figure 47*, the total analysis time may be reduced by at least a half. Such a reduction of time potentially allows for a faster preventive recall of a food product from sale, and for a clinical case, accelerate treatment and prevent the dire consequences of loss of health, or, in extreme cases, life.

The results of the chemometric analysis of PCA, which allows for the objective spectral identification of the analyte of biological origin, permitted the distinction of *C. jejuni*, *C. coli*, *C. lari*, and *C. upsaliensis* - testers in this experiment. In the case of the path with the growth of bacteria on the mCCDA medium, the discrimination of thermotolerant bacteria was 85% in accuracy, in the case of Skirrow agar medium and Columbia blood agar it was possible to obtain 96% accuracy. In an attempt to apply the method in the study of food samples, it was possible to differentiate *C.jejuni*, thanks to the combination of the spectrum obtained with the SERS technique and chemometric analysis, from four other strains (cultured on mCCDA medium) with the accuracy of 89%.

113

Further research with other food pathogens is required to properly develop the method. It should also be validated on other types of food samples. In order to accelerate the operation of the method, its automation is crucial. Currently, the measurement of several dozen spectra and their PCA analysis requires from one to two hours of work. It is also necessary to execute the full script for the assumptions of the procedure and laboratory activities (*Figure 47*). A direct capture and concentration of a bacterial sample in order to skip the multiplication stage or the parallel analysis of many species and strains within one sample seems to be interesting path to consider. The above are challenges that need to be addressed in order to develop a robust and efficient technique for the analysis of environmental and clinical samples.

The research conducted and described in this subsection led to the fulfilment of the second, third, fifth, sixth and seventh of the individual thesis goals.
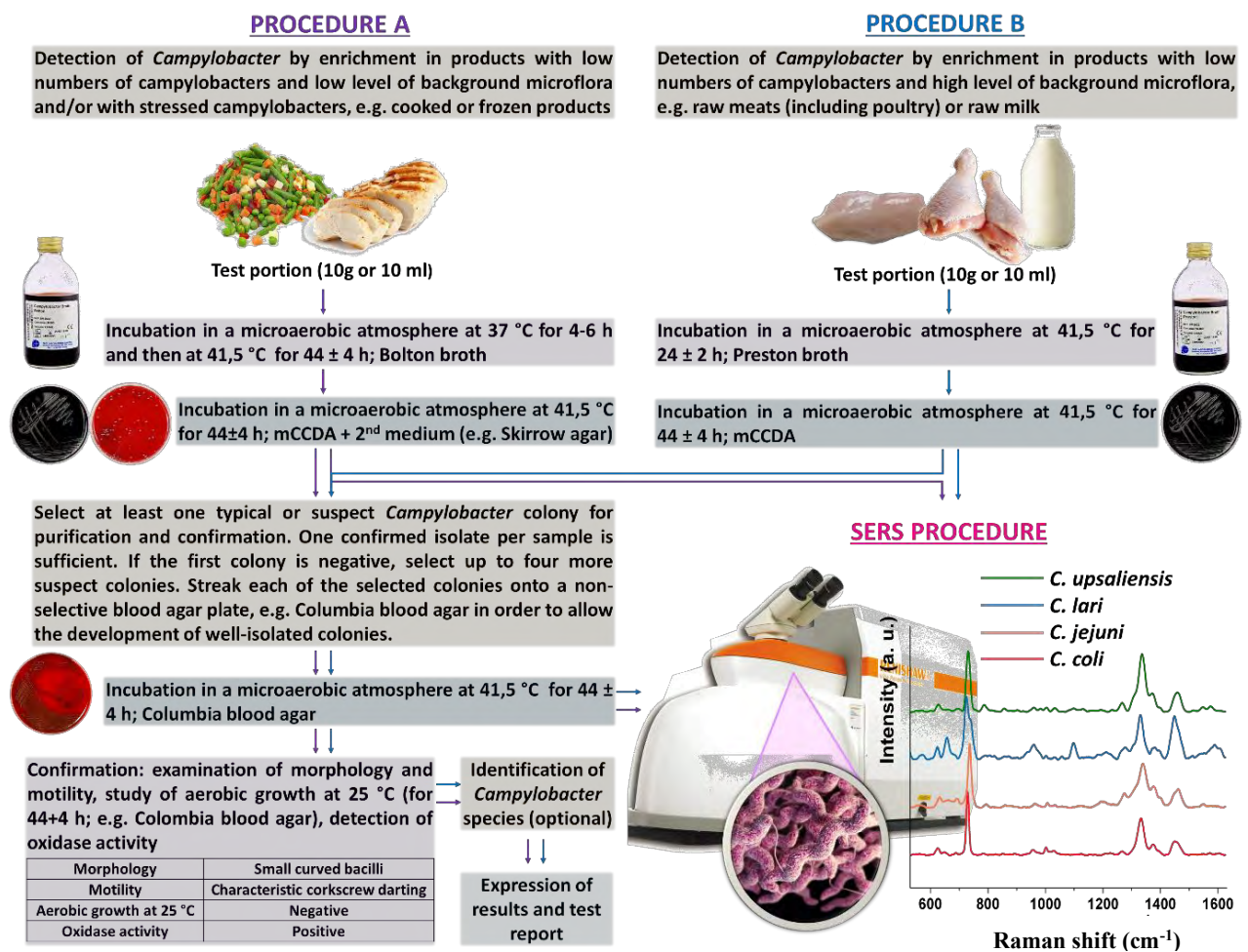
Figure 47. The scheme representing different procedures for Campylobacter spp. detection in food samples. Both procedures are including ISO standards and SERS-based approach [190].

7.2.5 Silicon-based SERS platform as a sensor for obtaining spectroscopic signatures of periodontitis.

The Ag/PV SERS platforms, described in the Chapter 7.2.4, demonstrated a number of advantages that render them a very good sensor for molecular and biological analyses. However, their disadvantages were defined as well, over time, with their production and usage. The biggest one is the problem of homogeneity and repeatability of PV-waste obtained from the Bruk-Bet Solar Tarnów, Poland. The advantage of reusing production waste in the long run, emerged to be an issue. The decisive departure of producers from polycrystalline panels in favour of those based on a monocrystalline structure created a vision of a complete lack of this substrate in the future [201]. In addition, there are various reasons for rejecting them from the production process, i.e., their defects may, over time, affect the spectral image through its own contribution in the form of signals from potential contaminants. Furthermore, cutting panels with a glass cutter often results in undesirable shapes and dimensions of the substrates and large losses of the base material.

Having experience with PV, it appears that the nanostructures of silicon or silicon nitride are a promising matrix to create, with the help of PVD deposition of active metal in the SERS technique, platforms with desirable properties in biological and molecular analysis. Using the laser ablation method in Group 1 at the Institute of Physical Chemistry, Warsaw, Poland, a technique for modifying the surface of a silicon wafer as a matrix for the production of the SERS substrate was developed [202]. Laser ablation is a subtractive technique consisting of the fabrication of micropatterns through the removal of small fractions of a substrate material under a focused pulsed laser beam [203].

The method developed in the cooperation inside the Group 1, mentioned above, was optimised for the best enhancement factor for the Raman reporter in the form of para-mercaptobenzoic acid. The calculated EF was at the level of 10^8 and the standard deviation (SD) at 7% for 10^{-6} M solution of p-MBA based on the intensity of the band at 1073 cm^{-1}. The optimized SERS substrate also exhibits excellent stability for up to six months. Laser processing allows to scale the fabrication process and make cuts in the processed material, thanks to which the silicon does not require additional cutting and you can fabricate platforms of the desired shape and size [202].

A femtosecond laser with a wavelength of 1030 nm, pulse duration of 300 fs and frequency of 300 kHz was used for the ablation process. The following parameters were

established to achieve the rough and best-enhancing silicon (p-type doped, with crystal orientation <100> and resistivity of 1–30 Ωcm) surface:

i. the arrangement of scanning layers (perpendicular);

ii. the fluence (E_d = 2293 J×m^{-2});

iii. the beam scanning speed of silicon substrate (v = 1.5 m×s^{-1});

iv. the distance between the scanning lines (d = 30 μm), the repetition rate (f = 300 kHz),

v. the number and pattern of repetitions (double layer is two ablation layers with the mutual orientation of 90°).

The influence of the type (Ag, Ag/Au alloys) and the thickness of the deposits onto silicon active metal layers (from 10 nm to 100 nm with the step of 10 nm) on the SERS efficiency also was examined. The best result was obtained for 100 nm of the silver layer with the average size of the silver crystallites ranging from 25.4 nm to 44.8 nm, whereas the nanoaggregates were between 60 nm and 100 nm.

The influence of the type of the applied metal in the vapour deposition process and the thickness of the layer were also investigated. The highest enhancement factor was obtained for the 100 nm silver layer with the average size of the silver crystallites ranging from 25.4 nm to 44.8 nm, whereas the nanoaggregates were between 60 nm and 100 nm. Responsiveness to material of biological origin was tested on the basis of Candida species and the calculated standard deviation of the results was 2.8%.

The optimized process allows for full control over the SERS substrate preparation procedure, which makes it extremely valuable in the context of research. It is currently the main type of substrate used among the group where it was developed and forms the basis of the SERS technique development process in analytical applications.

In the run-up to the COVID-19 pandemic, it was proposed that *Porphyromonas gingivalis*, which is the keystone pathogen implicated in the development of gum disease (periodontitis) [204, 205], could be related to the development of a neurodegenerative illness known as Alzheimer's disease [206]. The presence of bacteria of this species was detected in the brains of Alzheimer's disease patients. In order to detect this potential factor of neurodegenerative disease, a sensor will be developed to enable for it to be tagged and identified. SERS spectroscopy is the right tool for this type of measurement because of its sensitivity and, together with chemometric analysis, it may also provide the specificity necessary to identify microbial analyte. In order to supply an informative background, bacterial species from oral bacterial flora, usually accompanying *P. gingivalis* were also tested: *Aggregatibacter actinomycetemcomitans*, *Streptococcus* spp.. The frequency of

116

periodontal diseases diagnosed among children, adolescents and adults qualifies them to a group of social diseases. As a consequence of such illnesses, there are, among others, e.g., loosening and loss of teeth. They are caused by: inadequate, poor periodontal hygiene, avitaminosis, abnormal bite, habitual teeth grinding, smoking, excessive alcohol consumption, hormonal disorders, systemic disorders, improper diet, numerous abnormal, prosthetic restorations or disorders of saliva production [207, 208].

In order to increase the sensitivity of the sensor, I have developed and fully characterized the magnetic silver nanoparticles (Fe_2O_3@Ag NPs), which can adsorb on the surface of bacteria and additionally serve for their magnetic separation from the matrix in the form of a body fluid. **Details on the materials and devices used in the experiments may be found in Appendix 5.**

The preparation of Si/Ag SERS Platforms. The preparation of the silicon-based SERS substrate consists of five main steps. In this variant, instead of a laser beam, a cutting saw was used for the formation of squares (3.5×3.5 mm). The mechanical cutting saw was implemented (type: Disco DAD 2H/6TM) at the Institute of Electronic Materials Technology in Warsaw, Poland. They are also the producer of the silicon wafers that are applied in the procedure. Subsequently, the silicon surfaces were washed with great care with deionized water. Next, all of the residues were removed and the cut wafers were dried in a stream of argon. Afterward, the silicon surface was modified with the use of a femtosecond laser (based on potassium yttrium tungstate, with 1030 nm wavelength, repetition rate 300 kHz, and a single pulse set to 300 fs). In the final step, the modified silicon surface was sputtered with 100 nm of silver.

The measurements of SERS spectra by P. gingivalis and A. actinomycetemcomitans and chemometric analysis of the obtained results. I have tested five strains of *P. gingivalis* to verify the potential of the SERS technique to distinguish between strains of the same bacterial species. The measurements were conducted for strains grown on solid and liquid media. Twenty-five measurements were made each time using a portable Bruker Bravo spectrometer, while testing its potential in the study of microorganisms with SERS spectroscopy.

In the case of bacteria cultured on solid (agar) media, about three single bacterial colonies were selected and suspended in 500 µL of a sterile saline solution (0.9% NaCl) via an inoculation loop. Then, bacteria were gently mixed with the saline solution by an automatic pipette. In the case of bacteria grown in liquid media, 500 µL of each culture was placed in a 1.5 mL tube. Next, both types of samples were centrifuged (5 min, 1070×g),

117

the supernatants were discarded, and the pellets were suspended in 500 μL of the sterile saline solution. The washing procedure was repeated three times. The concentration of bacteria in each sample was at the level of 10^8 cfu×mL^{-1} (colony forming unit×mL^{-1}), as the cell suspension was equivalent to the 0.5 McFarland turbidity standard [209].
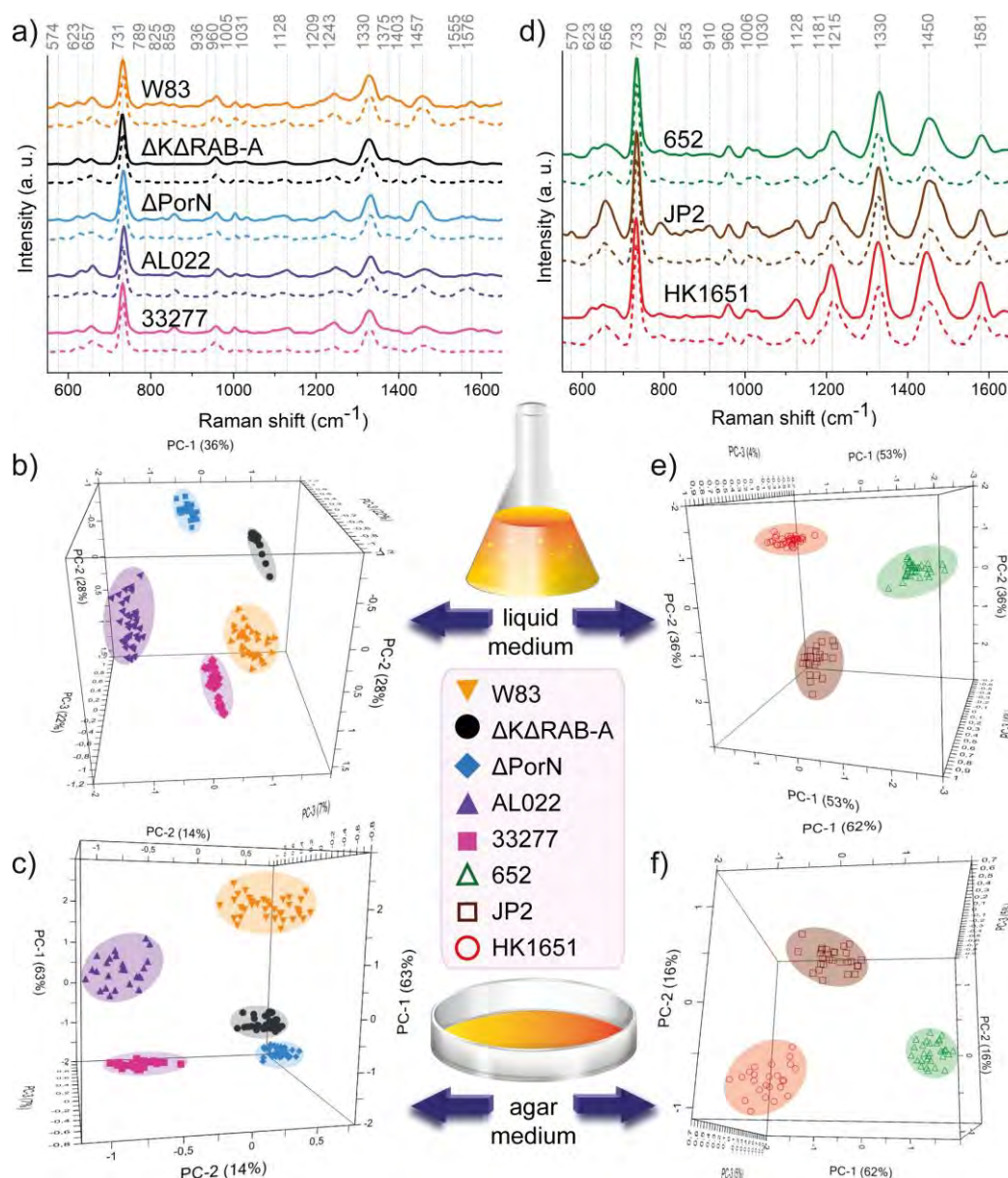
Figure 48. The SERS spectra (a, d) and three-dimensional (3D) PCA plots (b, c, e, f) obtained for five investigated P. gingivalis strains and three A. actinomycetemcomitans strains. The spectra marked with solid lines in the images (a and d) and PCA results from the images (b and e) present the findings obtained for bacteria grown on agar media, while the spectra marked with dashed lines in the images (a and d) and PCA results from the images (c and f) present the findings obtained for bacteria grown in liquid media [210].

After the final centrifugation step and supernatant removal, the pellets were suspended in 20 μL of the sterile saline solution. About 5 μL of each mixture was used for

SERS measurements by placing it onto the SERS substrate 5 min before measurement (to let the sample dry). Each strain was then cultured independently three times, both on solid (agar) and in liquid media.

The spectra (*Figure 48*) obtained from averaging all the measurements (each single spectra presented in this section was averaged from at least 25 single evaluations - amount of spectra collected for a single sample) were dominated by bands in the range 550 to 1650 cm^{-1}. The most intense were the bands at the Raman shift 730 and 1330 cm^{-1}, attributed to the vibrations to the in-plane ring breathing mode of adenine and to CH_3 / CH_2 wagging, respectively [137, 211]. The remaining bands may be linked to metabolites of purine degradation other than adenine and AMP, e.g., guanine, xanthine, hypoxanthine, uric acid, and to bacterial cell wall components, e.g., phospholipids and proteins [191, 212, 213]. The spectra marked with the solid line were obtained for the strains measured on the solid medium, and the ones with dashed line, for those grown on the liquid medium. This way of presentation will also appear in the results presented later. The spectra for bacteria grown on the same type of medium show great similarity with each other, the differences were only noticed in the intensities and the intensity ratios between the bands. The band at 1243 cm^{-1} assigned to Amide III vibrations [214] was exceedingly characteristic for all bacteria of the species studied. The differences in the spectra of diverse strains may result from the presence or absence of antigens and / or secreted chemical substances as well as different metabolites specific to the given strain. In the case of dissimilarities between the spectra measured for the same strain and on the solid and liquid medium, they may result from the reverse mechanism of interaction between the bacterial organism and its metabolites. Culturing in a liquid medium, where the mixing function is ensured in order to ensure even access to the nutrients of the medium, additionally causes a continuous change of the position of bacterial cells and frees them from access to metabolites. On a solid medium, where the movement of bacteria is limited, they are exposed to the continuous presence of metabolites within their outer barrier, which may, in turn, induce changes in their metabolism. As a consequence, their composition changes, which, due to the high sensitivity of SERS, is noticeable in the recorded spectrum.

The PCA method was used to compare and distinguish the spectra. With its help, it was possible to distinguish all five strains grown under both types of conditions. In the case of first three principal components (PC-1, PC-2, and PC-3), they were responsible together for 86% of the variance in the data, while comparing bacteria grown on agar media, and for 84% of the variance in the data in the case of liquid cultures.

I have measured three *A. actinomycetemcomitans* strains in order to verify the possibility of distinguishing the tested strains of *P. gingivalis* from other bacteria associated with localised aggressive periodontitis. The experiments were performed again under the same regime and conditions as the previous ones. The obtained spectra were similar to each other, regardless of the measurement conditions, i.e., the type of medium used for all strains. The spectra were again dominated by bands at about 733 and 1330 cm^{-1}. They also demonstrated strong bands at 1215, 1450, and 1581 cm^{-1}, which may be assigned to C–N stretching / Amide III / thymine, CH$_3$ / CH$_2$ deformation, and the C≡C bending mode of phenylalanine, respectively [137]. There were also numerous bands of lower intensities, e.g., at 623 cm^{-1} (C – C twisting in protein), 656 cm^{-1} (C – S stretching, hypoxanthine, xanthine, guanine), 960 cm^{-1} (C≡C deformation, adenine, guanine, NAD$^+$), 1006 cm^{-1} (phenylalanine, C–C aromatic ring stretching), 1128 cm^{-1} (≡C–O–C≡ in unsaturated fatty acids in lipids), and 1181 cm^{-1} (tyrosine) [133, 194, 212, 215-217]. Again, the differences between the spectra may be attributed to the intensity and the ratio of the intensity of the bands between the strains. Similarly, the PCA analysis made it possible to distinguish the three tested strains, despite a great similarity in the spectra obtained as a result of their measurements. The PC-1, PC-2, and PC-3 values together yielded 93% of the total variance in the case of strains cultured on agar plates and 83% when analysing bacteria grown in the liquid medium. The high spectral similarity demonstrated how powerful an analytical tool chemometrics is, when trying to identify with the spectroscopic method.

Additionally, to check the possibility of distinguishing *P. gingivalis* from other bacterial strains present in the oral cavity, two more strains were selected: *S. mitis* 3705/04 and *S. pseudopneumoniae* 6178/12. The first is normally present in the saliva microbiota, while the other is an emerging respiratory tract pathogen, and thus it may also be detected in human saliva. The measurements were made on the same principle as the previous ones (but only solid medium-based bacterial culture was conducted) and their results are presented below (*Figure 49*).

120
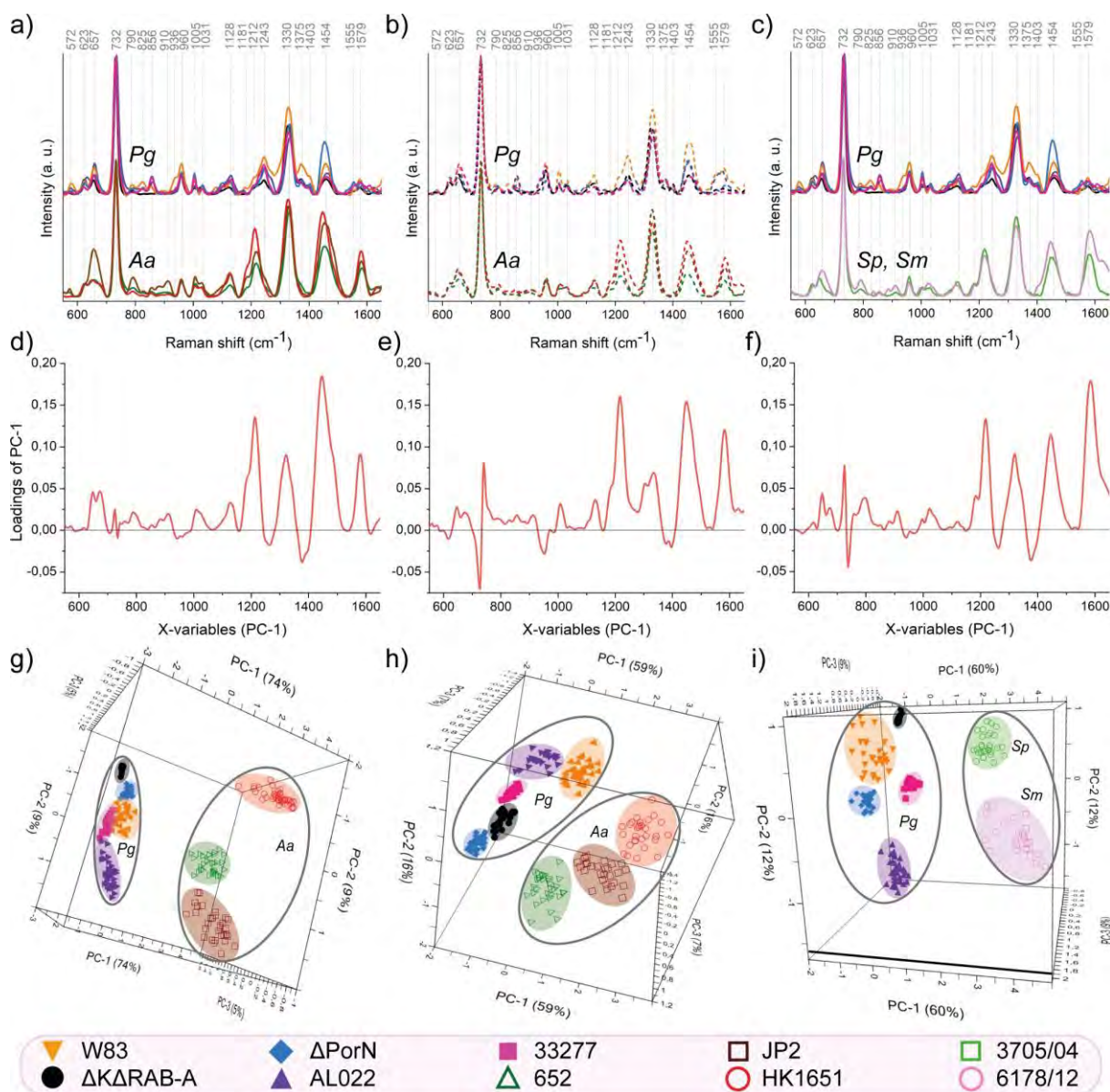
Figure 49. The Compiled SERS spectra (a–c), loading plots (d–f), and PCA (g–i) of P. gingivalis (Pg), A. actinomycetemcomitans (Aa), and Streptococcus spp. (S. mitis -Sm, and S. pseudopneumonia -, Sp) strains. The images (a, c, d, f, g, i) present results obtained for bacteria grown on agar media, while the images (b, e, h) present findings obtained for bacteria grown on liquid media [210].

As the distinction between the two spectra is possible for the two of streptococcal species due to the large differences in the intensity ratios of the obtained bands, the focus was on their comparison with the spectra of *P. gingivalis*. These differences mainly concerned the presence of the bands 1185 and 1217 cm^{-1}, which were noticeable in the spectra of streptococci and absent in spectroscopic images of *P. gingivalis*. At a further stage of differentiation, one can use the PCA analysis and the loading plot of PC-1 versus the Raman shift. The band at 1580 cm^{-1}, which was weak with *P. gingivalis* and extremely strong with

streptococcal strains, contributes to the distinction. Other fingerprints that distinguish these two groups of bacteria were the bands at 1217, 1328, and 1451 cm^{-1}. PC-1 together with PC-2 and PC-3 reached 81% of variability, which indicates that all seven strains can be effectively distinguished in this comparison.

In the case of a comparative analysis between *P. gingivalis* and *A. actinomycetemcomitans*, the results obtained for bacteria grown on agar-based and liquid media were separated. The significant difference was the low intensity band at about 910 cm^{-1}, present only in the case of *A. actinomycetemcomitans* strains. Likewise, bands at around 860, 1375, and 1400 cm^{-1} were discernible only for *P. gingivalis* and absent or exceptionally weak in intensity for the other three strains. The bands around 1005 and 1031 cm^{-1} were well separated in the spectra of *P. gingivalis* and overlap with *A. actinomycetemcomitans*. The band at 1215 cm^{-1} for *A. actinomycetemcomitans* was shifted to 1209 cm^{-1} in the case of the other five strains, in addition, the band at 1243 cm^{-1} was absent for the former.

The PCA analysis made it possible to separate the eight analysed strains into two groups, containing the spectra for bacteria from the same species and their mutual distinction. The most important bands for the distinction according to the analysis of PC-1 loading vs Raman shift were 1212, 1330, 1454, and 1579 cm^{-1}. The same was true for bacteria cultivated on a solid and a liquid medium. The accuracy of this separation reached 88% in the case of bacteria grown on agar plates and 82% for bacteria from planktonic cultures. Importantly, the black colour of colonies of wild-type strains bacteria did not affect the obtained results, which is usually the case with stained cells, which had already been confirmed in independent studies and in the previously described experiment [146]. The dark colour was due to accumulation of heme on the cell surface [218, 219]. The obtained results indicate that identification with SERS method is possible not only at the species level but also at the level of the strain. Most importantly, it is possible to distinguish the target microbial analyte from accompanying material under oral-saliva conditions.

The portable spectrometer used for the research resulted to be sufficiently resolving to ensure the possibility of identification at the level of subtle differences in the spectra. It also proved sufficient sensitivity and stability for hardware and software. During the experiments, the spectrometer worked in battery mode and with a constant power source. This indicates its high flexibility and the possibility of application in field or laboratory conditions.

The studies of human saliva with the use of a sensor, placed in a microfluidic system. In order to gather bacteria from saliva and to separate them magnetically and increase

the sensitivity of the method, nanoparticles with plasmonic and magnetic properties were prepared. Ultimately, the nanoparticles must be spectrally neutral in the fingerprint range for bacteria (about 550-1800 cm^{-1}) and have certain magnetic properties. Their synthesis was inspired by an already existing method which was appropriately modified [220]. Optimizing their synthesis was developed by the undergraduate staff in Group 1, the PAS Institute of Physical Chemistry.

The developed synthesis pathway is a one-step thermal decomposition of silver acetate salt in the presence of iron (III) oxide nanoparticles. Fe_2O_3 nanospheres having an average diameter of less than 50 nm were initially grated in an agate mortar with silver acetate with a mass ratio of 1:10. The mixture obtained in this way was transferred to plastic containers, and agate balls were added to it. Subsequently, the substrates were ground for 30 min in a Retsch MM400 mixer ball mill with a frequency of 20 Hz. The obtained powder was transferred to a round-bottom boat ceramic crucible and placed in a Carbolite tube furnace. The mixture was heated up to 200 °C at a rate of 10 °C×min^{-1}, and then, it was kept in a nitrogen atmosphere at 200 °C for 2 h. The furnace was cooled to ambient temperature with the product kept in a protective nitrogen atmosphere. Next, it was purified by suspending it in 500 mL of distilled water. Additionally, an ultrasonic bath was applied at this stage. Finally, the suspension was poured over the neodymium magnet till the supernatant became transparent. The final product was dried at ambient temperature thanks to which the nonmagnetic phase and all of the residuals from the synthesis were removed from the product in the supernatant phase.

In order to compare the properties of the nanoparticles obtained for the experiment with the literature data, I have performed absorption measurements using the UV-VIS spectroscopy method (*Figure 50*). In addition, 150 different nanoparticles were measured and counted from their SEM images (*Figure 51*). Each diameter measurement was coducted three times and the obtained results were averaged. Measurements, averaging and calculations of diameters and standard deviations were performed in Image J (*Figure 52*).
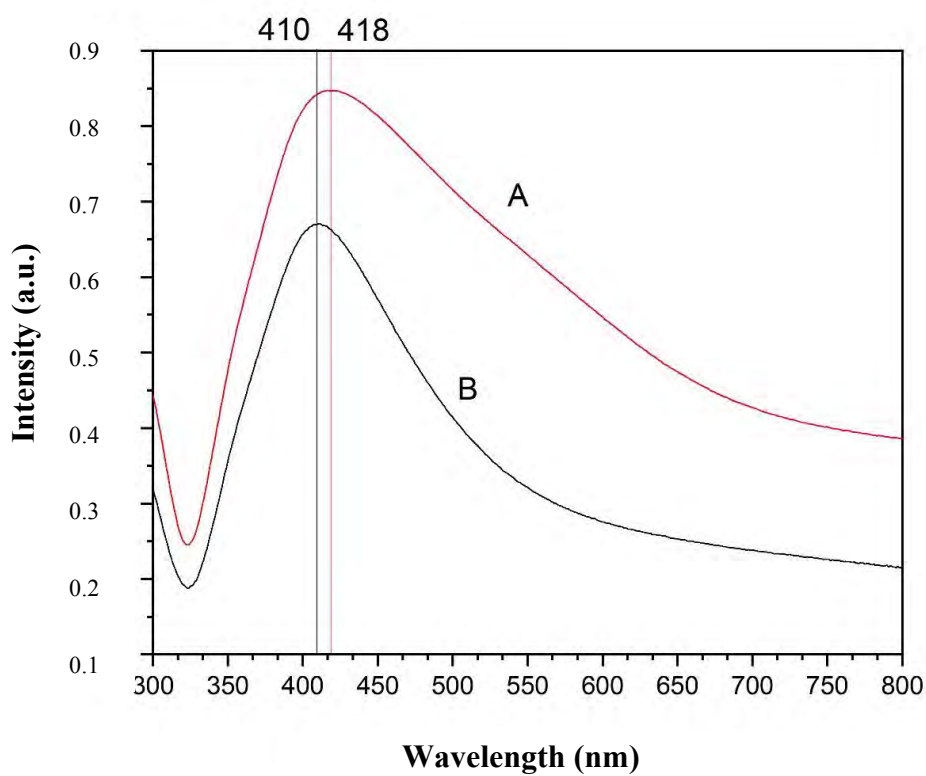
Figure 50. The comparison of absorption spectra of Fe₂O₃ @Ag, (A) sample with a mass ratio of Fe₂O₃ to silver acetate 1:10, (B) literature data [220].
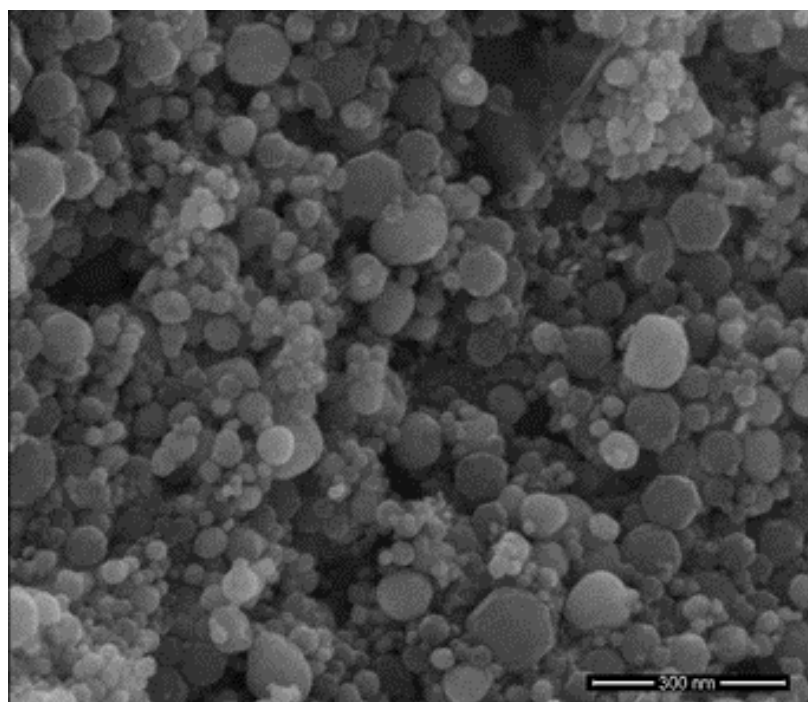
Figure 51. The SEM image of Fe₂O₃@Ag nanoparticles obtained by thermal reduction of silver acetate in the presence of iron (III) oxide microspheres with 1:10 weight ratio ofFe₂O₃ to silver acetate.

124
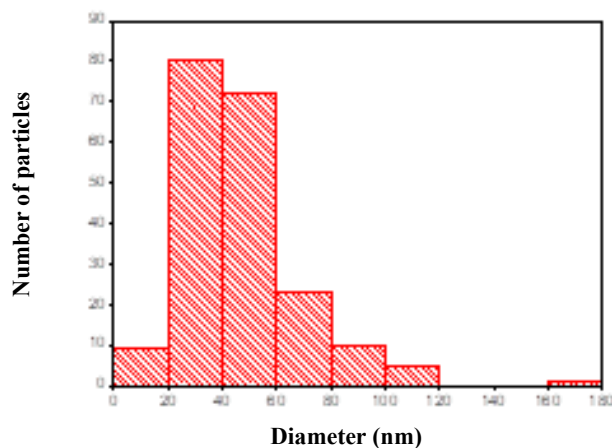
Figure 52. The size distribution of the obtained Fe$_2$O$_3$@Ag nanoparticles with 1:10 weight ratio of Fe$_2$O$_3$ to silver acetate.

The obtained Fe$_2$O$_3$@Ag UV-VIS spectrum (A) of prepared sample is characterised by an absorption maximum at 418 nm. The obtained results corresponded to the spectra available in the literature for Fe$_2$O$_3$@Ag nanoparticles (B). The absorption maximum of sample (A) was slightly shifted towards a longer wavelength than that of sample (B), probably due to the different content of silver and organic residues in both samples. The standard deviation of the measured nanoparticle diameters was ±21 nm. The mean, calculated size of the nanoparticles expressed as the median was 41±2 nm. The obtained results suggested that the size of nanoparticles was similar to the size of nanostructures on the surface of Si/Ag solid substrates and that the shape of the obtained nanoparticles was spherical. The dimensions were optimal for obtaining additional signal enhancement.

For creating a lab-on-a-chip environment I have developed the microfluidic chip. It consisted of a main channel with a width of 0.60 mm and two entries for needles with a diameter of 0.80 mm, one exit through a needle with a diameter of 0.80 mm and a zone for placing the Si/Ag platform, a cover plate with a hole and milled on gasket and quartz glass. The whole set was closed with a cover plate with a milled space for o-ring and a central opening.

The system included a quartz glass with dimensions of 20×20 mm, which allowed for the collection of signal during the experiment. More details of the designing process may be found in Appendix 5.

An infusion pump system was used for the automated control of the flow. For the injection of the analyte and the buffer, that contained suspension of NPs, into the microfluidic system and collection of the separated fractions, blunt-ended needles with an outer diameter

125

of 0.8 mm were installed in the holes that were drilled the in appropriate places in the plates. Polyethylene (PE) tubings with an inner diameter of 0.8 mm were applied to connect the chip with an infusion syringe pump and the residue container.

In the first variant of the experiment, the aim was to check the potential influence of nanoparticles on the spectrum of bacteria. The scheme of the second variant of the experiment and the spectra and PCA results are presented below, along with the SEM images of analytes (*Figure 53*).
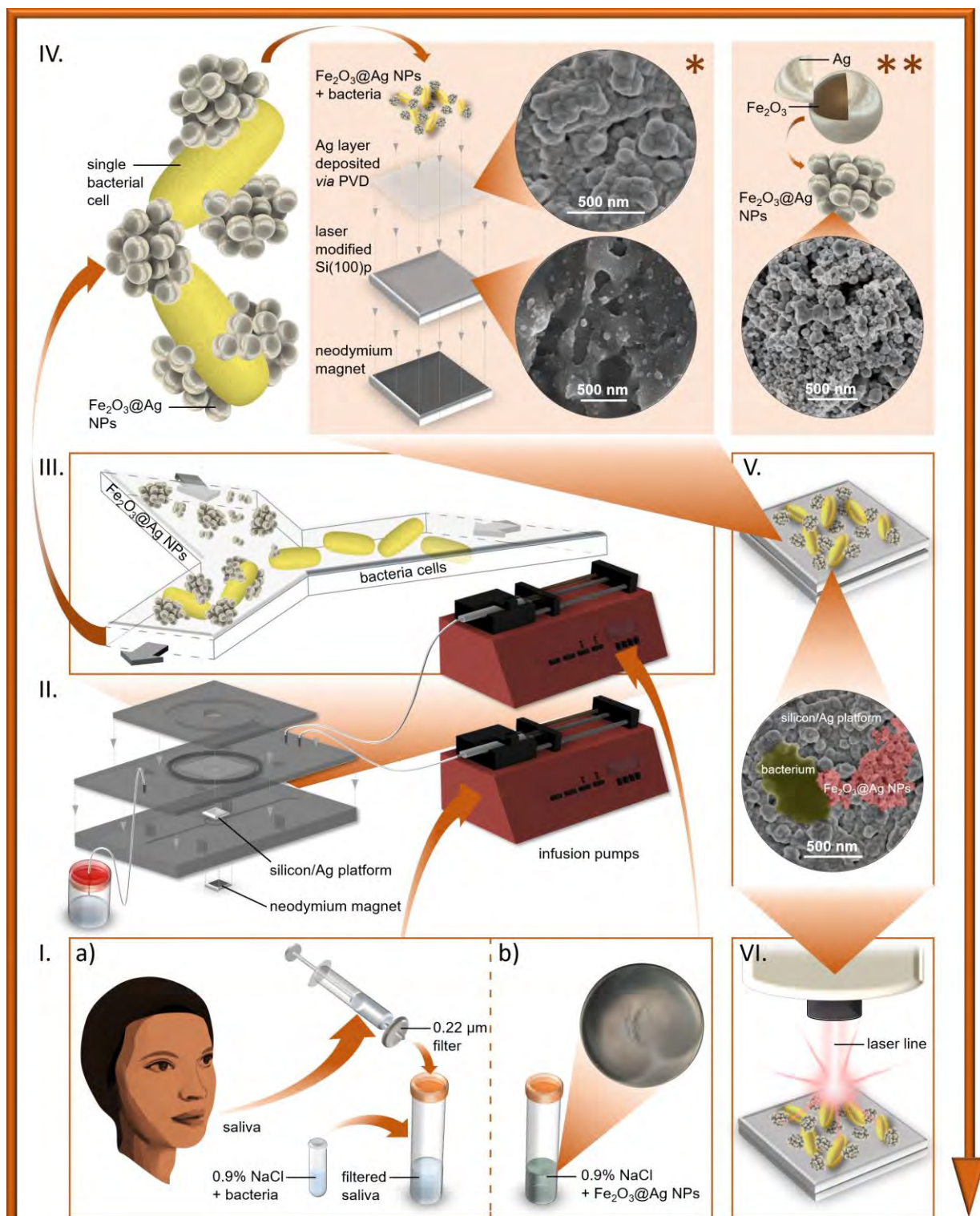
Figure 53. The experiment comprised collection, filtration, and inoculation of human saliva (Ia); the preparation of the solution of Fe₂O₃@Ag nanoparticles (Ib); the mixing both types of solutions in a microfluidic chip (II); the adsorption of bacterial cells to Fe₂O₃@Ag nanoparticles and formation of bacteria–nanoparticles aggregates (III); the magnetic attraction of the aggregates to the Si/Ag SERS platform placed over neodymium magnet (* and ** represent the arrangement and the SEM images of the Si/Ag substrate and of Fe₂O₃@Ag nanoparticles, respectively) (IV); the adsorption of bacteria–nanopartciles aggregates to the Si/Ag SERS platform (V); and the SERS measurements of the sample (VI) [210].
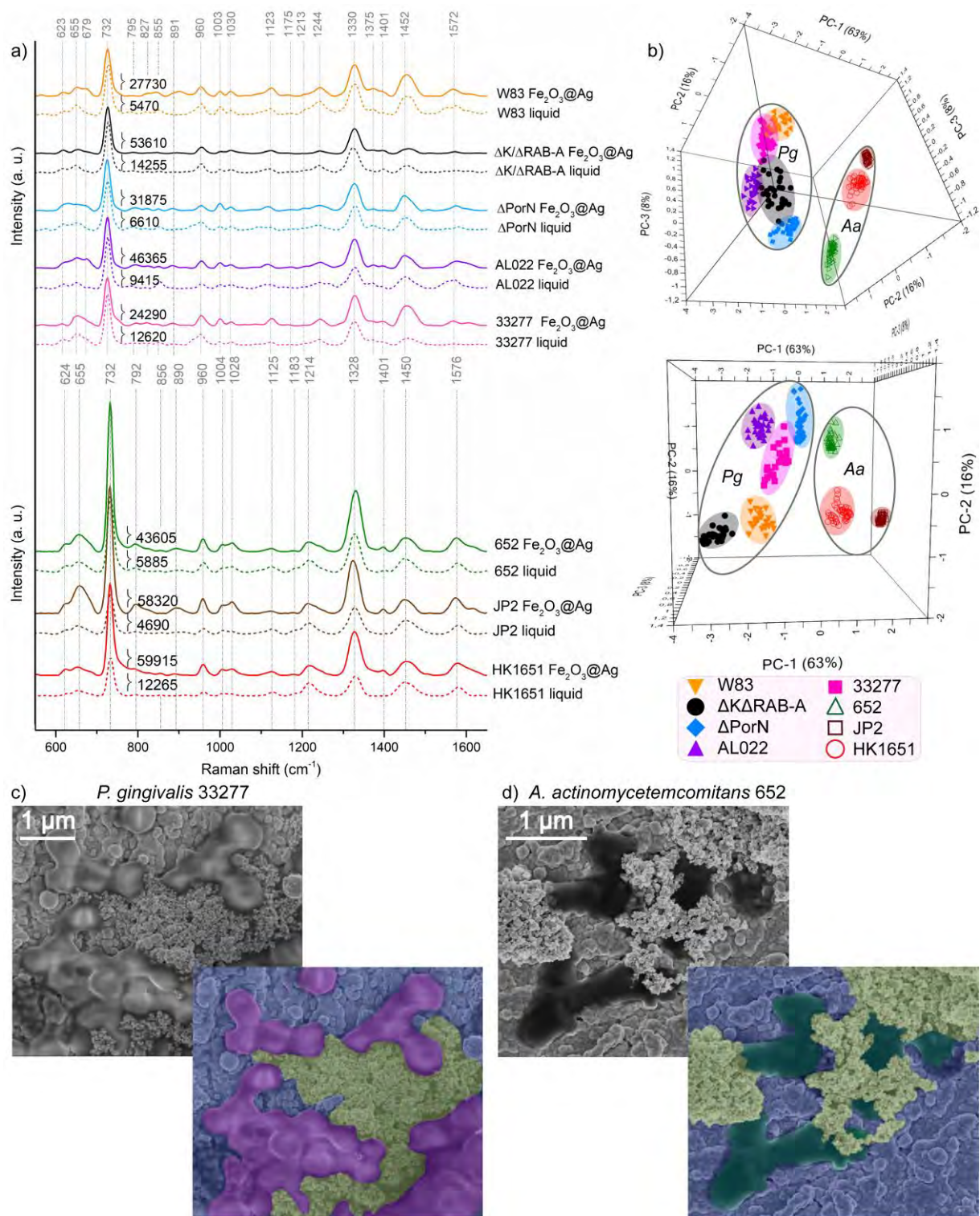
Figure 54. (a) The SERS spectra, (b) the PCA results and (c, d) the SEM images obtained for bacterial strains belonging to P. gingivalis or A. actinomycetemcomitans species. The spectra marked with solid lines present findings obtained for bacteria grown in liquid media, which were next rinsed, and dispersed in the saline solution, mixed with Fe₂O₃@Ag nanoparticles, and magnetically attracted to the Si/Ag SERS substrate in the microfluidic chip. The spectra marked with dashed lines are given for comparison and show results obtained for bacteria grown in liquid media and placed over the Si/Ag SERS substrate. The numbers given close to the band at around 730 cm⁻¹ represent average counts for this particular band before normalisation [210].

For *P. gingivalis* and *A. actinomycetemcomitans* the spectral differences for strains, measured in a series of experiments with nanoparticles, were identical to those without them (*Figure 54*). A significant difference between the spectral intensities, visible in the comparison of the results of the experiment in the microfluidic system (solid line) and those from the experiments on Si/Ag substrates without the use of nanoparticles (intensity values available in the graphic) was noted. 3D-PCA demonstrated the possibility of separating five strains belonging to *P. gingivalis* and three strains of *A. actinomycetemcomitans*. PC-1 together with PC-2 and PC-3 was responsible for 87% of the variance in the data, when compared with these two species.

The SEM images of *P. gingivalis* 33277 and *A. actinomycetemcomitans* are presented in duplicates in two rows: top row demonstrating the unmodified SEM photographs, while the bottom row presenting the same, but coloured in postproduction to highlight individual elements or structures: bacterial cells. The cells are marked with pink or green colour, Si/Ag platform is coloured in blue and Fe_2O_3@Ag NPs in yellow. The signal enhancement obtained after simultaneous application of two different SERS substrates indicated that Fe_2O_3@Ag NPs had a significant contribution to the overall SERS effect. This effect may find an explanation. The SEM photos demonstrated that the bacteria were close to the nanoparticles, which may result in the formation of additional 'hot spots'. These 'hot spots' found their place between the nanostructures on the surface of the SERS solid substrate. They were also found on the periphery and in the extreme upper parts of the bacteria on the substrate. As the detector in the spectrometer registers Raman backscatter, the part of the signal scattered directly on the platform was further scattered or absorbed by bacterial cells on the way to the detector. The signal backscattered and enhanced on the nanoparticles to the side and above the bacterium did not encounter any further obstacles and went directly to the detector. This was most likely the reason for the large difference in signal intensity between experiments [221].

Each bacterium is adsorbed to magnetic nanoparticles or connected to other cell(s). This is associated with the action of the silver shell of nanoparticles against Gram-negative bacteria, or, more precisely, with the interaction of nano-Ag with sulphur or phosphorus-containing proteins building the bacterial cell wall [222]. Because the core of Fe_2O_3@Ag NPs exhibits strong magnetic properties, it is possible to attract (via the neodymium magnet located beneath the SERS platform) the nanoparticles that are adsorbed to bacterial cells, directly from liquid samples to the surface of the Si/Ag SERS substrate.

129

In the second variant of the experiment, the detection and identification of the bacteria took place from human saliva and not from saline buffer. For this purpose, two different bacterial strains (*P. gingivalis* ΔPorN and *A. actinomycetemcomitans* HK1651) were separately mixed with 1 mL of filtered human saliva and then with 1 mL of the 0.9% NaCl aqueous solution of magnetic NPs (with a concentration of 1 mg×mL^{-1}) in a microfluidic chip. The flow in both inlet channels was set at 100 μL×min^{-1} (the same concentration of nanoparticles and flow values were used in the first variant of the experiment). Additionally, the spectra of filtered saliva were measured (*Figure 55*) in a system with nanoparticles and a solid medium in order to check the potential influence on the spectra of bacteria.
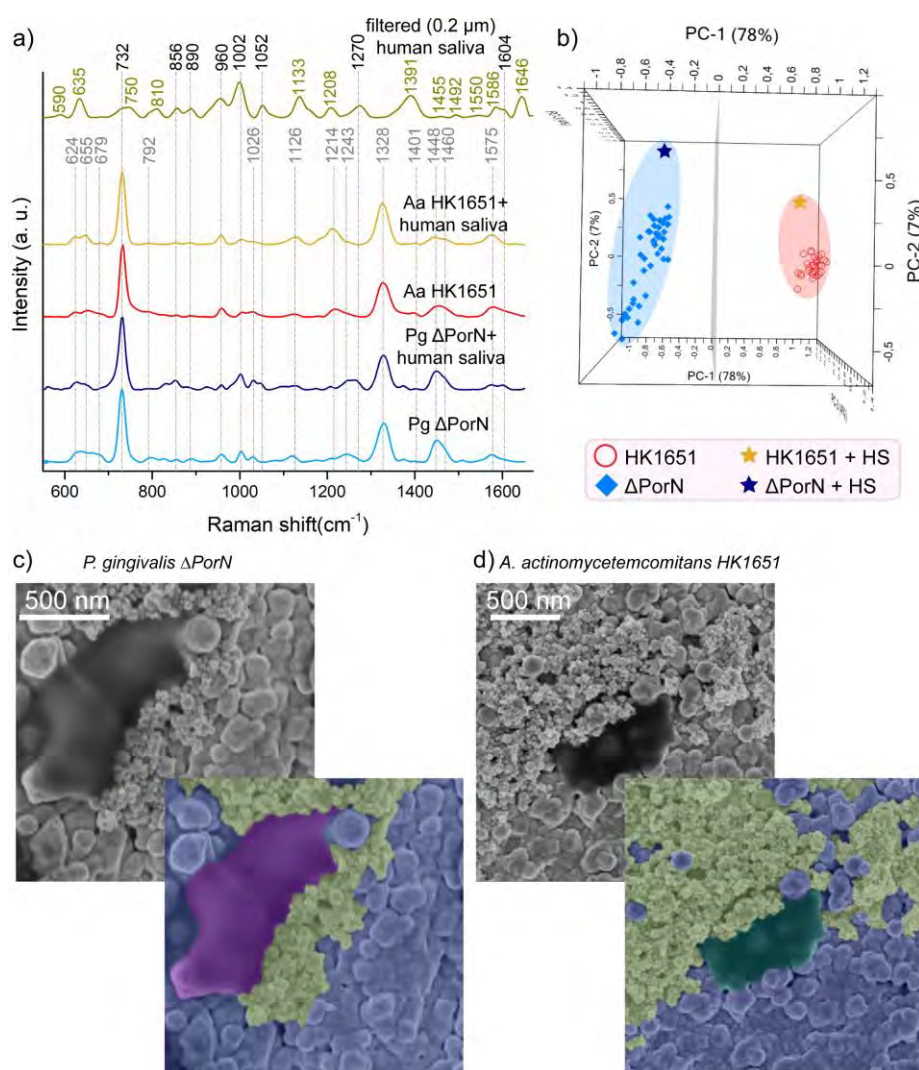
Figure 55. (a) The SERS spectra, (b) the PCA and (c,d) the SEM images obtained for two selected bacterial strains belonging to P. gingivalis ΔPorN or A. actinomycetemcomitans HK165, both mixed with human saliva (HS) and Fe₂O₃@Ag nanoparticles, and magnetically attracted to the Si/Ag SERS substrate in microfluidic chip. All of the spectra represent bacteria previously grown in liquid media. The spectra of filtered human saliva, P. gingivalis ΔPorN, and A. actinomycetemcomitans HK1651 in (a) were given for comparison [210].

The human saliva used in the experiments was obtained from a healthy male volunteer. Before the experiments, the saliva was placed in a syringe and filtered by applying syringe filters with pore sizes of 0.2 μm.

The obtained spectrum of filtered saliva, presented many characteristic signals: 635 cm^{-1} (C-C twisting of tyrosine), 750 cm^{-1} (ring breathing mode of tryptophan), 810 cm^{-1} (uric acid), 856 cm^{-1} (ring breathing mode of tyrosine), 890 cm^{-1} (structural protein modes, uric acid), 960 cm^{-1} (hydroxyapatite, xanthine), 1002 cm^{-1} (phenylalanine's C–C twisting), 1052 cm^{-1} and 1133 cm^{-1} (C–O stretching in carbohydrates and C–N stretching in proteins), 1208 cm^{-1} (tryptophan, tyrosine, phenylalanine – protein assignment), 1270 cm^{-1} (Amide III band in proteins), 1391 cm^{-1} (CH rocking), 1586 cm^{-1} (phenylalanine, hydroxyproline, hypoxanthine), 1604 cm^{-1} (C═C in-plane bending mode of phenylalanine and tyrosine), and 1646 cm^{-1} (Amide I) [137, 223, 224]. Minor differences from the literature data may be due to the fact that filtered saliva was used to avoid introducing bacteria from the oral flora into the experiment. However, the rich spectrum of saliva did not significantly affect the changes in the spectra of the bacteria. The changes were limited to an increase in the intensity of the bands at around 1126 and 1214 cm^{-1} for *A. actinomycetemcomitans* HK1651 and may have been caused by that the spectrum of filtered human saliva exhibiting bands almost in the same regions: 1133 and 1208 cm^{-1}. In the case of *P. gingivalis* ΔPorN, one can notice differences in the intensity of the bands at around 856 and 1002 cm^{-1} and the appearance of weak intensity bands at around 1052, 1270, and 1604 cm^{-1}. Again, all these slight changes were related to the influence of the spectrum of the filtered saliva on the spectrum of bacteria.

In order to present the possibility of identifying the bacteria, treating the spectra of *P. gingivalis* ΔPorN and *A. actinomycetemcomitans* HK1651, obtained during the variant of the experiment with saline buffer, as the spectra constituting the database, they were compared against the average spectra of the same bacterial strains in the experiment with filtered saliva. The single spectra represented by yellow (ΔPorN + human filtered saliva) and navy blue (HK1651 + human filtered saliva) stars are located in close proximity to the groups representing the SERS measurement of the corresponding 'reference' bacteria. The PC-1 reached 78% of total variance and together with PC-2 and PC-3 the value of 89% of variance was obtained. The SEM pictures of the bacteria after this experiment are presented below the spectrum. The presentation is identical to the description for the *Figure 54*.

As in the experiments with nanoparticles, an additional strong signal enhancement was noted, a series of experiments using saline in a microfluidic system were performed on the *A. actinomycetemcomitans* 652 strain at the concentration used for all experiments

131

$(10^8 \text{ cfu} \times \text{mL}^{-1}, 0.5 \text{ McFarland turbidity standards})$ and a series of its dilutions in order to estimate performance of the method. Results are presented in *Figure 56*.
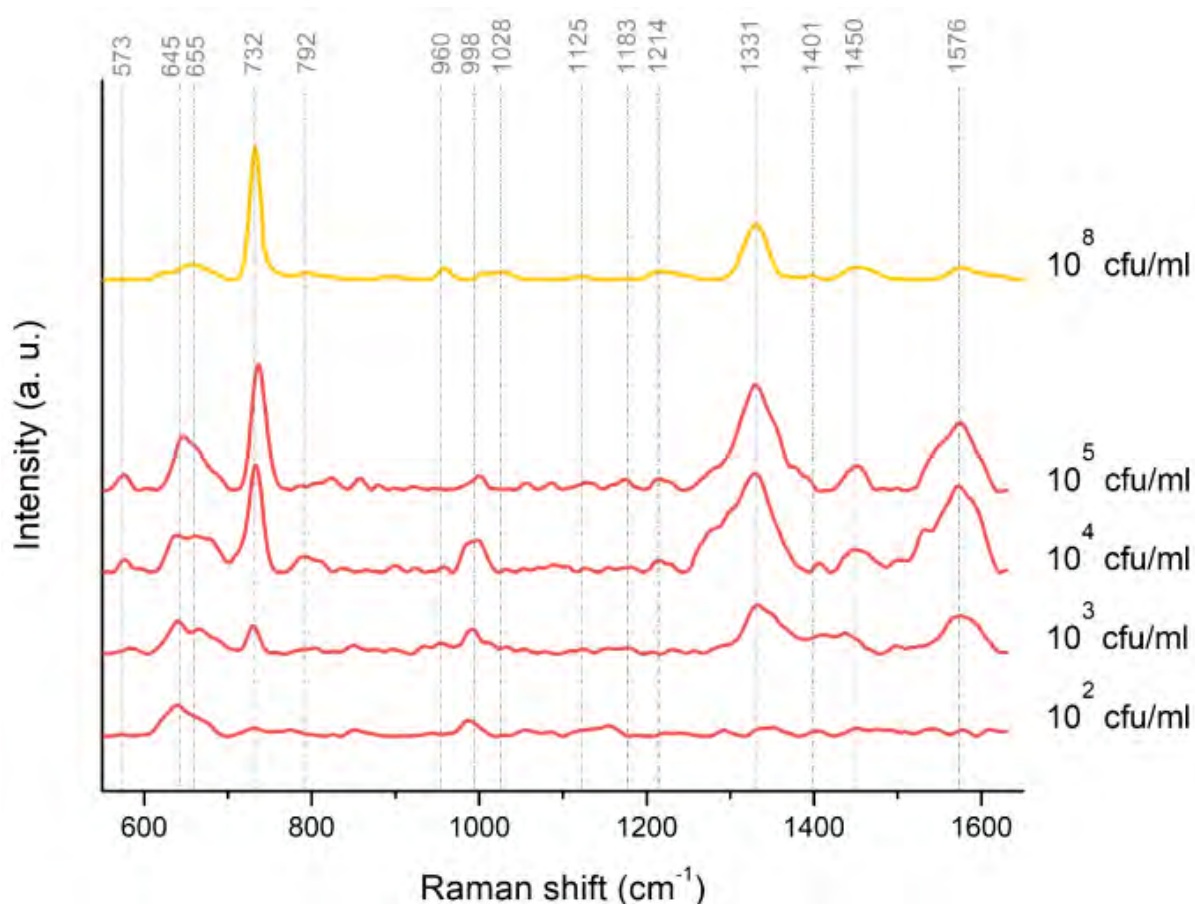
Figure 56. The stacked spectra measured to estimate the limit of detection (LOD). In order to verify the LOD, 1 mL of each of the following concentrations of A.actinomycetemcomitans 652: 10^5, 10^4, 10^3, and $10^2 cfu \times mL^{-1}$ (red spectra) was placed in the microfluidic device. The samples were prepared by serial dilution of the initial sample which was adjusted for 0.5 McFarland turbidity standards (10^8 cfu$\times$mL^{-1}). The spectrum of A. actinomycetemcomitans 652 (dark yellow), collected during standard measurement and described in the main manuscript, was presented for comparison.

The limit of detection (LOD) obtained from the experiments was at the level of 10^3 cfu$\times$mL^{-1}. Such a LOD value is sufficient to detect bacteria in human saliva, where the expected concentration is usually in the range between 10^4 and 10^8 cfu$\times$mL^{-1} [225, 226].

The conclusions. I managed to proof that for detection purposes portable devices can be used and the spectrum can be recorded sufficient to identify a microbiological hazard in no more than 45 seconds (the length of a single measurement with nanoparticles and on the platforms themselves, including data transmission to a computer). The applied PCA analysis allowed for the separation of the SERS spectra of bacteria belonging to different species (with

82, 88, and 91% of accuracy, depending on the analysed sample). Such a high separation of results coupled with exceedingly fast identification is an undisputed advantage of the SERS-PCA technique. Additionally, the similar effect was obtained for bacterial strains belonging to the same species.

In the case of experiments with the use of magnetoseparation and a microfluidic system, it was proved that nanoparticles can be effectively used for additional signal enhancement and bind to protein elements of cell walls. The lab-on-a-chip system, which I have created, controlled by infusion pumps and a mobile Raman spectrometer, additionally enables the miniaturisation of the measuring system, reduces the number of tools necessary for laboratory work and enables identification measurements in the magneto-separation zone. The obtained SERS signal was relatively strong, which is highly beneficial, especially when detecting low concentrations of bacteria in clinical samples. Additionally, the PCA performed for bacteria suspended in human saliva allowed us to separate *P. gingivalis* from *A. actinomycetemcomitans* strains with 89% accuracy. Furthermore, the sample can be prepared in a rapid and label-free manner and as a result, there is also no need for expensive reagents.

In a series of experiments, I proved that SERS spectroscopy performed on the developed Ag/Si substrates allows for the identification and detection of bacteria causing periodontal disease. The same bacteria are also reported to be present in the brain tissue of Alzheimer's patients. This makes the developed method an analytical tool that in the future can be practically used in research in hospital or clinical diagnostics with the real-life samples (and with actual analytes concentrations). The research conducted and described in this subsection led to the fulfilment of the first, fourth, fifth and sixth of the individual thesis goals.

7.3 Detection of circulating tumor cells using microfluidics and the PV/Ag and by shell-isolated nanoparticle-enhanced Raman Spectroscopy (SHINERS) – tandem

Another important field of diagnostics, in which that SERS may be implemented is related with detection of presence of cancer in the human body. The circulating tumour cells (CTCs) are living cancer cells separated from the primary tumour, which are responsible for the development and expansion of the metastasis form of cancer [227]. Their isolation and detection from human blood is an important, non-invasive way to observe the appearance or

133

evolution of a tumour. Disease-control allows for the preparation of treatment. The methodology of physical isolation of cells suspected of originating from the tumour requires multiple steps: (i) density-based cell separation size, (ii) negative selection of leukocytes with the usage of antibodies against hematopoietic cells or the depletion of leukocytes and erythrocytes, (iii) label based magnetic separation on magnetic beads modified with antibodies for tumour specific markers; (iv) segregation based on size, charge, migratory properties and deformability [228, 229]. As these types of cells require specialistic knowledge and experience, this process is exceptionally demanding and time-limiting for the progress of the entire diagnostic procedure. In order to confirm the correct typing, the CTCs involve the following techniques: polymerase chain reaction (PCR), reverse transcription PCR (RT-PCR), fluorescence scanning microscopy, immunofluorescence assays, flow cytometry analysis based on monoclonal antibodies or laser scanning cytometers [229-231]. Overall, the examination is highly time-consuming and expensive, which has a negative impact on quick and common access to diagnostics. Lately, CTCs detection techniques have undertaken novel approach based on miniaturized, nanomaterials and microfluidic reactions [232]. By using a microfluidic system with proven geometry, a set of peristaltic or infusion pumps and SERS spectroscopy, it is possible to miniaturize and greatly speed up the analysis of clinical blood samples. The high sensitivity of the SERS method on the developed and optimized Ag/PV media combined with the additional sensitivity provided by SHINs (shell-isolated nanoparticles) in the form of silica coated silver nanoparticles, may ensure the detection of cells in real blood at the clinical concentration level. Additionally, in order to distinguish between different types of CTCs, in order to more precisely define the place of spread of the disease, principal component analysis (PCA) was used to analyse the SERS data in the terms of: (i) distinguishing the spectral differences among the studied cells; (ii) extracting individual biochemical information from SERS features of each particular type of cell, and (iii) developing the models, which permit the simultaneous differentiation and classification of CTCs in complex clinical samples. In order to achieve the above-mentioned purposes in the studies presented below, the efficient capturing and accurate detection of renal carcinoma cell (Caki-1), cervical carcinoma cell line (HeLa) in the whole blood samples were performed. For the first time, a technology has been developed that allows simultaneous separation from whole blood and detection, using the SERS phenomenon, of selected tumour lines. **Details on the materials and devices used in the experiments may be found in Appendix 6.**

The cells cultivation and preparation, blood samples. The renal cell carcinoma (Caki-1) and epithelioid cervical carcinoma (HeLa) cell lines were used for experiments. The

renal carcinoma Caki-1 and epithelioid cervical carcinoma HeLa cells were cultured in RPMI-1640 and DMEM media, respectively. Both media were supplemented with 10% FBS, streptomycin (100 µg×mL^{-1}) and penicillin (100 U×mL^{-1}). The cell cultures were cultivated at 37 °C, in humidified atmosphere of 5% CO_2. During experiments the cancer cells were cultured in 25 cm^2 cell culture flasks. After reaching 80% of confluence, the cells were washed with PBS buffer and trypsinised (0.5% trypsin, 0.02% EDTA solution). Subsequently, the cells were collected, centrifuged at 250×g for 5 min at room temperature, resuspended in PBS and centrifuged again. After last centrifugation cells were resuspended in 20 µL of PBS and stored on ice. All the media and chemical reagents were obtained from Sigma-Aldrich (St. Louis, MO, USA). The initial concentration (after cultivation step) of cancer cells in PBS was ca. 0.44×10^6 cells×mL^{-1} and was further spiked into the human whole blood diluted with PBS to the 20% of hematocrit level with the final ratio of 1:800 cancer cells to blood cells (comparable to clinical samples). The cell cultures were conducted by Dr Joanna Danielewicz-Trzcińska at the Department of Molecular Biology, Faculty of Biology of the University of Warsaw.

The human blood samples derived from 10 healthy volunteers, available by courtesy of Regional Blood Centre (Warsaw, Poland) were used in our studies. An informed consent was obtained from all subjects (healthy volunteers).

The fabrication of Ag/PV SERS-active platform. The principles of preparation of SERS-remained unchanged, according to section 7.1.3 of the thesis. Polycrystalline, silicon-based photovoltaic panels had been provided to us thanks to the courtesy of Bruk-Bet Solar Tarnów, Poland as a post-production rest. A photovoltaic sample at 40×40 mm was placed in beaker filled with acetone. The first step was sonication for 10 minutes in ultrasonic bath at temperature 50 °C. Then, the acetone was exchanged and the step was repeated. After 10 minutes the beaker was filled with isopropyl alcohol and the sample was sonicated for 10 minutes at temperature 50 °C. Subsequently, the sample was sonicated for 10 minutes in distilled water (Millipore) at ambient temperature. The cleaned photovoltaic device was then dried for 30 minutes at 50 °C and placed in sterile Petri dish or immediately placed in Physical Vapor Deposition (PVD) device and sputtered with layer of silver. The prepared SERS platform was ready for use. In order to get smaller-sized platforms, 40×40 mm piece was cut with a glass-cutter.

The synthesis of SHINs. Silver nanoparticles were prepared using modified standard Turkevich's method of the synthesis of gold and silver nanoparticles [233]. To synthesize silver nanoparticles, 125 mL of 10^{-3} M aqueous solution of AgNO$_3$ was placed in a round-

bottom flask and heated to boiling under stirring. In the next step, 10 mL of a 1% solution of sodium citrate was added and the obtained mixture was kept boiling for 30 min while stirring. Then, the obtained sol was cooled to room temperature and allowed to age overnight in dark before deposition of the silica layer.

The silica layer on the silver nanoparticles has been formed by the decomposition of tetraethyl orthosilicate. In the first stage, the sol of nanoparticles was centrifuged at 5×10^3 g for 15 min. After centrifugation the supernatant was carefully removed, and the precipitate was redispersed in a smaller amount of water (to increase concentration of nanoparticles 10 times). Then, 1 mL of concentrated aqueous sol of the metal nanoparticles was introduced to 9 mL of isopropanol while vigorously stirring and 0.19 mL of 25% ammonia aqueous solution and 4 μL of tetraethyl orthosilicate were added to the aqueous / isopropanol sol of Ag nanoparticles. The mixture was stirred for 30 min at 28 °C. After that time the obtained sol of silica-covered nanoparticles was concentrated by centrifuging for 15 min at 5×10^3 g, the supernatant was poured out and the precipitate was redispersed in water. The average diameter of obtained silver nanoparticles determined from the analysis of 500 TEM images was equal to 53 ± 11 nm and the thickness of the formed SiO_2 layer was about 2-5 nm. This cleaning procedure was repeated four times. The nanoparticles were prepared at the Laboratory of Spectroscopy and Intermolecular Interactions, Faculty of Chemistry, University of Warsaw by Dr Jan Krajczewski.

The CTCs isolation in microfluidic device from the whole human blood. The proposed geometry of the microfluidic system was aimed at possibly simple and effective separation of the desired neoplastic cells. Two effects were used in the experiments: (i) inertial lift force and (ii) Dean flow [234, 235]. Based on the cellular size of the CTCs (20–30 μm), which is larger in comparison to diameter of other blood cells (2–15 μm) [236, 237], the size-based separation can be performed. Additionally, the proposed chip is equipped with an integration zone, where the separated cells, suspended in the PBS buffer with nanoparticles, are deposited on a fixed SERS platform and their spectra are measured. In order to evaluate the separation strategy of our system, in the first step, the studied cancer cells (HeLa, Caki-1) were spiked into the human whole blood diluted with PBS to the 20% of hematocrit level with the final ratio of 1:800 cancer cells to blood cells (comparable to clinical samples [238]). Then, the resulting mixture of cancer cells and blood flows from the syringe (the flow driven by an infusion pump) was introduced into the system via Inlet 1. Subsequently, it was focused by mixture of PBS fluid with SHINs that was injected via Inlet 2. The diagram and the course of the two types of flow are presented in *Figure 57*.
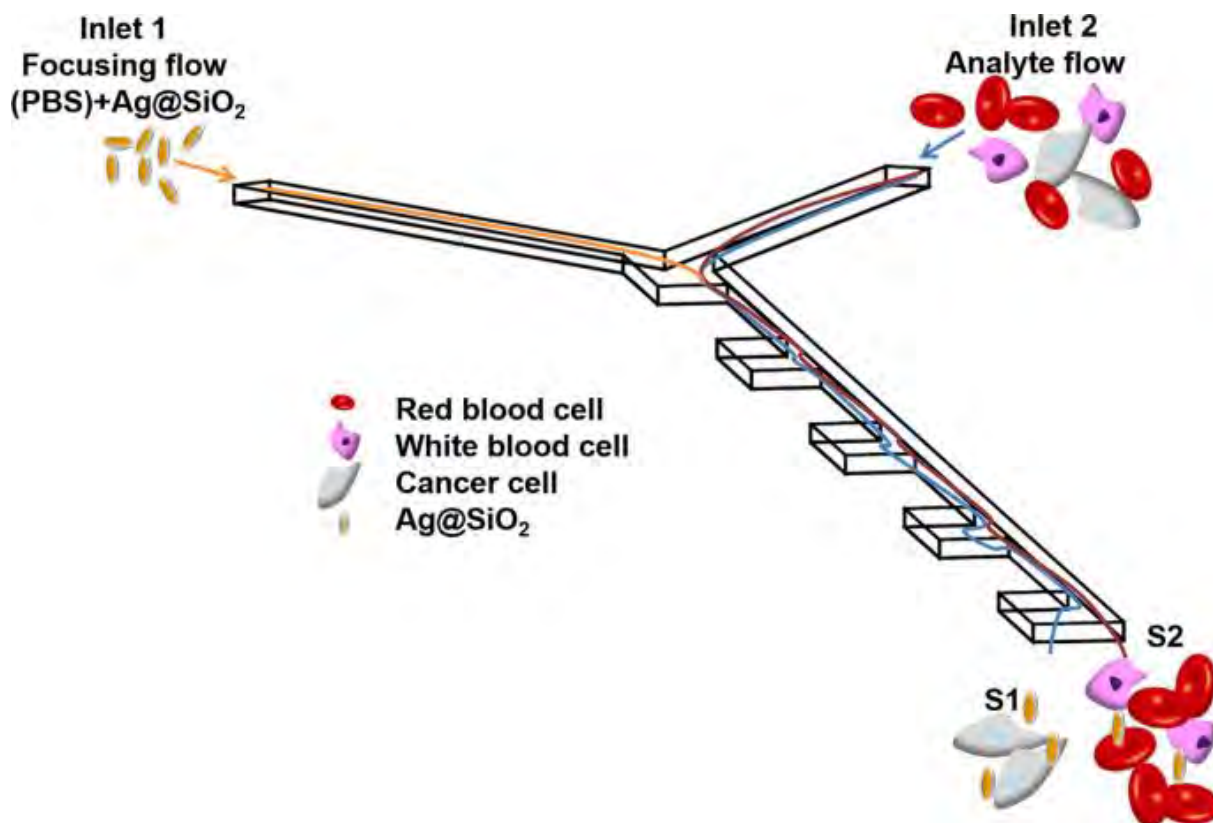
Figure 57. The schematic view of cancer cell isolation from whole blood. Through Inlet 1, a focus stream containing Ag@SiO$_2$ suspended in PBS solution was introduced into the system, and human whole blood was introduced through Inlet 2. The flow rate was optimized individually for each experiment in order to obtain the best possible separation of S1 and S2 flows at the chip exit [239]. The dimensions of the nanoparticles and blood components do not correspond to the true scale in which the geometry of the microfluidic system is presented.

The hydrodynamics of the separation technique was inspired by the works in which it was experimentally confirmed and theoretically analysed [192, 235]. The cancer cells movement is mainly caused by the inertial lift force. Therefore, these large cells move towards sidewall S1. The smaller cells of the blood composition, which movement is mainly influenced by Dean flow at each entrance of the concentration region, flow towards sidewall S2. The stream of isolated CTCs passes through the optical chamber with incorporated SERS-active platform and were finally analysed by recorded SHINERS spectra.

Apart from two infusion pumps, two syringes with needles connected to the inputs by means of Teflon hoses, few simple and cheap reagents and the microfluidic system itself, the isolation procedure does not require additional elements. This a great advantage of a given method, significantly simplifying the experiment and shortening its time. In addition,

the detection and identification in the next step by means of spectroscopic measurements ensures a quick recognition of the analyte.

      The SHINERS investigations. As with the spectra of bacteria cells, the spectra of cancer cells or blood cells differ from each other due to the dissimilarities in the amount and composition of amino acids, proteins, nucleic acids, lipids. The differences make it possible to distinguish various cancer cell lines from the blood and from each other [168]. In order to detect and identify cells in a microfluidic system, the first step was to measure their spectra from pre-cultures and get acquainted with their spectral image, directly on PV/Ag platform. The cells were applied on the platform at the starting concentration and the measurement was started immediately after the spectrometer was set up. The results of the experiment are presented below in *Figure 58*.
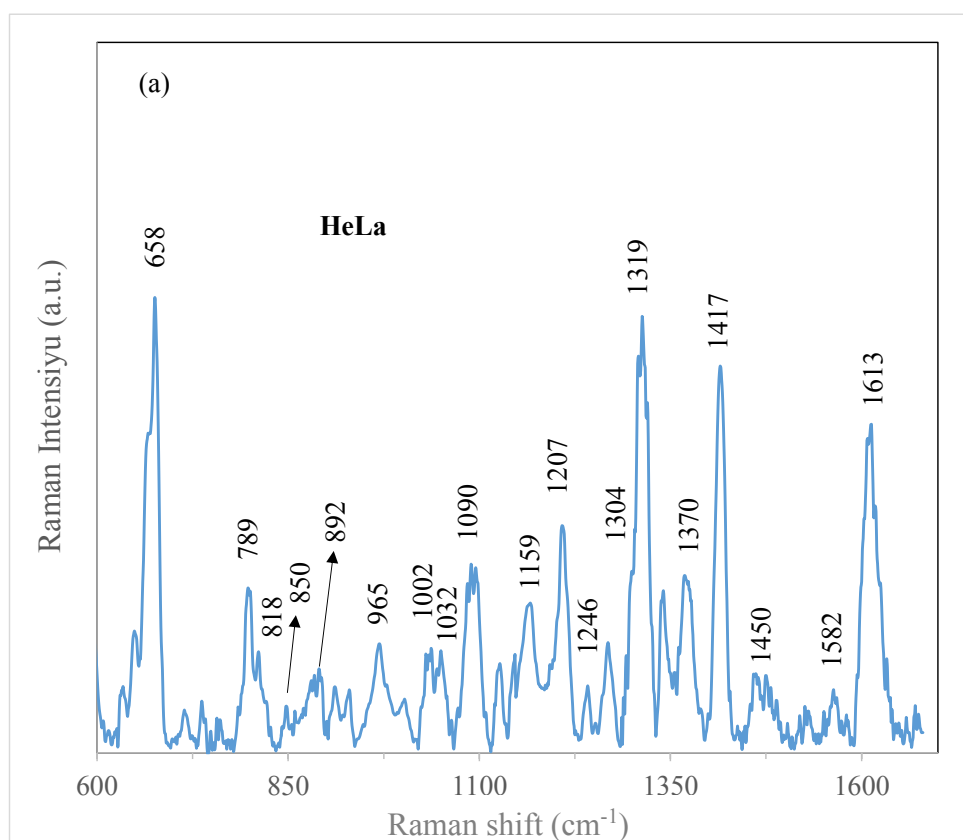
Figure 58. The reference SERS spectra of (a) HeLa and (b) Caki-1cells placed directly from pre-cultures onto the SERS substrate. The spectra were averaged over 40 SHINERS spectra for each cell types. The single spectrum acquisition took 20 s, by using this mapping mode. The incident laser power was set at about 2.5 mW [239].
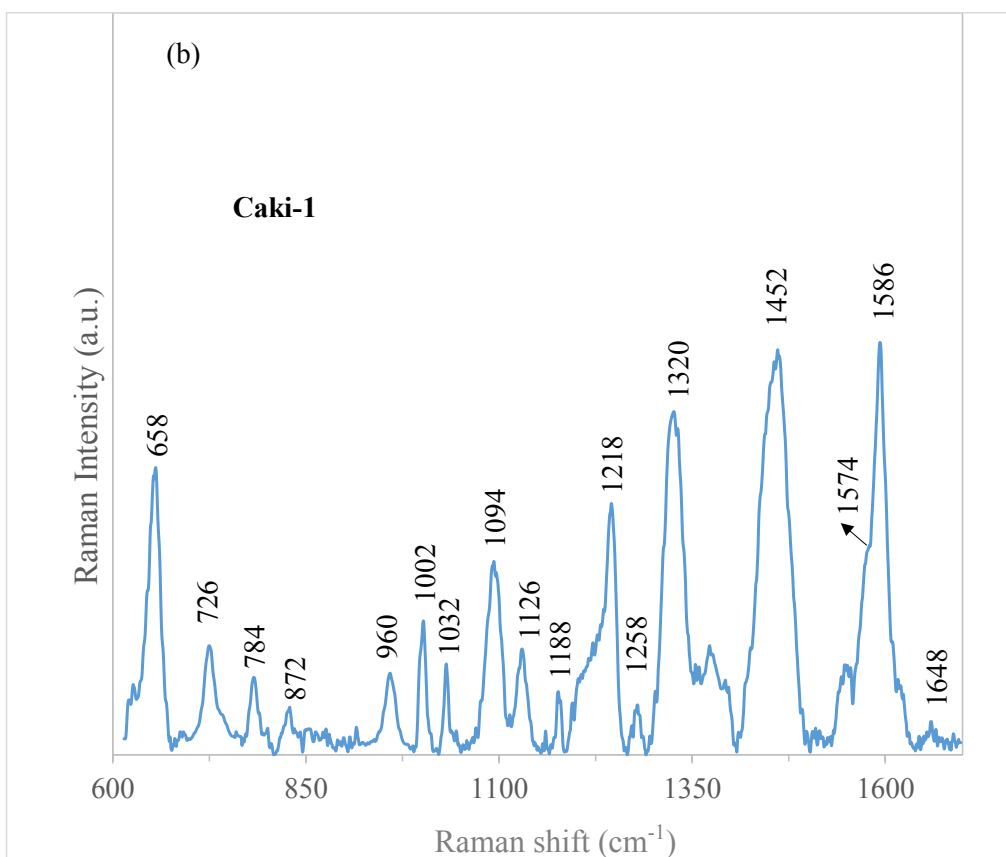
Figure 58. The continuation from page 138.

The following table presents the main SERS bands observed in the analysed cells and the corresponding bands assignments [175, 240-244].

Table 9. The assignment of SERS bands depicted in Figure 58.

Observed SERS band (cm^{-1})	Vibrational mode	Assignment
638	C-S stretch	globin and cellular components (cysteine)
716	$d(COO^-)$	globin and cellular components (amino-acids)
796	n(pyr breathe), n_6	porphyrin
863	$g(C_mH)$	porphyrin
904	C-C stretch	globin and cellular components (glutamic acid, isoleucine, threonine, lysine)
956	C-C stretch	globin and cellular components (proteins)

139

1002	indole assymetric ring breathe	globin and cellular components (phenylalanine)
1027	in plane ring CH deform	globin and globin and cellular components (phenylalanine)
1104	C-N, C-C stretch	globin and cellular components (proteins, lipids)
1127	C-N, C-C stretch	globin and cellular components (proteins)
1215	$d(C_mH)$, n_{13}'or n_{42}	porphyrin
1257	CH_2 wagging $d(CH_2 / CH_3)_6$	globin (glutamic acid) and cellular components (proteins, lipids: Amide III)
1286	$g(C_mH)$, n_{21}	porphyrin
1326	CH_2 wagging	globin and cellular components (phenylalanine, glutamic acid, serine, methionine, histidine)
1342	CH_2 scissoring CH_3 deformation	globin and cellular components; glutamic acid, aspartic acid, asparagine, glutamine; alanine, leucine, valine, isoleucine
1446	$d(CH_2 / CH_3)$	globin and porphyrin
1488	CH and ring	tryptophan
1562		porphyrin (skeletal mode) and cellular components
1609		porphyrin

In the next step, I performed an experiment in a microfluidic system with the use of blood collected from the patient. In one embodiment, HeLa cells were added to the blood and, in the other, Caki-1 cells. The spectrum of blood was measured by placing the Ag/PV platform in the collection tank for the separated blood. having completed the separation experiment and measured the spectra of the cells of the tumour line, the platform was transferred to the microscope stage of the spectrometer and the evaluation was performed.
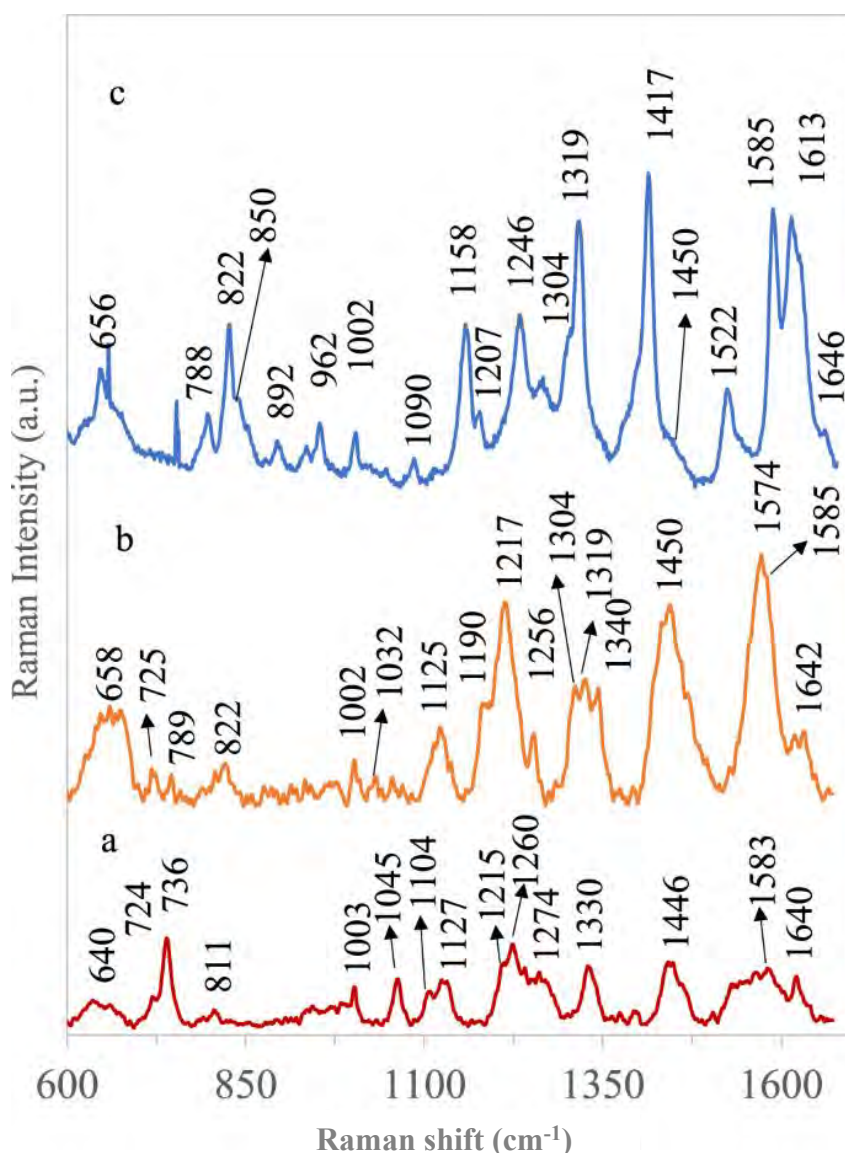
Figure 59. The averaged and normalized SHINERS spectra of (a) blood cells, (b) Caki-1, and (c) HeLa cells recorded on Ag/PV SERS platform in microfluidic device [239].

The spectra (*Figure 59*) obtained from the material gathered as a result of separation from the blood in the microfluidic system and those obtained after direct deposition of the analyte on the platform were extremely similar to each other. The spectra revealed common spectroscopic features characteristic for the eukaryotic cell [166]: the band-shoulders around 1256 cm^{-1} and 1600 cm^{-1} were assigned to Amide I bands, aromatic amino acid contributions appeared around 1002 cm^{-1} (phenylalanine) and 656 cm^{-1} (tyrosine). The vibrational modes of nucleic acid were present at 789 and 1090 cm^{-1}. In addition, the spectra of both cell lines presented individual characteristics in the form of bands observed for the sample containing Caki-1 cells, i.e. the band at 1417 cm^{-1} corresponded to adenine and guanine, nucleic acid nucleotides and the band at 1522 cm^{-1} associated with carotene [137]. In addition, there were

differences in the form of changes in the intensity of the bands present in the spectra of both cell lines, that is: in the spectrum of Caki-1 appeared a highly intensive band at 1450 cm^{-1} and a week band at 822 cm^{-1}. Both corresponded to the structural protein modes of tumours [245]. These two bands were also present in the spectrum of HeLa cells but with changed relative intensities.

In the SHINERS spectrum of blood cells, that consist mainly of leucocytes and erythrocytes, multiple bands appeared that are typical for porphyrin -1215, 1446, 1583 cm^{-1}, globin vibrations - 640, 724, 1003, 1260, and 1330 cm^{-1}, and some others, which may include contribution from proteins and lipids (1104, 1127, 1260 cm^{-1}) [246-249].

The most prominent bands for globin and cellular components, cysteine, appeared at 640 cm^{-1}, for thiocyanate 736 cm^{-1}, 1003 cm^{-1}, C-C vibration of phenylalanine , in plane ring CH deformation mode of phenylalanine 1045 cm^{-1}, C-N, C-C stretch in plane of protein 1127 cm^{-1}, proteins, lipids: Amide III 1260 cm^{-1}, globin and cellular components 1330 cm^{-1}, globin and porphyrin 1446 cm^{-1} [168, 170, 172].

The spectroscopic data revealed, that the CTCs can be distinguished from blood cells thanks to the bands at 656 cm^{-1} (C-C twisting mode of tyrosine), 1158 cm^{-1} (CH$_2$CH$_3$ bending modes of lipids), 1319 cm^{-1} (CH$_3$ deformation mode of collagen), 1417 cm^{-1} (C = C stretching in quinoid ring), 822 and 1450 cm^{-1} (structural protein modes of tumours). The band at 1450 cm^{-1} was assigned to overlapping asymmetric CH$_2$ bending and CH$_2$ scissors vibrations. Phospholipids, elastin, and collagen were also recognized to present a band in this region [173-175]. All the differences reflected the changes in biochemical pattern between normal, healthy blood cells and uncontrollably mutating and developing cancer cells.

Due to the fact that nanoparticles are segregated in the same system as the stream of neoplastic cells and they do not end up in the container for the separated blood, the recorded spectrum of blood is characterized by a much lower intensity than the SHINERS spectra. In order to verify how SHINs affect the spectral intensity of tumour cells, the experiment was repeated without the addition of nanoparticles to the focusing stream.
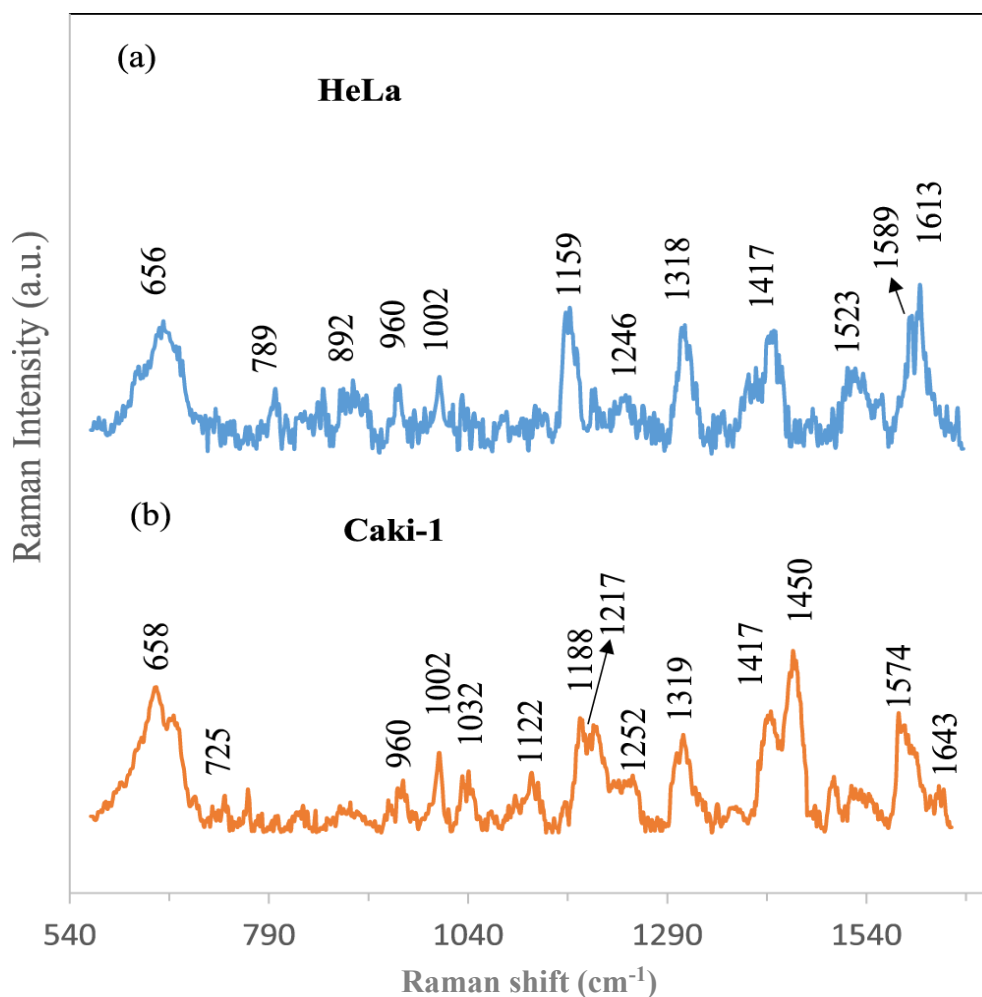
Figure 60. The averaged and normalized SERS spectra of (a) HeLa and (b) Caki-1, cells recorded on Ag/PV SERS platform in microfluidic device without shell-isolated nanoparticles [239].

As one may note in *Figure 60*, the intensity of the spectra obtained without the addition of nanoparticles was several times lower than those recorded in the SHINERS method. Therefore, an increase in the sensitivity of the method was confirmed by the application of additional 'hot spots', created in a similar way as those explained in Chapter 7.1.5 of the following thesis. Additionally, on a sample of 100 measured SHINERS spectra, the calculations of relative standard deviation (RSD) were performed for the strong signals at 658 and 1613 cm^{-1} and the achieved result was 8% and 7.2%, respectively. This result indicates a high repeatability of the method and the potential for its further development towards ensuring applicability.

Finally, in order to introduce objective identification of individual analytes into the method, the results of the experiment with SHINs, i.e., the spectra of both cell lines and blood, were subjected to PCA analysis (40 spectra of each analyte). The principal component

143

scores (*Figure 61*) demonstrated that only two PCs (PC-1 and PC-2) were important for analysed cells differentiation. The PC-1 and PC-2 resulted in the sum of the variance at 89%. In this way, these two PCs allowed for an effective differentiation between all studied cells.
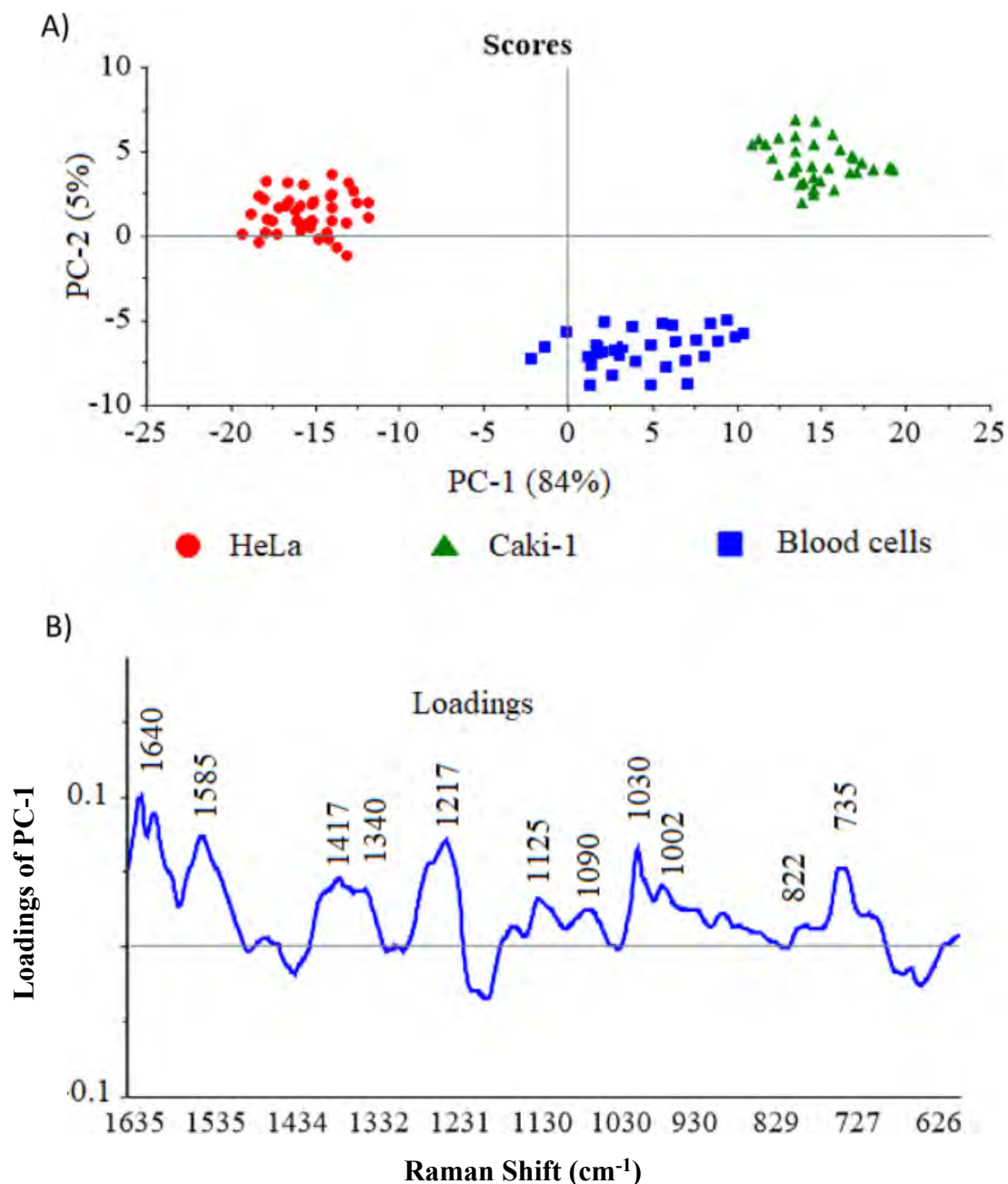
Figure 61. The plots of (A) two dimensional PC-1 versus PC-2 scores component calculated for blood cells (blue squares), HeLa (red dots) and Caki-1 (green triangles) cells and (B) corresponding PC-1 loading data [239].

The plot of scores related to PC-1 to PC-2 demonstrated that all spectral data could be divided into three groups corresponding to blood cells (blue), renal cell carcinoma (Caki-1) (blue) and HeLa (red). The cluster of blood cells proved the relatively lower homogeneity in

comparison to cancer cells. This might have been related to the more complex structural changes of all expected cells in filtered blood e.g., erythrocytes and lymphocytes. the loading of PC-1 gave insight into the bands that were the most significant for the cells differentiations. Following bands provided a high input into the differentiation: 735 cm^{-1} (thiocyanate), 1030 cm^{-1} (phenylalanine and / or lipid), 1217 cm^{-1} (Amide III), 1340 cm^{-1} (proteins, glutamic acid, serine, methionine, histidine), 1417 cm^{-1} (C=C stretching in quinoid ring), 1585 cm^{-1} (phenylalanine, tyrosine) and 1640 cm^{-1} (Amide I). There were other wavenumbers at about 822, 1090, 1125 cm^{-1} that also contribution to PC-1 in the same direction as the most intensive loadings. As one may notice, many spectral bands presented above were consistent with the SHINERS features commented in the spectra analysis, performed earlier in this section.

The conclusions. In a series of experiments, an effective, non-invasive and label-free method of isolation, detection and identification of CTCs was developed. Its strength is the sensor in the form of a combination of a SERS-active platform based on photovoltaic cell (Ag/PV) and appropriately designed SHINs (shell-isolated nanoparticles) in the form of silica coated silver nanoparticles that additionally improved SERS sensitivity and allowed for maintaining a high reproducibility and stability of recorded SERS signals. Another advantage is the constructed microfluidic device for high-throughput isolation of cancer cells from whole blood samples. The entire procedure in conjunction with PCA was applied for improving the efficient screening, detection, and discrimination of a particular CTCs in complex biological samples. The developed statistical model allowed for a diagnosis accuracy of 89% in the differentiation of blood cells, renal cell carcinoma (Caki-1) and cervical carcinoma (HeLa) cells, based on the SHINRS spectra of the individual cells. It was proven that the developed device for the CTCs separation and analysis presents a colossal potential for inventing the personalized cancer treatment solution. The research conducted and described in this section led to the fulfilment of the third, fourth, fifth and sixth of the individual thesis goals.

7.4 DEP-SERS-based analysis of the environmental and clinical samples.

Among the many species of Gram-positive and Gram-negative bacteria that pose a threat to human health and life through their consumption with food, one of the greatest threats are cronobacters. These *Cronobacter* spp. are foodborne pathogens posing a particular risk to infants. They may cause conditions such as sepsis, meningitis, necrotising enterocolitis as a result of the consumption of contaminated infant formula powder and may survive during transit in the newborn stomach [250]. They have a particular ability to persist in dry environments (the pathogen is even capable of resisting osmotic pressure, high temperatures, drying and shows acid resistance at pH=3.0 [251] including powdered foods and, as a result, it may also affect immunocompromised adults [252, 253]. As part of the growing awareness and thanks to the development of statistics on this threat, the European Union introduced regulation (EC) No. 2073/2005 [254] as amended later by regulation (EU) No. 365/2010 [255], which requires the absence of *Cronobacter* spp. up to 30 units of 10 g test portions of dried infant formulae and dried dietary foods for special medical purposes intended for infants below six months of age. The regulation concerned includes 7 species: *C. sakazakii, C. malonaticus, C. turicensis, C. muytjensii, C. dublinensis, C. universalis* and *C. condimenti*. Originally, the methodology of bacteria detection was regulated by the ISO/TS 22964: 2006 standard [256], however, it was updated to the standard EN ISO 22964: 2017 [257], as it was demonstrated that several isolates of *Cronobacter* spp. did not grow well in the media and under conditions described in the previous standard [258].

In connection with the attempt to use the SERS method to detect and identify all seven *Cronobacter* strains, the bacteria that are considered as accompanying bacteria in contaminated food (and also may pose a health hazard to adults and children) was additionally tested. To further increase the similarity between companion bacteria, related species from the Enterobacteriaceae family were selected: *Escherichia coli* (3 strains), *Enterobacter cloacae* (5 strains) and *Salmonella enterica* (5 serovars). *E. coli* strains do not cause disease when naturally living in the guts [259]. However, the virulent strains may cause for example: gastroenteritis, urinary tract infections or neonatal meningitis. *Enterobacter cloacae* is a regular member of the normal guts flora of many humans [260]. As for Salmonella, some strains are associated with infections in immunocompromised individuals, which generally results in food poisoning, when a person ingests foods containing a high concentration of the bacteria. It may cause diseases such as: urinary tract and respiratory tract infections. In all

146

cases, infants and young children are much more susceptible to infection, easily achieved by ingesting even only a small number of bacteria.

Having measured the spectra of the above-mentioned bacteria and analysing their spectra using PCA in order to verify the method for distinguishing these bacteria, the spectra of environmental *Cronobacter* strains were examined in order to differentiate them from the accompanying strains. This experiment was supposed to verify the usefulness of the SERS application in the case of a large number of strains found in the real samples in comparison with their standards from libraries of bacterial strains.

Additionally, an experiment was conducted to simulate a real clinical situation. The obtained clinical strain of *C. sakazakii* from the blood of an infected infant was added to a sample of infant formula. An attempt was made to isolate the pathogenic bacteria and detect them on the SERS platform using the dielectrophoretic effect and the microfluidic system. Its surface topography (created with the use of a femtosecond laser) allowed at the same time to isolate bacteria from the matrix in a flow using the DEP phenomenon and to perform spectroscopic measurements on the centrally located SERS-active 'island' to obtain spectra. The spectra collected during this experiment were used to identify the strain based on PCA analysis with the use of previously used reference spectra. **Details on the materials and devices used in the experiments may be found in Appendix 7.**

The bacterial strains. Seven strains of *Cronobacter* spp. were obtained for the purpose of experiment: *C. sakazakii (*ATCC 29544)*, C. malonaticus* (LMG 23826)*, C. turicensis* (LMG 23827)*, C. muytjensii* (ATCC 51 329)*, C. dublinensis* (LMG 23823)*, C. universalis* (LMG 9529) and *C. condiment* (LMG 26250). Five strains of *Enterobacter cloacae* were obtained for the purpose of experiment: *E. cloacae* (CCUG 3012), *E. cloacae* (DSM 6254), *E. cloacae* (DSM 30062), *E. cloacae* (DSM 109592), *E. cloacae* (DSM 10593). Three strains of *Escherichia coli* and five serovars of *Salmonella enterica* were obtained from the Institute of Microbiology, Faculty of Biology, University of Warsaw, Poland: *E. coli* 517, *E. coli* DH5α, *E. coli* TG1, *S. virchow*, *S. typhimurium*, *S. saintpaul*, *S. oranienburg* and *S. entriritidis*.

Additionally, 26 strains (*Table 10.*) of *Cronobacter* spp. of environmental origin were obtained from Department of Molecular Mirobiology, Faculty of Biology, University of Warsaw, Poland:

147

Table 10. The list of the environmental strains of Cronobacter bacteria used in the experiments.

Strain	Source of isolation	Year of isolation
MK_1	Milk	2017
MK_2	Herbes de Provence	2017
MK_3	Blackground pepper	2017
MK_4	Herby pepper	2017
MK_5	Basil leaves	2017
MK_6	Oregano leaves	2017
MK_7	Spicy pepper	2017
MK_8	Pepper herby	2017
MK_9	Herbal tea	2017
MK_10	Oregano leaves	2018
MK_11	Herbes de Provence	2018
MK_12	Tarragon	2018
MK_13	Marjoram leaves	2018
MK_14	Basil leaves	2018
MK_15	Sweet pepper	2018
MK_16	Sweet pepper	2018
MK_18	Sweet pepper	2019
MK_19	Herbes de Provence	2019
MK_20	Herbes de Provence	2019
MK_25	Herby pepper	2019
MK_26	Basil leaves	2019
MK_28	Sweet pepper	2019
MK_29	Basil leaves	2019
MK_31	Marjoram leaves	2019
MK_32	Basil leaves	2019
MK_37	Herbes de Provence	2019

One clinical strain of *Cronobacter sakazakii* was obtained from the blood of an infected infant and donated by Prof. Anna Skoczyńska (the National Reference Centre for Bacterial Meningitis in the National Medicines Institute, Warsaw, Poland).

The preparation of Si/Ag SERS Platforms. The preparation of a silicon-based SERS substrate, consisted of five main steps. The cutting saw was used for the formation of squares (3.5×3.5 mm) from the silicon wafer. A mechanical cutting saw was implemented (type: Disco DAD 2H/6TM) at the Institute of Electronic Materials Technology in Warsaw, Poland. They were also the producer of the silicon wafers that were applied in the procedure. Secondly, the silicon surfaces were washed with great care with deionized water. Next, all of

148

the residues were removed and the cut wafers were dried in a stream of argon. Afterward, the silicon surface was modified with the use of a femtosecond laser (based on potassium yttrium tungstate, with 1030 nm wavelength, repetition rate of 300 kHz, and a single pulse set to 300 fs. In the final step, the modified silicon surface was sputtered with 100 nm of silver.

For the experiments with the use of DEP and the microfluidic system, a separate series of SERS media with built-in electrodes was prepared to perform the dielectrophoretic separation of bacteria. First, the substrates were prepared according to the standard procedure, with the difference that the square, on which the surface was modified, was about 5 x 5 mm. Then, in order to create the appropriate geometry of the electrodes and the 'island' active in the SERS technique the linearly polarized beam from previously described femtosecond laser was delivered to a computer-controlled vertically adjustable sample-holding platform through a galvanometric scanner and focusing optics with the focal length of f=163 mm. The resulting beam focal spot diameter was 60 μm. Using the same parameters as for the laser surface ablation process, in order to create a matrix for nanoplasmonic structures, the conductive layer was removed, in line with the geometry (*Figure 62 (a)*) developed in Group 1 of the Institute of Physical Chemistry of the Polish Academy of Sciences [261].
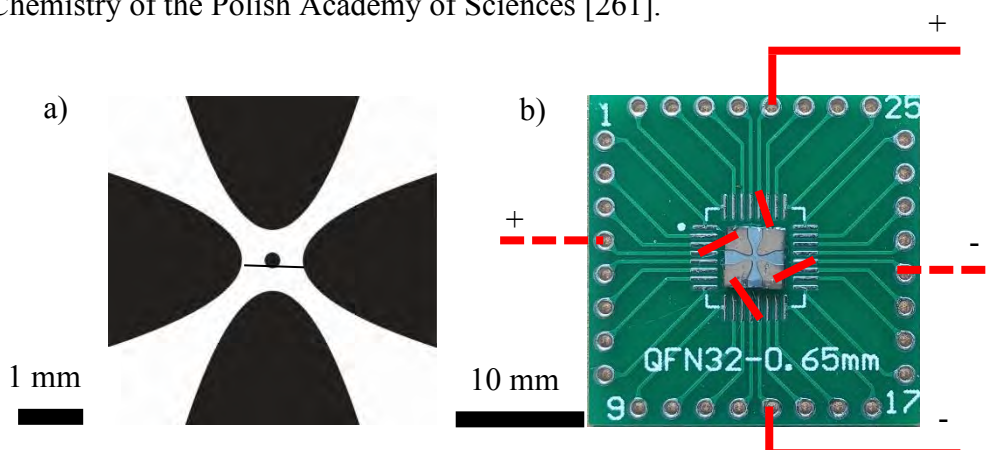
Figure 62. The symmetry of the electrodes and the 'SERS island' mapped on the surface of the SERS Si/Ag platform by laser ablation (a). The black area shows the parts unmodified by the ablation process, while the white area demonstrates the laser working area; PCB adapter - QFN32/QFP32 with localized SERS-DEP chip. The continuous red lines and the dashed lines depict the diagram of electrical connections made by soldering and silver conductive paste.

The SERS-DEP chip, which I have developed, was glued to the PCB of the adapter - QFN32/QFP32 with cyanoacrylate glue. The electrodes on the SERS-DEP substrate were connected to the electrical leads on the PCB using Conductive Silver Cement. These, in turn, were soldered to copper electric wires, to which the outputs from the Siglent SDG 2042X Function Generator were later connected, and the function sequence and voltage

149

between the electrodes were monitored and fine-tuned with the UNI-T UPO2074CS oscilloscope. The schematic diagram of all electrical connections is presented in *Figure 62 (b)*. The layout of the microfluidic chip is depicted in *Figure 63*.

The measurement of Cronobacter bacteria spectra of reference and environmental strains with identification by PCA analysis. I have examined seven strains of cronobacters to test the potential of the SERS technique to distinguish them. The measurements were made for strains grown on solid media. Twenty-five evaluations were made each time using a portable Bruker Bravo spectrometer, while testing its potential in the study of microorganisms with SERS spectroscopy.
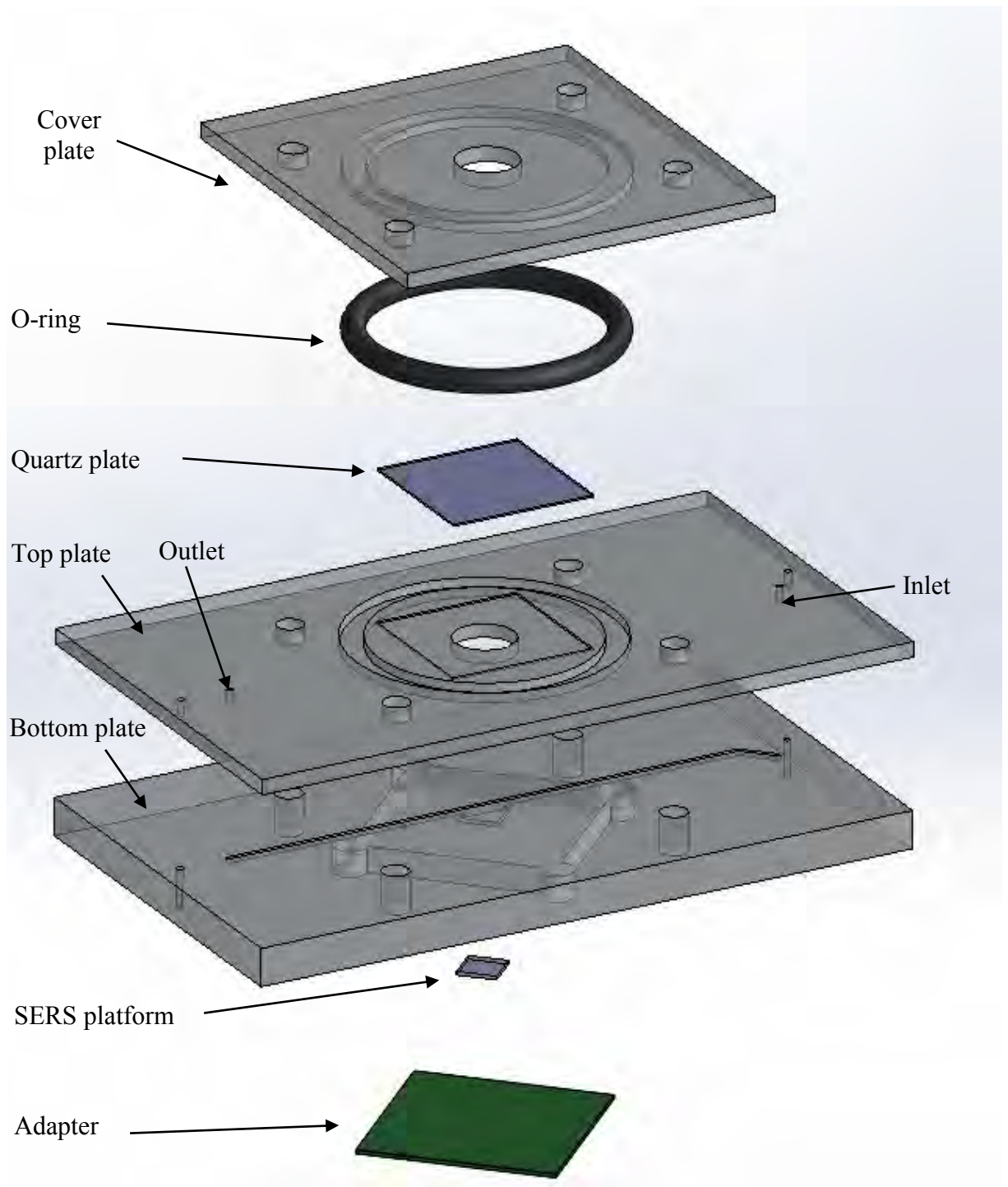
Figure 63. The diagram of the microfluidic system: cover plate with a pocket for an O-ring, a hole for the laser beam and holes for screws coupling (M3) the element with the system; sealing O-ring; quartz glass with dimensions of 19.00x19.00x0.55 mm; the upper part of the microfluidic system with an O-ring milling, a through hole (8 mm in diameter) for the laser beam, Inlet and Outlet holes (0.8 mm in diameter), two holes for positioning pins and holes for screws fixing the system with a cap element; the lower part of the microfluidic system with a channel with a thickness and height of 0.6 mm made in the upper part of the system, milling for the adapter - QFN32/QFP32 and milling for the SERS-DEP platform, which on the diagonal of the system is a through hole (6 mm in diameter) giving access to the 'SERS island' by the analyte, two holes for positioning pins and holes for screws fixing the system with the cover element; SERS-DEP platform; Adapter - QFN32/QFP32.

151
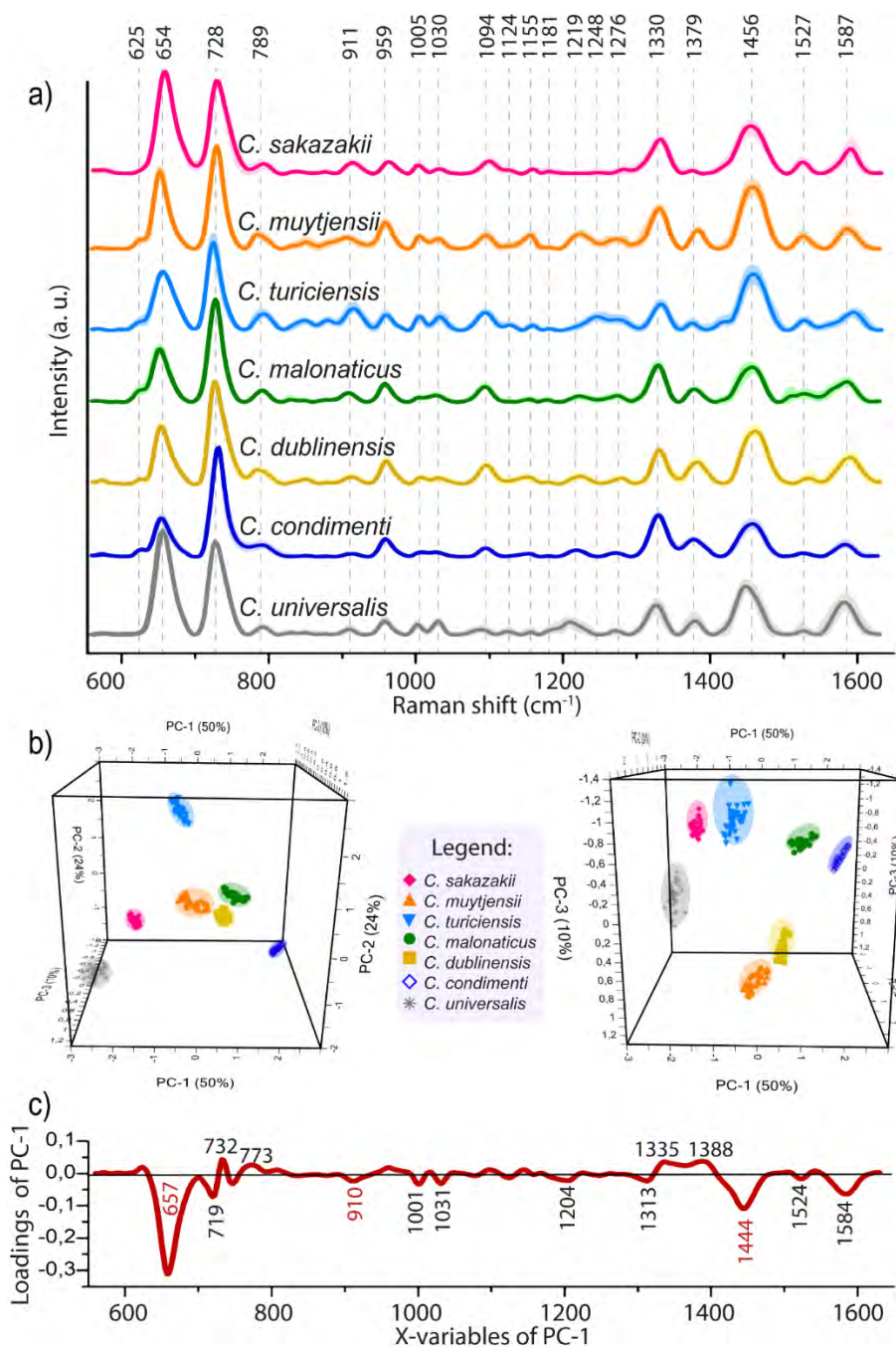
Figure 64. The spectra of seven reference strains of the genus Cronobacter (a). The thick line represents the spectrum averaged from 25 measurements, while a paler shade of the same colour, for a given species, depicts all the overlapping spectra of a given species. A three-dimensional representation of the PCA analysis, is presented in two views for better insight into the results (b). The loading of PC-1 analysis result demonstrating the contribution of the diagnostic bands to the differentiation of the analysed bacterial species (c).

The recorded signals (*Figure 64.*) were characteristic of the spectra of bacteria. The spectral image was dominated by intense signals at 654 cm^{-1} (C-S stretching, C-C twisting of proteins tyrosine), 728 cm^{-1} (adenine - FAD, NAD) and medium-intense signals at 959 cm^{-1}

152

(C=C def., C-N stretching), 1094 cm^{-1} (O-P-O (DNA), C-C or C-O-C stretching), 1330 cm^{-1} (CH$_3$, CH$_2$ wagging), 1456 cm^{-1} (CH$_3$, CH$_2$ deformation) and 1587 cm^{-1} (C=C bending mode - phenylalanine). In addition, the spectrum demonstrates characteristic signals of low intensity and at the same time variable in case of intensity for different species at 625 cm^{-1} (C-C twisting- protein), 789 cm^{-1} (ring breathing mode of cytosine, uracil), 911 cm^{-1} (C=C def., C-N stretching), 1005 cm^{-1} (phenylalanine, C-C aromatic ring stretching), 1030 cm^{-1} (C-N stretching, C-C stretching- phospholipids carbohydrates), 1124 cm^{-1} (=C-OC= - unsaturated fatty acids in lipids), 1155 cm^{-1} (CH$_2$CH$_3$ bending modes of lipids), 1181 cm^{-1} (C-O ring, aromatic - proteins), 1219 cm^{-1} (Amide III - random, thymine), 1248 cm^{-1} (Amide III), 1276 cm^{-1} (Amide III), 1379 cm^{-1} (tryptophan, guanine) and 1527 cm^{-1} (cytosine) [137, 191, 213, 262].

The differences in the spectral image for all seven species made it possible to distinguish them by PCA analysis, with a PC-1 score of 50%, a total of PC-1.2 and 3 of 84% and accuracy of 90%. The single spectra represented by symbols with corresponding colours are visible on the three-dimensional compilation of the PC analyses. The spectra were characteristically divided into coherent groups of points, corresponding to a given species. They were well grouped and spatially separated. Significant differences visible to a naked eye were the variable intensity ratio of the bands at 654 and 728 cm^{-1} between species and significant differences in intensity, shape and slight differences in the shift of the band around 1456 cm^{-1} may be observed. The mutual comparison of as many as 7 different species becomes very difficult using only visual analysis, therefore the loadings of PC-1 were compiled in the X-variables of PC-1 function. This analysis proved that the 657 and 1444 cm^{-1} bands made the greatest contribution to the diversity of spectra, which were clearly a component of the band at 1456 cm^{-1} with a large half-width. A smaller but significant input was given by the bands at 719, 732 (band at 728 cm^{-1}), 773, 1335, 1388, and 1584 cm^{-1}.

The above results clearly show that the combined SERS-PCA method is well suited to differentiate the tested *Cronobacter* species. Despite the intrinsic similarities, the disparities in the composition of the membrane and the metabolites of the tested material make it possible to distinguish them. These are satisfactory preliminary results and reference data for further experiments with clinical material. Previously however, 26 strains of *Cronobacter* spp. of environmental origin were measured. The tested strains were assigned to the corresponding species using the 16S rRNA analysis performed at the Institute of Microbiology, Faculty of

Biology, University of Warsaw, Poland. The colours of the spectra in the *Figure 65.* below correspond to the colours of the species of the reference spectra presented above (*Figure 64*).
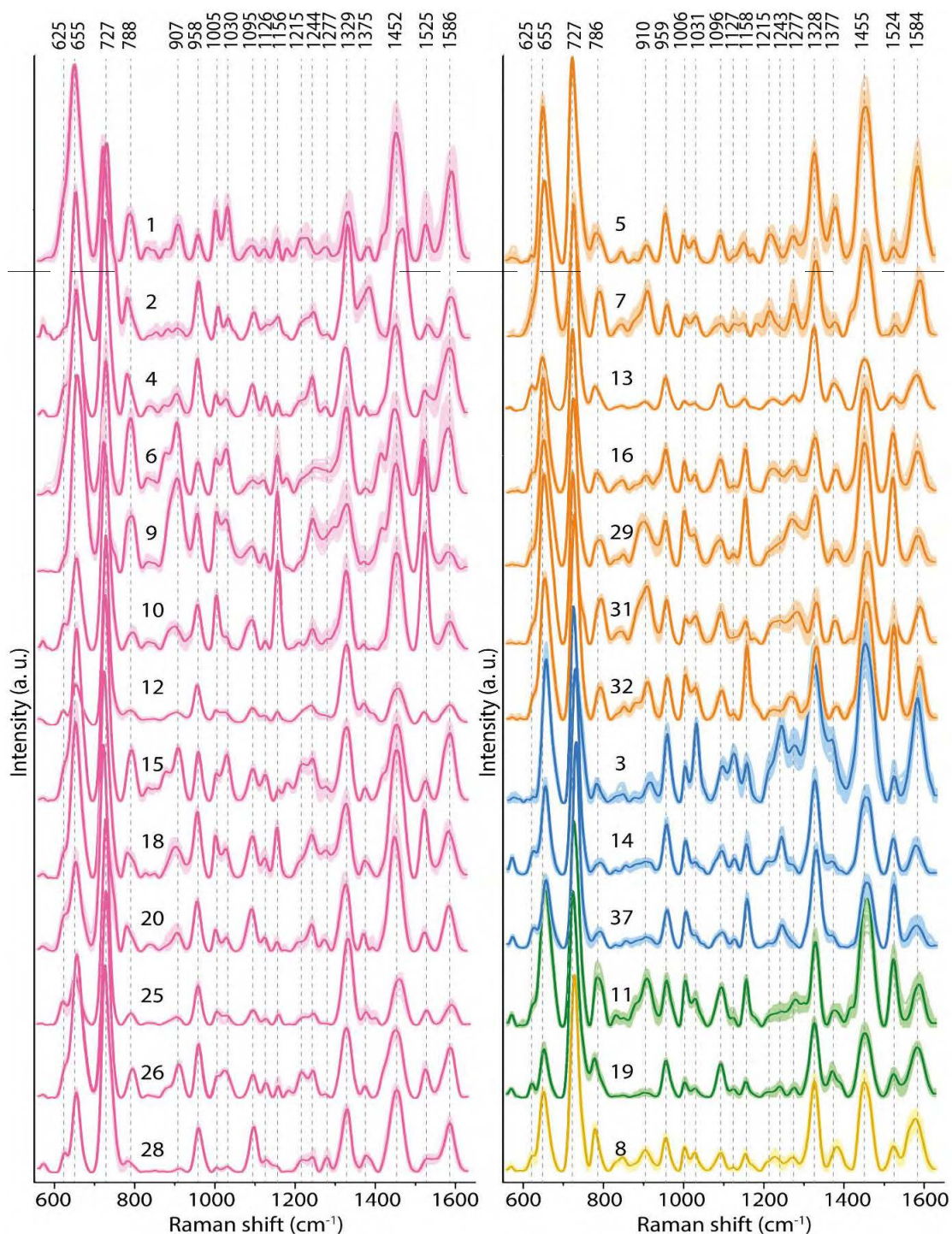
Figure 65. The SERS spectra of twenty-six environmental strains of the genus Cronobacter (a). The thick line represents the spectrum averaged from 25 measurements, while a paler shade of the same colour, for a given species, depicts all the overlapping spectra of a given species. The spectra: 1,2,4,6,9,10,12,15,18,20,25,26 and 28 represent the spectral image of the strains belonging to the species C. sakazakii; 5,7,13,16,29,31,32 - C. muytjensii; 3,14, 37 - C. turiciensis; 11,19 - C. malonaticus; 8 - C. dublinensis.

The spectra presented above demonstrated the presence of bands at Raman shifts and intensities consistent with the data obtained for the standard strains. The large number of the results did not allow for an in-depth, empirical comparative analysis. The PCA analysis of the spectra of environmental and reference strains was performed in the further part of the study together with data from *Cronobacter* companion strains.

The SERS measurement of environmental, companion strains of bacteriaalong with identification by comparison with PCA analysis. Three *Escherichia coli* strains, five *Salmonella enteritidis* serovars and five *Enterobacter cloacae* strains were measured. All strains, that I have examined, were environmental strains and their comparative analysis with environmental and standard *Cronobacter* spp. bacteria was directly aimed at testing the SERS method, combined with statistical PCA analysis of the obtained spectra, in research on multiple microbiological hazards in clinical and environmental samples. The obtained results are presented below (*Figure 66*).

155
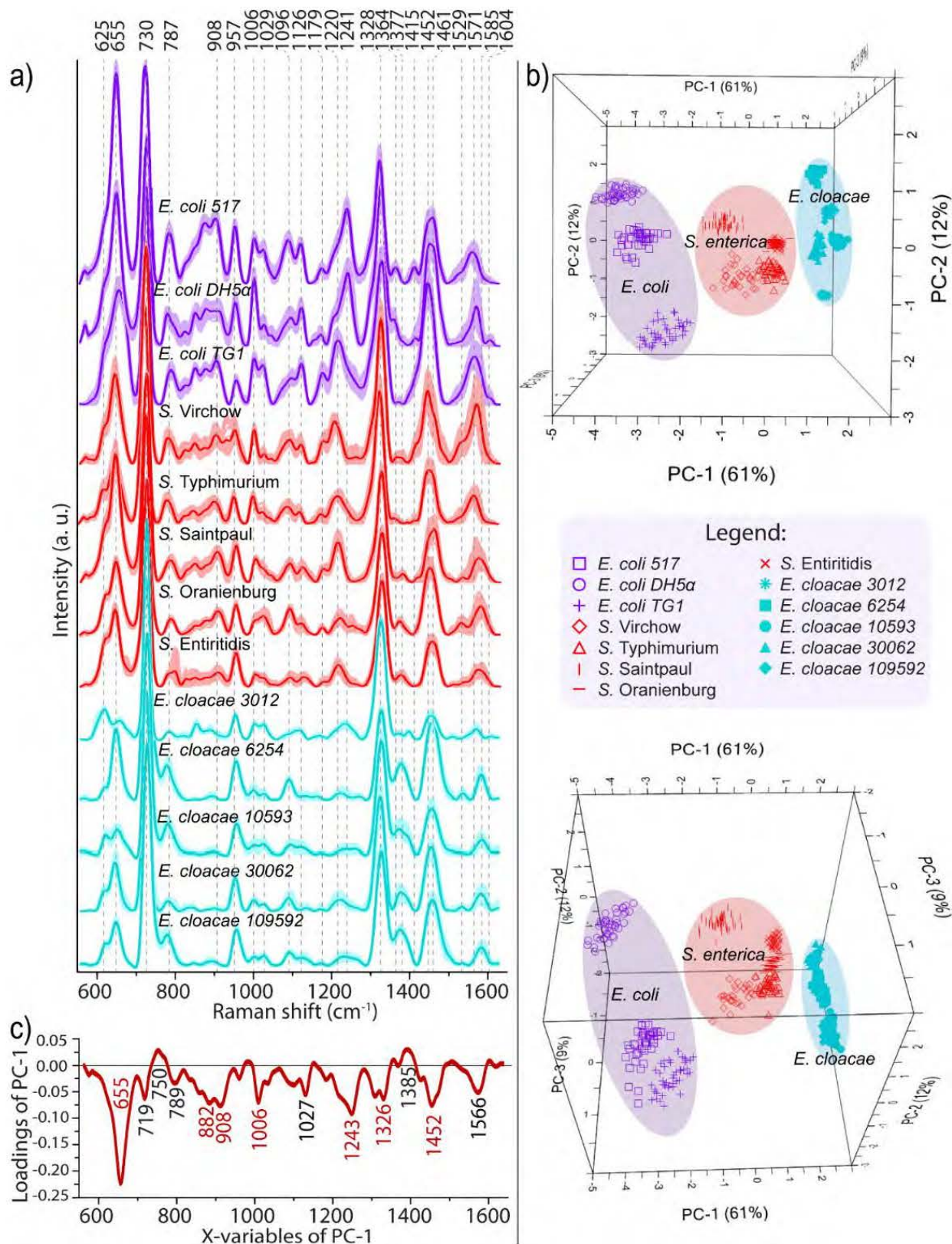
Figure 66. The SERS spectra of environmental, companion strains (a). The thick line represents the spectrum averaged from 25 measurements, while a paler shade of the same colour for, a given species, depicts all the overlapping spectra of a given species. A three-dimensional representation of the PCA analysis of tested strains (b). The loading of PC-1 analysis result demonstrating the contribution of the diagnostic bands to the differentiation of the analysed bacterial species (c).

156

The obtained spectral results (*Figure 66.*) were very 'rich' in terms of the number of signals and demonstrated top quality (high intensity and high signal-to-noise ratio), which, as in the case of *Cronobacter* spp. spectra, made them a good material for analysis. Similarly, as in the previous case, the large number of different strains made simple analysis difficult. What was characteristic were the classic properties of bacteria spectra, distinguished by the presence of intense bands at around 655, 730, 957, 1364, and 1452 cm^{-1}. Their assignments were corresponding to those of *Cronobacter* spp.

The PCA analysis made it possible to clearly distinguish three groups of points representing single spectra. Each of them enabled the division of the collected spectra into those belonging to bacteria from the three studied species. The separation for the three principal components was 82% in total, and accuracy was 80%. These results indicated at the same time the possibility of distinguishing the examined bacteria at the species level and their close relationship and morphological similarity, manifested by a similar spectral 'fingerprint'. The analysis of the loadings of the PC-1 dependency and Raman shift presented a slightly different picture of the performed analysis. In the *Figure 66 (c)*, thirteen bands may be observed, which similarly contributed to the differentiation of the analysed spectra. The largest impact to differentiation among them was due to a band at about 655 cm^{-1} and a similarly high level came from differences in the course of bands 882, 908, 1006, 1243, 1326, and 1452 cm^{-1}. The remaining visible bands made a much smaller contribution to the result. This analysis demonstrated that the additional data from the PCA analysis was crucial for the interpretation of the results and indicated, potentially, which of the recorded signals were the most characteristic for the tested microorganisms, and thus being crucial for their further differentiation in the tested material.

Next, the PCA analyses were performed with the use of spectra for standard and environmental strains of *Cronobacter* spp. To increase the transparency of the results, all spectra from each species were averaged. In addition, only five strains of *Cronobacter* spp. were used in the comparative analysis, as only five out of seven tested reference strains found their environmental equivalents among the bacteria collected for research. The results are presented below.
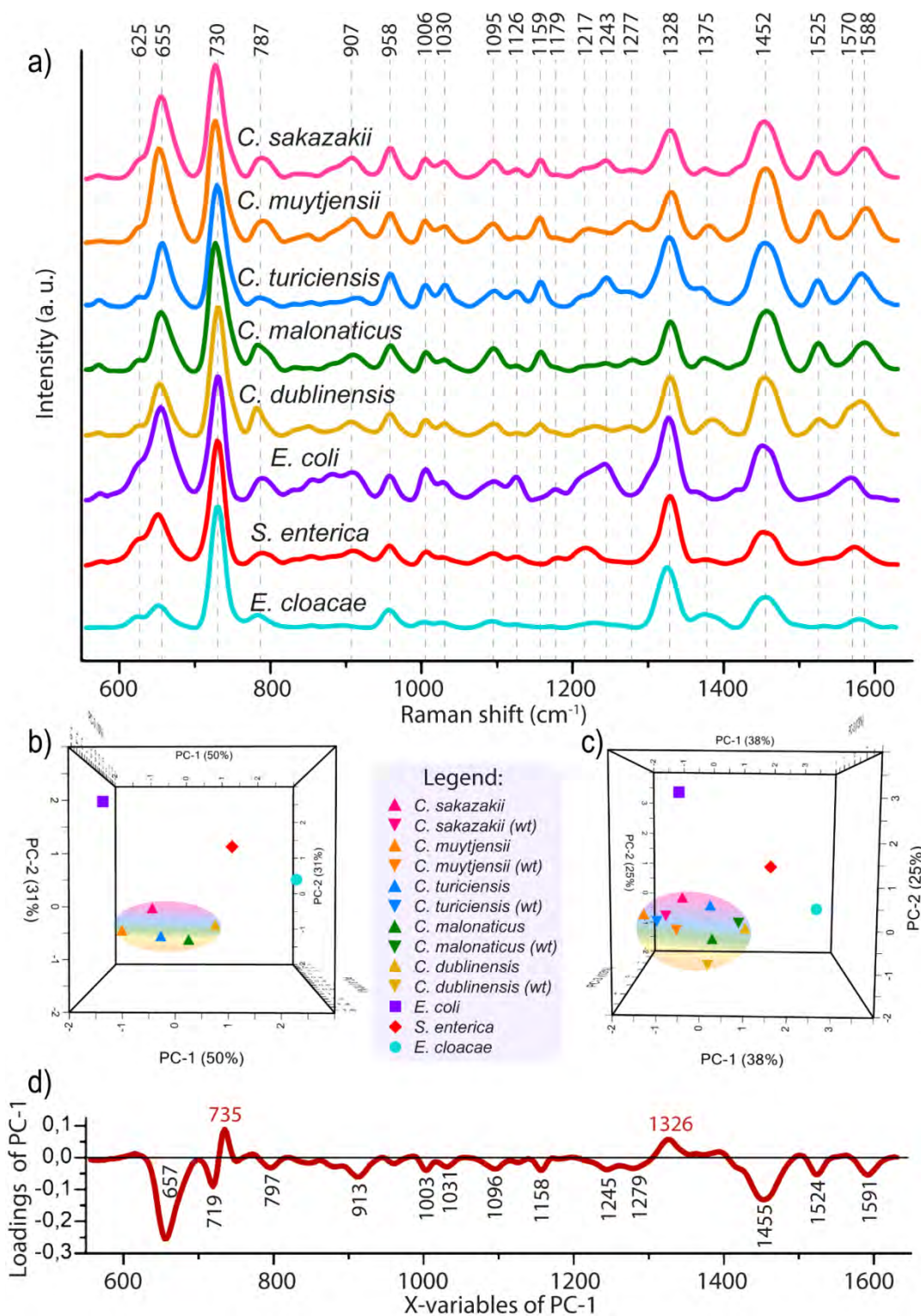
Figure 67. The SERS spectra of five species of Cronobacter spp. (standard and environmental - wt) stacked with. E. coli, S. enteritidis and E. cloacae environmental strains (a). The single spectrum is averaged from all measurements for given species. A three-dimensional representation of the PCA analysis of tested species: (b) with standard Cronobacter species and (c) both standard and environmental Cronobacter species. The loading of PC-1 analysis result demonstrating the contribution of the diagnostic bands to the differentiation of the analysed bacterial species (c).

http://rcin.org.pl

All the compiled spectra (*Figure 67.*) demonstrated a great similarity in terms of signals, their Raman shift values and intensity. The greatest differences were visible in the area from about 1000 to 1330 cm^{-1} in the case of *E. coli, S. enterica* and *E. cloacae* strains, respectively. Due to a large number of bands in this area, the PCA analysis again significantly facilitated the analysis, differentiation and allowed for drawing conclusions regarding the obtained data. In the case of comparing the reference spectra for *Cronobacter* spp. and the companion strains (*Figure 67 (b)*), the results for the averaged spectra split as expected, i.e., one group of points was created representing the spectral data for cronobacters and the companion strains separated from them, and from each other. The total distribution of points reached 91% with the accuracy of 92%. In the case of the analysis, which took into account the standard and environmental strains of *Cronobacter* bacteria and the other three strains (*Figure 67 (c)*), the distribution of points in the three-dimensional representation was almost identical. Additionally, the points representing the spectra of the reference and environmental *Cronobacter* strains were close to each other, which indicated an extremely close similarity of these microorganisms. In this case, the overall differentiation reached 76% and the accuracy 90%. The lower value for the percentages of PC values resulted from the exceedingly similar spectral image obtained for the reference and environmental strains of the same *Cronobacter* species. In a large group of points, which would be the single spectra, their species distinction would be impossible, but with a high probability they could still be assigned to the genus *Cronobacter*.

The Loadings of PC-1 analysis allows, by standard, to notice the similarities and spectral differences of the tested bacterial strains. In order to simplify the analysis, it was performed for comparison with the reference and accompanying strains (*Figure 67(d)*). It is clearly visible that the bands at 735 and 1326 cm^{-1} were present in each spectrum and constituted a great similarity to them, while the bands at 657, 719, 1455, 1524, and 1591 cm^{-1} contributed to the diversity. Particularly noteworthy was the band at 1524 cm^{-1}. While the other signals responsible for the distinction differed mainly in the shift value and intensity, the 1524 cm^{-1} band appeared to be extremely characteristic for bacteria of the genus *Cronobacter* and was practically absent in the other spectra presented above in this series of experiments. This fact may of course be noticed by conducting ordinary spectral analysis, but it was clearly confirmed by statistical analysis. Its relatively small contribution to the distinction was due to its original low intensity compared to the bands at 655, 730 or 1452 cm^{-1} but it was no less important.

159

The obtained results clearly confirmed the usefulness of the SERS-PCA method in the identification of the considered microbiological hazard, even in the case of the simultaneous identification of closely related strains present in the intestinal flora.

The isolation of the clinical strain of Cronobacter sakazakii from infant milk using the phenomenon of dielectrophoresis and microfluidics and its identification using the SERS-PCA method. In the consequence of the performed measurements of reference and clinical strains, control data was obtained for the experiment with the clinical strain of *Cronobacter sakazakii*. I carried out the following experiment, exploiting negative DEP effect, using the calculations developed in Group 1 and on the basis of experiments with *E. coli* bacteria that belong to the same family, i.e. Enterobacteriaceae [261]. As a result of these works, it was found that for the immobilisation of bacteria on the SERS platform, a suitable solution was to apply the negative phenomenon of dielectrophoresis (nDEP) in a system of four electrodes. Between each pair, a sinus function was applied with frequency (f) of 450 kHz, voltage (U) of o10 V, time of deposition (t) of 180 s, and the distance between tip of electrodes (R) was 0.9 mm. In the described experiment, only the deposition time was extended due to the large volume of the analyte. Suspension of the clinical strain of *C. sakazakii* at the level of 10^8 cfu×mL^{-1} (equivalent to the 0.5 McFarland turbidity standard) was added to 3 mL of Bebilon Advance baby milk (recommended for newborns) - prepared in accordance with the instructions on the packaging.

Thereafter, the suspension of the bacteria in the milk was passed through a sterile syringe filter polyethersulfone membrane with 0.1 micrometre in diameter holes. This way, the bacteria remained on the primary side of a filter surface and were separated from the content of the baby's milk. Additionally, in order to get rid of the milk residues, 3 mL of tenfold diluted PBS buffer was passed through the filter. Such a dilution of the buffer resulted from the necessity to use it in the experiment with nDEP and was taken into account in the calculations performed for the previous experiments. A syringe was then connected to the outlet of the filter and the positron controlled by an infusion pump system. Using this kit, 10-fold diluted PBS buffer washed away the bacteria on the primary side of the membrane and transported them through the main channel using a PTFE tube, connected to an inlet in a microfluidic system. The flow was set at 100 microliters per minute and was maintained until the syringe emptied.

At the moment of introducing the suspension into the system, the function generator was activated with the aforementioned parameters. The progress of the set function was controlled by an oscilloscope attached to one of the electrode pairs. After emptying the

160

syringe, the voltage on the generator was disconnected and the SERS spectra were collected using a Bruker Bravo spectrometer perpendicular to the surface of the SERS platform. The remaining buffer solution along with the non-immobilized bacteria was channelled further to an outlet and then through the PTFE tube to diabetes insipidus.

The collected spectra, as an experimental test, were subjected to PCA analysis against the spectra collected for twenty-six environmental *Cronobacter* strains, five environmental control *E. cloacae* strains, five environmental control *S. enterica* strains and three environmental control *E. coli* strains. Additionally, to simplify the analysis, all the spectra analysed for a given species were averaged to one spectrum and re-analysed by PCA. The obtained results are presented below (*Figure 68*).
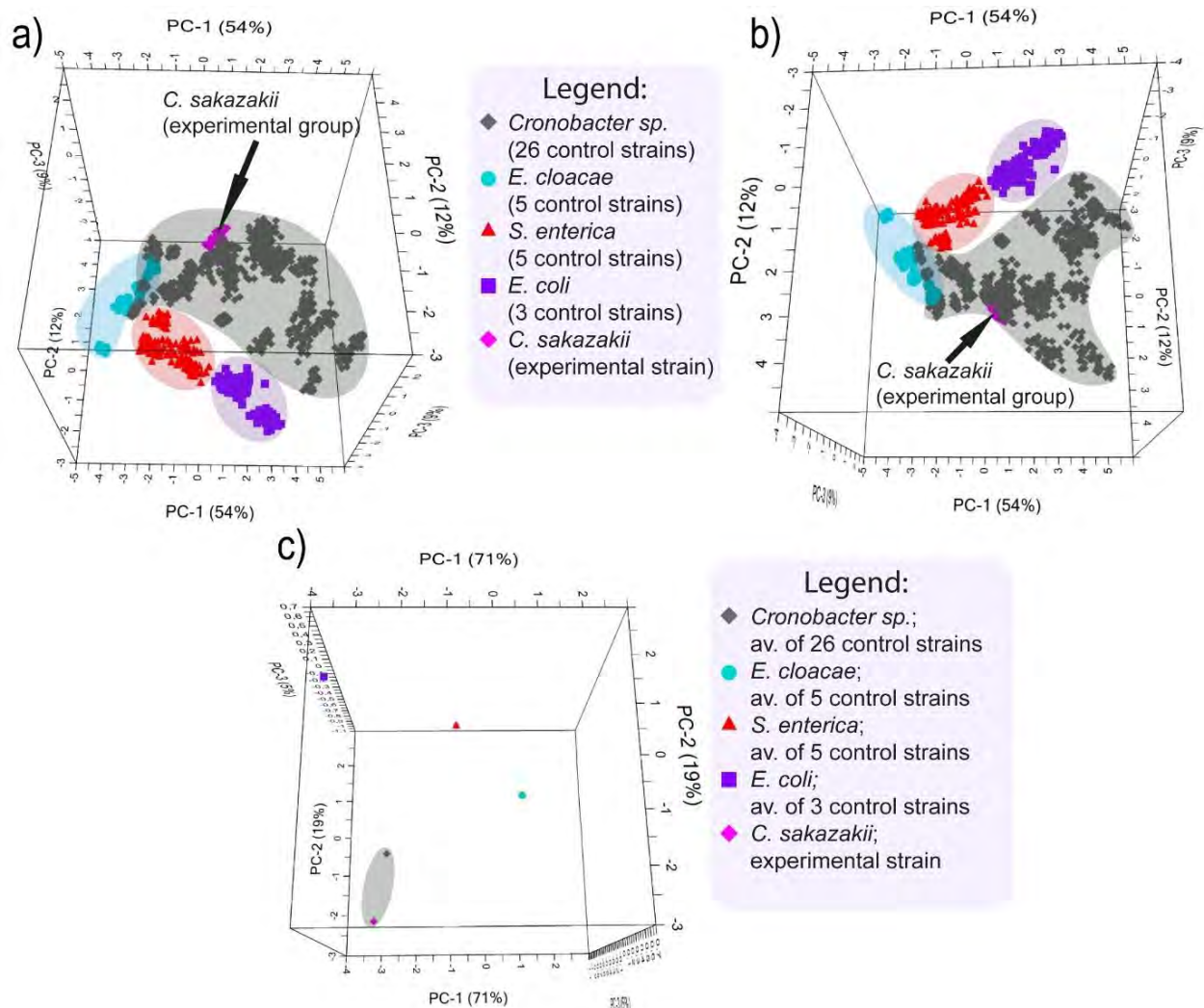
Figure 68. The three-dimensional representation of the PCA analysis of tested species: (a and b) with experimental group of clinical strain of Cronobacter sakazakii and control strains; (c) simplified analysis where each points represents all spectra collected for each species that have been averaged before statistical analysis was performed.

The above comparison (*Figure 68*.), with the participation of non-averaged data, clearly enabled the division of the obtained spectra into groups corresponding to the four analysed species. The experimental group was assigned to the 'point cloud' representing the spectra collected for the bacteria *Cronobacter* spp. The results were presented in two projections for better orientation in three-dimensional space. The sum of the percentages for the three PCs reached 75% and the accuracy 89%. An important fact is, however, that this result mainly concerned the division into data species. The location of the analytical points for the experimental clinical group of *Cronobacter sakazakii* left no doubt as to its belonging to this species. As for the simplified analysis, an extremely clear division of the points obtained was again noticeable. Two of them, representing the averaged environmental strains and the average score for the clinical strain, were close together in the same quadrant. In this case, the sum of the PC was 95% and the accuracy 98%. Thus, averaging the spectra for the same experimental groups resulted in an increase in the total value of PC in comparison with the analysis of non-averaged spectra. This is a good way to increase the accuracy and precision of the identification analysis in the case of a very large number of variables, such as numerous single SERS spectra. Such averaging may be treated as the resultant spectral image for a given microorganism, which eliminates the variability of spectra, caused for example by the measurement time, a change in the environment of bacteria caused by the excretion of metabolites or changes in the structure of their cell membranes as a response to food and moisture deprived conditions, in which the measurement takes place in additional exposure to laser light. This result additionally confirmed the well-established rule, according to which a large number of results for a repeated experiment, averaged, is the best approximation of its actual result.

The conclusions. The research related to bacteria posing a microbiological hazard to infants and, in extreme cases, to adults, proved the possibility of implementing a method using SERS spectroscopy and statistical analysis of PCA results in the detection of this type of threat. The measurement and analysis of the results for the reference and environmental strains clearly demonstrated the possibility of identification at the species level in the collective hazard analysis. The results for closely related reference and environmental species somehow indicated the possibility of spectroscopic confirmation of the similarity of these organisms thanks to their spectral images. Additionally, the developed microfluidic system and an integrated platform for the separation of bacteria from the matrix in the form of baby's milk and the simultaneous SERS measurements proved to be effective. It

enabled the immobilisation of the bacteria in the selected zone and the effective measurement of their spectra. The PCA analysis again proved to be an invaluable tool in the analysis of the results, and it was additionally found that the reduction of the number of tested variables by averaging the groups of spectra corresponding to the analysed groups of analytes allowed for an effective increase in discrimination. This was confirmed by obtaining similar results for this type of approach and analysis for all individual spectra of the same analytes. The obtained results constituted an important step towards further research on the possibility of a wider use of SERS spectroscopy and the solutions developed as part of the presented research in the form of microfluidic platforms and systems, in standard environmental or clinical tests. The research conducted and described in this section led to the fulfilment of the first, fourth, fifth, sixth and seventh of the individual thesis goals.

8.   Summary and discussion

The presented thesis contains several basic assumptions, thanks to which SERS spectroscopy could find practical application in the detection and identification of microbiological hazards and cancer cells. The main task was to determine the requirements for an efficient, fast, cost-effective, repeatable and reliable analyte preparation path and its analysis with the use of selected spectroscopy techniques, and based on the PCA method - analysis of the collected test results. The first and most important step to achieve this task was to develop the SERS platforms that would meet the assumptions of simplicity of production, reproducibility of the manufacturing process, even distribution of the nanoplasmonic structures, ensuring high enhancement factor and reproducibility of test results. I have successfully developed several types of completely novel, solid SERS platforms and formed a continuum in the development of this technology (*Table 11*.). First platforms were created by modifying ready-made matrices of future substrates with the SERS – active metal. The final outcome was the development of a method of laser ablation of the silicon surface and its modification by means of metal physical vapor deposition (PVD). In addition, the developed platforms may assume predetermined shapes and dimensions, and their geometry may be modified in order to create, for example, electrodes that were used to separate microbial material using the phenomenon of dielectrophoresis. These platforms are now being used as standard for all kinds of measurements in the research group in which they were developed and optimised. The experience gained in the production of various types of substrates enriched the final effect with several additional parameters, not taken into account at the beginning, such as, for example, the possibility of long storage without losing properties - tests in the developing group proved the possibility of their effective use even after several months. In addition, they do not self-corrode, are chemically and mechanically resistant and do not add additional signals to the spectrum, apart from the band at 519-521 cm^{-1}, characteristic of silicon [263] (that platform partially consist of), and is often used as a calibration band for spectrometers. It is then an additional asset and not an analytical obstacle.

In addition to the solid SERS platform, the research resulted in a need to create nanoparticles that would additionally adsorb the target analyte and, using a selected physical property, thicken it in the measurement area. The phenomenon of magnetism was chosen for this property. In this way I developed magnetic Fe_2O_3@Ag nanoparticles, which additionally,

164

due to the silver layer constituting the shell in core-shell nanoparticles, are a source of additional signal enhancement in the SERS technique. The method of their production does not require the use of complex reactions, and being based on the thermal decomposition of one of the substrates, it ensures the formation of nanoparticles that do not provide additional signals for analysis from unreacted reagents or residual solvents. The process of cleaning them from non-magnetic residues is really straightforward. The production process itself, apart from the ball mill and the furnace with the possibility of maintaining an anaerobic atmosphere, also does not require the use of complicated and high-cost measures. The nanoparticles have been successfully used for isolation from the suspension, concentration and enhancement of the spectroscopic signal for *Porphyromonas gingivalis* bacteria on a SERS platform. In addition, they were also used in other works carried out in the research group. The properties, characteristics, as well as advantages and disadvantages of the developed SERS platforms have been summarized in *Table 11*. The common feature of the developed nanoplasmonic structures is a similar size distribution: 35 ± 5 nm. With the exception of nanoparticles, nanostructures are part of larger structures with dimensions up to 2-3 μm. Such a surface topography of SERS substrates allows bacterial cells and fragments of eukaryotic cells to 'arrange' in these structures. In this way, they are closer to the 'hot spots' and their number increases, effectively enhancing inelastically scattered radiation.

Another important task for the success of further experiments was the development of the optimal culture conditions for bacteria (which were one of the main analytes in the planned research - including the cultivation time and the potential influence of the medium on the spectra obtained) and the measurement conditions - including the type and power of the laser line, optimal time for sample preparation, length of measurement time. I have obtained the data for the development of an efficient protocol for further experiments, including those conducted for eukaryotic cells or body fluids such as blood or saliva. This part of the work made it possible to obtain repeatable and reliable test results and set out a method of working with almost any microbiological analyte. What is more, the developed analytical path allows to obtain valuable spectra for various types of analysis, almost with every attempt. Laboratory reality is significantly different from 'dry data' appearing in publications and other studies, and not every attempt to obtain a result, regardless of the technique and type of analyte, is successful. That is why this part of the work is extremely useful and is a big step towards creating a practical application in the analysis of microbiological hazards or in the diagnosis of food or environmental samples. In addition, it ensures reproducibility of experiments and

165

repeatability of results regardless of the place of testing. The use of two, extremely different in terms of construction, spectrometers in the course of the conducted research additionally confirms this thesis - the obtained spectra were characterized by the presence and repetitive Raman shift for the bands characteristic for bacteria. Moreover, the developed method enables quick measurement of the tested material, up to a dozen or so measurement minutes, and depending on the software used for the PCA analysis, an equally quick comparative analysis of the results for the experimental and reference groups.

The series of substrates and the research protocol, that I have developed, allowed for the examination of various types of material through bacterial prokaryotic cells (Gram-positive, Gram-negative, aerobic, anaerobic and those preferring limited access to oxygen) to eukaryotic cancer cells and body fluids in the form of blood and saliva. Bacterial strains isolated from food, environmental samples, various collections as well as clinical samples were tested. A large variety of the tested material allowed for the collection of an enormous amount of data, which, after being analysed, exhibited diversity, which at the same time led to drawing conclusions about the characteristic elements of the spectra for various types of tested samples. Both bacterial and neoplastic cells and various body fluids display spectra so characteristic that they can be divided into different groups of samples. Additionally, an analysis of these spectra was performed and specific bands found their assignments. In this way, another dependence was discerned, according to which the spectra for a specific group of analytes are so diverse, that it is possible to assign them to a specific kind, species or even strain, in the case of bacterial cells. In the case of cancer cells and fluids, the spectra possess such a characteristic pattern of bands that it is possible to identify the analyte on their basis. The PCA analysis in material identification is almost indispensable in the analysis of a large number of data to determine the type of sample. By using the spectral data for the type of microbial sample under investigation as experimental data and comparing them by chemometric analysis with the spectral data of hazards or companion strains that may be in the sampling area or in the food sample, one can obtain the result of data separation and find the assignment of the analyte to a specific species, and sometimes even a strain in the case of bacteria. This creates the need for a database that could serve in the future as an application of SERS spectroscopy in routine research. The split values obtained as the sum of all PCs used in the analysis varied from seventy to over ninety percent with an accuracy of over 90%. In the case of simplified analyses, where all spectra for a given species were averaged, the correctness of the analysis was at the level of currently used methods, described in the

166

theoretical part of the following thesis. As for the research underpinning the application of the method in various applications, these are considered to be satisfactory results.

It is worth emphasising that all the obtained analyses, and hence the spectra, were attained in a label-free mode. No specific antibodies, antigens or ligands were used in the conducted research. Consequently, the obtained spectral data corresponds directly to the morphology of biological analytes. And these properties emerged to be sufficient to distinguish between them.

In order to isolate analytical material from various matrices, both for cancerous and bacterial cells, it was possible to successfully implement microfluidic systems. Their properties resulting from micrometric channel geometries enabled the miniaturisation of processes using such phenomena as laminar and turbulent flow, mixing of nanolitre volumes of substrates, and process automation with the use of infusion or peristaltic pumps. It was possible to successfully isolate neoplastic cells from the blood, concentrate bacteria in the area of signal integration, as well as provide conditions for an effective application of dielectrophoresis in the area of micrometre dimensions. These systems, called lab-on-a-chip, form an important path in the development of the proposed SERS-PCA technique, as they provide the possibility of testing food, environmental or clinical samples for a specific hazard with a high reproducibility and without the use of costly and time-consuming equipment or processes.

The obtained results proved that the main thesis of this dissertation was correct and its individual goals have been achieved. They clearly demonstrated that SERS spectroscopy is an effective, sensitive and universal technique for the detection of a wide range of samples. Combining it with chemometric, statistical PCA analysis creates an useful and powerful analytical tool, named SERS-PCA. Further development of combining chemometric analysis spectroscopy and systems for the extraction of analyte from the matrix taken for testing is especially desirable and necessary for the actual implementation of this methodology in routine tests. Ultimately, the positivity of just another detection technique requiring skilled personnel is not attractive enough. Automation or partial automation of the sample preparation, measurement and analytical process is much more enticing and it is the direction in which activities in this science will be focused in the near future.

Table 11. The overview of the properties of the developed SERS substrates.

Compared feature	SERS substrates			
	Ag/SSWM	Ag/PV	Si/Ag	Fe_2O_3@Ag
Type	Solid, mesh	Solid	Solid	Magnetic nanoparticles
Average nanostructures size	33 ± 14 nm	31 ± 11 nm	35 ± 2 nm	41 ± 2 nm
Enhancement Factor value	4.2×10^6	2.1×10^6	1.0×10^8	9.7×10^7
Tested application	Bacteria, tumour cells, organic compounds	Bacteria, tumour cells, organic compounds	Bacteria, organic compounds	Bacteria, organic compounds
Special tested application	Long-time laser exposition measurements	Spectroelechtochemistry	Integrated SERS-DEP platform	Label free magnetoseparation of bacteria, label based magnetoseparation of CTCs
Shelf life	24-48h	6 months	6 months	1 month
Pros	• Excellent heat conduction • Multiple applications	• Good stability • Multiple applications	• Multiple applications • Good stability • Full control of the manufacturing process • The ability to control the dimensions, geometry and architecture of the surface • Possible introduction of mass production	• Simple substrates • Ease of preparation and cleaning • Wide range of applications • Magnetic properties • They are a source of additional reinforcement when used with solid SERS substrates
Cons	• Short service life due to corrosion • The quality depends on the source of supply of the matrix substrate • Relatively low enhancement factor value	• The quality depends on the source of supply of the matrix substrate • Relatively low enhancement factor value	• The complexity of the setup for laser ablation process	• Lower durability than solid SERS substrates • Possible slight contamination with amorphous carbon

168

9. List of journal articles

Articles based on the research conducted as part of this dissertation:

1. T. Szymborski, E. Witkowska, **K. Nicinski**, Z. Majka, T. Krehlik, T. Deskur, K. Winkler, A. Kaminska, Steel Wire Mesh as a Thermally Resistant SERS Substrate, *Nanomaterials (Basel)*, 8 (2018).

2. E. Witkowska, **K. Niciński**, D. Korsak, T. Szymborski, A. Kaminska, Sources of variability in SERS spectra of bacteria: comprehensive analysis of interactions between selected bacteria and plasmonic nanostructures, *Analytical and Bioanalytical Chemistry*, (2019).

3. **K. Niciński**, E. Witkowska, D. Korsak, K. Noworyta, J. Trzcińska-Danielewicz, A. Girstun, A. Kamińska, Photovoltaic cells as a highly efficient system for biomedical and electrochemical surface-enhanced Raman spectroscopy analysis, *RSC Advances*, 9 (2019) 576-591.

4. E. Witkowska, **K. Niciński**, D. Korsak, B. Dominiak, J. Waluk, A. Kamińska, Nanoplasmonic sensor for foodborne pathogens detection. Towards development of ISO-SERS methodology for taxonomic affiliation of Campylobacter spp, *Journal of Biophotonics*, 13 (2020) e201960227.

5. E. Witkowska, A.M. Łasica, **K. Niciński**, J. Potempa, A. Kamińska, In Search of Spectroscopic Signatures of Periodontitis: A SERS-Based Magnetomicrofluidic Sensor for Detection of Porphyromonas gingivalis and Aggregatibacte ractinomycetemcomitans, *ACS Sensors*, 6 (2021) 1621-1635.

6. **K. Niciński**, J. Krajczewski, A. Kudelski, E. Witkowska, J. Trzcińska-Danielewicz, A. Girstun, A. Kamińska, Detection of circulating tumor cells in blood by shell-isolated nanoparticle–enhanced Raman spectroscopy (SHINERS) in microfluidic device, *Scientific reports*, 9 (2019) 1-14.

7. T. Szymborski, Y. Stepanenko, **K. Niciński**, P. Piecyk, S.M. Berus, M. Adamczyk-Popławska, A. Kamińska, Ultrasensitive SERS platform made via femtosecond laser micromachining for biomedical applications, *Journal of Materials Research and Technology*, 12 (2021) 1496-1507.

Other publications:

1. A. Kamińska, T. Szymborski, E. Witkowska, E. Kijeńska-Gawrońska, W. Świeszkowski, **K. Niciński**, J. Trzcińska-Danielewicz, A. Girstun, Detection of Circulating Tumor Cells Using Membrane-Based SERS Platform: A New Diagnostic Approach for 'Liquid Biopsy'. *Nanomaterials*, 9 (2019), 366.

2. M. Fronczak, P. Strachowski, **K. Niciński**, M. Krawczyk, W. Kaszuwara, M. Bystrzejewski, Synthesis and adsorptive properties of sulfonated nanocomposites based on carbon-encapsulated iron nanoparticles and styrene-p-divinylbenzene copolymer*, Separation Science and Technology*, 55:14(2020), 2470-2481.

3. S. Berus, E. Witkowska, **K. Niciński**, E. Sadowy, W. Puzia, P. Ronkiewicz, A. Kamińska, Surface-enhanced Raman scattering as a discrimination method of Streptococcus spp. and alternative approach for identifying capsular types of S. pneumoniae isolates, Spectrochimica Acta Part A: *Molecular and Biomolecular Spectroscopy*, 233 (2020), 118088.

4. M. Czaplicka, **K. Niciński**; A. Nowicka; T. Szymborski; I. Chmielewska, J. Trzcińska-Danielewicz; A. Girstun, A. Kamińska, Effect of Varying Expression of EpCAM on the Efficiency of CTCs Detection by SERS-Based Immunomagnetic Optofluidic Device, *Cancers*, 12 (2020), 3315.

5. A. Kowalska, M. Czaplicka, A. Nowicka, **K. Niciński, A.** Piotrowska, A. Kamińska, Association between grade brain tumours and the interleukin-10 receptor subunit alpha based on surface-enhanced Raman spectroscopy and multivariate analysis, *Journal of Raman Spectroscopy*, 52(11) (2021), 1788.

6. R. de Lima Oliveira, **K. Niciński,** M. Pisarek, A. Kaminska, T. Arne, G. Pasternak, J.C. Colmenares, Porous Heteroatom-Doped Carbons: Efficient Catalysts for Selective Oxidation of Alcohols by Activated Persulfate. *ChemCatChem,* (2022), e202200787

10. List of patents and patent applications

1. Patent: **Pat.238794**

   Platform for surface-enhanced Raman effect, method of preparing such a platform, method for determining substances and / or microorganisms using such a platform, use of such a platform for direct detection and / or identification of substances and / or microorganisms, especially bacteria, using the surface-enhanced Raman effect technique or in combination with electrochemical measurements. 2018, P. 426643, Poland; **K. Niciński**, E. Witkowska, D. Korsak, J. Trzcińska-Danilewicz, A. Girstun, T. Szymborski, A. Michota-Kamińska.

2. Patent application

   Platform for the detection and / or identification of microorganisms, especially bacteria, using the Surface Enhanced Raman Effect (SERS) technique, the method of preparation, application and measuring using such a platform. 2018, P.424152, Poland; T. Szymborski, E. Witkowska, **K. Niciński**, A. Michota-Kamińska.

3. Patent: **Pat.239296**

   Method for detecting thermotolerant bacteria of the genus Campylobacter spp. in food. 2019, P.430701, Poland; E. Witkowska, **K. Niciński**, B. Dominiak, D. Korsak, J. Waluk, A. Michota-Kamińska.

4. Patent application

   The method of manufacturing a silicon platform for SERS measurements, silicon platform for SERS measurements and the use of a silicon platform for SERS measurements of biological samples. 2020, P.434300, Poland; T. Szymborski, Y. Stepanenko, P. Piecyk, **K. Niciński**, and A. Michota-Kamińska.

11. List of Tables

12. List of Figures

173

175

176

13. List of Equations

14. List of abbreviations

3D	three-dimensional
AFM	Atomic force microscopy
ATCC	American Type Culture Collection
BHI	Brain Heart Infusion
Caki-1	Human Renal Cancer Cell Line
CCA	Chromogenic Coliform Agar
CCD	Charge-Coupled Device
CFU	Colony Forming Unit
CNC	Computer Numerical Control
CTC	Circulating Tumor Cell
DEP	Dielectrophoresis
DMAB	4.4′-dimercaptoazobenzene
DNA	Deoxyribonucleic Acid
EDTA	Ethylenediamine Tetraacetic Acid
EF	Enhancement Factor
ELISA	Enzyme-linked Immunoassay
FAD	Flavin Adenine Dinucleotide
HeLa	Henrietta Lacks[1]
ISO	International Organization for Standardization
LB	Lysogeny Broth
LOD	Limit of Detection
LSPR	Localized Surface Plasmon Resonance
mCCDA	modified Charcoal-Cefoperazone-Deoxycholate Agar
NAD	Nicotinamide Adenine Dinucleotide
NP.	Nanopartcile
p-ATP	p-aminothiophenol
PC	Principal Component
PCA	Principal Component Analysis
PCR	Polymerase Chain Reaction
PE	Polyethylene
PLA	Polylactic acid
p-MBA	p-mercaptobenzoic *acid*
PTFE	Polytetrafluoroethylene
PV	Photovoltaic
PVD	Physical Vapor Deposition
RNA	Ribonucleic Acid
RPM	Revolutions Per Minute
RSD	Relative Standard Deviation
RT-PCR	Reverse Transcription–Polymerase Chain Reaction
SEM	Scanning Electron Microscopy
SERS	Surface Enhanced Raman Spectroscopy / Scattering
SHINs	Shell-Isolated Nanoparticles
SHINERS	Shell-Isolated Nanoparticle-Enhanced Raman Spectroscopy
spp.	Several Species

---

[1] Is an immortal cell line used in scientific research, named after and derived from cervical cancer cells taken from the name of the patient.

SSWM	Stainless Steel Wire Mesh
TBX	Tryptone Bile X-Glucuronide
TEM	Transmission Electron Microscopy
TSY	Trypticase Soy–Yeast
TSYEA	Trypticase Soy–Yeast Extract Agar
UV-VIS	Ultraviolet-Visible spectrophotometry
XPS	X-Ray Photoelectron Spectroscopy

15. Appendix section

Appendix 1

The chemicals and materials. *P*-mercaptobenzoic acid (*p*-MBA) and phosphate-buffered saline (PBS) packs (10 mM, pH=7.2) were obtained from Sigma-Aldrich (Dorset, UK) and used without further purification. Water (resistivity over 18 MΩ), purified using a Milli-Q plus 185 system was used throughout the process. Stainless steel wire mesh was obtained from Anping County Huijin Wire Mesh Co., Ltd., Anping, China. Each type of mesh wire was purchased in quantity of $1m^2$ and deposited rolled in room temperature prior to use. To sputter a layer of silver the PVD equipment was used (EM MED020, Leica, Heerbrugg, Switzerland). The silver target was obtained from Mennica Metale Szlachetne, Warsaw, Poland. The target diameter was 54 mm, thickness was 0.5 mm. The vacuum during the silver sputtering was on the level of 10^{-2} mbar, whereas the sputtering current was 25 mA.

The bacteria culture. *E. coli* and *B. subtilis* were obtained from the Department of Applied Microbiology, Institute of Microbiology, University of Warsaw, Warsaw, Poland.

The Raman and SERS Spectroscopy conditions and instrumentation. The measurements were conducted with a Renishaw inVia Raman system (Wotton-under-Edge, Gloucestershire, UK) equipped with a 785 nm diode laser (Wotton-under-Edge, Gloucestershire, UK). The light from the laser was passed through a line filter and focused on a sample mounted on an X–Y–Z translation stage with a 50× microscope objective, Numerical Aperture (NA)=0.75. The beam diameter was approximately 5 μm. The laser power at the sample was 5 mW or less. The microscope was equipped with 1200 grooves per mm grating, cut-off optical filters, and a 1024×256 pixel Peltier-cooled RenCam CCD detector (Wotton-under-Edge, Gloucestershire, UK), which allowed registering the Stokes part of Raman spectra with 5–6 cm^{-1} spectral resolution and 2 cm^{-1} wavenumber accuracy. The experiments were performed at ambient conditions using a back-scattering geometry. The time required for completing a single SERS spectrum was 4 seconds for *p*-MBA and 40 seconds for bacteria.

The obtained spectra were processed with an OPUS software (Bruker Optic GmbH 2012 version, Ettlingen, Germany). The spectra were smoothed with Savitsky-Golay filter, the background was removed using baseline correction, and then the spectra were normalized using a so-called Min-Max normalisation.

The Scanning Electron Microscopy (SEM). The observations were performed under high vacuum using the FEI Nova NanoSEM 450 (Hillsboro, OR, USA). The accelerating voltage was in range from 2 to 10 kV. The SSWM samples with bacteria cells were observed without any additional layer of gold.

Appendix 2

The materials and chemicals. To sputter a layer of silver the PVD equipment was used (EM MED020, Leica, Heerbrugg, Switzerland). The silver target was obtained from Mennica Metale Szlachetne, Warsaw, Poland. The target diameter was 54 mm, thickness was 0.5 mm. The vacuum during the silver sputtering was on the level of 10^{-2} mbar, whereas the sputtering current was 25 mA.

The bacterial species. Bacterial strains: *E. coli* K12 and *B. subtilis* 168 were obtained from the Department of Applied Microbiology, University of Warsaw, Poland.

The culture conditions and sample preparation. Cultures of *E. coli* and *B. subtilis* were maintained in Trypticase soy–yeast extract agar (TSYEA) (Oxoid, Basingstoke, Hampshire, UK) at 4 °C throughout the study period and stored at −80 °C in brain heart infusion (BHI) broth supplemented with 20% glycerol.

The following culture media were purchased from Biocorp, Poland: Luria–Bertani (LB) agar medium, BHI agar, and Mannitol Egg Yolk Polymyxin (MEYP) agar for cultivation of *B. subtilis* and LB agar medium, BHI agar, Tryptone Bile X-Glucuronide (TBX) agar, and Chromogenic Coliform Agar (CCA) for cultivation of *E. coli*. All the plates were incubated at 37 °C for 24 h. Additionally, the plates with LB agar and *E. coli* or *B. subtilis* were cultured for 48 h and 72 h to check the influence of the culture duration on the SERS spectrum.

The Raman and SERS spectroscopy. The measurements were conducted with a Renishaw inVia Raman system equipped with a 300 mW diode laser–emitting 785 nm line, a 50 mW He-Ne laser–emitting 633 nm line, a 50 mW diode laser–emitting 532 nm line, and a 200 mW He-Cd laser–emitting 325 nm line. These lines were used as an excitation source (λex). The light from the lasers was passed through a line filter and focused on a sample mounted on an X–Y–Z translation stage with a ×20 microscope objective (NA = 0.25). The beam diameter was approximately 5 μm. The laser power at the sample was 1.5, 1.0, 1.2, and 1.6mW, respectively, for 785, 633, 532 and 325 nm laser lines. For the 785 nm laser line, the power levels 0.08, 0.1, 0.8, 1.5, 8.0, and 16.0 mW were also tested. The microscope was

equipped with three different diffraction gratings (1200 grooves/mm - for the 785 nm line, 1800 grooves/mm - for the 633 nm and 532 nm lines, and 2400 grooves/mm - for the 325 nm line), cut off optical filters, and a 1024×256-pixel Peltier-cooled RenCam CCD detector, which allowed registering the Stokes part of Raman spectra with 5–6 cm^{-1} spectral resolution and 2 cm^{-1} wave number accuracy. The experiments were performed at ambient conditions using a back-scattering geometry.

The Scanning Electron Microscopy (SEM). The observations were performed under high vacuum using the FEI Nova NanoSEM 450. The accelerating voltage was in a range from 2 kV up to 10 kV. The wire mesh samples with bacterial species were observed without any additional layer of gold.

Appendix 3

The chemicals and materials. *P*-aminothiophenol (*p*-ATP) and phosphate-buffered saline (PBS) packs (10mM, pH = 7.2) were obtained from Sigma-Aldrich (Dorset, UK) and used without further purification. Water (resistivity over 18 MΩ), purified using a Milli-Q plus 185 system was used throughout the process. PV panels were obtained from Bruk-Bet Solar Tarnów, Poland as a post-production residue. To sputter a layer of silver the PVD equipment was used (EM MED020, Leica, Heerbrugg, Switzerland). The silver target was obtained from Mennica Metale Szlachetne, Warsaw, Poland. The target diameter was 54 mm, thickness was 0.5 mm. The vacuum during the silver sputtering was on the level of 10^{-2} mbar, whereas the sputtering current was 25 mA.

The electrochemical measurements were carried out using μAUTOLABIII/FRA2.

All the media and reagents were obtained from Sigma-Aldrich (St. Louis, MO, USA). The bacterial species used in the experiment were obtained from the Department of Bacterial Genetics, Faculty of Biology of the University of Warsaw. The growth of bacteria was conducted at the Department of Molecular Microbiology, Faculty of Biology, University of Warsaw by Dr Dorota Korsak.

The tumour cells cultures were conducted by Dr Joanna Danielewicz-Trzcińska at the Department of Molecular Biology, Faculty of Biology of the University of Warsaw.

The Raman and SERS spectroscopy. The Raman and SERS spectroscopy measurements were carried out with a Renishaw inVia Raman system equipped with a 785 nm diode laser. The light from the laser was passed through a line filter and focused on a sample mounted on an X–Y–Z translation stage with a 50× microscope objective, NA = 0.25. The laser beam diameter, defined as twice the radius of a circle encompassing the area

185

with 86% of the total power, was about 2.5 μm; approximately the same values were attained from the experimentally obtained laser spot image and from the theoretical formula (4λf/πD). The experiments were performed at ambient conditions using a back-scattering geometry at 1.5 mW power at the sample. The microscope was equipped with 1200 grooves per mm grating, cut off optical filters, and a 1024×256 pixel Peltier-cooled RenCam CCD detector, which allowed registering the Stokes part of the Raman spectra with 5–6 cm^{-1} spectral resolution and 2 cm^{-1} wave number accuracy. The experiments were performed at ambient conditions using a back-scattering geometry.

The Scanning Electron Microscopy (SEM). The Scanning Electron Microscopy observations were performed under high vacuum using the FEI Nova NanoSEM 450. The accelerating voltage ranged from 2 up to 10 kV. The PV/Ag samples were observed without any additional layer of gold.

The Atomic Force Microscopy (AFM). The atomic force microscopy imaging was performed by using a Multimode 8 AFM microscope by Bruker (Germany) equipped with Nanoscope V controller and piezoelectric scanner type E with a 10×10 μm scanning area. The system was controlled by Multimode 8.15 software from Bruker. All images were collected in ScanAssyst™ mode using a 650 nm silicon tip on a silicon nitride cantilever with dimensions 115×25 μm (length × width). Resonant frequency of the cantilever was 70kHz and its spring constant was 0.4 N×m^{-1}. Raw images were flattened using 1st order procedure. In order to calculate sample roughness, four images with a 5×5 μm area were recorded in different places on the sample surface. Then, the roughness (R_a) of each recorded image was calculated using NanoScope Analysis software by Bruker and the average roughness value was obtained. The measurements were carried out by Dr Krzysztof Noworyta in the Research Group No. 18, Institute of Physical Chemistry, PAS, Warsaw.

The XPS measurement. The X-ray photoelectron spectroscopic measurements were performed using a PHI 5000 VersaProbe (ULVAC-PHI) spectrometer with monochromatic Al Kα radiation (hν = 1486.6 eV) from an X-ray source operating at a 100 μm spot size, 25 W and 15 kV. The survey XPS spectra were collected with a hemispherical analyser at the pass energy of 117.4 and an energy step size of 0.4 eV. The X-ray beam was incident at the sample surface at an angle of 45° with respect to the surface normal, and the analyser axis was located at 45° with respect to the surface. The XPS data were evaluated by MultiPak v.9 software using the set of sensitivity factors supplied by PHI.2.3.6.

The electrochemical SERS measurements. The measurements were carried out by Dr Krzysztof Noworyta in the Research Group No. 18, Institute of Physical Chemistry, PAS, Warsaw.

The fabrication of a spectroelectrochemical system. The system has been designed using MasterCAM software and then micromachined with a computer numerical-controlled (CNC) milling machine (ErgWind, type MFG4025P) in a 5 mm polycarbonate (PC) slab (Bayer). The system was made at the Laboratory of Microfabrication, Institute of Physical Chemistry PAS, Warsaw.

Appendix 4

The growth media for bacteria strains cultivation. Bolton broth, as well as modified charcoal-cefoperazone-deoxycholate agar (mCCDA), Skirrow agar, and Columbia blood agar were purchased from Oxoid (Basingstoke, United Kingdom). Sodium chloride, acetone, isopropyl alcohol, sucrose, hydrochloric acid, ethylenediaminetetraacetic acid (EDTA), and lysozyme were purchased from Linegal Chemicals (Warsaw, Poland), mutanolysin—from A&A Biotechnology (Gdynia, Poland), GeneMATRIX Bacterial & Yeast Genomic DNA Purification Kit—from EURX (Gdansk, Poland), Pfu polymerase and GeneJET Gel Extraction and DNA Cleanup Micro Kit—from Thermo Fisher Scientific (Waltham, Massachusetts). The growth of bacteria was conducted at the Department of Molecular Microbiology, Faculty of Biology, University of Warsaw by Dr Dorota Korsak.

The SERS database of thermotolerant Campylobacters spp. control strains. *C. jejuni* NCTC 11351, *C. coli* ATCC 33559, *C. upsaliensis* ATCC 43954 and *C. lari* ATCC BAA-1060 were cultured on mCCDA, Skirrow agar and Columbia blood agar were grown in a microaerobic atmosphere at 41.5 °C for 44 ±4 h. Next, the bacteria were subjected to the SERS experiments. The cultivation process for each *Campylobacter sp*. and on each type of culture medium was performed in triplicate and the obtained SERS results were averaged and placed in the bacterial SERS database.

The bacteria sample preparation for SERS measurements. All types of bacteria colonies were collected via 1 μL loop. Afterwards, bacteria cells were suspended in sterile saline solution (500 μL) and centrifuged for 3 minutes at 1070×g. The supernatant was discarded and the bacterial cells were resuspended in sterile saline solution. The centrifugation process was repeated three times to obtain a solution of bacterial cells without additional contaminations from culture media. After final centrifugation, the pellet of bacterial cells was resuspended in saline solution (~5–10 μL). About 2.5 μL of such bacterial solution

was placed over freshly prepared SERS substrate and dried for a few minutes in sterile conditions.

The SERS substrates. In order to enhance the Raman signal of bacterial cells the previously developed SERS substrate, based on PV panels were used. The PV panels from production waste were obtained from Bruk-Bet Solar Tarnów, Poland.

In order to prepare such SERS substrates, the PV cells were divided into pieces of ~0.5 cm×0.5 cm, placed in a beaker filled with acetone, and put in a shaker. After 40 minutes of shaking at room temperature, acetone solution was replaced with isopropyl alcohol and then with Millipore water, and the process was repeated. Finally, the SERS substrates were dried with compressed pure nitrogen and sputtered with 8 nm layer of silver via Physical Vapor Deposition (PVD) device (Quorum Q150T ES). The sputtering process conditions were as follows: (a) 25 mA current, (b) argon plasma, (c) 10^{-2} mbar of working pressure. The silver targets of 4N purity, used in sputtering process, were provided by Mennica Metale (Warsaw, Poland). The substrates were used immediately after their preparation.

The Raman and SERS spectroscopy. The measurements were conducted with a Renishaw inVia Raman system equipped with a 300 mW diode laser emitting 785 nm light, which was used as an excitation source. The light from the laser was passed through a line filter and focused on a sample mounted on an X–Y–Z translation stage with a ×20 microscope objective, NA = 0.25. The beam diameter was approximately 5 μm, and the laser power at the sample was 1.5 mW. The microscope was equipped with diffraction grating with 1200 grooves per mm, cut-off optical filters, and a 1024×256 pixel Peltier-cooled RenCam CCD detector, which allowed for registration of the Stokes part of Raman spectra with 5 to 6 cm^{-1} spectral resolution and 2 cm^{-1} wavenumber accuracy. The experiments were performed at ambient conditions using a back-scattering geometry.

The spectra were recorded immediately after placing the analysed sample on the SERS substrate surface. During the period of about 10 minutes, the SERS spectra were repeatedly recorded for different 'hot spots' on the SERS platforms. At the same time, the focus of the laser beam was readjusted. The laser power at the sample was 1.5 mW. The time required for completing a single SERS spectrum was about 4 seconds.

The Scanning Electron Microscopy (SEM). In order to attach the SERS substrate to aluminium scanning electron microscopy (SEM) pin stubs Micro to NanoEM-TecAG42 (Ted Pella, Inc.) were used. The observations were performed under high vacuum using the FEI Nova NanoSEM 450. The accelerating voltage was in rage from 2 kV up to 10 kV.

The SERS spectra pre-processing. The pre-processing was performed using the OPUS software (Bruker Optic GmbH 2012 version). The spectra were smoothed with Savitzky–Golay filter (9 points) 49, the background was removed using baseline correction (concave rubber band correction; number of iterations: 10, number of baseline points: 64), and then the spectra were normalized using a Min-Max normalisation. All the spectra presented in this work were averaged from at least 25 SERS measurements. They were obtained from three different experiments (in each experiment different pieces of the SERS substrate and different bacterial cell colonies were used) conducted on different spots of one SERS substrate. The three-dimensional PCA and the cluster analysis were conducted with the use of Unscrambler software (CAMO software AS, version 10.3, Norway).

Appendix 5

The chemicals and materials. The silver target was purchased from Mennica Metale Szlachetne, Poland and sputtered via physical vapor deposition (PVD) (sputtering device: Quorum, Q150T ES, Laughton, U.K.). The vacuum during the process was at the level of 10^{-2} mbar, the sputtering current was 25 mA, and the process took place in an argon plasma atmosphere. The final thickness of the silver layer was controlled with a quartz crystal monitor.

The Fe_2O_3 nanospheres having an average diameter of less than 50 nm were purchased from Merck KGaA, Darmstadt, Germany. The silver acetate was purchased from Merck KGaA, Darmstadt, Germany.

The substrates were ground in a Retsch MM400 mixer ball. The obtained powder was heat-treated in Carbolite tube furnace (Keison Products, Chelmsford, Essex, U.K.).

An infusion pump system (Harvard Apparatus Pump Series, MA) was used for the automated control of the flow.

Bacterial strains. Five strains of *P. gingivalis* [33277 (wt), W83 (wt), ΔK/ΔRAB-A, ΔPorN, AL022] were obtained from the Institute of Microbiology, Faculty of Biology, University of Warsaw, Poland. The construction of *P. gingivalis*-mutated strains (ΔK/ΔRAB-A, ΔPorN) was reported before [264]. Three strains of *A. actinomycetemcomitans*[HK1651 (wt), JP2, 652 (wt)] were a kind gift from Prof. Donald R. Demuth (University of Louisville School of Dentistry, Louisville, Kentucky, United States), while two streptococcal strains, namely, *Streptococcus pseudopneumoniae* 6178/12 and *Streptococcus mitis* 3705/04, were donated by Prof. Anna Skoczyńska (the National Reference Centre for Bacterial Meningitis in the National Medicines Institute, Warsaw, Poland).

189

The culture media and growth conditions of bacterial strains. The *P. gingivalis* strains were grown in enriched BD BBL trypticase soy broth (eTSB per liter: 30 g of trypticase soy broth, 5 g of yeast extract, 5 mg of hemin, pH 7.5; 0.5 g of l-cysteine and 2 mg of menadione) and on eTSB blood agar (eTSB medium containing 1.5% agar and 5% defibrinated sheep blood) at 37 °C in anaerobic conditions using an Anoxomat Mark II system (90% nitrogen, 5% carbon dioxide, and 5% hydrogen). The cultures of mutated strains were additionally supplemented with appropriate antibiotics (erythromycin at 5 $\mu g \times mL^{-1}$ and / or tetracycline at 1 $\mu g \times mL^{-1}$ and chloramphenicol at 3.5 $\mu g \times mL^{-1}$).

The *A. actinomycetemcomitans* strains were grown in BD BBL brain heart infusion (BHI) broth and on BHI agar (1.5% agar), both supplemented with 40 $mg \times L^{-1}$ $NaHCO_3$, at 37 °C in microaerobic conditions using an Anoxomat Mark II system (85% N_2, 10% CO_2, 5% O_2), while streptococcal strains were cultured on Columbia blood agar at 37 °C in aerobic conditions.

All bacteria were grown to the early stationary phase (ca. 24 h in broth or 48h on plates in the case of *P. gingivalis* and *A. actinomycetemcomitans* or ca. 16 h on plates in the case of *S. pseudopneumoniae* and *S. mitis*). The bacterial strains belonging to *P. gingivalis* and *A. actinomycetemcomitans* were cultured both on solid (agar) and in a liquid medium to check if the culture conditions would alter for the SERS measurements. All cultures were conducted in the Department of Bacteria Genetics, Faculty of Biology, University of Warsaw by Dr Anna Łasica.

The Instrumentation: SERS Spectroscopy, Scanning Electron Microscopy, UV-VIS spectroscopy. To perform the SERS measurements, a Bruker's BRAVO spectrometer equipped with a Duo LASER (700–1100 nm) and a CCD camera was used. The spectrometer also has a function of fluorescence rejection, which was applied during all measurements. The laser power for both lasers was <100 mW, while the spectral resolution was 4 cm^{-1}. The SERS spectra were recorded repeatedly for 30 min. A single measurement, composed of three accumulations, each of 6 s, was completed after approximately 45 s (because of data processing and transfer). The results were next processed via OPUS software, ver.2012 (Bruker Optic GmbH, Germany). All of the single spectra presented in this section were averaged from at least 25 single measurements (number of spectra collected for a single sample).

After the SERS experiments, the SERS substrates with bacteria placed on them were subjected to SEM measurements, without prior treatment of the cells. The substrates were

190

attached to aluminium SEM pin stubs with conductive liquid silver paint (Pelco, Ted Pella, Inc.). The SEM measurements, performed under high vacuum, were obtained using an FEI Nova NanoSEM 450 scanning electron microscope. The range of the accelerating voltage was 2–10 kV.

The UV-VIS spectra were made using a Shimadzu, Japan UV-2700 spectrophotometer. They were made in the absorption mode, with a spectral resolution of 1 nm, in a 99.8% ethanol suspension. The concentration was adjusted by dilution and magnetic separation of aggregates until a clear solution with a faint green colour was obtained.

A McFarland densitometer, used in experiments was DEN-1B model, produced by Biosan.

The chemometric analysis of spectral data. All pre-processed data was transferred to the Unscrambler software (CAMO software AS, version 10.3, Norway), used for the three-dimensional PCA and the cluster analysis.

The fabrication of a microfluidic chip. The microfluidic system was designed with the use of MasterCAM software and milled in a 5 and 2 mm polycarbonate (PC) slab (Bayer) with a computer numerical-controlled (CNC) milling machine (ErgWind, type MFG4025P). To join two main milled elements, the PC slabs were pressed together at a high temperature (T = 130°C) for 30 min. The top cover was connected to the rest of the chip with screws and sealed with an O-ring. The chip was containing also square neodymium magnet with a thickness of 1 mm and external dimensions identical to the SERS platform, that was placed below the Si/Ag platform. The microfluidic chip was made at the Laboratory of Microfabrication, Institute of Physical Chemistry PAS, Warsaw.

The SERS spectra pre-processing. The pre-processing was performed using the OPUS software (Bruker Optic GmbH 2012 version). The spectra were smoothed with Savitzky–Golay filter (9 points) 49, the background was removed using baseline correction (concave rubber band correction; number of iterations: 10, number of baseline points: 64), and then the spectra were normalized using a Min-Max normalisation. All the spectra presented in this work were averaged from at least 25 SERS measurements. The spectra were obtained from three different experiments (in each experiment different pieces of SERS substrate and different bacterial cell colonies were used) conducted on different spots of a SERS substrate.

Appendix 6

The chemicals, materials and cell lines. The Caki-1 cell line purchased from ATCC was a kind gift from Professor Anna Czarnecka (Department of Oncology, Military Institute of Medicine, Warsaw, Poland). The HeLa cell line came from the European Collection of Cell Cultures (ECACC) and was supplied by Sigma-Aldrich (St. Louis, MO, USA).

The PVD device (Leica, EM MED020) was applied to sputter the Ag directly on the PV surface. No adhesion layer, i.e., chromium or titanium, was used between photovoltaic surface and the Ag layer. The thickness of the Ag layer was set to 8 nm for all analysed samples. The sputtering conditions: the current was 25 mA and the pressure was 10^{-2} mbar.

The fabrication of a microfluidic chip. The microfluidic chip was designed using MasterCAM software and then micromachined with a computer numerical-controlled (CNC) milling machine (ErgWind, type MFG4025P) in a 5 mm polycarbonate (PC) slab (Bayer).

The milled channels had the narrowest sections, 1.20 mm in length, 0.12 mm wide and 0.063 mm depth. The wider sections were 0.70 mm long and 0.35 mm wide. To join milled and plain PC slabs we pressed them together at high temperature (T = 130°C) for 30 minutes.

A high precision syringe pump system (Harvard Apparatus Pump Series, MA, USA) was used for automated control of flow. To inject the analyte and buffer into the system and collect the separated fractions, holes with a diameter of 0.8 mm were drilled in appropriate places of the plates. Blunt ended needles with an outer diameter of 0.8 mm were installed in the holes. Standard polyethylene (PE) tubings with an inner diameter of 0.8 mm were used for interconnection of the chip at the syringe pump. The SERS-active platform based onto photovoltaic array was placed onto the detection area chambers (DA) of the microfluidic chip to record SHINERS signals from this point. The detection points were open to air and the recorded SHINERS signals were not affected by the material of the microfluidic device. The microfluidic chip was made at the Laboratory of Microfabrication, Institute of Physical Chemistry PAS, Warsaw.

The SERS measurements. A Renishaw inVia Raman system was equipped with a 785 nm diode laser as excitation source. The light from the laser was focused on the measured sample with a×50 microscope objective, NA = 0.25. The beam diameter was approximately 2.5 μm. The spectroscopic maps were acquired by collecting SERS spectra over the previously defined range (36×36 μm) at each point on a grid with 3 μm spacing using an automated microscope stage. Typically, 40 SHINERS spectra for each cell types were

192

acquired for 20 s each, by using this mapping mode. The laser light measured at the sample gives power at about 2.5 mW.

The SEM measurements. The SEM images were acquired on the FEI Nova NanoSEM 450 instrument operating at an accelerating voltage of 10 kV.

The xhemometrics and data processing. All recorded SHINERS data was optimised for principal component analysis using following steps. Firstly, the spectra were smoothed with Savitzky-Golay filter, the background corrected (concave rubber band correction; no. of baseline points 34; no. of iterations 10), and normalized using OPUS software (Bruker Optic GmbH 2012 version). All the data was introduced to PCA analysis using the commercial Unscrambler@ software (CAMO software AS, version 10.3, Norway). The PCA was completed base onto the NIPLAS algorithm, validation (random with 20 segments), significance 0.05 and the 120 number of samples (SHINERS spectra).

Appendix 7

The chemicals and materials. The silver target was purchased from Mennica Metale Szlachetne, Poland and sputtered via physical vapor deposition (PVD) (sputtering device: Quorum, Q150T ES, Laughton, U.K.). The vacuum during the process was at the level of 10^{-2} mbar, the sputtering current was 25 mA, and the process took place in an argon plasma atmosphere. The final thickness of the silver layer was controlled with a quartz crystal monitor.

The conductive sliver cement was purchased from Ted Pella.

The experiments included usage of an infusion pump system and were conducted with Harvard Apparatus Pump Series, MA.

The culture media and growth conditions of bacterial strains. All of the above mentioned strains and serovars were cultured on Brain heart infusion (BHI), a nutrient-rich, agar-based medium for 24 h at 37 °C before the sample preparation process begun. All cultures were conducted in the laboratory of Department of Molecular Mirobiology, Faculty of Biology, University of Warsaw, Poland:

The sample preparation for SERS measurements. In the case of all bacteria cultured the growth procedure took place on solid (agar) media. Next, about three single bacterial colonies were selected and suspended in 500 μL of a sterile saline solution (0.9% NaCl) via an inoculation loop. Then, bacteria were gently mixed with the saline solution by an automatic pipette and centrifuged (5 min, 1070g), the supernatants were discarded, and the

pellets were suspended in 500 μL of the sterile saline solution. The washing procedure was repeated three times. The concentration of bacteria in each sample was at the level of 10^8 cfu×mL^{-1}, as the cell suspension was equivalent to the 0.5 McFarland turbidity standard (McFarland densitometer DEN-1B, Biosan)[209]. After the final centrifugation step and supernatant removal, the pellets were suspended in 20 μL of the sterile saline solution. About 5 μL of each mixture was used for the SERS measurements by placing it onto the SERS substrate 5 min before measurement in order to let the sample dry. Each strain was cultured independently three times.

The instrumentation for SERS spectroscopy. To perform SERS measurements, a Bruker's BRAVO spectrometer equipped with a Duo LASER (700–1100 nm) and a CCD camera was used. The spectrometer also had a function of fluorescence rejection, which was applied during all measurements. The laser power for both lasers was <100 mW, while the spectral resolution was 2–4 cm^{-1}. The SERS spectra were recorded repeatedly for 30 min. A single measurement, composed of three accumulations, each of 6 s, was completed after approximately 45 s (because of data processing and transfer). The results were next processed via OPUS software, ver.2012 (Bruker Optic GmbH, Germany). All of the single spectra presented in the article were averaged from at least 25 single measurements (number of spectra collected for a single sample).

The fabrication of a microfluidic chip. The microfluidic chip was designed using MasterCAM software and then micromachined with a computer numerical-controlled (CNC) milling machine (ErgWind, type MFG4025P) in a 5 and 2 mm polycarbonate (PC) slab (Bayer). The microfluidic chip was made at the Laboratory of Microfabrication, Institute of Physical Chemistry PAS, Warsaw

The SERS spectra pre-processing. The pre-processing was performed using the OPUS software (Bruker Optic GmbH 2012 version). The spectra were smoothed with Savitzky–Golay filter (9 points) 49, the background was removed using baseline correction (concave rubber band correction; number of iterations: 10, number of baseline points: 64), and then the spectra were normalized using a Min-Max normalisation. All the spectra presented in this work were averaged from at least 25 SERS measurements. The spectra were obtained from three different experiments (in each experiment different pieces of the SERS substrate and different bacterial cell colonies were used) conducted on different spots of a SERS substrate.

The chemometric analysis of spectral data. All pre-processed data were transferred to the Unscrambler software (CAMO software AS, version 10.3, Norway), used for the three-dimensional PCA and the cluster analysis.

16. References

[1] B.C. Windom, D.W. Hahn, Raman Spectroscopy, in: Q.J. Wang, Y.-W. Chung (Eds.) Encyclopedia of Tribology, Springer US, Boston, MA, 2013, pp. 2742-2747.

[2] E. Smith, G. Dent, Modern Raman spectroscopy: a practical approach, John Wiley & Sons2019.

[3] Z. Kęcki, Podstawy spektroskopii molekularnej, Wydawnictwo Naukowe PWN2013.

[4] L. Brillouin, Diffusion of light and x-rays by a transparent homogeneous body, Ann. Phys, 17 (1922) 88-122.

[5] A. Smekal, Zur quantentheorie der dispersion, Naturwissenschaften, 11 (1923) 873-875.

[6] C.V. Raman, K.S. Krishnan, A new type of secondary radiation, Nature, 121 (1928) 501-502.

[7] N. Colthup, Introduction to infrared and Raman spectroscopy, Elsevier2012.

[8] R. Pilot, R. Signorini, C. Durante, L. Orian, M. Bhamidipati, L. Fabris, A review on surface-enhanced Raman scattering, Biosensors, 9 (2019) 57.

[9] P. Colomban, G. Gouadec, Raman scattering theory and elements of Raman instrumentation, Raman Spectroscopy for Soft Matter Applications, John Wiley & Sons, Inc. Hoboken, NJ2009.

[10] A. Knebl, R. Domes, S. Wolf, C. Domes, J. Popp, T. Frosch, Fiber-enhanced Raman gas spectroscopy for the study of microbial methanogenesis, Analytical Chemistry, 92 (2020) 12564-12571.

[11] P. Vandenabeele, H. Edwards, Raman Spectroscopy in Archaeology and Art History: Volume 2, Royal Society of Chemistry2018.

[12] R. Löbenberg, N.A. Bou-Chacra, Raman spectroscopy for quantitative analysis in the pharmaceutical industry, Journal of Pharmacy & Pharmaceutical Sciences, 23 (2020) 24-46.

[13] W.J. Dufresne, C.J. Rufledt, C.P. Marshall, Raman spectroscopy of the eight natural carbonate minerals of calcite structure, Journal of Raman Spectroscopy, 49 (2018) 1999-2007.

[14] K.C. Doty, I.K. Lednev, Raman spectroscopy for forensic purposes: recent applications for serology and gunshot residue analysis, TrAC Trends in Analytical Chemistry, 103 (2018) 215-222.

[15] B. Vucelić-Radović, D. Lazić, M. Nikšić, Application of Molecular Methods and Raman Microscopy: Spectroscopy in Agricultural Sciences and Food Technology, Ubiquity Press2019.

[16] R. Bhartia, L.W. Beegle, L. DeFlores, W. Abbey, J. Razzell Hollis, K. Uckert, B. Monacelli, K.S. Edgett, M.R. Kennedy, M. Sylvia, Perseverance's scanning habitable environments with Raman and luminescence for organics and chemicals (SHERLOC) investigation, Space Science Reviews, 217 (2021) 1-115.

[17] G. Lopez-Reyes, M. Veneranda, J.A. Manrique, Á. González Martín, A. Moral, C. Perez-Canora, J.A. Rodríguez Prieto, A. Sanz Arranz, J. Saiz Cano, E. Lalla, The Raman laser spectrometer ExoMars simulator (RLS Sim): A heavy-duty Raman tool for ground testing on ExoMars, Journal of Raman Spectroscopy, 53 (2022) 382-395.

[18] W. Kiefer, M. Buback, G. Hoffmann, E. Korte, A. Roseler, E. Lentz, K. Gerwert, A. Leipertz, M. Spiekermann, Special techniques and applications, Infrared and Raman Spectroscopy-Methods and Applications. Weinheim (VCH), (1995) 465-517.

[19] M. Fleischmann, P.J. Hendra, A.J. McQuillan, Raman spectra of pyridine adsorbed at a silver electrode, Chemical physics letters, 26 (1974) 163-166.

[20] D.L. Jeanmaire, R.P. Van Duyne, Surface Raman spectroelectrochemistry: Part I. Heterocyclic, aromatic, and aliphatic amines adsorbed on the anodized silver electrode, Journal of electroanalytical chemistry and interfacial electrochemistry, 84 (1977) 1-20.

[21] M.G. Albrecht, J.A. Creighton, Anomalously intense Raman spectra of pyridine at a silver electrode, Journal of the american chemical society, 99 (1977) 5215-5217.

[22] E. Stern, R. Ferrell, Surface plasma oscillations of a degenerate electron gas, Physical Review, 120 (1960) 130.

[23] P.L. Stiles, J.A. Dieringer, N.C. Shah, R.P. Van Duyne, Surface-enhanced Raman spectroscopy, Annu Rev Anal Chem (Palo Alto Calif), 1 (2008) 601-626.

[24] B. Sharma, R.R. Frontiera, A.-I. Henry, E. Ringe, R.P. Van Duyne, SERS: Materials, applications, and the future, Materials today, 15 (2012) 16-25.

[25] E. Witkowska, Surface-enhanced Raman spectroscopy as a tool for efficient detection and differentiation of pathogenic bacteria and fungi, Institute of Physical Chemistry, Polish Academy of Sciences Warsaw, 2018.

[26] J.R. Lombardi, R.L. Birke, L.A. Sanchez, I. Bernard, S.C. Sun, The effect of molecular structure on voltage induced shifts of charge transfer excitation in surface enhanced Raman scattering, Chemical physics letters, 104 (1984) 240-247.

[27] M.R. Gartia, T.C. Bond, G.L. Liu, Metal− Molecule Schottky Junction Effects in Surface Enhanced Raman Scattering, The Journal of Physical Chemistry A, 115 (2011) 318-328.

[28] S. Schlücker, SERS microscopy: nanoparticle probes and biomedical applications, ChemPhysChem, 10 (2009) 1344-1354.

[29] K. Kneipp, Y. Wang, H. Kneipp, L.T. Perelman, I. Itzkan, R.R. Dasari, M.S. Feld, Single Molecule Detection Using Surface-Enhanced Raman Scattering (SERS), Physical Review Letters, 78 (1997) 1667-1670.

[30] E.C. Le Ru, P.G. Etchegoin, Quantifying SERS enhancements, MRS bulletin, 38 (2013) 631-640.

[31] Z.-Q. Tian, Z.-L. Yang, B. Ren, D.-Y. Wu, SERS from transition metals and excited by ultraviolet light, Surface-Enhanced Raman Scattering, Springer2006, pp. 125-146.

[32] J.A. Creighton, C.G. Blatchford, M.G. Albrecht, Plasma resonance enhancement of Raman scattering by pyridine adsorbed on silver or gold sol particles of size comparable to the excitation wavelength, Journal of the Chemical Society, Faraday Transactions 2: Molecular and Chemical Physics, 75 (1979) 790-798.

[33] Y.S. Yamamoto, T. Itoh, Why and how do the shapes of surface-enhanced Raman scattering spectra change? Recent progress from mechanistic studies, Journal of Raman Spectroscopy, 47 (2016) 78-88.

[34] https://www.oceaninsight.com/products/sampling-accessories/raman/sers/.

[35] https://www.silmeco.com/products/sers-substrate-custom/.

[36] https://www.renishaw.com/en/sers-ters--25811.

[37] http://www.madatec.com/RAMAN_files/Q-SERS%20G1_data%20sheet-Madatec.pdf.

[38] https://sersitive.eu.

[39] https://www.silmeco.com/products/sers-substrate-serstrate/.

[40] S.K. Das, E. Marsili, Bioinspired metal nanoparticle: synthesis, properties and application, Croacia: InTech2011.

[41] W. Xinxin Lian and Yuanjiang Lv and Haoliang Sun and David Hui and Guangxin, Effects of Ag contents on the microstructure and SERS performance of self-grown Ag nanoparticles/Mo–Ag alloy films, Nanotechnology Reviews, 9 (2020) 751--759.

[42] L.a.D.L.a.R.Y.a.L.Z.a.T.D.a.H.Y.a.C.T. Zhang, Light-Triggered Reversible Self-Assembly of Gold Nanoparticle Oligomers for Tunable SERS, Langmuir, 31 (2015) 1164-1171.

[43] N.K. Chaki, S.G. Sudrik, H.R. Sonawane, K. Vijayamohanan, Single phase preparation of monodispersed silver nanoclusters using a unique electron transfer and cluster stabilising agent, triethylamine, Chemical Communications, (2002) 76-77.

[44] R. Sato-Berrú, R. Redón, A. Vázquez-Olmos, J.M. Saniger, Silver nanoparticles synthesized by direct photoreduction of metal salts. Application in surface-enhanced Raman spectroscopy, Journal of Raman Spectroscopy: An International Journal for Original Work in all Aspects of Raman Spectroscopy, Including Higher Order Processes, and also Brillouin and Rayleigh Scattering, 40 (2009) 376-380.

[45] M.J.R.a.T. Pradeep, Solvothermal synthesis of silver nanoparticles from thiolates, Journal of Colloid and Interface Science, 268 (2003) 81-84.

[46] S.S.a.S. Seal, Cluster size effect observed for gold nanoparticles synthesized by sol-gel technique as studied by X-ray photoelectron spectroscopy, Nanostructured Materials, 11 (1999) 1181-1193.

[47] X.S.Z.a.L.Z. Jian Liu and Qihua Yang and, Pore size control of mesoporous silicas from mixtures of sodium silicate and TEOS, Microporous and Mesoporous Materials, 106 (2007) 62-67.

[48] Y. Ling-Feng Zhang and Min Li and Tie-Zhen Ren and Xinying Liu and Zhong-Yong, Ce-modified Ni nanoparticles encapsulated in SiO2 for COx-free hydrogen production via ammonia decomposition, International Journal of Hydrogen Energy, 40 (2015) 2648-2656.

[49] A.X. Wang, X. Kong, Review of Recent Progress of Plasmonic Materials and Nano-Structures for Surface-Enhanced Raman Scattering, Materials, 8 (2015).

[50] J. Zhang, M.R. Langille, C.A. Mirkin, Synthesis of Silver Nanorods by Low Energy Excitation of Spherical Plasmonic Seeds, Nano Letters, 11 (2011) 2495-2498.

[51] D. Yang Yang and Yan Cong and Jingyu Shang and Yang Liu and Guoqiang Fang and Jiahua Zhang and Bin, NIR LSPR-coupling of Ag nanorices and W18O49 nanowires: Application of LRET and SERS, Sensors and Actuators B: Chemical, 330 (2021) 129199.

[52] D.a.L.D.M.a.G.M.a.K.J.M. Aherne, Optical Properties and Growth Aspects of Silver Nanoprisms Produced by a Highly Reproducible and Rapid Synthesis at Room Temperature, Advanced Functional Materials, 18 (2008) 2005-2016.

[53] H. Shang Wang and Yanhong Tian and Su Ding and Yilong, Rapid synthesis of long silver nanowires by controlling concentration of Cu2+ ions, Materials Letters, 172 (2016) 175-178.

[54] M.B. Gebeyehu, T.F. Chala, S.-Y. Chang, C.-M. Wu, J.-Y. Lee, Synthesis and highly effective purification of silver nanowires to enhance transmittance at low sheet resistance with simple polyol and scalable selective precipitation method, RSC Advances, 7 (2017) 16139-16148.

[55] Q. Xue, W. Yao, J. Liu, Q. Tian, L. Liu, M. Li, Q. Lu, R. Peng, W. Wu, Facile Synthesis of Silver Nanowires with Different Aspect Ratios and Used as High-Performance Flexible Transparent Electrodes, Nanoscale Research Letters, 12 (2017) 480.

[56] R.M.a.A.K.a.S.W.-H. Mehmet Kahraman and Emma, Fundamentals and applications of SERS-based bioanalytical sensing, Nanophotonics, 6 (2017) 831--852 , lastchecked = 2022-2005-2016.

[57] P.G. Jamkhande, N.W. Ghule, A.H. Bamer, M.G. Kalaskar, Metal nanoparticles synthesis: An overview on methods of preparation, advantages and disadvantages, and applications, Journal of drug delivery science and technology, 53 (2019) 101174.

[58] J. Yu-Luen Deng and Yi-Je, Black silicon SERS substrate: Effect of surface morphology on SERS detection and application of single algal cell analysis, Biosensors and Bioelectronics, 53 (2014) 37-42.

[59] R. Ossig, Y.-H. Kwon, F. Hubenthal, H.-D. Kronfeldt, Naturally grown Ag nanoparticles on quartz substrates as SERS substrate excited by a 488 nm diode laser system for SERDS, Applied Physics B, 106 (2012) 835-839.

[60] B.S. Sheetz, Y.N.D. Bandara, B. Rickson, M. Auten, J.R. Dwyer, Rapid, General-Purpose Patterning of Silicon Nitride Thin Films Under Ambient Conditions for Applications

Including Fluid Channel and SERS Substrate Formation, ACS Applied Nano Materials, 3 (2020) 2969-2977.

[61] Z. Jie Zhang and Xiaolei Zhang and Simeng Chen and Tiancheng Gong and Yong, Surface-enhanced Raman scattering properties of multi-walled carbon nanotubes arrays-Ag nanoparticles, Carbon, 100 (2016) 395-407.

[62] C. Wenning Zhao and Zhimou Xu and Tangyou Sun and Sisi Liu and Xinghui Wu and Zhichao Ma and Jian He and Cunhua, Carbon cloth surface-decorated with silver nanoparticles for surface-enhanced Raman scattering, Journal of Alloys and Compounds, 584 (2014) 635-639.

[63] A.K.M. Jamil, E.L. Izake, A. Sivanesan, R. Agoston, G.A. Ayoko, A homogeneous surface-enhanced Raman scattering platform for ultra-trace detection of trinitrotoluene in the environment, Analytical Methods, 7 (2015) 3863-3868.

[64] K.S.a.E.L.I.a.A.P.O.M.a.T.W.a.H.W.a.T.T.a.G.A.A. Daniel, Fabrication of dual function disposable substrates for spectroelectrochemical nanosensing, Sensors and Actuators B: Chemical, 287 (2019) 9-17.

[65] Y.H.K.a.H.L.a.Q.C.a.Q.O.a.H.J. Jiaji Zhu and Akwasi Akomeah Agyekum and Felix, Qualitative and quantitative analysis of chlorpyrifos residues in tea by surface-enhanced Raman spectroscopy (SERS) combined with chemometric models, Lwt, 97 (2018) 760-769.

[66] A.C. Crawford, L.B. Laurentius, T.S. Mulvihill, J.H. Granger, J.S. Spencer, D. Chatterjee, K.E. Hanson, M.D. Porter, Detection of the tuberculosis antigenic marker mannose-capped lipoarabinomannan in pretreated serum by surface-enhanced Raman scattering, Analyst, 142 (2017) 186-196.

[67] H. Yunfei Tian and Peng Wu and Qin Liu and Xi Wu and Xiandeng, Mapping for total surface-enhanced Raman scattering to improve its quantification analysis, Talanta, 161 (2016) 151-156.

[68] A. Lashkaripour, R. Silva, D. Densmore, Desktop micromilled microfluidics, Microfluidics and Nanofluidics, 22 (2018) 31.

[69] K. Raj M, S. Chakraborty, PDMS microfluidics: A mini review, Journal of Applied Polymer Science, 137 (2020) 48958.

[70] A.V. Nielsen, M.J. Beauchamp, G.P. Nordin, A.T. Woolley, 3D Printed Microfluidics, Annual Review of Analytical Chemistry, 13 (2020) 45-65.

[71] S.H. Yazdi, I.M. White, Optofluidic Surface Enhanced Raman Spectroscopy Microsystem for Sensitive and Repeatable On-Site Detection of Chemical Contaminants, Analytical Chemistry, 84 (2012) 7992-7998.

[72] B.C. Galarreta, M. Tabatabaei, V. Guieu, E. Peyrin, F. Lagugné-Labarthet, Microfluidic channel with embedded SERS 2D platform for the aptamer detection of ochratoxin A, Analytical and Bioanalytical Chemistry, 405 (2013) 1613-1621.

[73] I.J. Hidi, M. Jahn, K. Weber, D. Cialla-May, J. Popp, Droplet based microfluidics: spectroscopic characterization of levofloxacin and its SERS detection, Physical Chemistry Chemical Physics, 17 (2015) 21236-21242.

[74] E. Koglin, J.M. Séquaris, P. Valenta, Surface enhanced raman spectroscopy of nucleic acid bases on Ag electrodes, Journal of Molecular Structure, 79 (1982) 185-189.

[75] W.A. Hassanain, E.L. Izake, Toward Label-Free SERS Detection of Proteins through Their Disulfide Bond Structure, SLAS Discovery, 25 (2020) 87-94.

[76] D. Yu, Q. Yin, J. Wang, J. Yang, Z. Chen, Z. Gao, Q. Huang, S. Li, SERS-Based Immunoassay Enhanced with Silver Probe for Selective Separation and Detection of Alzheimer's Disease Biomarkers, International journal of nanomedicine, 16 (2021) 1901-1911.

[77] A.A. Kowalska, A. Kaminska, W. Adamkiewicz, E. Witkowska, M. Tkacz, Novel highly sensitive Cu-based SERS platforms for biosensing applications, Journal of Raman spectroscopy, 46 (2015) 428-433.

[78] Y. Kwon, S.B. Nukala, S. Srivastava, H. Miyamoto, N.I. Ismail, J. Jousma, J. Rehman, S.-B. Ong, W.H. Lee, S.-G. Ong, Detection of viral RNA fragments in human iPSC cardiomyocytes following treatment with extracellular vesicles from SARS-CoV-2 coding sequence overexpressing lung epithelial cells, Stem Cell Research & Therapy, 11 (2020) 514.

[79] J.-H. Lee, B.-C. Kim, O. Byeung-Keun, J.-W. Choi, Rapid and sensitive determination of HIV-1 virus based on surface enhanced raman spectroscopy, Journal of biomedical nanotechnology, 11 (2015) 2223-2230.

[80] J.D. Driskell, Y. Zhu, C.D. Kirkwood, Y. Zhao, R.A. Dluhy, R.A. Tripp, Rapid and sensitive detection of rotavirus molecular signatures using surface enhanced Raman spectroscopy, PloS one, 5 (2010) 10222.

[81] P. Negri, A. Kage, A. Nitsche, D. Naumann, R.A. Dluhy, Detection of viral nucleoprotein binding to anti-influenza aptamersviaSERS, Chemical Communications, 47 (2011) 8635-8637.

[82] https://www.who.int/news-room/fact-sheets/detail/cancer.

[83] K.M. Koo, J. Wang, R.S. Richards, A. Farrell, J.W. Yaxley, H. Samaratunga, P.E. Teloken, M.J. Roberts, G.D. Coughlin, M.F. Lavin, P.N. Mainwaring, Y. Wang, R.A. Gardiner, M. Trau, Design and Clinical Verification of Surface-Enhanced Raman Spectroscopy Diagnostic Technology for Individual Cancer Risk Prediction, ACS Nano, 12 (2018) 8362-8371.

[84] J.U. Lee, W.H. Kim, H.S. Lee, K.H. Park, S.J. Sim, Quantitative and Specific Detection of Exosomal miRNAs for Accurate Diagnosis of Breast Cancer Using a Surface-Enhanced Raman Scattering Sensor Based on Plasmonic Head-Flocked Gold Nanopillars, Small, 15 (2019) 1804968.

[85] W.R. Premasiri, Y. Chen, J. Fore, A. Brodeur, L.D. Ziegler, SERS biomedical applications: diagnostics, forensics, and metabolomics, Frontiers and Advances in Molecular Spectroscopy, Elsevier2018, pp. 327-367.

[86] R. Das, S. Parveen, A. Bora, P. Giri, Origin of high photoluminescence yield and high SERS sensitivity of nitrogen-doped graphene quantum dots, Carbon, 160 (2020) 273-286.

[87] S. Cîntă Pînzaru, I. Pavel, N. Leopold, W. Kiefer, Identification and characterization of pharmaceuticals using Raman and surface-enhanced Raman scattering, Journal of Raman Spectroscopy, 35 (2004) 338-346.

[88] C.-H. Ho, S. Lee, SERS and DFT investigation of the adsorption behavior of 4-mercaptobenzoic acid on silver colloids, Colloids and Surfaces A: Physicochemical and Engineering Aspects, 474 (2015) 29-35.

[89] T. Sandvik, Selection and use of laboratory diagnostic assays in BVD control programmes, Preventive Veterinary Medicine, 72 (2005) 3-16.

[90] A.C.S. Talari, Z. Movasaghi, S. Rehman, I.u. Rehman, Raman Spectroscopy of Biological Tissues, Applied Spectroscopy Reviews, 50 (2015) 46-111.

[91] S. Kalasin, J. Dabkowski, K. Nüsslein, M.M. Santore, The role of nano-scale heterogeneous electrostatic interactions in initial bacterial adhesion from flow: A case study with Staphylococcus aureus, Colloids and Surfaces B: Biointerfaces, 76 (2010) 489-495.

[92] J. Ko, S.-G. Park, S. Lee, X. Wang, C. Mun, S. Kim, D.-H. Kim, J. Choo, Culture-free detection of bacterial pathogens on plasmonic nanopillar arrays using rapid Raman mapping, ACS applied materials & interfaces, 10 (2018) 6831-6840.

[93] C. Wang, C. Yu, Analytical characterization using surface-enhanced Raman scattering (SERS) and microfluidic sampling, Nanotechnology, 26 (2015) 092001.

[94] N. Duan, B. Chang, H. Zhang, Z. Wang, S. Wu, Salmonella typhimurium detection using a surface-enhanced Raman scattering-based aptasensor, International journal of food microbiology, 218 (2016) 38-43.

[95] N. Duan, Y. Yan, S. Wu, Z. Wang, Vibrio parahaemolyticus detection aptasensor using surface-enhanced Raman scattering, Food Control, 63 (2016) 122-127.

[96] L.-L. Tay, P.-J. Huang, J. Tanha, S. Ryan, X. Wu, J. Hulse, L.-K. Chau, Silica encapsulated SERS nanoprobe conjugated to the bacteriophage tailspike protein for targeted detection of Salmonella, Chemical Communications, 48 (2012) 1024-1026.

[97] S.K. Srivastava, H.B. Hamo, A. Kushmaro, R.S. Marks, C. Grüner, B. Rauschenbach, I. Abdulhalim, Highly sensitive and specific detection of E. coli by a SERS nanobiosensor chip utilizing metallic nanosculptured thin films, Analyst, 140 (2015) 3201-3209.

[98] Y. Zhang, X. Ye, G. Xu, X. Jin, M. Luan, J. Lou, L. Wang, C. Huang, J. Ye, Identification and distinction of non-small-cell lung cancer cells by intracellular SERS nanoprobes, RSC Advances, 6 (2016) 5401-5407.

[99] S. Cinta Pinzaru, A. Falamas, C.A. Dehelean, Molecular conformation changes along the malignancy revealed by optical nanosensors, Journal of Cellular and Molecular Medicine, 17 (2013) 277-286.

[100] S. Bamrungsap, A. Treetong, C. Apiwat, T. Wuttikhun, T. Dharakul, SERS-fluorescence dual mode nanotags for cervical cancer detection using aptamers conjugated to gold-silver nanorods, Microchimica Acta, 183 (2016) 249-256.

[101] A. Pramanik, S.R. Chavva, B.P. Viraka Nellore, K. May, T. Matthew, S. Jones, A. Vangara, P.C. Ray, Development of a SERS Probe for Selective Detection of Healthy Prostate and Malignant Prostate Cancer Cells Using ZnII, Chemistry – An Asian Journal, 12 (2017) 665-672.

[102] S. Lee, H. Chon, J. Lee, J. Ko, B.H. Chung, D.W. Lim, J. Choo, Rapid and sensitive phenotypic marker detection on breast cancer cells using surface-enhanced Raman scattering (SERS) imaging, Biosensors and Bioelectronics, 51 (2014) 238-243.

[103] X. Wu, L. Luo, S. Yang, X. Ma, Y. Li, C. Dong, Y. Tian, L.e. Zhang, Z. Shen, A. Wu, Improved SERS Nanoparticles for Direct Detection of Circulating Tumor Cells in the Blood, ACS Applied Materials & Interfaces, 7 (2015) 9965-9971.

[104] X. Xi, C. Liang, Perspective of Future SERS Clinical Application Based on Current Status of Raman Spectroscopy Clinical Trials, Frontiers in chemistry, 9 (2021) 665841-665841.

[105] A. Rahman, A.K. Rahman, Nanoscale Metrology of Line Patterns on Semiconductor by Continuous Wave Terahertz Multispectral Reconstructive 3-D Imaging Overcoming the Abbe Diffraction Limit, IEEE Transactions on Semiconductor Manufacturing, 32 (2019) 7-13.

[106] S.G. Kaminskyj, T.E. Dahms, High spatial resolution surface imaging and analysis of fungal cells using SEM and AFM, Micron, 39 (2008) 349-361.

[107] A. Curry, H. Appleton, B. Dowsett, Application of transmission electron microscopy to the clinical study of viral and bacterial infections: Present and future, Micron, 37 (2006) 91-106.

[108] Y. Seo, W. Jhe, Atomic force microscopy and spectroscopy, Reports on Progress in Physics, 71 (2007) 016101.

[109] J.N. Israelachvili, Intermolecular and surface forces, Academic press2011.

[110] C. Kittel, P. McEuen, Kittel's Introduction to Solid State Physics, John Wiley & Sons2018.

[111] J. Chastain, R.C. King Jr, Handbook of X-ray photoelectron spectroscopy, Perkin-Elmer Corporation, 40 (1992) 221.

[112] P. Van der Heide, X-ray photoelectron spectroscopy: an introduction to principles and practices, John Wiley & Sons2011.

201

[113] W. Doh, V. Papaefthimiou, S. Zafeiratos, Applications of synchrotron-based X-ray photoelectron spectroscopy in the characterization of nanomaterials, Surface science tools for nanomaterials characterization, (2015) 317-366.

[114] H. Abdi, L.J. Williams, Principal component analysis, Wiley interdisciplinary reviews: computational statistics, 2 (2010) 433-459.

[115] R. Bro, A.K. Smilde, Principal component analysis, Analytical Methods, 6 (2014) 2812-2831.

[116] J. Hutchings, C. Kendall, B. Smith, N. Shepherd, H. Barr, N. Stone, The potential for histological screening using a combination of rapid Raman mapping and principal component analysis, Journal of biophotonics, 2 (2009) 91-103.

[117] P.A. Mosier-Boss, Review on SERS of Bacteria, Biosensors, 7 (2017) 51.

[118] S. Sauer, M. Kliem, Mass spectrometry tools for the classification and identification of bacteria, Nature Reviews Microbiology, 8 (2010) 74-82.

[119] K. Imagawa, Y. Mizukami, S. Miyazaki, Regulatory convergence of medical devices: a case study using ISO and IEC standards, Expert Review of Medical Devices, 15 (2018) 497-504.

[120] M. Mochizuki, S. Asatyas, K. Suthiwanich, T. Hayashi, Thiol molecules as temperature sensors for surface-enhanced Raman scattering measurements of heat-sensitive materials, Chemistry Letters, 45 (2016) 1207-1209.

[121] M. De Jesus, K. Giesfeldt, M. Sepaniak, Use of a sample translation technique to minimize adverse effects of laser irradiation in surface-enhanced Raman spectrometry, Applied spectroscopy, 57 (2003) 428-438.

[122] J.S. Suh, D.H. Jeong, M.S. Lee, Effect of inhomogeneous broadening on the surface photochemistry of phthalazine, Journal of Raman spectroscopy, 30 (1999) 595-598.

[123] B. Song, Simple and fast fabrication of superhydrophobic metal wire mesh for efficiently gravity-driven oil/water separation, Marine pollution bulletin, 113 (2016) 211-215.

[124] Y. Yoshida, Y. Inoue, A. Shimosaka, Y. Shirakawa, J. Hidaka, Effect of aperture structure of Dutch weave mesh on flow resistivity, Journal of Chemical Engineering of Japan, 48 (2015) 730-741.

[125] S. Lebedev, O. Gefle, E. Amitov, D.Y. Berchuk, D. Zhuravlev, Poly (lactic acid)-based polymer composites with high electric and thermal conductivity and their characterization, Polymer Testing, 58 (2017) 241-248.

[126] T. Szymborski, E. Witkowska, K. Nicinski, Z. Majka, T. Krehlik, T. Deskur, K. Winkler, A. Kaminska, Steel Wire Mesh as a Thermally Resistant SERS Substrate, Nanomaterials (Basel), 8 (2018).

[127] A. Michota, J. Bukowska, Surface-enhanced Raman scattering (SERS) of 4-mercaptobenzoic acid on silver and gold substrates, Journal of Raman Spectroscopy, 34 (2003) 21-25.

[128] Y. Fang, N.-H. Seong, D.D. Dlott, Measurement of the distribution of site enhancements in surface-enhanced Raman scattering, Science, 321 (2008) 388-392.

[129] C. Novara, S. Dalla Marta, A. Virga, A. Lamberti, A. Angelini, A. Chiadò, P. Rivolo, F. Geobaldo, V. Sergo, A. Bonifacio, SERS-active Ag nanoparticles on porous silicon and PDMS substrates: A comparative study of uniformity and Raman efficiency, The Journal of Physical Chemistry C, 120 (2016) 16946-16953.

[130] J.B. Herzog, M.W. Knight, Y. Li, K.M. Evans, N.J. Halas, D. Natelson, Dark plasmons in hot spot generation and polarization in interelectrode nanoscale junctions, Nano letters, 13 (2013) 1359-1364.

[131] S.P. Hastings, P. Swanglap, Z. Qian, Y. Fang, S.-J. Park, S. Link, N. Engheta, Z. Fakhraai, Quadrupole-enhanced Raman scattering, ACS nano, 8 (2014) 9025-9034.

[132] W.F. Pearman, M. Lawrence-Snyder, S.M. Angel, A.W. Decho, Surface-enhanced Raman spectroscopy for in situ measurements of signaling molecules (autoinducers) relevant to bacteria quorum sensing, Applied Spectroscopy, 61 (2007) 1295-1300.

[133] T. Luna-Pineda, K. Soto-Feliciano, E. De La Cruz-Montoya, L.C.P. Londoño, C. Ríos-Velázquez, S.P. Hernández-Rivera, Spectroscopic characterization of biological agents using FTIR, normal Raman and surface-enhanced Raman spectroscopies, Chemical and Biological Sensing VIII, International Society for Optics and Photonics, 2007, pp. 65540K.

[134] J. Guicheteau, L. Argue, D. Emge, A. Hyre, M. Jacobson, S. Christesen, Bacillus spore classification via surface-enhanced Raman spectroscopy and principal component analysis, Applied spectroscopy, 62 (2008) 267-272.

[135] Y. Chao, T. Zhang, Surface-enhanced Raman scattering (SERS) revealing chemical variation during biofilm formation: from initial attachment to mature biofilm, Analytical and bioanalytical chemistry, 404 (2012) 1465-1475.

[136] F. Madzharova, Z. Heiner, M. Gühlke, J. Kneipp, Surface-enhanced hyper-Raman spectra of adenine, guanine, cytosine, thymine, and uracil, The Journal of Physical Chemistry C, 120 (2016) 15415-15423.

[137] Z. Movasaghi, S. Rehman, I.U. Rehman, Raman spectroscopy of biological tissues, Applied Spectroscopy Reviews, 42 (2007) 493-541.

[138] M.L. Laucks, A. Sengupta, K. Junge, E.J. Davis, B.D. Swanson, Comparison of psychro-active arctic marine bacteria and common mesophillic bacteria using surface-enhanced Raman spectroscopy, Applied spectroscopy, 59 (2005) 1222-1228.

[139] J. Zhang, Q. Huang, G. Yao, Z. Ke, H. Zhang, Y. Lu, SERS study of transformation of phenylalanine to tyrosine under particle irradiation, Journal of Molecular Structure, 1072 (2014) 195-202.

[140] C. Krafft, L. Neudert, T. Simat, R. Salzer, Near infrared Raman spectra of human brain lipids, Spectrochimica Acta Part A: Molecular and Biomolecular Spectroscopy, 61 (2005) 1529-1535.

[141] R.K. Dukor, Vibrational spectroscopy in the detection of cancer, Handbook of vibrational spectroscopy, (2006).

[142] A. Walter, A. Marz, W. Schumacher, P. Rosch, J. Popp, Towards a fast, high specific and reliable discrimination of bacteria on strain level by means of SERS in a microfluidic device, Lab Chip, 11 (2011) 1013-1021.

[143] M.C. Demirel, P. Kao, N. Malvadkar, H. Wang, X. Gong, M. Poss, D.L. Allara, Bio-organism sensing via surface enhanced Raman spectroscopy on controlled metal/polymer nanostructured substrates, Biointerphases, 4 (2009) 35-41.

[144] M. Veres, M. Füle, S. Tóth, M. Koós, I. Pócsik, Surface enhanced Raman scattering (SERS) investigation of amorphous carbon, Diamond and Related Materials, 13 (2004) 1412-1415.

[145] C. Greulich, D. Braun, A. Peetsch, J. Diendorf, B. Siebers, M. Epple, M. Köller, The toxic effect of silver ions and silver nanoparticles towards bacteria and human cells occurs in the same concentration range, RSC advances, 2 (2012) 6981-6987.

[146] E. Witkowska, K. Nicinski, D. Korsak, T. Szymborski, A. Kaminska, Sources of variability in SERS spectra of bacteria: comprehensive analysis of interactions between selected bacteria and plasmonic nanostructures, Anal Bioanal Chem, (2019).

[147] Y. Liu, K. Chao, M.S. Kim, X. Nou, Rapid screening and species identification of E. coli, Listeria, and Salmonella by SERS technique, Defense and Security 2008: Special Sessions on Food Safety, Visual Analytics, Resource Restricted Embedded and Sensor Networks, and 3D Imaging and Display, SPIE, 2008, pp. 54-62.

203

[148] C. Fan, Z. Hu, A. Mustapha, M. Lin, Rapid detection of food- and waterborne bacteria using surface-enhanced Raman spectroscopy coupled with silver nanosubstrates, Appl Microbiol Biotechnol, 92 (2011) 1053-1061.

[149] K. Shrivas, S. Sahu, G.K. Patra, N.K. Jaiswal, R. Shankar, Localized surface plasmon resonance of silver nanoparticles for sensitive colorimetric detection of chromium in surface water, industrial waste water and vegetable samples, Analytical Methods, 8 (2016) 2088-2096.

[150] N.E. Marotta, L.A. Bottomley, Surface-enhanced Raman scattering of bacterial cell culture growth media, Applied spectroscopy, 64 (2010) 601-606.

[151] B.W. Peterson, P.K. Sharma, H.C. van der Mei, H.J. Busscher, Bacterial cell surface damage due to centrifugal compaction, Applied and environmental microbiology, 78 (2012) 120-125.

[152] A. Takada, K. Matsushita, S. Horioka, Y. Furuichi, Y. Sumi, Bactericidal effects of 310 nm ultraviolet light-emitting diode irradiation on oral bacteria, BMC Oral Health, 17 (2017) 1-10.

[153] L. Galli, V. Brusa, R. Rodríguez, M. Signorini, J.M. Oteiza, G.A. Leotta, Escherichia coli in food products, Escherichia coli in the Americas, Springer2016, pp. 173-203.

[154] R.W. Miles, Photovoltaic solar cells: Choice of materials and production methods, Vacuum, 80 (2006) 1090-1097.

[155] L. Zhou, S. Zhuang, C. He, Y. Tan, Z. Wang, J. Zhu, Self-assembled spectrum selective plasmonic absorbers with tunable bandwidth for solar energy conversion, Nano Energy, 32 (2017) 195-200.

[156] I.C.G. Thanos, An in-situ Raman spectroscopic study of the reduction of HNO3 on a rotating silver electrode, Journal of Electroanalytical Chemistry and Interfacial Electrochemistry, 200 (1986) 231-247.

[157] S. Hy, Felix, Y.-H. Chen, J.-y. Liu, J. Rick, B.-J. Hwang, In situ surface enhanced Raman spectroscopic studies of solid electrolyte interphase formation in lithium ion battery electrodes, Journal of Power Sources, 256 (2014) 324-328.

[158] K. Niciński, E. Witkowska, D. Korsak, K. Noworyta, J. Trzcińska-Danielewicz, A. Girstun, A. Kamińska, Photovoltaic cells as a highly efficient system for biomedical and electrochemical surface-enhanced Raman spectroscopy analysis, RSC Advances, 9 (2019) 576-591.

[159] A. Trügler, J.-C. Tinguely, G. Jakopic, U. Hohenester, J.R. Krenn, A. Hohenau, Near-field and SERS enhancement from rough plasmonic nanoparticles, Physical Review B, 89 (2014) 165409.

[160] Y. Zhao, X. Liu, D.Y. Lei, Y. Chai, Effects of surface roughness of Ag thin films on surface-enhanced Raman spectroscopy of graphene: spatial nonlocality and physisorption strain, Nanoscale, 6 (2014) 1311-1317.

[161] A. Matikainen, T. Nuutinen, T. Itkonen, S. Heinilehto, J. Puustinen, J. Hiltunen, J. Lappalainen, P. Karioja, P. Vahimaa, Atmospheric oxidation and carbon contamination of silver and its effect on surface-enhanced Raman spectroscopy (SERS), Scientific Reports, 6 (2016) 37192.

[162] Y. Song, P.J. Swedlund, G.J. McIntosh, B.C.C. Cowie, G.I.N. Waterhouse, J.B. Metson, The Influence of Surface Structure on H4SiO4 Oligomerization on Rutile and Amorphous TiO2 Surfaces: An ATR-IR and Synchrotron XPS Study, Langmuir, 28 (2012) 16890-16899.

[163] J. Tang, F.S. Ou, H.P. Kuo, M. Hu, W.F. Stickle, Z. Li, R.S. Williams, Silver-coated Si nanograss as highly sensitive surface-enhanced Raman spectroscopy substrates, Applied Physics A, 96 (2009) 793-797.

[164] A. Kamińska, T. Szymborski, T. Jaroch, A. Zmysłowski, A. Szterk, Gold-capped silicon for ultrasensitive SERS-biosensing: Towards human biofluids analysis, Materials Science and Engineering: C, 84 (2018) 208-217.

[165] Y.S. Hu, J. Jeon, T.J. Seok, S. Lee, J.H. Hafner, R.A. Drezek, H. Choo, Enhanced Raman Scattering from Nanoparticle-Decorated Nanocone Substrates: A Practical Approach to Harness In-Plane Excitation, ACS Nano, 4 (2010) 5721-5730.

[166] L. Noorani, M. Stenzel, R. Liang, M.H. Pourgholami, D.L. Morris, Albumin nanoparticles increase the anticancer efficacy of albendazole in ovarian cancer xenograft model, Journal of Nanobiotechnology, 13 (2015) 25.

[167] W.-T. Cheng, M.-T. Liu, H.-N. Liu, S.-Y. Lin, Micro-Raman spectroscopy used to identify and grade human skin pilomatrixoma, Microscopy Research and Technique, 68 (2005) 75-79.

[168] U. Neugebauer, J.H. Clement, T. Bocklitz, C. Krafft, J. Popp, Identification and differentiation of single cells from peripheral blood by Raman spectroscopic imaging, Journal of Biophotonics, 3 (2010) 579-587.

[169] N. Stone, C. Kendall, J. Smith, P. Crow, H. Barr, Raman spectroscopy for identification of epithelial cancers, Faraday Discussions, 126 (2004) 141-157.

[170] I. Notingher, C. Green, C. Dyer, E. Perkins, N. Hopkins, C. Lindsay, L.L. Hench, Discrimination between ricin and sulphur mustard toxicity in vitro using Raman spectroscopy, Journal of The Royal Society Interface, 1 (2004) 79-90.

[171] M.F.K. Fung, M.K. Senterman, N.Z. Mikhael, S. Lacelle, P.T.T. Wong, Pressure-tuning fourier transform infrared spectroscopic study of carcinogenesis in human endometrium, Biospectroscopy, 2 (1996) 155-165.

[172] N. Stone, C. Kendall, N. Shepherd, P. Crow, H. Barr, Near-infrared Raman spectroscopy for the classification of epithelial pre-cancers and cancers, Journal of Raman Spectroscopy, 33 (2002) 564-573.

[173] Z. Huang, A. McWilliams, H. Lui, D.I. McLean, S. Lam, H. Zeng, Near-infrared Raman spectroscopy for optical diagnosis of lung cancer, International Journal of Cancer, 107 (2003) 1047-1052.

[174] U. Utzinger, D.L. Heintzelman, A. Mahadevan-Jansen, A. Malpica, M. Follen, R. Richards-Kortum, Near-Infrared Raman Spectroscopy for in vivo Detection of Cervical Precancers, Applied Spectroscopy, 55 (2001) 955-959.

[175] C. Krafft, T. Knetschke, A. Siegner, R.H.W. Funk, R. Salzer, Mapping of single cells by near infrared Raman microspectroscopy, Vibrational Spectroscopy, 32 (2003) 75-83.

[176] D.P. Fromm, A. Sundaramurthy, A. Kinkhabwala, P.J. Schuck, G.S. Kino, W.E. Moerner, Exploring the chemical enhancement for surface-enhanced Raman scattering with Au bowtie nanoantennas, The Journal of Chemical Physics, 124 (2006) 061101.

[177] C. Chenal, R.L. Birke, J.R. Lombardi, Determination of the Degree of Charge-Transfer Contributions to Surface-Enhanced Raman Spectroscopy, ChemPhysChem, 9 (2008) 1617-1623.

[178] M. Sun, H. Xu Direct Visualization of the Chemical Mechanism in SERRS of 4-Aminothiophenol/Metal Complexes and Metal/4-Aminothiophenol/Metal Junctions, ChemPhysChem, 10 (2009) 392-399.

[179] Y.-F. Huang, D.-Y. Wu, H.-P. Zhu, L.-B. Zhao, G.-K. Liu, B. Ren, Z.-Q. Tian, Surface-enhanced Raman spectroscopic study of p-aminothiophenol, Physical Chemistry Chemical Physics, 14 (2012) 8485-8497.

[180] M. Osawa, N. Matsuda, K. Yoshii, I. Uchida, Charge transfer resonance Raman process in surface-enhanced Raman scattering from p-aminothiophenol adsorbed on silver: Herzberg-Teller contribution, The Journal of Physical Chemistry, 98 (1994) 12702-12707.

[181] R.L. Scharff, Economic burden from health losses due to foodborne illness in the United States, Journal of food protection, 75 (2012) 123-131.

[182] N. Coutrelis, European Union food law update, J. Food L. & Pol'y, 2 (2006) 121.

[183] ISO 6579-1:2017. 2017 Microbiology of the food chain—Horizontal method for the detection, enumeration and serotyping of Salmonella—Part 1: Detection of S*almonella* spp.

[184] ISO 11290-1:2017 . 2017 Microbiology of the food chain—Horizontal method for the detection and enumeration of L*isteria monocytogenes* and of Listeria spp. - Part 1: Detection method.

[185] ISO 22964:2017. 2017 Microbiology of the food chain - Horizontal method for the detection of Cronobacter spp.

[186] European Commission Regulation, 2017. Comission Regulation of August 23, 2017 amending Regulation (EC) No 2073/2005 as regards Campylobacter in broiler carcases, 2017/1495/EC. Official Journal of the European Union, L 218/1, 24.8.2017.

[187] E.F.S.A.a.E.C.f.D.P.a. Control, The European Union summary report on trends and sources of zoonoses, zoonotic agents and food-borne outbreaks in 2017, EFSa Journal, 16 (2018).

[188] M.A. Strid, J. Engberg, L.B. Larsen, K. Begtrup, K. Mølbak, K.A. Krogfelt, Antibody responses to Campylobacter infections determined by an enzyme-linked immunosorbent assay: 2-year follow-up study of 210 patients, Clinical Diagnostic Laboratory Immunology, 8 (2001) 314-319.

[189] S.A. Barghouthi, A universal method for the identification of bacteria based on general PCR primers, Indian journal of microbiology, 51 (2011) 430-444.

[190] E. Witkowska, K. Niciński, D. Korsak, B. Dominiak, J. Waluk, A. Kamińska, Nanoplasmonic sensor for foodborne pathogens detection. Towards development of ISO-SERS methodology for taxonomic affiliation of Campylobacter spp, Journal of Biophotonics, 13 (2020).

[191] E. Witkowska, D. Korsak, A. Kowalska, A. Janeczek, A. Kamińska, Strain-level typing and identification of bacteria–a novel approach for SERS active plasmonic nanostructures, Analytical and bioanalytical chemistry, 410 (2018) 5019-5031.

[192] A. Walter, A. März, W. Schumacher, P. Rösch, J. Popp, Towards a fast, high specific and reliable discrimination of bacteria on strain level by means of SERS in a microfluidic device, Lab on a Chip, 11 (2011) 1013-1021.

[193] R.M. Jarvis, A. Brooker, R. Goodacre, Surface-enhanced Raman scattering for the rapid discrimination of bacteria, Faraday Discuss, 132 (2006) 281-292; discussion 309-219.

[194] M. Demirel, P. Kao, N. Malvadkar, H. Wang, X. Gong, M. Poss, D. Allara, Bio-organism sensing via surface enhanced Raman spectroscopy on controlled metal/polymer nanostructured substrates, Biointerphases, 4 (2009) 35-41.

[195] J. Guicheteau, L. Argue, A. Hyre, M. Jacobson, S.D. Christesen, Raman and surface-enhanced Raman spectroscopy of amino acids and nucleotide bases for target bacterial vibrational mode identification, Chemical and Biological Sensing VII, International Society for Optics and Photonics, 2006, pp. 62180O.

[196] M. Kahraman, A.I. Zamaleeva, R.F. Fakhrullin, M. Culha, Layer-by-layer coating of bacteria with noble metal nanoparticles for surface-enhanced Raman scattering, Anal Bioanal Chem, 395 (2009) 2559-2567.

[197] X. Yang, C. Gu, F. Qian, Y. Li, J.Z. Zhang, Highly sensitive detection of proteins and bacteria in aqueous solution using surface-enhanced Raman scattering and optical fibers, Analytical chemistry, 83 (2011) 5888-5894.

[198] Z. Movasaghi, S. Rehman, D.I. ur Rehman, Fourier transform infrared (FTIR) spectroscopy of biological tissues, Applied Spectroscopy Reviews, 43 (2008) 134-179.

[199] W. Premasiri, Y. Chen, P. Williamson, D. Bandarage, C. Pyles, L. Ziegler, Rapid urinary tract infection diagnostics by surface-enhanced Raman spectroscopy (SERS): identification and antibiotic susceptibilities, Analytical and bioanalytical chemistry, 409 (2017) 3043-3054.

[200] J. Xu, J.W. Turner, M. Idso, S.V. Biryukov, L. Rognstad, H. Gong, V.L. Trainer, M.L. Wells, M.S. Strom, Q. Yu, In situ strain-level detection and identification of Vibrio parahaemolyticus using surface-enhanced Raman spectroscopy, Analytical chemistry, 85 (2013) 2630-2637.

[201] M. Mirzaei, M.Z. Mohiabadi, A comparative analysis of long-term field test of monocrystalline and polycrystalline PV power generation in semi-arid climate conditions, Energy for Sustainable Development, 38 (2017) 93-101.

[202] T. Szymborski, Y. Stepanenko, K. Niciński, P. Piecyk, S.M. Berus, M. Adamczyk-Popławska, A. Kamińska, Ultrasensitive SERS platform made via femtosecond laser micromachining for biomedical applications, Journal of Materials Research and Technology, 12 (2021) 1496-1507.

[203] R.E. Russo, Laser ablation, Applied Spectroscopy, 49 (1995) 14A-28A.

[204] S.S. Socransky, Dental biofilms: difficult therapeutic targets, Periodontol 2000, 28 (2002) 12-55.

[205] R. Teles, F. Teles, J. Frias-Lopez, B. Paster, A. Haffajee, Lessons learned and unlearned in periodontal microbiology, Periodontology 2000, 62 (2013) 95-162.

[206] S.S. Dominy, C. Lynch, F. Ermini, M. Benedyk, A. Marczyk, A. Konradi, M. Nguyen, U. Haditsch, D. Raha, C. Griffin, Porphyromonas gingivalis in Alzheimer's disease brains: Evidence for disease causation and treatment with small-molecule inhibitors, Science advances, 5 (2019).

[207] G. Hajishengallis, Periodontitis: from microbial immune subversion to systemic inflammation, Nature Reviews Immunology, 15 (2015) 30-44.

[208] R.J. Genco, W.S. Borgnakke, Risk factors for periodontal disease, Periodontology 2000, 62 (2013) 59-94.

[209] A. Zapata, S. Ramirez-Arcos, A comparative study of McFarland turbidity standards and the Densimat photometer to determine bacterial cell density, Current microbiology, 70 (2015) 907-909.

[210] E. Witkowska, A.M. Łasica, K. Niciński, J. Potempa, A. Kamińska, In Search of Spectroscopic Signatures of Periodontitis: A SERS-Based Magnetomicrofluidic Sensor for Detection of Porphyromonas gingivalis and Aggregatibacter actinomycetemcomitans, ACS Sensors, 6 (2021) 1621-1635.

[211] P. Kubryk, R. Niessner, N.P. Ivleva, The origin of the band at around 730 cm−1 in the SERS spectra of bacteria: a stable isotope approach, Analyst, 141 (2016) 2874-2878.

[212] A.G. Andrew, M.S. James, A.J. James, L.C. Susan, M.S. Kevin, SERS of whole-cell bacteria and trace levels of biological molecules, Proc.SPIE, 2002.

[213] W.R. Premasiri, J.C. Lee, A. Sauer-Budge, R. Théberge, C.E. Costello, L.D. Ziegler, The biochemical origins of the surface-enhanced Raman spectra of bacteria: a metabolomics profiling by SERS, Analytical and Bioanalytical Chemistry, 408 (2016) 4631-4647.

[214] T. Lemma, A. Saliniemi, V. Hynninen, V.P. Hytönen, J.J. Toppari, SERS detection of cell surface and intracellular components of microorganisms using nano-aggregated Ag substrate, Vibrational Spectroscopy, 83 (2016) 36-45.

[215] Y. Chen, W.R. Premasiri, L.D. Ziegler, Surface enhanced Raman spectroscopy of Chlamydia trachomatis and Neisseria gonorrhoeae for diagnostics, and extra-cellular metabolomics and biochemical monitoring, Scientific Reports, 8 (2018) 5163.

[216] B. Sjöberg, S. Foley, B. Cardey, M. Enescu, An experimental and theoretical study of the amino acid side chain Raman bands in proteins, Spectrochimica Acta Part A: Molecular and Biomolecular Spectroscopy, 128 (2014) 300-311.

[217] D. Yang, H. Zhou, N.E. Dina, C. Haisch, Portable bacteria-capturing chip for direct surface-enhanced Raman scattering identification of urinary tract infection pathogens, Royal Society Open Science, 5 180955.

[218] A.M. Lasica, T. Goulas, D. Mizgalska, X. Zhou, I. De Diego, M. Ksiazek, M. Madej, Y. Guo, T. Guevara, M. Nowak, Structural and functional probing of PorZ, an essential bacterial surface component of the type-IX secretion system of human oral-microbiomic Porphyromonas gingivalis, Scientific Reports, 6 (2016) 1-22.

[219] A. Sroka, M. Sztukowska, J. Potempa, J. Travis, C.A. Genco, Degradation of host heme proteins by lysine-and arginine-specific cysteine proteinases (gingipains) of Porphyromonas gingivalis, Journal of Bacteriology, 183 (2001) 5609-5616.

[220] G. Sharma, P. Jeevanandam, A Facile Synthesis of Multifunctional Iron Oxide@Ag Core–Shell Nanoparticles and Their Catalytic Applications, European Journal of Inorganic Chemistry, 2013 (2013) 6126-6136.

[221] T.-Y. Liu, K.-T. Tsai, H.-H. Wang, Y. Chen, Y.-H. Chen, Y.-C. Chao, H.-H. Chang, C.-H. Lin, J.-K. Wang, Y.-L. Wang, Functionalized arrays of Raman-enhancing nanoparticles for capture and culture-free analysis of bacteria in human blood, Nature communications, 2 (2011) 1-8.

[222] E. Sawosz, A. Chwalibog, K. Mitura, S. Mitura, J. Szeliga, T. Niemiec, M. Rupiewicz, M. Grodzik, A. Sokołowska, Visualisation of morphological interaction of diamond and silver nanoparticles with Salmonella enteritidis and Listeria monocytogenes, Journal of nanoscience and nanotechnology, 11 (2011) 7635-7641.

[223] C.K. Muro, L. de Souza Fernandes, I.K. Lednev, Sex determination based on Raman spectroscopy of saliva traces for forensic purposes, Analytical chemistry, 88 (2016) 12489-12493.

[224] V. Moisoiu, M. Badarinza, A. Stefancu, S.D. Iancu, O. Serban, N. Leopold, D. Fodor, Combining surface-enhanced Raman scattering (SERS) of saliva and two-dimensional shear wave elastography (2D-SWE) of the parotid glands in the diagnosis of Sjögren's syndrome, Spectrochimica Acta Part A: Molecular and Biomolecular Spectroscopy, 235 (2020) 118267.

[225] V.I. Haraszthy, P.K. Sreenivasan, Microbiological and clinical effects of an oral hygiene regimen, Contemporary clinical trials communications, 8 (2017) 85-89.

[226] N. Salako, V. Rotimi, R. Preeta, F. Khodakhast, The bacteriology of the supragingival plaque of child dental patients in Kuwait, Medical Principles and Practice, 13 (2004) 191-195.

[227] R.A. Ghossein, S. Bhattacharya, J. Rosai, Molecular detection of micrometastases and circulating tumor cells in solid tumors, Clinical Cancer Research, 5 (1999) 1950-1960.

[228] S. Nagrath, L.V. Sequist, S. Maheswaran, D.W. Bell, D. Irimia, L. Ulkus, M.R. Smith, E.L. Kwak, S. Digumarthy, A. Muzikansky, Isolation of rare circulating tumour cells in cancer patients by microchip technology, Nature, 450 (2007) 1235-1239.

[229] M. Yu, S. Stott, M. Toner, S. Maheswaran, D.A. Haber, Circulating tumor cells: approaches to isolation and characterization, Journal of Cell Biology, 192 (2011) 373-382.

[230] K. Pantel, C. Alix-Panabières, Real-time liquid biopsy in cancer patients: fact or fiction?, Cancer research, 73 (2013) 6384-6388.

[231] T.M. Gorges, K. Pantel, Circulating tumor cells as therapy-related biomarkers in cancer patients, Cancer Immunology, Immunotherapy, 62 (2013) 931-939.

[232] H.J. Yoon, M. Kozminsky, S. Nagrath, Emerging role of nanomaterials in circulating tumor cell isolation and analysis, ACS nano, 8 (2014) 1995-2017.

[233] B. Enustun, J. Turkevich, Coagulation of colloidal gold, Journal of the American chemical society, 85 (1963) 3317-3328.

[234] A.A.S. Bhagat, H. Bow, H.W. Hou, S.J. Tan, J. Han, C.T. Lim, Microfluidics for cell separation, Medical & biological engineering & computing, 48 (2010) 999-1014.

[235] M.G. Lee, J.H. Shin, C.Y. Bae, S. Choi, J.-K. Park, Label-free cancer cell separation from human whole blood using inertial microfluidics at low shear stress, Analytical chemistry, 85 (2013) 6213-6218.

[236] S. Zheng, H.K. Lin, B. Lu, A. Williams, R. Datar, R.J. Cote, Y.-C. Tai, 3D microfilter device for viable circulating tumor cell (CTC) enrichment from blood, Biomedical microdevices, 13 (2011) 203-213.

[237] R.I. Handin, S.E. Lux, T.P. Stossel, Blood: principles and practice of hematology, Lippincott Williams & Wilkins2003.

[238] S. Riethdorf, H. Fritsche, V. Müller, T. Rau, C. Schindlbeck, B. Rack, W. Janni, C. Coith, K. Beck, F. Jänicke, Detection of circulating tumor cells in peripheral blood of patients with metastatic breast cancer: a validation study of the CellSearch system, Clinical cancer research, 13 (2007) 920-928.

[239] K. Niciński, J. Krajczewski, A. Kudelski, E. Witkowska, J. Trzcińska-Danielewicz, A. Girstun, A. Kamińska, Detection of circulating tumor cells in blood by shell-isolated nanoparticle–enhanced Raman spectroscopy (SHINERS) in microfluidic device, Scientific reports, 9 (2019) 1-14.

[240] T.C. Bakker Schut, P.J. Caspers, G.J. Puppels, A. Nijssen, F. Heule, M.H.A. Neumann, D.P. Hayes, Discriminating Basal Cell Carcinoma from its Surrounding Tissue by Raman Spectroscopy, Journal of Investigative Dermatology, 119 (2002) 64-69.

[241] A. Taleb, J. Diamond, J.J. McGarvey, J.R. Beattie, C. Toland, P.W. Hamilton, Raman Microscopy for the Chemometric Analysis of Tumor Cells, The Journal of Physical Chemistry B, 110 (2006) 19625-19631.

[242] N. Uzunbajakava, A. Lenferink, Y. Kraan, B. Willekens, G. Vrensen, J. Greve, C. Otto, Nonresonant Raman imaging of protein distribution in single human cells, Biopolymers, 72 (2003) 1-9.

[243] W.A. El-Said, T.-H. Kim, H. Kim, J.-W. Choi, Analysis of Intracellular State Based on Controlled 3D Nanostructures Mediated Surface Enhanced Raman Scattering, PLOS ONE, 6 (2011) e15836.

[244] I. Notingher, S. Verrier, H. Romanska, A.E. Bishop, J.M. Polak, L.L. Hench, In situ characterisation of living cells by Raman spectroscopy, Spectroscopy, 16 (2002) 43-51.

[245] H.H. Wang, C.Y. Liu, S.B. Wu, N.W. Liu, C.Y. Peng, T.H. Chan, C.F. Hsu, J.K. Wang, Y.L. Wang, Highly Raman-Enhancing Substrates Based on Silver Nanoparticle Arrays with Tunable Sub-10 nm Gaps, Advanced Materials, 18 (2006) 491-495.

[246] S. Stewart, P.M. Fredericks, Surface-enhanced Raman spectroscopy of amino acids adsorbed on an electrochemically prepared silver surface, Spectrochimica Acta Part A: Molecular and Biomolecular Spectroscopy, 55 (1999) 1641-1660.

[247] N.A. Brazhe, S. Abdali, A.R. Brazhe, O.G. Luneva, N.Y. Bryzgalova, E.Y. Parshina, O.V. Sosnovtseva, G.V. Maksimov, New insight into erythrocyte through in vivo surface-enhanced Raman spectroscopy, Biophys J, 97 (2009) 3206-3214.

[248] J.L. Lippert, L.E. Gorczyca, G. Meiklejohn, A laser Raman spectroscopic investigation of phospholipid and protein configurations in hemoglobin-free erythrocyte ghosts, Biochim Biophys Acta, 382 (1975) 51-57.

[249] D.F. Wallach, S.P. Verma, Raman and resonance-Raman scattering by erythrocyte ghosts, Biochim Biophys Acta, 382 (1975) 542-551.

[250] J. Farmer, M. Asbury, F. Hickman, D. Brenner, The Enterobacteriaceae study group: Enterobacter sakazakii: a new species of" Enterobacteriaceae" isolated from clinical specimens, Int J Syst Bacteriol, 30 (1980) 569-584.

[251] F. Casalinuovo, P. Rippa, L. Battaglia, N. Parisi, Isolation of Cronobacter spp. (Enterobacter Sakazakii) from Artisanal Mozzarella, Italian journal of food safety, 3 (2014) 1526-1526.

[252] G. Kalyantanda, L. Shumyak, L.K. Archibald, Cronobacter species contamination of powdered infant formula and the implications for neonatal health, Frontiers in pediatrics, 3 (2015) 56.

[253] J. Chap, P. Jackson, R. Siqueira, N. Gaspar, C. Quintas, J. Park, T. Osaili, R. Shaker, Z. Jaradat, S. Hartantyo, International survey of Cronobacter sakazakii and other Cronobacter spp. in follow up formulas and infant foods, International journal of food microbiology, 136 (2009) 185-188.

[254] https://www.fsai.ie/uploadedFiles/Reg2073_2005(1).pdf.

[255] https://www.fsai.ie/uploadedFiles/Reg365_2010.pdf.

[256] https://www.iso.org/standard/41258.html.

[257] https://www.iso.org/standard/64708.html.

[258] A. de Benito, N. Gnanou Besse, I. Desforges, B. Gerten, B. Ruiz, D. Tomás, Validation of standard method EN ISO 22964:2017 — Microbiology of the food chain — Horizontal method for the detection of Cronobacter spp, International Journal of Food Microbiology, 288 (2019) 47-52.

[259] J.N. Martinson, N.V. Pinkham, G.W. Peters, H. Cho, J. Heng, M. Rauch, S.C. Broadaway, S.T. Walk, Rethinking gut microbiome residency and the Enterobacteriaceae in healthy human adults, The ISME Journal, 13 (2019) 2306-2318.

[260] S. Bhar, M.J. Edelmann, M.K. Jones, Characterization and proteomic analysis of outer membrane vesicles from a commensal microbe, Enterobacter cloacae, Journal of Proteomics, 231 (2021) 103994.

[261] A.B. Nowicka, M. Czaplicka, T. Szymborski, A. Kamińska, Combined negative dielectrophoresis with a flexible SERS platform as a novel strategy for rapid detection and identification of bacteria, Analytical and Bioanalytical Chemistry, 413 (2021) 2007-2020.

[262] A.A. Guzelian, J.M. Sylvia, J.A. Janni, S.L. Clauson, K.M. Spencer, SERS of whole-cell bacteria and trace levels of biological molecules, SPIE2002.

[263] İ. Doğan, R. Gresback, T. Nozaki, M. van de Sanden, Chemical analysis of ligand-free silicon nanocrystal surfaces by surface enhanced Raman spectroscopy, arXiv preprint:1412.8622, (2014).

[264] M. Rapala-Kozik, G. Bras, B. Chruscicka, J. Karkowska-Kuleta, A. Sroka, H. Herwald, K.-A. Nguyen, S. Eick, J. Potempa, A. Kozik, Adsorption of components of the plasma kinin-forming system on the surface of Porphyromonas gingivalis involves gingipains as the major docking platforms, Infection and immunity, 79 (2011) 797-805.

210